Homochiral Metal Complexes for Biodegradable Polymer Synthesis

Jean-Charles Buffet

This thesis is submitted for the degree of

Doctor of Philosophy

of the

University of Edinburgh

November 2009

Declaration

Except where specific reference has been made to other sources, the work presented in this thesis is the original work of the author. It has not been submitted, in whole or in part, for any other degree.

Jean-Charles Buffet

November 2009

Abstract

Chapter One introduces the principle of alkoxide and phosphine oxide as ligands for lanthanides and electropositive metals, ligand self-recognition, stereoselective polymerisation of lactide, fixation of CO_2 and finally copolymerisation of CO_2 and epoxide.

Chapter Two shows the synthesis of the proligands *rac*-HL^R (a racemic phosphine oxide-alkoxide, **A**, where R = ^{t}Bu, Ph or C_6H_3-Me-3,5) and explores the resolution into diastereomeric *RRR*- and *SSS*-$M(L^R)_3$ to afford C_3–symmetric $M(L^R)_3$ complexes, **B** (where M = Sc, Lu, Y, In, Bi or La). It also demonstrates that the process is under thermodynamic control and driven by ligand self-recognition *via* the synthesis of *bis*(L^R) adducts $(L^R)_2MX$, **C**, (where M = Y or In and X = $N(SiMe_3)_2$ or OC_6H_3-^{t}Bu$_2$-2,6) and mono(L^R) adducts $(L^R)MX_2$, **D** (where M = Al or In and X = $N(SiMe_3)_2$, CH_2SiMe_3 or Me). Finally, it outlines the fixation of CO_2 into an indium-amide bond.

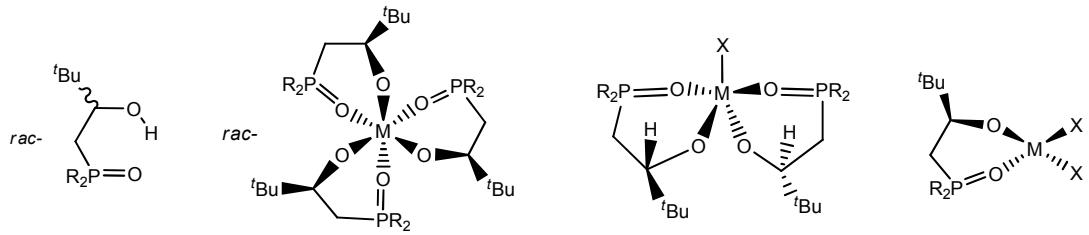

A **B** **C** **D**

Chapter Three contains a detailed investigation of the potential of the M^{III} complexes as initiators for the stereoselective polymerisation of lactide, ε-caprolactone, glycolide and copolymerisation of lactide and ε-caprolactone, lactide and glycolide and CO_2 and epoxide.

Chapter Four investigates the use of *rac*-HL^{tBu} in the resolution into diastereomeric *RR*- and *SS*-$M(L^{tBu})_2$ complexes, **E** (where M = Ca, Zn or Sn), and of *rac*-HL^{Ph} into $[M(L^R)_2]_2$ complexes, **F** (where M = Mg, Co or Sn and R = Ph or C_6H_3-Me-3,5) and mono-(L^{tBu}) adducts $(L^{tBu})MgX$, **G** (X = $N(SiMe_3)_2$ or OC_6H_3-^{t}Bu$_2$-2,6). It also

describes the synthesis of protonated M^{II} complexes $(HL^{R})MCl_2$, **H** (where M = Mg, Zn or Sn and R = ^{t}Bu or Ph). Finally, it details the polymerisation of lactide and its copolymerisation with glycolide using M^{II} complexes as initiators.

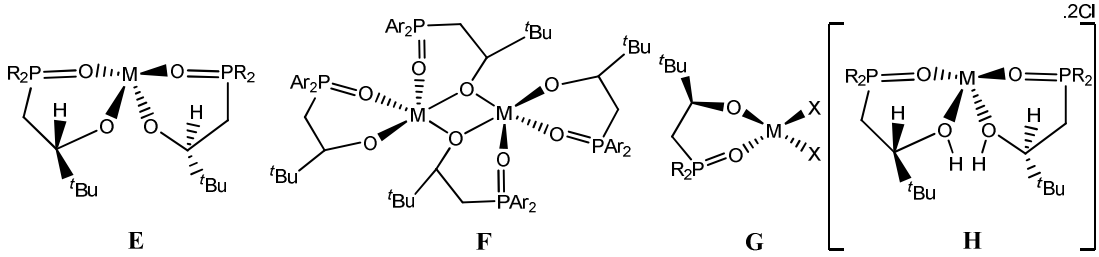

E **F** **G** **H**

Chapter Five gives full experimental details and analytical data for the herein described novel compounds.

Acknowledgements

I would like to thank my supervisor Prof. Polly L. Arnold to have accepted a polymer chemist in her group but also for her encouragement and “joie de vivre” throughout my PhD.

I would like to thank Dr. Claire Wilson, Prof. Sandy Blake, Dr. Anna Collins and Dr. Fraser White (X-ray crystallography); Dr. Adrienne Davis, Mr. Juraj Bella and Dr. Marika De Cremoux (NMR spectroscopy); Mr. Tony Hollingworth, Mr. Graham Coxhill and Dr. Ali Abda-Sadal (mass spectrometry); Mr. Stephen Boyer (elemental analysis) and Professors Howdle and Bradley (GPC).

Thanks also to past and present Post-Docs, Dr. Steve Liddle, Dr. Chris Carmichael, Dr. Sergey Zlatogorsky and Dr. Lorena Postigo for their help and answers to my numerous questions.

Thanks to Mr. Stuart Gorringe to have been a fantastic (despite being far too tall) project student.

Thanks to all past and present members of the Arnold and Love group to make my life so fully exciting, including the coffee break and Uno games.

Thanks to my family for their understanding and support.

Special Thanks to my wonderful girlfriend to cope with stress during the writing of this work and to have accepted to proof-read this manuscript.

Abbreviations

acac	acetylacetonate
Ar	C_6H_3-Me-3,5
BzOH	benzyl alcohol
Cat	catalyst
Conv.	conversion
DABAL	Bis(trimethylaluminum)–1,4-diazabicyclo[2.2.2]-octane
DABCO	1,4-diazabicyclo[2.2.2]-octane
DCM	dichloromethane
DI	diastereomeric index which represents the percentage in the desired diastereomer (*i.e RRR/SSS* or *RR/SS*).
DME	1,2-dimethoxyethane
eq.	equivalents
Eq.	equation
ES	electrospray
GPC	gel permeation chromatography
IR	infra-red
LA	lactide
M_w	weight average molecular weight
M_n	number average molecular weight
$M_{n,\ exp}$	experimental molecular weight
$M_{n,\ theo}$	theoretical molecular weight
MS	mass spectrometry
N"	$N(SiMe_3)_2$
NMR	nuclear magnetic resonance
OAr	OC_6H_3-^{t}Bu$_2$-2,6
oct	octanoate (2-ethylhexanoate)
PCL	polycaprolactone
PDI	polydispersity index

PDLA	poly-*D*-lactide (*i.e.* poly-*R*-lactide)
PGL	polyglycolide
Ph	phenyl
PLA	polylactide
PLLA	poly-*L*-lactide (*i.e.* poly-*S*-lactide)
ppm	part per million
Pybox	pyridine bis(oxazoline)
ROP	ring-opening polymerisation
RT	room temperature
^{t}Bu	*tert*-butyl
THF	tetrahydrofuran
T_g	glass transition temperature
T_m	melting point
TMS	$SiMe_4$
trisox	*tris*(oxazoline)

Table of Contents

Chapter 1: Introduction

Chapter 2: Synthesis of M^{III} complexes

Chapter 3: Polymerisation using M^{III} complexes

Chapter 4: Synthesis of $M(L^R)_2$ complexes and their use as polymerisation initiators

Chapter 5: Experimental

Chapter 1: Introduction

1.1 General Introduction

A great number and variety of homogeneous lanthanide catalysts are now used in industry and academia as low cost, low-toxicity, Lewis acidic coordination catalysts.[1-3] In the search for new asymmetric catalysts, chiral C_3-symmetric complexes are emerging as interesting competitor systems to the ubiquitous C_2-symmetric systems.[4-6]

The polymerisation of the biorenewable monomer *rac*-lactide into the biodegradable polymer polylactide (PLA) provides an interesting challenge for new chiral catalysts; the physical properties of the lactide polymers are highly dependent on the polymer stereochemistry.[7-9]

1.2 Alkoxides as ligands for lanthanides and electropositive metals

Alkoxide complexes are known for practically every element of the s, p, d and f blocks of the Periodic Table. They behave generally as one-electron ligands (˙OR) with notable flexibility; however, they can function sometimes in a 'non-innocent' manner, showing more than one electronic and structural configuration with a variable (terminal, μ_2- or μ_3-bridging) behaviour.

Coordination numbers of 3-6 are typically noted for the d-block elements, but higher formal coordination numbers are often observed in lanthanide $Ln(OR)_3$ complexes. Lewis basic solvents can be employed to 'break up' higher nuclearity species.

In 1991, a review by Mehrotra *et al.* described the syntheses, chemical properties, and spectroscopic characteristics of alkoxo and aryloxo $M(OR)_n$ (where M = Sc, Y or Ln).[10] Four years later, a short review by Hubert-Pfalzgraf described the implications of lanthanide complexes as molecular precursors in materials science.[11]

In 1996, Anwander reported some of the structural aspects of $Ln(OR)_n$ and functionalised ligands emphasising the design and synthesis of ligand environments to create tailored precursors.[12] In the decade following these reviews, numerous advances have been realised in the syntheses, characterisation, and structural elucidation of various molecules containing Ln-OR fragments.[13-17] Recently, a remarkable review by Boyle *et al.* described in details the advances in structurally characterised lanthanide alkoxide, aryloxide and silyloxide complexes.[18]

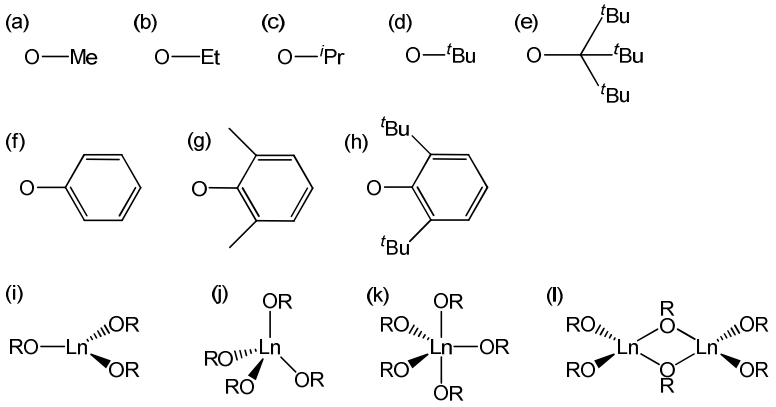

Figure 1.1: Schematic drawing of common alkoxides ((a) methoxide (OMe), (b) ethoxide (OEt), (c) *iso*-propoxide (O^{i}Pr), (d) *tert*-butoxide (O^{t}Bu) and (e) tri-*tert*-butylmethoxide (TBM)); phenoxides ((f) phenoxide (OPh), 2,6-dimethyl phenoxide (DMP) and 2,6-di-*tert*-butyl phenoxide (DBP)) and central cores ((i) trigonal planar (tp), (j) tetrahedral (td), (k) trigonal biplanar (tbp) and (l) dinuclear tetrahedral).[18]

In 1995, a review by Hermann *et al.* discussed the use of metal alkoxides as precursors in chemical vapour deposition (CVD) and explored this method for most of the metals of the Periodic Table.[19]

Arguably the greatest advances in alkoxide organometallic chemistry for electropositive metals within the last decade have come in the field of single-site initiators for the polymerisation of polar monomers. This will be discussed later in this Chapter (see section 1.6.3 and 1.6.4).

1.3 Phosphine oxide as ligands for electropositive metals

Complexes of the lanthanides with 'hard' donor ligands are of considerable interest as the possibility of a covalent contribution to the bonding should be maximised in such complexes. Phosphine oxide complexes, mainly those of triphenylphosphine oxide are well known in lanthanide chemistry.[20-24] In 1992, Aspinall *et al.* reported a classical example of a lanthanide phosphine oxide complex $[LaL_2(PPh_2)(Ph_3PO)]$ (where $L = N(SiMe_3)_2$).[25]

Recently organophosphine oxide-substituted binaphthol ligands have emerged as potential ligands for enantioselective transformations catalysed by large lanthanide ions.[26]

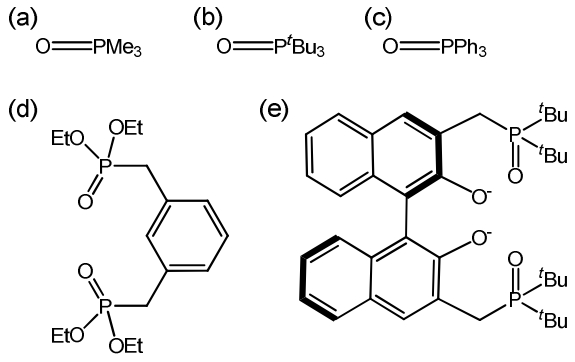

Figure 1.2: Schematic drawing of common phosphine oxides ((a) trimethylphosphine oxide, (b) tri-*tert*-butylphosphine oxide, (c) triphenylphosphine oxide and selected aryl phosphine oxide (d) and (e)

1.4 Ligand self-recognition

Ligand self-recognition is when, in the most simplified system, a chiral ligand L forms a $[ML_2]^{2+}$ type of metal complex (M : L ratio of 1 : 2). When the resulting $[ML_2]^{2+}$ complex is obtained from a racemic mixture of *R* and *S* ligands, both the homochiral *RR*-$[ML_2]^{2+}$ or *SS*-$[ML_2]^{2+}$ and the heterochiral *RS*-$[ML_2]^{2+}$ species are usually obtained. A ligand is said to be self-recognising if the homochiral complex is formed in preference to the heterochiral one (Figure 1.3).[27-29]

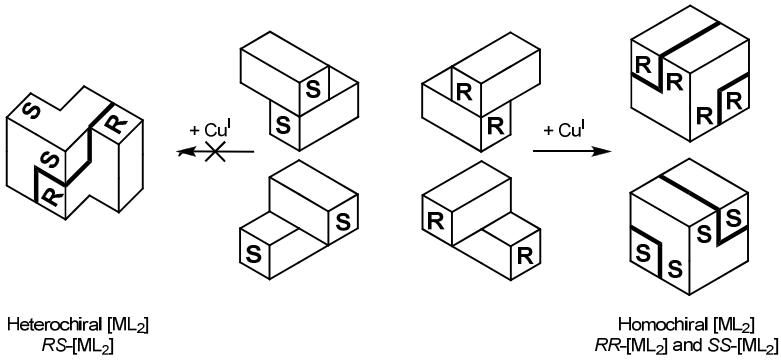

Figure 1.3: Stack's representation of ligand self-recognition[30]

A few examples of ligand self-recognition based solely on chirality exist in transition metal chemistry and have helped define the requirements for ligand self-recognition. Ligands must be rigid, sized to fit the correct number around the metal centre, project chirality and assemble to generate a more compact structure than a heterochiral ligand would.

One approach to induce self-recognition in smaller coordination compounds is to develop chiral ligands that are capable of recognition in the process of the complex formation.

Stack *et al.* have reported ligand recognition in dimeric Cu^{I} complexes of tetradentate ligands that have a *trans*-1,2-cyclohexane diamine frame (*trans*-1,2-cyclohexane diamine contains two chiral carbon centers, *RR* or *SS* enantiomer of **A**), (Figure 1.4).[30]

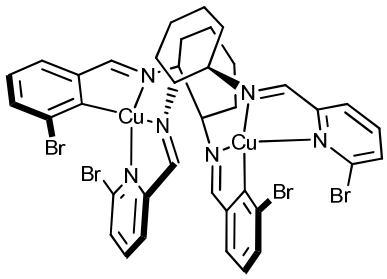

$[Cu_2\mathbf{A}_2]^{2+}$

Figure 1.4: Dimeric Cu^{I} complex of *trans*-1,2-cyclohexane diamine, $[Cu_2\mathbf{A}_2]^{2+}$

The equimolar reaction of enantiopure *RR*-**A** with $[Cu(MeCN)_4]CF_3SO_3$ in 1 : 1 ratio of CH_2Cl_2 : CH_3CN generated the binuclear species *Λ,Λ*-$[\{RR\text{-}Cu(\mathbf{A})\}_2]^{2+}$ stereospecifically, while *rac*-**A** led to two discrete homochiral metal complexes *Λ,Λ*-$[\{RR\text{-}Cu(\mathbf{A})\}_2]^{2+}$ and *Δ,Δ*-$[\{SS\text{-}Cu(\mathbf{A})\}_2]^{2+}$. These ligands are intrinsically helical and bind two Cu^I centers in a 2 + 2 configuration to generate the M_2L_2 complexes.[30]

Zema *et al.* have synthesised similar ligands in enantiomerically pure forms and have isolated pure homochiral *RR/SS*-$[Cu_2(\mathbf{B})_2]^{2+}$ complexes that form exclusively as (*P*) or (*M*) double helices from the enantiomerically pure *bis*-imino *bis*-quinoline ligands *RR*- and *SS*-**B** (Figure 1.5).[31]

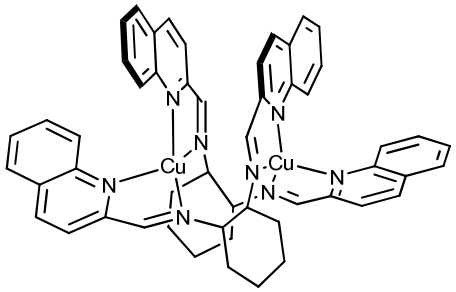

$[Cu_2(R,R\text{-}\mathbf{B})_2]^{2+}$

Figure 1.5: *trans*-1,2-cyclohexane diamine based complex, $[Cu_2(RR\text{-}\mathbf{B})_2]^{2+}$

Both ligands form 2 : 2 helical complexes with $Cu^I(ClO_4)$; a chiral double helix of (*M*) handedness, in which the two ligands are entwined in such an arrangement that half of each ligand is inequivalent to the other half of the same ligand.[31, 32]

Mascharak *et al*. have established the formation of homochiral dimeric Cu^{II} complexes $[RR\text{-}Cu_2(\mathbf{C})_2](ClO_4)_2$ and $[SS\text{-}Cu_2(\mathbf{C})_2](ClO_4)_2$ in equal amounts from a racemic mixture of a chiral ligand *N*-(1,2-*bis*(2-pyridyl)ethyl)pyridine-2-carboxamide (PEAH), H**C** (Figure 1.6), and $Cu(ClO_4)_2{\cdot}6H_2O$ in DMF.[33]

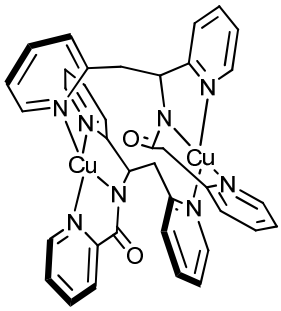

$[Cu_2(R,R\text{-}\mathbf{C})_2]^{2+}$

Figure 1.6: Homochiral dimeric Cu^{II} complexes $[RR\text{-}Cu_2(\mathbf{C})_2]^{2+}$

Oxazolines are essential ligands in asymmetric catalysis and also important synthons for stereoselective synthesis.[34, 35]

The synthesis of enantiopure helicates using chiral *bis*(oxazolyl) pyridine ligands, **D** and **E** (Figure 1.7) with $Ag^{I}(BF_4)$ in solution have been reported by Williams *et al.*. A *rac*-**D** produced $[RR\text{-}Ag_2(\mathbf{D})_2](BF_4)_2$ and $[SS\text{-}Ag_2(\mathbf{D})_2](BF_4)_2$ by homochiral self-assembly.

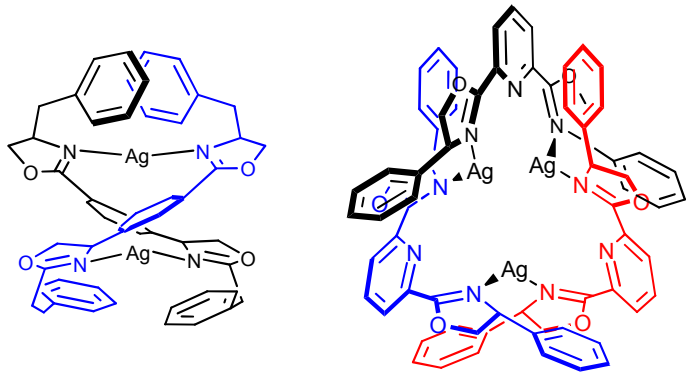

$[Ag_2(S,S\text{-}\mathbf{D})_2]^{2+}$ $[Ag_3(R,R\text{-}\mathbf{E})_3]^{3+}$

Figure 1.7: $[SS\text{-}Ag_2(\mathbf{D})_2]^{2+}$ and $[RR\text{-}Ag_3(\mathbf{E})_3]^{3+}$ complexes

The solution studies on a closely related racemic ligand **E** gave similar results as with **D**. Both **D** and **E** form enantiopure helicates with Ag^{I}, but the type of helix differs. **D** forms a double helix, $[Ag_2(\mathbf{D})_2]^{2+}$; the complex has D_2 symmetry with pseudo-twofold axes passing through the silver ions and through the pyridine groups. The compound obtained with **E** was a circular trinuclear helix, $[Ag_3(\mathbf{E})_3]^{3+}$, with

crystallographic C_3-symmetry and consists of trigonal planes of Ag^I ions with the ligands bridging the sides of the triangle.[29]

The success of the C_2-symmetric *bis*(oxazolines) (BOX) and pyridine-*bis*(oxazolines) (pybox) discovered in the early 1990s has established them as very good ligands. In contrast, the development and application of *tris*(oxazolines) has been much slower. Several *tris*(oxazolines) have been synthesised during the last decade;[36-39] the first example was reported by Katsuki *et al*. in 1995.[40, 41]

Hong *et al.* have investigated the self-assembly of chiral *tris*(oxazoline) ligands, **F**, around Ag^I ions. The ligands **F** (Figure 1.8) act as a *tris*monodentate unit and give rise to D_3-symmetric, dimeric, trinuclear complexes. Reaction of an equimolar mixture of *S*-**F** and *R*-**F** in the presence of three equivalents of $AgNO_3$ afforded a mixture of the homochiral complexes *SSS*-$[Ag_3(\mathbf{F})_2]^{3+}$ and *RRR*-$[Ag_3(\mathbf{F})_2]^{3+}$ by ligand self-recognition. No trace of heterochiral products was observed.[42]

Gade *et al.* used chiral polydentate ligands such as ^{i}Pr-*tris*oxaline, **G** (Figure 1.8) to form C_3-symmetric *tris*(oxazoline) scandium complexes [$ScCl_3$(^{i}Pr-trisox)].[39, 43]

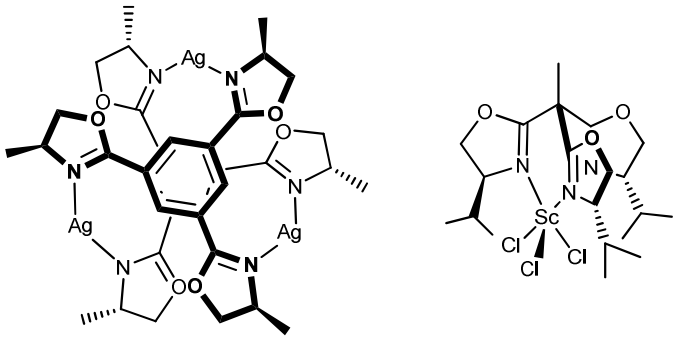

$[Ag_3F_2]^{3+}$ $ScCl_3G_3$

Figure 1.8: Chiral trismonodentate oxazoline, **F** and **G.**

Another approach involves the coordination of three enantiopure C_2-symmetric biaryl ligands to make a homochiral LnL_3 complex.[1, 44, 45]

In 1993, Shibasaki *et al.* showed the first complex of a lanthanide metal and a binol derivative with a heterometallic alkali-metal lanthanide *tris*(binaphtholate) complex.[46] The general formula of the catalyst is $[M(THF)_2]_3[Ln(binol)_3(H_2O)]$, **H**

(Figure 1.9) and crystal structures have now been reported for $[Na(THF)_2]_3[Ln(binol)_3(H_2O)]$ (Ln = La, Pr and Eu).[47] The complexes have C_3 symmetry, with the Ln ion sitting slightly above (approximately 0.4 Å) the plane of the three alkali-metal ions and the H_2O bound along the C_3 axis. For *R*-binol complexes the stereochemistry at the Ln ion is always Δ, and conversely *S*-binol gives rise to Λ stereochemistry at Ln.

Anhydrous alkali-metal lanthanide binaphtholates were prepared cleanly by the protonolysis reaction of lanthanide *tris*(silylamides) with MHbinol (M = Na or Li).[48,49]

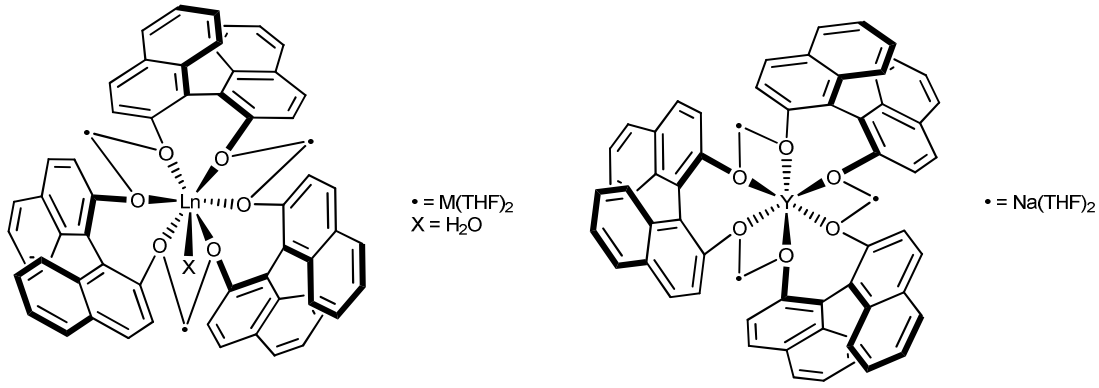

H **I**

Figure 1.9: Hetero alkali-metal lanthanide *tris*(binaphtholate), **H** and **I**

The most successful asymmetric and bifunctional lanthanide-based catalysts are based on $Na_3[Ln(binol)_3]$ (Figure 1.9); the first example of spontaneous resolution of three molecules of a racemic ligand at a lanthanide/alkali metal centre. The reaction of $YN"_3$ with *rac*-NaHbinol affords an equal mixture of the heterobimetallic *RRR/SSS*-$Na_3[Y(binol)_3]$ complexes, **I** (Figure 1.9). However, all other lanthanide/alkali metal combinations give different combinations of the heterochiral *RRS-/SSR*- complexes.[49]

1.5 Homochiral electropositive metal complexes

The binding of lanthanides of different sizes inside the chiral enantiopure nonaazamacrocycles, **J**, made by Lisowski *et al.* has been shown to generate enantiopure helical complexes of the form Ln**J**. For example, while the (*M*)-helical complex is the kinetic product formed with the all-*R*-enantiomer of the macrocycle, both (*M*)- and (*P*)-helical complexes are formed over time and are favoured for early and late lanthanides respectively (Figure 1.10).[50]

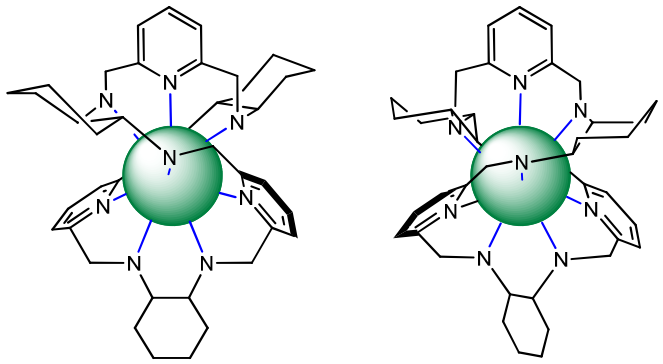

Figure 1.10: (*M*)- and (*P*)-helical complexes of chiral nonaazamacrocycles, **J**

Scott *et al.* recently reported the formation of several optically enantiopure complexes *R*-[Fe**K**$_3$]$^{2+}$ of an enantiopure chiral ligand *R*-2-phenylglycinol **K,** and $Fe(ClO_4)_2 \cdot 6H_2O$ in MeCN (Figure 1.11). The authors proved these compounds to be the first characterised [Fe**K**$_3$]$^{2+}$ complexes.[51]

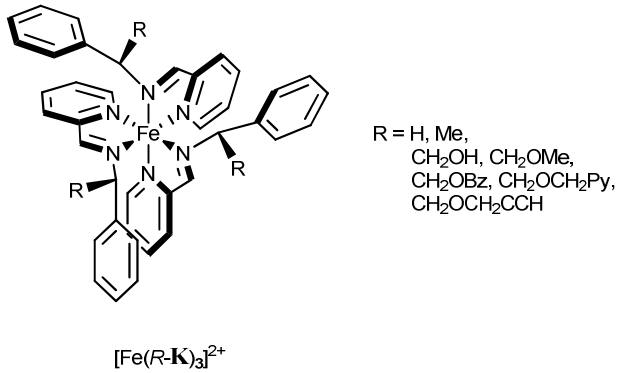

Figure 1.11: Complexes *R*-[FeK$_3$]$^{2+}$of ligand *R*-2-phenylglycinol, **K**

1.6 Polymerisation of lactide

1.6.1 General background

1.6.1.1 Applications of polylactides

In recent years, biodegradable polymers from biorenewable resources have received a great deal of attention as alternatives to traditional petrochemical-based polymers. In particular, poly(lactic acid) (PLA) has received a large amount of industrial interest (Figure 1.12). Cargill-Dow LLC and other companies have developed the infrastructure for both the manufacture and processing of PLA.[52] This has caused a significant drop in the cost of the plastic and has led to an increased use of PLA in a number of applications such as textile, packaging, pharmaceutical and biotechnology industries.[53]

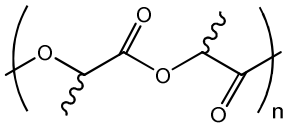

Figure 1.12: Molecular structure of poly lactic acid, PLA.

A current industrial use for PLA is disposable packaging in the food and beverage industry. Under suitable conditions the plastic containers will degrade to carbon dioxide and water. PLA has been used in the medical industry for many years; one of its first applications was in sutures for surgical procedures (PLA mixed with poly(glycolic acid)). The sutures need not be removed and are gradually degraded by the body's natural pathways. Similarly, screws made of PLA are used for fixing fragments of bones. As the screws degrade over time, secondary surgeries are not required in order to remove them after the healing process has been achieved. Current research has focused on controlled drug delivery. Here, the drug is encapsulated in a polymer matrix; the active drug is slowly and continually released over time as the polymer is degraded.[54]

The production of PLA starts from a starch or sugar feedstock, which is processed to yield *D*-glucose. Optically pure *L*-lactic acid is generated by the fermentation

process using bacteria of the genera Lactobacillus.[55] The synthesis of lactide is achieved by a depolymerisation process to afford the lactide monomer (Scheme 1.1).

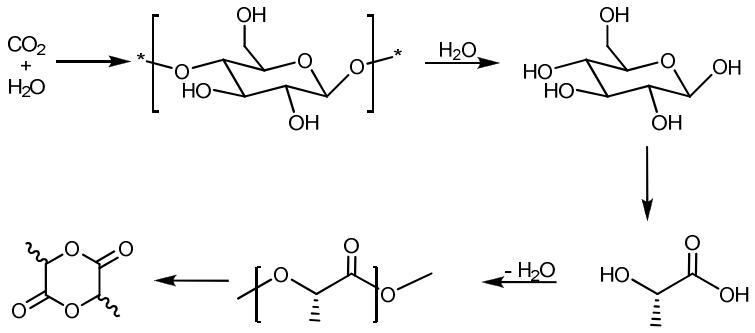

Scheme 1.1: Synthesis of lactide monomer from natural resources

There are a number of possible microstructures for PLA due to the different ways of incorporating the isomers of lactide (LA) into the polymer chain (Figure 1.13).

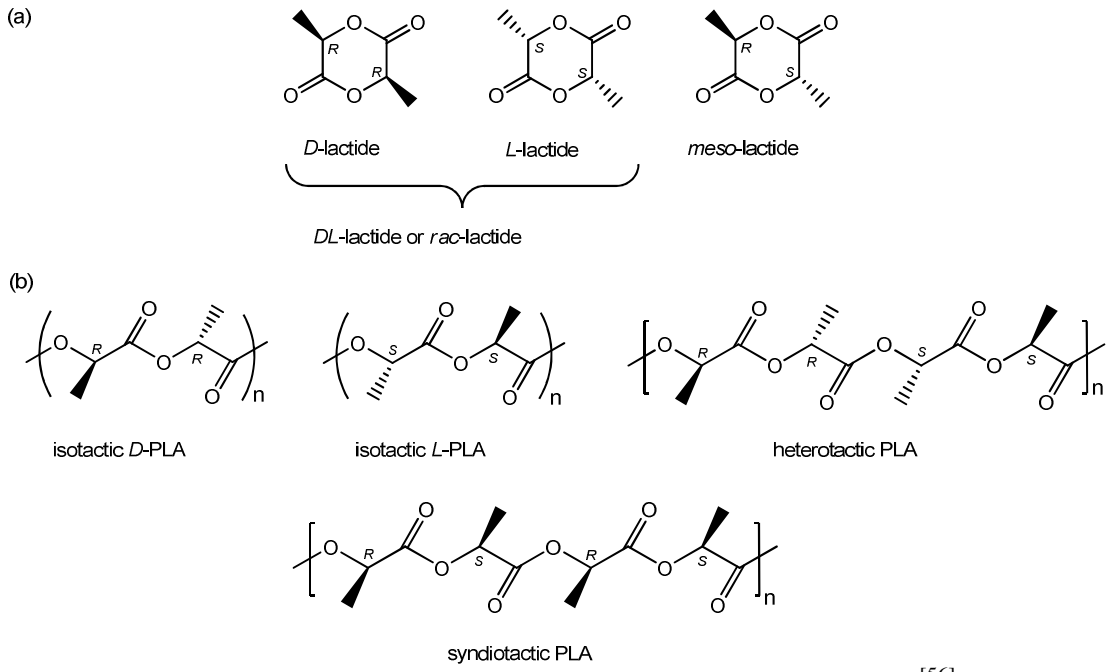

Figure 1.13: a) Isomers of lactide and b) microstructures of polylactide[56]

1.6.1.2 Degradation process of the polylactides

Degradation of PLA occurs through two mechanisms: hydrolysis of the polyester chain and enzymatic degradation. The rate of hydrolysis is dependent on a number of factors, including the molecular weight and the crystallinity of the polymer. Acidic

or basic conditions can be used to catalyse the hydrolysis; elevating both the temperature and humidity increases the hydrolysis rate. Once the polymer has been hydrolysed into small oligomeric chains (< 4000 g/mol) bacteria and other microorganisms can further degrade the polymer to carbon dioxide and water. Although PLA degrades relatively easily in comparison with traditional plastics, further research into the infrastructure required for large-scale degradation of the plastic as well as for monomer recovery/recycling is required.

1.6.1.3 Industrial process

A catalyst participates in reactions to increase its rate but is not consumed by the overall reaction; an initiator is consumed during the reaction.

The most widely used complex used as an initiator for the industrial preparation of PLA is undoubtedly Sn^{II}(octanoate), $Sn(oct)_2$, **L** (Figure 1.14). Aluminium alkoxides such as $Al(O^iPr)_3$ have also proven to be efficient catalysts for the ROP of cyclic esters but are significantly less active than $Sn(oct)_2$. Thus, much interest has been devoted to zinc derivatives as potential non-toxic catalysts, such as $Zn(lact)_2$, **M**, that allow for better control of the molecular weight of the resulting polymers compared with zinc powder.

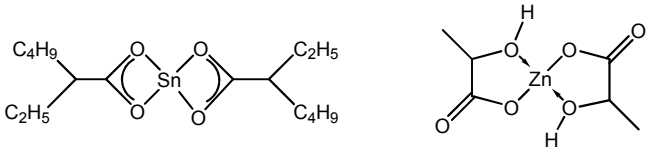

L **M**

Figure 1.14: Tin octanoate, **L** and zinc lactate, **M**

1.6.2 Mechanistic considerations

1.6.2.1 General considerations

The ring-opening of lactide occurs due to relief of a larger than normal ring-strain for lactide when compared to other six-membered rings. In this case, the high degree

of ring-strain is due to the unusual geometric conformation imposed on the ring by the presence of the two ester groups;[57] the ester groups are nearly planar forcing the ring into an irregular skew-boat conformation with the methine protons in the axial positions and the methyl substituents in the equatorial positions of the structure. The ring-opening of the strained lactide drives the polymerisation; standard enthalpy of polymerisation is -23 $kJ.mol^{-1}$ and standard entropy of polymerisation is -0.04 $kJ.K^{-1}.mol^{-1}$ for the formation of poly(*L*-lactic acid).[58]

The three-step coordination-insertion mechanism for the ROP of cyclic esters was first elucidated in 1971 by Dittrich.[59] The first experimental proof for such a mechanism in the $Al(O^iPr)_3$ initiated polymerisation of lactide was independently reported in the late 1960s by Kricheldorf[60] and Teyssié.

The first step of the coordination-insertion mechanism consists of the coordination of the monomer to the Lewis-acidic metal centre (Scheme 1.2, i).

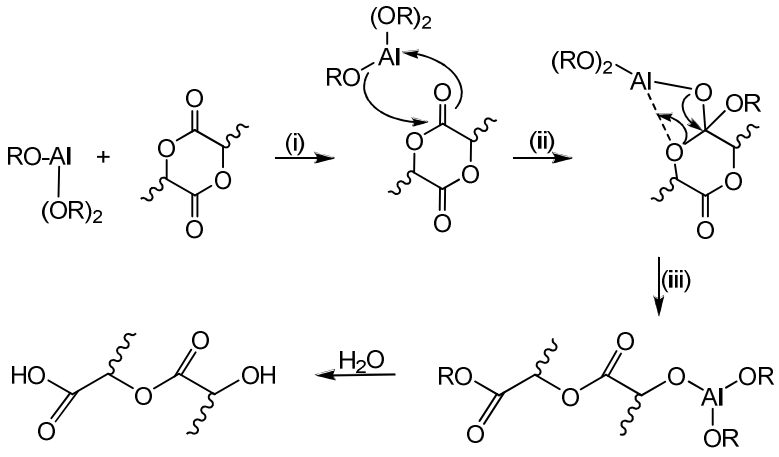

Scheme 1.2: Coordination-insertion mechanism for the $Al(O^iPr)_3$-catalysed ROP of *rac*-lactide.

The monomer subsequently inserts into one of the aluminium-alkoxide bonds *via* nucleophilic addition of the alkoxide group to the carbonyl carbon (ii) followed by ring opening *via* acyl-oxygen cleavage (iii). Hydrolysis of the active metal-alkoxide bond leads to the formation of hydroxyl end groups.

$Sn(oct)_2$ is inherently more active than $Al(O^iPr)_3$ but the polymerisation was found to be even faster and better controlled when $Sn(oct)_2$ was combined with a protic reagent such as an alcohol. The mechanism for the $Sn(oct)_2$-catalysed ROP has been the subject of much more controversy and several initiation pathways were proposed.[61] In a majority of these mechanisms, co-initiation with a hydroxyl-group-containing compound [*e.g.* H_2O, alcohol or hydroxyl-carboxylic acid (denoted herein as ROH)] has been assumed. Support for the coordination-insertion mechanism has recently been obtained theoretically (Scheme 1.3).[62] $Sn(OAc)_2$ was used as a model for $Sn(oct)_2$ and two molecules of methanol were found to coordinate to the metal centre.

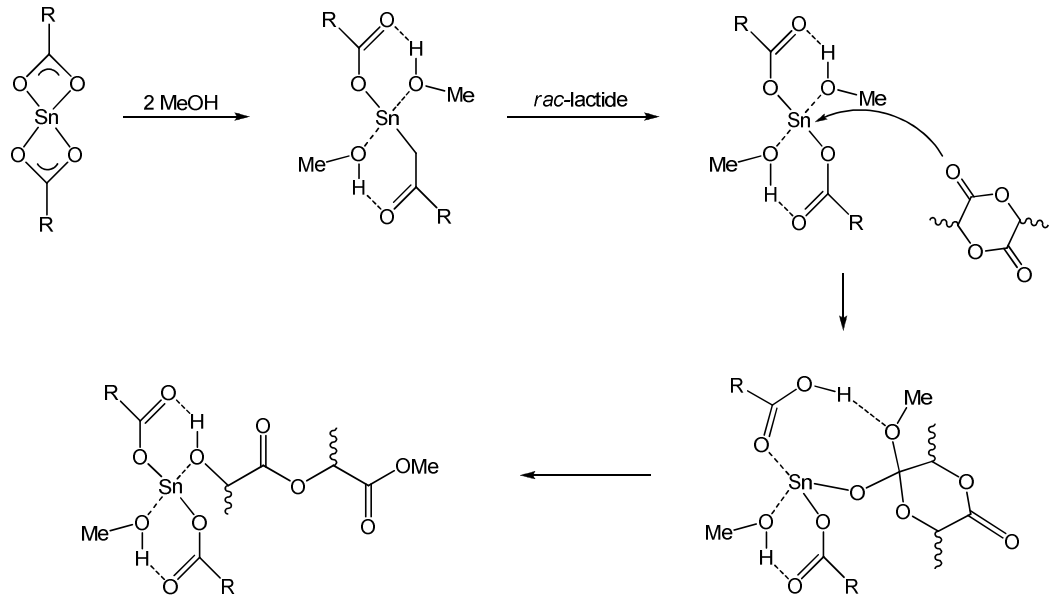

Scheme 1.3: Calculated mechanism for the $Sn(oct)_2$-catalysed ROP of lactide.

Recently, Kowalski *et al.*[63] have shown that at least one of the active species is RO-Sn-oct, reversibly formed as shown in Scheme 1.4. The results of kinetic studies of cyclic ester polymerisation initiated with "pure" $Sn(oct)_2$, $Sn(OR)_2$, $Sn(oct)_2$/ROH, $Sn(OR)_2$/octanoate and various mixtures of these also revealed that the actual initiator is the Sn^{II} alkoxide, formed in the exchange reactions between carboxylate and alkoxide in $Sn(oct)_2$ and ROH, respectively.[64]

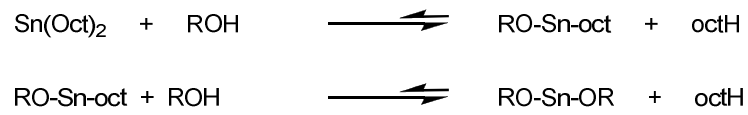

Scheme 1.4: Results of mechanistic studies on $Sn(oct)_2$

Comparatively, the mechanism of $Zn(lact)_2$ catalysed ROP has been much less studied. However, the combination of $Zn(lact)_2$ with a primary alcohol was demonstrated to increase its activity and allow for a better control of the polymerisation, as in the case of $Sn(oct)_2$.[65]

Transesterification is the major chain transfer mechanism in the polymerisation of lactide.[66] In such coordination-insertion polymerisations the efficiency of the molecular-weight control depends on the ratio $k_{propagation}/k_{initiation}$ but also from the extent of transesterification reactions that can occur.[67] This leads to a scrambling in the molecular weights observed for the polymers, and a broadening of the PDI.

For intramolecular transesterification, two growing polymer chains come together and a random exchange of polymer ends occurs, backbiting leading to macrocyclic structures and shorter chains (Scheme 1.5).

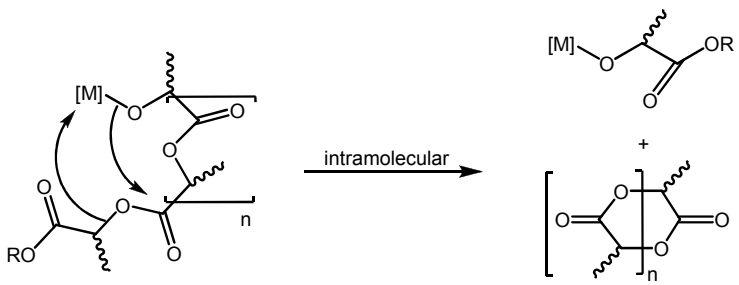

Scheme 1.5: Intramolecular transesterification side reactions

Alternatively the transesterification can occur through an intermolecular process causing the formation of cyclic polymers, through chain redistributions (Scheme 1.6).[68]

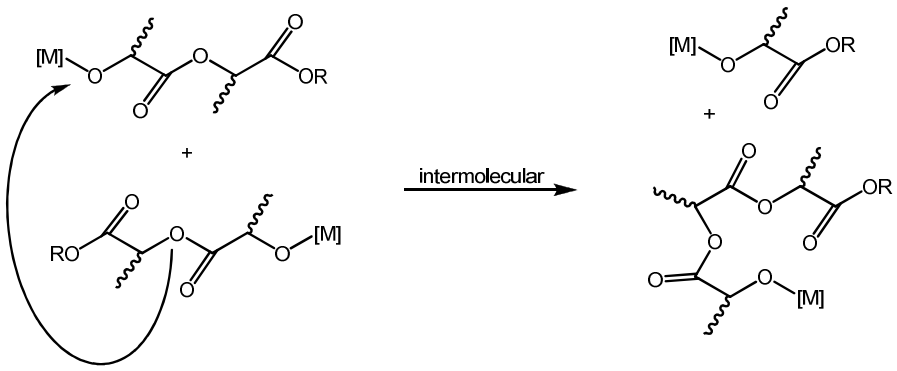

Scheme 1.6: Intermolecular transesterification side reactions

1.6.2.2 Control of the microstructure by living polymerisation

Achieving control over polymer microstructures is often accomplished by using a living polymerisation (from which chain transfer and chain termination are absent). In many cases, the rate of chain initiation is fast compared with the rate of chain propagation, so that the number of kinetic-chain carriers is essentially constant throughout the polymerisation.

If a polymerisation is truly living, the molecular weight distribution (M_n or M_w) of the polymer chains is uniform and the rate of consumption of monomer is constant throughout the polymerisation. It also follows that the molecular weight of the polymer will increase linearly with conversion until one hundred percent conversion is achieved. The polydispersity index (PDI) is defined as the weight average molecular weight divided by the number average molecular weight (M_w/M_n). If no termination processes are present in the system, it is possible to restart the polymerisation after complete conversion *via* addition of more monomer.

Since the pioneering work of Klein *et al.* in the 1950s,[69] metal-based catalytic systems have been the focus of considerable attention for the polymerisation of cyclic esters,[70] and numerous studies have been carried out to elucidate the mechanism of such polymerisations. Through variation in the nature of the metal centre and the surrounding ligands, a broad range of initiators have been prepared and evaluated.[71]

1.6.3 Living polymerisation of *rac*-lactide with single-site initiators

It has been found that a number of metals are capable of polymerising lactide including group 2 (magnesium[56, 72-80] and calcium[56, 77, 81-83]), group 3 and lanthanides (yttrium[84-102] and the lanthanides[71, 86, 87, 100, 102-108]), transition metals (zinc[56, 71, 73, 76, 77, 108-111] and iron[112-115]), group 13 (aluminium[68, 71, 72, 88, 116-126] and indium[127, 128]) and group 14 (tin[63, 108, 129-132] and germanium[133, 134]).

A general formula for these catalysts is $(L_n)MR$, where (L_n) are ancillary ligands that do not play an active role in the polymerisation but do strongly influence the metal centre and its behaviour in the polymerisation, M is a Lewis acidic metal centre and R is the initiating group. In general, the most effective initiator group is an alkoxide but alkyls, amides, and halides have been found to initiate the polymerisation. These metal-mediated polymerisations are thought to occur through a coordination-insertion mechanism as shown with the $Al(O^iPr)_3$ (Scheme 1.3).

The first ancillary ligand systems developed for the polymerisation of lactide were the metalloporphyrins, **N**, synthesised by Inoue *et al.* in the late 1980s (Figure 1.15).[135] These systems gave polymers of narrow molecular weight distribution, in high yield. The incoming monomer and the initiator require a *cis*-arrangement in order for the coordination-insertion mechanism to be viable. In the case of the porphyrinato ligands, the metal is completely encompassed by a very rigid ligand in the equatorial plane, leaving only two trans axial sites for the coordination of the initiator and the monomer.

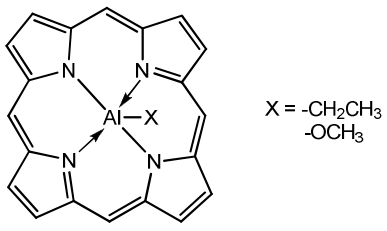

N

Figure 1.15: Example of Al^{III} metalloporphyrin system

It was postulated that a more flexible ligand might allow for a unimolecular pathway for chain growth because of the less constrained geometry at the metal centre. Bertrand *et al.* developed aluminium, zinc, samarium and tin diamidoamino complexes, **O**, for the polymerisation of lactide (Figure 1.16).[108, 124]

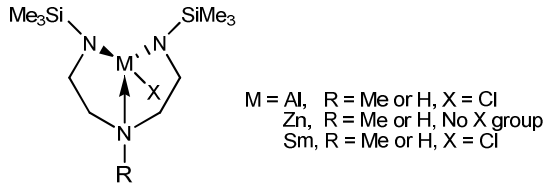

O

Figure 1.16: Metal diamidoamino complexes, **O**

SALEN-(salicylic aldehyde and ethylene diamine) based catalysts, **P**, have been widely studied for the polymerisation of lactide. Inspired by the porphyrinato systems of Inoue, the range of SALEN catalysts includes aluminium,[121, 123, 136-138] yttrium,[88] titanium,[139] iron[140] and tin[141] (Figure 1.17).

The polymers formed using these catalysts have narrow molecular weight distributions and a linear relationship is observed between the conversion and molecular weight, implying living polymerisation.

The SALAN analogues of these complexes have also been synthesised (the imine is reduced to a secondary amine or reductively aminated to give the tertiary amine) and are active for polymerisation of lactide.[120] A half-salan based ligand, **Q**, developed by Tolman *et al.* was a landmark catalyst for the polymerisation of lactide; it was the most active catalyst at the time of the report (Figure 1.17).[111] The high activity of the tridentate system was attributed to facile coordination of lactide to the coordinatively unsaturated metal centre.

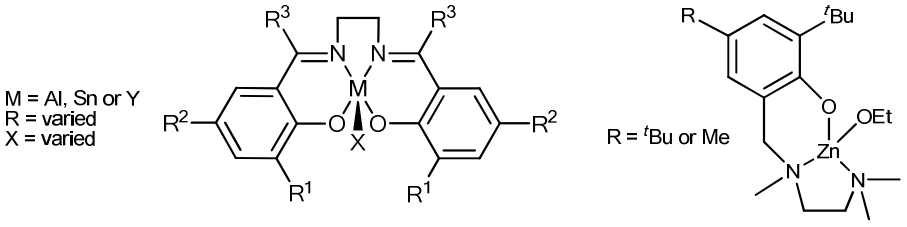

P **Q**

Figure 1.17: SALEN, **P** and half-SALAN Zinc, **Q** initiators.

Finally, β-Diiminate complexes, **R**, have also received a large amount of attention as catalysts. Analogues of magnesium,[72, 75, 142] iron[114] and zinc[72, 75, 142, 143] catalysts have been reported (Figure 1.18). In general, these catalysts display the characteristics of living systems. The magnesium β-diiminate catalysts are among the most active catalysts currently known for the metal-mediated ROP of lactide; the zinc systems are also highly active and exhibit some stereoselectivity in the polymerisation.[111, 144]

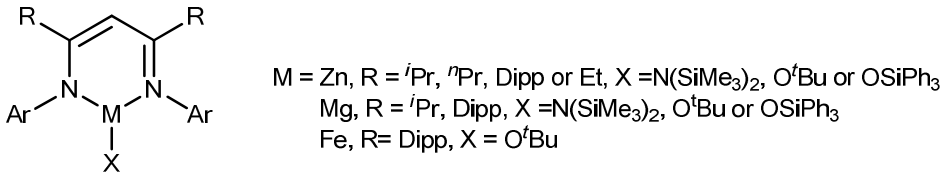

R

Figure 1.18: β-Diiminate complexes, **R**.

However, there is a problem with the β-Diiminate complexes; upon degradation amines are formed and can be toxic.

1.6.4 Stereoselective ROP of *rac*-lactide

1.6.4.1 General overview

Stereochemistry is one of the most critical factors determining the physical and mechanical properties of a polymeric material. Polymers that have stereocenters in the repeat unit can exhibit two structures of maximum order, isotactic and

syndiotactic. Because of their stereoregularity, isotactic and syndiotactic polymers are typically crystalline; an important feature for many applications because it increases the melting point and the glass transition temperature. One of the most promising methodologies for the synthesis of stereoregular polymers is the design and implementation of single-site catalysis.[145]

Two mechanisms are possible for stereoselective polymerisations of lactide by single-site metal-based catalysis: enantiomorphic site control and chain-end control. In enantiomorphic site control, a chiral catalyst will selectively polymerise one enantiomer of a monomer preferentially over the opposite enantiomer. In chain-end control the stereoselectivity of the polymerisation is controlled by the chirality of the last incorporated monomer in the growing chain. The mechanism by which stereocontrol is achieved is hard to determine; polymers resulting from the two different mechanisms can have very similar microstructures. Also, the two mechanisms can act in tandem to provide the observed stereocontrol.

Stereoerrors occur during polymerisation for systems that are not ideal. Occasionally the "wrong" enantiomer is incorporated. The way these stereoerrors are propagated in the growing polymer chain can provide invaluable evidence for determining which mechanism is responsible for stereoselectivity. In the case of enantiomorphic site control once an error occurs it is corrected by the selectivity of the catalyst and the "right" enantiomer continues to be polymerised. In chain-end control, the enantiomer being polymerised is switched once an error occurs.

1.6.4.2 Isotactic polylactide

Isotactic polylactide (Figure 1.19) can be obtained by polymerising enantiopure monomer or by the chiral resolution of *rac*-lactide using an enantioselective catalyst. It has been found that a number of metals are capable of stereoselectively polymerising *rac*-lactide with high isotacticity including magnesium,[72] yttrium,[87, 98, 104, 146] zirconium,[147] zinc,[72] aluminium[88, 98, 120-123, 125, 148-151] and the lanthanides[104, 152, 153].

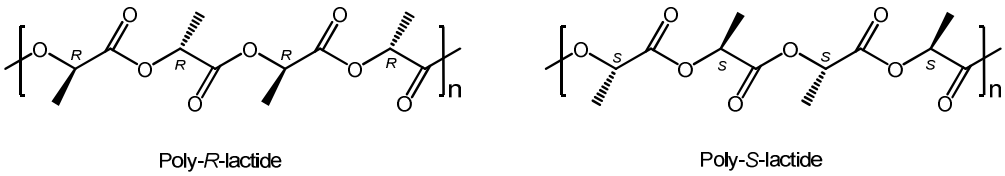

Figure 1.19: Isotactic polylactide

When the interaction between polymers having different tacticities or configurations prevail over one between polymers with the same tacticity or configuration, a stereoselective association of the former polymer pair takes place. Such association is described as stereocomplexation or stereocomplex formation. It can be divided into two different categories: stereocomplexes or stereoblock (Figure 1.20).[154]

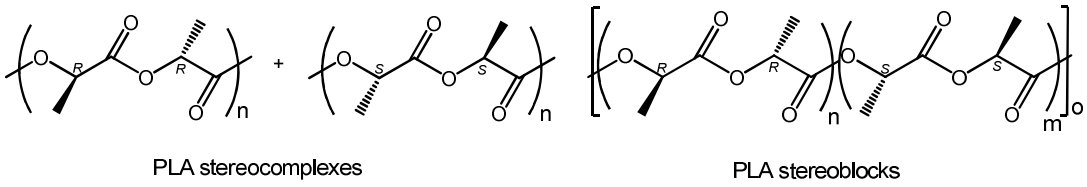

Figure 1.20: Stereocomplexes and stereoblocks of polylactide

The first approach to kinetic resolution of *rac*-lactide into isotactic polylactides was investigated with aluminium complexes supported by SALEN ligands derived from *RR*-binaphthyldiamine (**S**, Figure 1.21). Spassky's,[155] and Coates, results in stereoselective ROP of lactides suggests a strategy for the direct preparation of the polylactide stereocomplex from *rac*-lactide. It has been shown that *rac*-SALEN catalysts can be used to polymerise *rac*-lactide to produce stereocomplexes of PLLA and PDLA. In this case, the *RR*-catalyst polymerises *D*-lactide preferentially to form PDLA, and the *SS*-catalyst polymerises *L*-lactide to form PLLA.

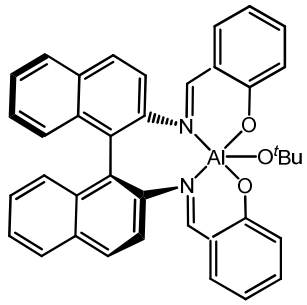

S

Figure 1.21: Aluminium SALEN initiators, **S**, for polymerisation of *rac*-lactide

The exact nature of the resulting stereoregular polylactides has been the subject of some controversery. Baker initially claimed the formation of stereocomplexes based on powder X-Ray diffraction analysis,[122] but detailed NMR studies by Coates[88] and Feijen[121] demonstrated later that PLA stereoblocks were formed instead of PLA stereocomplexes. An alternate proposal is that the polymer is in fact a stereoblock PLA with alternating block of *R*-lactide and *S*-lactide in the main chain.

1.6.4.3 Syndiotactic Polylactides

According to Bernoullian statistics, syndiotactic PLA (Figure 1.22) may be prepared from *meso*-lactide provided that the propagating chain end shows a propensity for *r*-dyad placement between monomer units.[156]

It has been found that a number of metals are capable of stereoselectively polymerising *meso*-lactide with high syndiotacticity including magnesium,[55] yttrium,[73, 86, 88] zinc[72, 73] and aluminium[88, 148, 157].

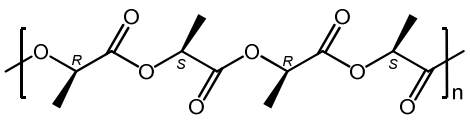

Figure 1.22: Syndiotactic polylactide

Chain-end stereocontrol was investigated by Coates *et al.* with the β-diiminate complex **T** (Figure 1.23).[72] NMR analyses revealed the formation of syndiotactic

polylactides, P_r, with 76 % racemic linkages between monomer units. From the polymerisation data, it is apparent that the identity of the initiating group significantly affects both the molecular weight and the polydispersity of the polymers. In particular, amide, ethyl and acetyl are clearly inferior initiating units as they yield polymers with broad polydispersities and molecular weights that compare poorly with theoretical values. Unfortunately, the replacement of zinc by magnesium led to initiators that yielded atactic PLA.

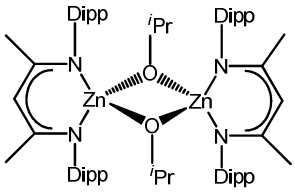

T

Figure 1.23: β-Diiminate zinc complex, **T**

Coates *et al.* have reported better results for the chiral SALEN-based aluminium complex **S** (Figure 1.21). This enantiomerically pure complex leads to more syndiotactic polylactides (up to 96 % racemic linkages). However stereocontrol is completely lost upon replacement of aluminium by other metals such as yttrium.

1.6.4.4 Heterotactic Polylactides

The preparation of heterotactic polylactides (Figure 1.24) from *rac*-lactide is due to insertion of *L*-lactide and *D*-lactide and therefore requires chain-end control. It has been found that a number of metals are capable of stereoselectively polymerising *rac*-lactide with high heterotacticity including group 2 (magnesium[72, 75, 142] and calcium[158]), group 3 (yttrium[85, 86, 90, 96] and scandium[159]), transition metals (zirconium[160, 161] and zinc[72, 75, 76, 142, 143, 162, 163]), group 13 (aluminium[89, 148] and indium[164]) and group 14 (germanium[133] and tin[165]).

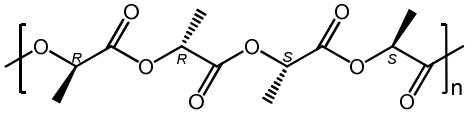

Figure 1.24: Heterotactic polylactide.

Coates *et al.* demonstrated that β-diiminate dinuclear complex **T** (Figure 1.23) catalysed the stereoselective ROP of *rac*-lactide, yielding a polymer with a highly heterotactic microstructure (stereoselectivities of 90 % at room temperature and 94% at 0 °C).[143] The *iso*propyl groups at the aryl substituents were found to play a key role on the chain-end control, as indicated by the decreased heterotacticities observed with ethyl (79 % at room temperature) and *n*-propyl groups (76 % at room temperature). This methodology has been successfully applied in complexes **U** (Figure 1.25).[120]

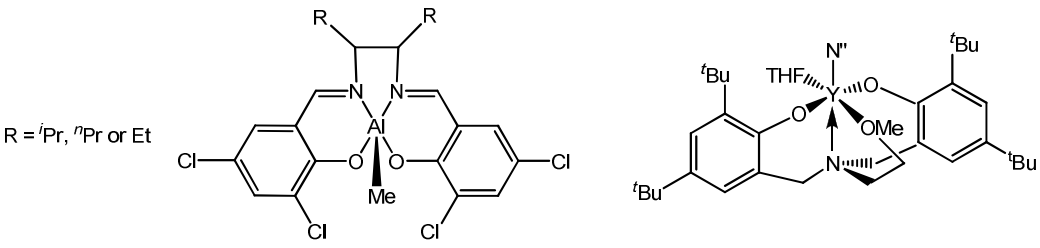

U **V**

Figure 1.25: Initiators for the synthesis of heterotactic polylactides from *rac*-lactide

The 3,5-dichlorophenoxides, $\mathbf{U_1}$ (R = Me) and $\mathbf{U_2}$ (R = CH_2Ph), are appreciably more active than their dimethyl analogues. This is most likely a consequence of the greater electrophilicity of the aluminum centers in $\mathbf{U_1}$ and $\mathbf{U_2}$. In case of $\mathbf{U_2}$, 96 % heterotactic PLA is obtained.

In 2004, Carpentier demonstrated the first example of a group 3 complex (Y^{III} centre with bulky bisphenolato ancillary ligands) which rapidly polymerised *rac*-lactide into predominantly heterotactic PLA. The yttrium complex **V** (Figure 1.25) led to stereoselectivities of 80 % in THF but only 60 % in toluene at room temperature.[90] The chain-end control was similar magnitude for alkyl and amido co-ligands but significantly lower for the lanthanum derivative (64 % in THF).

1.7 Reaction with CO_2

1.7.1 General overview

Small carbon-containing molecules such as CH_4, CO and CO_2 are attractive chemical feedstocks as they are inexpensive and readily available. To activate these small inert molecules, a potent electron source is needed to reduce their thermodynamically stable bonds. Fixation of CO_2 in its intact form may represent the first fundamental step for stoichiometric and catalytic activation of such a molecule by means of transition-metal complexes.

CO_2 has a Lewis-acidic carbon and weakly Lewis basic oxygen atoms; it is therefore not surprising that it can undergo various reactions in the coordination sphere of transition-metal compounds, such as insertion into M-X bonds (X = C, H, O or N).

In the 1970s, several groups worked on reactions of the fixation of CO_2 into organic compounds catalysed by transition metal complexes.[166-168] For example, dimethyl formamide (DMF) has been synthesised from dimethyl amine, CO_2 and H_2 in benzene in the presence of transition metal complexes; however, the reaction was slow with a low yield.[169]

The 1980s and 1990s hold examples of reactions of CO_2 fixation at a metal centre *via* insertion in the metal-ligand bond, Several reviews have tried to explain the various organometallic reactions of CO_2.[170-172] Hence, copolymerisation of CO_2 and epoxide with metal complexes have been studied extensively (*cf.* Section 1.5).

1.7.2 Fixation of CO_2 into a metal-amide bond

Recent results in magnesium chemistry gave some insights into the mechanism of the insertion of a molecule of CO_2 into a metal-amide bond.

Sita *et al.* describe a new class of oxo-transfer that involves an exchange between CO_2 and a divalent Group 14 $M\{N(SiMe_3)_2\}_2$, in which the process produced trimethylsilyl isocyanate (Equation 1.1). [173]

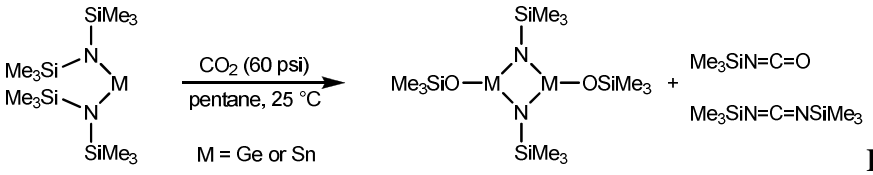

Eq. 1.1

Following, this work, Ching-Cheng *et al.* reported the attempted insertion of a CO_2 molecule into $Mg\{N(SiMe_3)_2\}_2$ which led to the claim of the first linear bonding mode of CO_2 in the magnesium-aluminum compounds $[\{R_2Al(\mu\text{-}NSiMe_3)(\mu\text{-}OSiMe_3)\ Mg(THF)_2(\mu\text{-}K^2\text{-}O_2C)\}_3]$ (R=Me or Et) **W** (Figure 1.22), which were obtained by bubbling CO_2 through a mixture of AlR_3 and $Mg\{N(SiMe_3)_2\}_2$ in THF.[174]

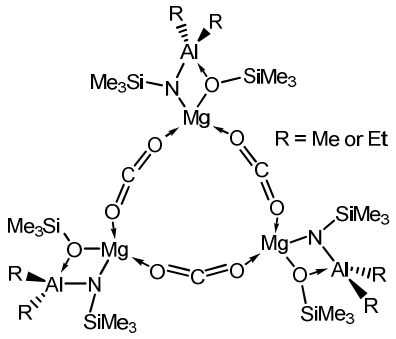

W

Figure 1.22: Proposed linear bonding mode of CO_2 in the magnesium-aluminum compounds (now disproven).

These results were recently contested by Gambarotta *et al*. who reported after new calculation fixation of the isocyanate in the magnesium-aluminium adduct (Scheme 1.7).[175]

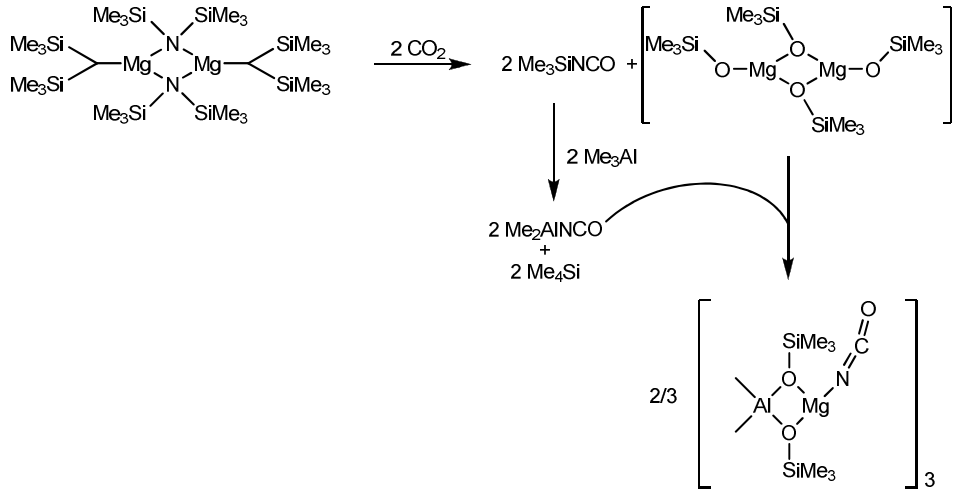

Scheme 1.7: Formation of isocyanate by-product

Recently, Meyer *et al.* reported their studies of the CO_2 activation by insertion into a U-N(amide) bond where a different group on of one of the nitrogen atoms changed the outcome of the fixation.[176] The reaction of CO_2 with the uranium complex $\mathbf{X_1}$ led to the creation of a uranium-oxygen triple bond complex, $\mathbf{X_2}$, and elimination of an isocyanate. The driving force is likely the formation and release of the thermodynamically stable isocyanate, R-NCO. (Equation 1.2).

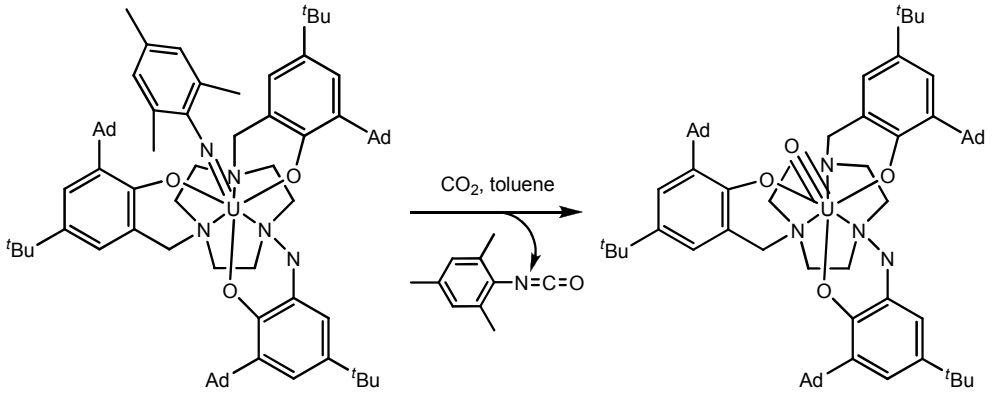

$\mathbf{X_1}$ $\mathbf{X_2}$ **Eq. 1.2**

In $\mathbf{Y_1}$, use of an amido ligand led to the formation of $\mathbf{Y_2}$ *via* insertion of CO_2 into a amide bond (Equation 1.3), the isocyanate formation and the extrusion from the complexes is not possible and allowed the retention of the mesityl ligand.

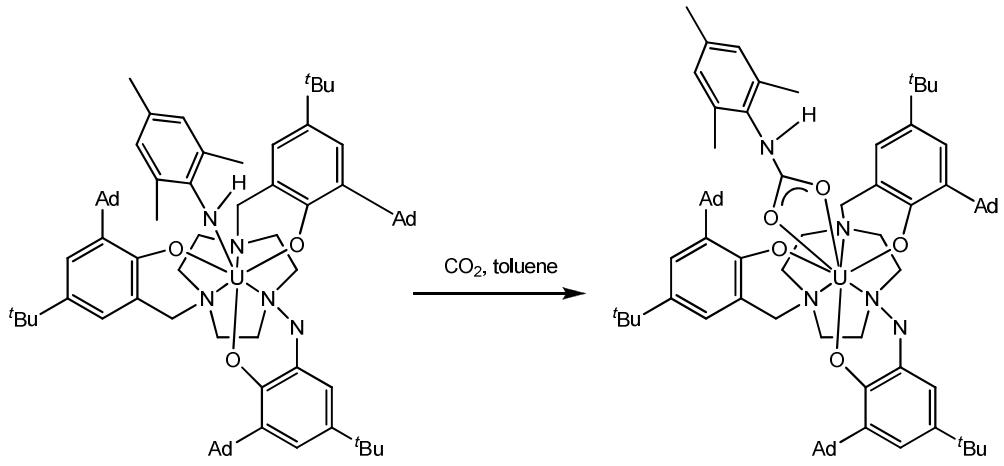

Y_1 Y_2 **Eq. 1.3**

1.8 Copolymerisation CO_2 and epoxide

1.8.1 General Background

CO_2 is an abundant, inexpensive, non-toxic and biorenewable resource that is an attractive raw material for important industrial processes; its copolymerisation with an epoxide produces polycarbonates which possess outstanding properties including strength, lightness, durability and high transparency.[177]

Inoue *et al.* demonstrated 40 years ago that it is possible to couple CO_2 and propylene oxide in the presence of a catalyst derived from a 1 : 1 mixture of $(CH_3CH_2)_2Zn$ and water.[178] This process is illustrated in Equation 1.4, generating a cyclic carbonate.

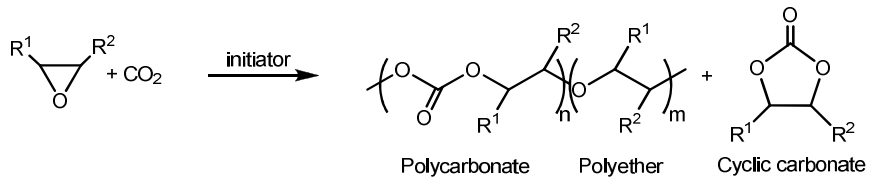

Eq. 1.4

This cyclic carbonate was proposed by Kuran *et al.* as a possible result from degradation of the growing copolymer chain, *i.e.* the back-biting mechanism (Scheme 1.7).[179]

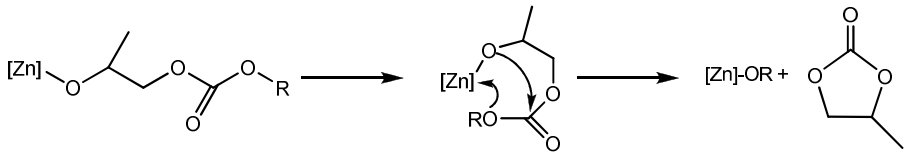

Scheme 1.8: Proposed mechanism for the formation of the cyclic byproduct.

In the late 1990s, Darensbourg *et al.* employed well-defined zinc *bis*(phenoxides) **AA** (Figure 1.26), as homogeneous catalysts for the cyclohexene oxide/CO_2 copolymerisation and obtained a better mechanistic understanding of this catalytic process (Scheme 1.9).[180, 181]

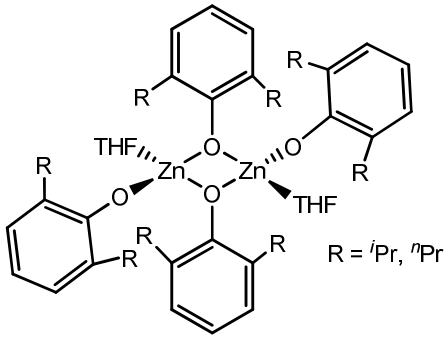

AA

Figure 1.26: Dimeric zinc bis(phenoxides) **AA.**

The most significant advance in this area came with the contribution from Coates's laboratory, which involved the use of monomeric and dimeric zinc catalysts containing β-diiminate ligands. Dramatic changes in catalytic activities for cyclohexene oxide/CO_2 copolymerisation were noted for variations in the stereoelectronic character of the (β-diiminate)Zn(OR) complex, **AB** (Figure 1.27).[182]

For example, for the zinc species where R^1 = H and R^2 = R^3 = Et, a TOF of 239 h^{-1} at 50 °C and 6.9 bar was obtained. However, upon changing R^1 = CN, R^2 = Me and R^3 = ^{i}Pr, the TOF increases to 2290 h^{-1} under the same reaction conditions.

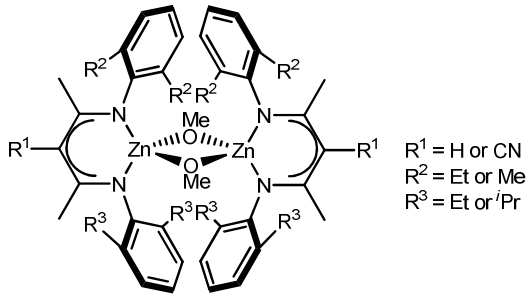

AB

Figure 1.27: (β-Diiminate)Zn(OMe) complex, **AB.**

1.8.2 Mechanistic considerations

The alternating copolymerisation of epoxides/CO_2 is a two-step process; the insertion of CO_2 into a metal alkoxide is followed by insertion of epoxide into a metal carbonate (Scheme 1.9).

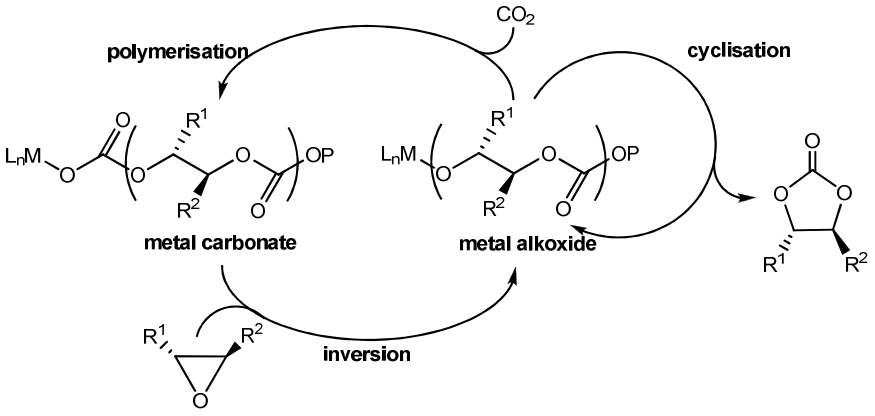

Scheme 1.9: Mechanism of the copolymerisation of CO_2 and epoxide.[183]

Cyclic species are a common by-product of the copolymerisation of CO_2 and aliphatic epoxides as they are thermodynamically more stable than polycarbonates. Their formation results from degradation of the growing polycarbonate chain by depolymerisation or 'backbiting'. The percentage of polymer (as a proportion of cyclic species) typically increases at lower reaction temperature.[184]

1.8.3 Copolymerisation by single-site catalysts

Several very good and extensive reviews have been written during last decade on this subject.[183, 185-190] It has been found that a number of metal complexes are capable of stereoselectively copolymerising CO_2 and various epoxides including those based on the lanthanides,[191] chromium,[192-198] manganese,[199-201] cobalt,[202-206] zinc,[207-217] cadmium[217, 218] and aluminium.[219, 220]

Following the research of Inoue, zinc complexes have been used the most extensively as initiators for copolymerisation of CO_2 and epoxide. Darensbourg *et al.* reported *bis*(salicylaldiminato)-zinc complexes, **AC** (Figure 1.28) which copolymerised propylene oxide and CO_2 with 99 % carbonate linkages, M_n of 41 000 g/mol and PDI of 10.3.[221] β-Diiminate zinc catalysts, **AD** (Figure 1.28) discovered by Coates have proved to be highly active.

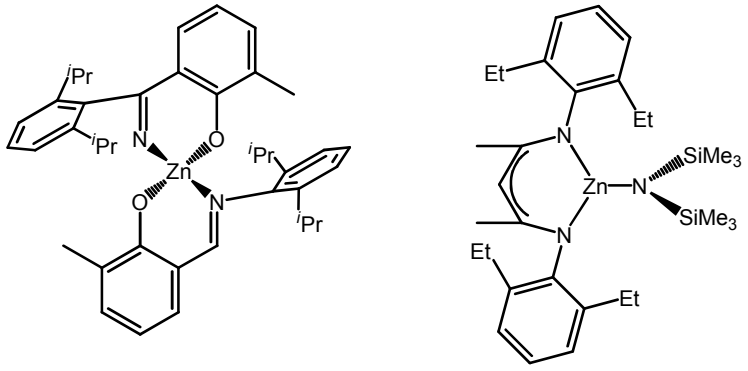

AC **AD**

Figure 1.28: Zinc catalysts for CO_2 and epoxide copolymerisation, **AC** and **AD**

Salen cobalt reported by Coates *et al.* exhibit moderate activities for the copolymerisation of propylene oxide and CO_2. At 25 °C and 55 atm CO_2, **AE** (Figure 1.29) catalysed the copolymer formation with 95 % carbonate linkages, M_n of 15 300 g/mol and a PDI of 1.22.[222] Repo *et al.* described bridged *bis*(phenoxyiminato) cobalt complexes, **AF** (Figure 1.29) showing activities of 900 h^{-1}.[202]

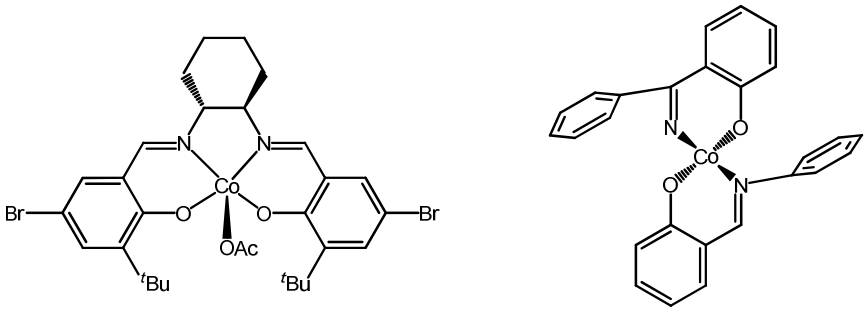

AE **AF**

Figure 1.29: Cobalt catalyst for CO_2 and epoxide copolymerisation, **AE** and **AF**

[1] H. C. Aspinall, *Chem. Rev.* **2002**, *102*, 1807.
[2] M. Shibasaki, N. Yoshikawa, *Chem. Rev.* **2002**, *102*, 2187.
[3] P. N. O'Shaughnessy, K. M. Gillespie, P. D. Knight, I. J. Munslow, P. Scott, *Dalton Trans.* **2004**, 2251.
[4] S. E. Gibson, M. P. Castaldi, *Angew. Chem., Int. Ed.* **2006**, *45*, 4718.
[5] I. Katsuki, Y. Motoda, Y. Sunatsuki, N. Matsumoto, T. Nakashima, M. Kojima, *J. Am. Chem. Soc.* **2002**, *124*, 629.
[6] M. Lama, O. Mamula, G. Kottas, F. Rizzo, L. De Cola, A. Nakamura, R. Kuroda, H. Stoeckli-Evans, *Chem. Eur. J.* **2007**, *13*, 7358.
[7] M. H. Chisholm, Z. Zhou, *J. Mater. Chem.* **2004**, *14*, 3081.
[8] H. Ma, J. Okuda, *Macromolecules* **2005**, *38*, 2665.
[9] O. Dechy-Cabaret, B. Martin-Vaca, D. Bourissou, *Chem. Rev.* **2004**, *104*, 6147.
[10] R. C. Mehrotra, A. Singh, U. M. Tripathi, *Chem. Rev.* **1991**, *91*, 1287.
[11] L. G. Hubert-Pfalzgraf, *New J. Chem.* **1995**, *19*, 727.
[12] R. Anwander, *Top. Curr. Chem.* **1996**, *179*, 149.
[13] D. C. Bradley, R. C. Mehrotra, I. P. Rothwell, A. Singh, *Alkoxo and aryloxo Derivatives of Metals*, Academic Press, New York, **2001**.
[14] N. Y. Turova, E. P. Turevskaya, V. G. Kessler, M. I. Yanovskaya, *The Chemistry of Metal Alkoxide*, Kluwer Academic Publishers, Boston, **2002**.
[15] D. C. Bradley, *Chem. Rev.* **1989**, *89*, 1317.
[16] K. G. Caulton, L. G. Hubert-Pfalzgraf, *Chem. Rev.* **1990**, *90*, 969.
[17] C. D. Chandler, C. Roger, M. J. Hampden-Smith, *Chem. Rev.* **1993**, *93*, 1205.
[18] T. J. Boyle, L. A. M. Ottley, *Chem. Rev.* **2008**, *108*, 1896.
[19] W. A. Hermann, N. W. Huber, O. Runte, *Angew. Chem., Int. Ed.* **1995**, *34*, 2187.
[20] D. C. Bradley, J. S. Ghotra, F. A. Hart, M. B. Hursthouse, P. R. Raithby, *J. Chem. Soc., Dalton Trans.* **1977**, 1166.
[21] G. B. Deacon, G. D. Fallon, C. M. Forsyth, B. M. Gatehouse, P. C. Junk, A. Philosof, P. A. White, *J. Organomet. Chem.* **1998**, *565*, 201.
[22] J. E. Cosgriff, G. B. Deacon, B. M. Gatehouse, *Aust. J. Chem.* **1993**, *46*, 1881.
[23] W. J. Evans, J. W. Grate, R. J. Doedens, *J. Am. Chem. Soc.* **1985**, *107*, 1671.
[24] J. Guan, R. D. Fischer, *J. Organomet. Chem.* **1997**, *532*, 147.
[25] H. C. Aspinall, S. R. Moore, A. K. Smith, *J. Chem. Soc., Dalton Trans.* **1992**, 153.
[26] X. Yu, T. J. Marks, *Organometallics* **2007**, *26*, 365.
[27] J.-M. Vincent, C. Philouze, I. Pianet, J.-B. Verlhac, *Chem. Eur. J.* **2000**, *6*, 3595.
[28] C. Provent, G. Bernardinelli, A. F. Williams, N. Vulliermet, *Eur. J. Inorg. Chem.* **2001**, 1963.
[29] C. Provent, E. Rivara-Minten, S. Hewage, G. Brunner, A. F. Williams, *Chem. Eur. J.* **1999**, *5*, 3487.
[30] M. A. Masood, J. E. Eric, T. D. P. Stack, *Angew. Chem., Int. Ed.* **1998**, *37*, 928.

[31] V. Amendola, L. Fabbrizzi, C. Mangano, P. Pallavicini, E. Roboli, M. Zema, *Inorg. Chem.* **2000**, *39*, 5803.
[32] V. Amendola, L. Fabbrizzi, L. Linati, C. Mangano, P. Pallavicini, V. Pedrazzini, M. Zema, *Chem. Eur. J.* **1999**, *5*, 3679.
[33] J. M. Rowland, M. M. Olmstead, P. K. Mascharak, *Inorg. Chem.* **2002**, *41*, 1545.
[34] F. Fache, E. Schulz, M. L. Tommasino, M. Lemaire, *Chem. Rev.* **2000**, *100*, 2159.
[35] H. A. McManus, P. J. Guiry, *Chem. Rev.* **2004**, *104*, 4151.
[36] J. Zhou, Y. Tang, *Chem. Soc. Rev.* **2005**, *34*, 664.
[37] S.-G. Kim, K.-H. Kim, J. Jung, S. K. Shin, K. H. Ahn, *J. Am. Chem. Soc.* **2002**, *124*, 591.
[38] S. Bellemin-Laponnaz, L. H. Gade, *Angew. Chem., Int. Ed.* **2002**, *41*, 3473.
[39] L. H. Gade, G. Marconi, C. Dro, B. D. Ward, M. Poyatos, S. Bellemin-Laponnaz, H. Wadepohl, L. Sorace, G. Poneti, *Chem. Eur. J.* **2007**, *13*, 3058.
[40] K. Kawasaki, S. Tsumura, T. Katsuki, *Synlett* **1995**, 1245.
[41] Y. Kohmura, T. Katsuki, *Tetrahedron Lett.* **2000**, *41*, 3941.
[42] H.-J. Kim, D. Moon, M. S. Lah, J.-I. Hong, *Angew. Chem., Int. Ed.* **2002**, *41*, 3174.
[43] L. H. Gade, S. Bellemin-Laponnaz, *Chem. Eur. J.* **2008**, *14*, 4142.
[44] M. Shibasaki, H. Sasai, T. Arai, *Angew. Chem., Int. Ed.* **1997**, *36*, 1236.
[45] M. Shibasaki, H. Sasai, T. Arai, T. Lida, *Pure Appl. Chem.* **1998**, *70*, 1027.
[46] H. Sasai, T. Suzuki, N. Itoh, K. Tanaka, T. Date, K. Okamura, M. Shibasaki, *J. Am. Chem. Soc.* **1993**, *115*, 10372.
[47] H. Sasai, T. Arai, Y. Satow, K. N. Houk, M. Shibasaki, *J. Am. Chem. Soc.* **1995**, *117*, 6194.
[48] H. C. Aspinall, J. L. M. Dwyer, N. Greeves, A. Steiner, *Organometallics* **1999**, *18*, 1366.
[49] H. C. Aspinall, J. F. Bickley, J. L. M. Dwyer, N. Greeves, R. V. Kelly, A. Steiner, *Organometallics* **2000**, *19*, 5416.
[50] J. Gregolinski, P. Starynowicz, K. T. Hua, J. L. Lunkley, G. Muller, J. Lisowski, *J. Am. Chem. Soc.* **2008**, *130*, 17761.
[51] S. E. Howson, L. E. N. Allan, N. P. Chmel, G. J. Clarkson, R. v. Gorkum, P. Scott, *Chem. Commun.* **2009**, 1727.
[52] R. E. Drumright, P. R. Gruber, D. E. Henton, *Adv. Mater.* **2000**, *12*, 1841.
[53] B. Gupta, N. Revagade, J. Hilborn, *Prog. Polym. Sci.* **2007**, *32*, 455.
[54] R. Langer, *Acc. Chem. Res.* **2000**, *33*, 94.
[55] A. N. Vaidya, R. A. Pandey, S. Mudliar, M. S. Kumar, T. Chakrabarti, S. Devotta, *Crit. Rev. Environ. Sci. Technol.* **2005**, *35*, 429.
[56] C. A. Wheaton, P. G. Hayes, B. J. Ireland, *Dalton Trans.* **2009**, 4832.
[57] G. J. Van Hummel, S. Harkema, F. E. Kohn, J. Feijen, *Acta Crystallogr., Sect. B* **1982**, *B38*, 1679.
[58] A. Duda, S. Penczek, *Macromolecules* **1990**, *23*, 1636.
[59] W. Dittrich, R. C. Schulz, *Angew. Makromol. Chem.* **1971**, *15*, 109.
[60] H. R. Kricheldorf, M. Berl, N. Scharnagl, *Macromolecules* **1988**, *21*, 286.

[61] P. J. A. In't Veld, E. M. Velner, P. Van De Witte, J. Hamhuis, P. J. Dijkstra, J. Feijen, *J. Polym. Sci., Part A: Polym. Chem.* **1997**, *35*, 219.
[62] M. Ryner, K. Stridsberg, A.-C. Albertsson, H. von Schenck, M. Svensson, *Macromolecules* **2001**, *34*, 3877.
[63] A. Kowalski, J. Libiszowski, T. Biela, M. Cypryk, A. Duda, S. Penczek, *Macromolecules* **2005**, *38*, 8170.
[64] A. Duda, S. Penczek, A. Kowalski, J. Libiszowski, *Macromol. Symp.* **2000**, *153*, 41.
[65] H. R. Kricheldorf, I. Kreiser-Saunders, D.-O. Damrau, *Macromol. Symp.* **2000**, *159*, 247.
[66] H. R. Kricheldorf, I. Kreiser-Saunders, *Makromol. Chem.* **1990**, *191*, 1057.
[67] S. Penczek, A. Duda, R. Szymanski, *Macromol. Symp.* **1998**, *132*, 441.
[68] P. Dubois, C. Jacobs, R. Jerome, P. Teyssie, *Macromolecules* **1991**, *24*, 2266.
[69] J. Kleine, H. H. Kleine, *Makromol. Chem.* **1959**, *30*, 23.
[70] W. Kuran, *Prog. Polym. Sci.* **1998**, *23*, 919.
[71] B. J. O'Keefe, M. A. Hillmyer, W. B. Tolman, *J. Chem. Soc., Dalton Trans.* **2001**, 2215.
[72] B. M. Chamberlain, M. Cheng, D. R. Moore, T. M. Ovitt, E. B. Lobkovsky, G. W. Coates, *J. Am. Chem. Soc.* **2001**, *123*, 3229.
[73] M. H. Chisholm, N. W. Eilerts, J. C. Huffman, S. S. Iyer, M. Pacold, K. Phomphrai, *J. Am. Chem. Soc.* **2000**, *122*, 11845.
[74] H.-Y. Tang, H.-Y. Chen, J.-H. Huang, C.-C. Lin, *Macromolecules* **2007**, *40*, 8855.
[75] M. H. Chisholm, J. Gallucci, K. Phomphrai, *Inorg. Chem.* **2002**, *41*, 2785.
[76] M. H. Chisholm, J. C. Gallucci, K. Phomphrai, *Inorg. Chem.* **2005**, *44*, 8004.
[77] M. H. Chisholm, J. Gallucci, K. Phomphrai, *Chem. Commun.* **2003**, 48.
[78] B. Lian, C. M. Thomas, O. L. Casagrande, Jr., T. Roisnel, J.-F. Carpentier, *Polyhedron* **2007**, *26*, 3817.
[79] J. Ejfler, M. Kobylka, L. B. Jerzykiewicz, P. Sobota, *Dalton Trans.* **2005**, 2047.
[80] T. Chivers, C. Fedorchuk, M. Parvez, *Organometallics* **2005**, *24*, 580.
[81] M. H. Chisholm, J. C. Gallucci, K. Phomphrai, *Inorg. Chem.* **2004**, *43*, 6717.
[82] H.-Y. Chen, H.-Y. Tang, C.-C. Lin, *Polymer* **2007**, *48*, 2257.
[83] Z. Zhong, M. J. K. Ankone, P. J. Dijkstra, C. Birg, M. Westerhausen, J. Feijen, *Polym. Bull.* **2001**, *46*, 51.
[84] R. H. Platel, A. J. P. White, C. K. Williams, *Chem. Commun.* **2009**, 4115.
[85] A. Amgoune, C. M. Thomas, J.-F. Carpentier, *Macromol. Rapid Commun.* **2007**, *28*, 693.
[86] A. Amgoune, C. M. Thomas, T. Roisnel, J.-F. Carpentier, *Chem. Eur. J.* **2006**, *12*, 169.
[87] W. Miao, S. Li, H. Zhang, D. Cui, Y. Wang, B. Huang, *J. Organomet. Chem.* **2007**, *692*, 4828.
[88] T. M. Ovitt, G. W. Coates, *J. Am. Chem. Soc.* **2002**, *124*, 1316.
[89] X. Liu, X. Shang, T. Tang, N. Hu, F. Pei, D. Cui, X. Chen, X. Jing, *Organometallics* **2007**, *26*, 2747.

[90] C.-X. Cai, A. Amgoune, C. W. Lehmann, J.-F. Carpentier, *Chem. Commun.* **2004**, 330.
[91] R. H. Platel, L. M. Hodgson, A. J. P. White, C. K. Williams, *Organometallics* **2007**, *26*, 4955.
[92] R. H. Platel, A. J. P. White, C. K. Williams, *Inorg. Chem.* **2008**, *47*, 6840.
[93] R. H. Platel, L. M. Hodgson, C. K. Williams, *Polym. Rev.* **2008**, *48*, 11
[94] Y. Yang, S. Li, D. Cui, X. Chen, X. Jing, *Organometallics* **2006**, *26*, 671.
[95] L. M. Hodgson, A. J. P. White, C. K. Williams, *J. Polym. Sci., Part A: Polym. Chem.* **2006**, *44*, 6646.
[96] L. M. Hodgson, R. H. Platel, A. J. P. White, C. K. Williams, *Macromolecules* **2008**, *41*, 8603.
[97] A. Alaaeddine, A. Amgoune, C. M. Thomas, S. Dagorne, S. Bellemin-Laponnaz, J.-F. Carpentier, *Eur. J. Inorg. Chem.* **2006**, *2006*, 3652.
[98] A. Alaaeddine, C. M. Thomas, T. Roisnel, J.-F. Carpentier, *Organometallics* **2009**, *28*, 1469.
[99] I. Westmoreland, J. Arnold, *Dalton Trans.* **2006**, 4155.
[100] G. G. Skvortsov, M. V. Yakovenko, P. M. Castro, G. K. Fukin, A. V. Cherkasov, J.-F. Carpentier, A. A. Trifonov, *Eur. J. Inorg. Chem.* **2007**, 3260.
[101] P. L. Arnold, J.-C. Buffet, R. P. Blaudeck, S. Sujecki, C. Wilson, *Chem. Eur. J.* **2009**, *15*, 8241.
[102] P. L. Arnold, J.-C. Buffet, R. P. Blaudeck, S. Sujecki, A. J. Blake, C. Wilson, *Angew. Chem., Int. Ed.* **2008**, *47*, 6033.
[103] Y. Luo, X. Wang, J. Chen, C. Luo, Y. Zhang, Y. Yao, *J. Organomet. Chem.* **2009**, *694*, 1289.
[104] R. Heck, E. Schulz, J. Collin, J.-F. Carpentier, *J. Mol. Catal. A* **2007**, *268*, 163.
[105] H. Ma, T. P. Spaniol, J. Okuda, *Dalton Trans.* **2003**, 4770.
[106] H. Ma, T. P. Spaniol, J. Okuda, *Angew. Chem., Int. Ed.* **2006**, *45*, 7818.
[107] H. Ma, T. P. Spaniol, J. Okuda, *Inorg. Chem.* **2008**, *47*, 3328.
[108] A. Dumitrescu, B. Martin-Vaca, H. Gornitzka, J.-B. Cazaux, D. Bourissou, G. Bertrand, *Eur. J. Inorg. Chem.* **2002**, 1948.
[109] Y. Huang, W.-C. Hung, M.-Y. Liao, T.-E. Tsai, Y.-L. Peng, C.-C. Lin, *J. Polym. Sci., Part A: Polym. Chem.* **2009**, *47*, 2318.
[110] J.-C. Wu, B.-H. Huang, M.-L. Hsueh, S.-L. Lai, C.-C. Lin, *Polymer* **2005**, *46*, 9784.
[111] C. K. Williams, L. E. Breyfogle, S. K. Choi, W. Nam, V. G. Young, M. A. Hillmyer, W. B. Tolman, *J. Am. Chem. Soc.* **2003**, *125*, 11350.
[112] B. J. O'Keefe, S. M. Monnier, M. A. Hillmyer, W. B. Tolman, *J. Am. Chem. Soc.* **2001**, *123*, 339.
[113] D. S. McGuinness, E. L. Marshall, V. C. Gibson, J. W. Steed, *J. Polym. Sci., Part A: Polym. Chem.* **2003**, *41*, 3798.
[114] V. C. Gibson, E. L. Marshall, D. Navarro-Llobet, A. J. P. White, D. J. Williams, *J. Chem. Soc., Dalton Trans.* **2002**, 4321.
[115] X. Wang, K. Liao, D. Quan, Q. Wu, *Macromolecules* **2005**, *38*, 4611.
[116] N. Iwasa, M. Fujiki, K. Nomura, *J. Mol. Catal. A* **2008**, *292*, 67.

[117] H. Du, A. H. Velders, P. J. Dijkstra, Z. Zhong, X. Chen, J. Feijen, *Macromolecules* **2009**, *42*, 1058.
[118] T. V. Mahrova, G. K. Fukin, A. V. Cherkasov, A. A. Trifonov, N. Ajellal, J.-F. Carpentier, *Inorg. Chem.* **2009**, *48*, 4258.
[119] D. Pappalardo, L. Annunziata, C. Pellecchia, *Macromolecules* **2009**, *42*, 6056.
[120] P. Hormnirun, E. L. Marshall, V. C. Gibson, A. J. P. White, D. J. Williams, *J. Am. Chem. Soc.* **2004**, *126*, 2688.
[121] Z. Zhong, P. J. Dijkstra, J. Feijen, *J. Am. Chem. Soc.* **2003**, *125*, 11291.
[122] C. P. Radano, G. L. Baker, M. R. Smith, *J. Am. Chem. Soc.* **2000**, *122*, 1552.
[123] Z. Zhong, P. J. Dijkstra, J. Feijen, *Angew. Chem., Int. Ed.* **2002**, *41*, 4510.
[124] N. Emig, H. Nguyen, H. Krautscheid, R. Reau, J.-B. Cazaux, G. Bertrand, *Organometallics* **1998**, *17*, 3599.
[125] T. M. Ovitt, G. W. Coates, *J. Polym. Sci., Part A: Polym. Chem.* **2000**, *38*, 4686.
[126] M. H. Chisholm, J. C. Gallucci, K. T. Quisenberry, Z. Zhou, *Inorg. Chem.* **2008**, *47*, 2613.
[127] I. Peckermann, A. Kapelski, T. P. Spaniol, J. Okuda, *Inorg. Chem.* **2009**, *48*, 5526.
[128] A. F. Douglas, B. O. Patrick, P. Mehrkhodavandi, *Angew. Chem., Int. Ed.* **2008**, *47*, 2290.
[129] A. P. Dove, V. C. Gibson, E. L. Marshall, H. S. Rzepa, A. J. P. White, D. J. Williams, *J. Am. Chem. Soc.* **2006**, *128*, 9834.
[130] N. Nimitsiriwat, V. C. Gibson, E. L. Marshall, M. R. J. Elsegood, *Dalton Trans.* **2009**, 3710.
[131] N. Nimitsiriwat, V. C. Gibson, E. L. Marshall, M. R. J. Elsegood, *Inorg. Chem.* **2008**, *47*, 5417.
[132] N. Nimitsiriwat, E. L. Marshall, V. C. Gibson, M. R. J. Elsegood, S. H. Dale, *J. Am. Chem. Soc.* **2004**, *126*, 13598.
[133] A. J. Chmura, Christopher J. Chuck, Matthew G. Davidson, M. D. Jones, M. D. Lunn, Steven D. Bull, M. F. Mahon, *Angew. Chem., Int. Ed.* **2007**, *46*, 2280.
[134] A. Finne, Reema, A.-C. Albertsson, *J. Polym. Sci. Part A: Polym. Chem.* **2003**, *41*, 3074.
[135] T. Aida, S. Inoue, *Acc. Chem. Res.* **1996**, *29*, 39.
[136] M. H. Chisholm, N. J. Patmore, Z. Zhou, *Chem. Commun.* **2005**, 127.
[137] D. Bourissou, B. Martin-Vaca, A. Dumitrescu, M. Graullier, F. Lacombe, *Macromolecules* **2005**, *38*, 9993.
[138] Z. Tang, X. Pang, J. Sun, H. Du, X. Chen, X. Wang, X. Jing, *J. Polym. Sci., Part A: Polym. Chem.* **2006**, *44*, 4932.
[139] C. K. A. Gregson, I. J. Blackmore, V. C. Gibson, N. J. Long, E. L. Marshall, A. J. P. White, *Dalton Trans.* **2006**, 3134.
[140] C. K. A. Gregson, V. C. Gibson, N. J. Long, E. L. Marshall, P. J. Oxford, A. J. P. White, *J. Am. Chem. Soc.* **2006**, *128*, 7410.
[141] D. Agustin, G. Rima, H. Gornitzka, J. Barrau, *J. Organomet. Chem.* **1999**, *592*, 1.

[142] M. H. Chisholm, J. C. Huffman, K. Phomphrai, *J. Chem. Soc., Dalton Trans.* **2001**, 222.
[143] M. Cheng, A. B. Attygalle, E. B. Lobkovsky, G. W. Coates, *J. Am. Chem. Soc.* **1999**, *121*, 11583.
[144] R. C. Pratt, B. G. G. Lohmeijer, D. A. Long, R. M. Waymouth, J. L. Hedrick, *J. Am. Chem. Soc.* **2006**, *128*, 4556.
[145] G. W. Coates, *Chem. Rev.* **2000**, *100*, 1223.
[146] N. Nomura, R. Ishii, Y. Yamamoto, T. Kondo, *Chem. Eur. J.* **2007**, *13*, 4433.
[147] G. Zi, Q. Wang, L. Xiang, H. Song, *Dalton Trans.* **2008**, 5930.
[148] H. Du, A. H. Velders, P. J. Dijkstra, J. Sun, Z. Zhong, X. Chen, J. Feijen, *Chem. Eur. J.* **2009**, *15*, 9836.
[149] M. Bouyahyi, E. Grunova, N. Marquet, E. Kirillov, C. M. Thomas, T. Roisnel, J.-F. Carpentier, *Organometallics* **2008**, *27*, 5815.
[150] P. Hormnirun, E. L. Marshall, V. C. Gibson, R. I. Pugh, A. J. P. White, *Proc. Natl. Acad. Sci. U. S. A.* **2006**, *103*, 15343.
[151] N. Nomura, R. Ishii, M. Akakura, K. Aoi, *J. Am. Chem. Soc.* **2002**, *124*, 5938.
[152] Q. Wang, L. Xiang, H. Song, G. Zi, *J. Organomet. Chem.* **2009**, *694*, 691.
[153] A. Otero, J. Fernandez-Baeza, A. Lara-Sanchez, C. Alonso-Moreno, I. Marquez-Segovia, L. F. Sanchez-Barba, A. M. Rodriguez, *Angew. Chem., Int. Ed.* **2009**, *48*, 2176.
[154] H. Tsuji, *Macromolecular Bioscience* **2005**, *5*, 569.
[155] N. Spassky, M. Wisniewski, C. Pluta, A. Le Borgne, *Macromol. Chem. Phys.* **1996**, *197*, 2627.
[156] F. A. Bovey, P. A. Mirau, *NMR of Polymers*, Academic, San Diego, Calif., San Diego, **1996**.
[157] T. M. Ovitt, G. W. Coates, *J. Am. Chem. Soc.* **1999**, *121*, 4072.
[158] D. J. Darensbourg, W. Choi, O. Karroonnirun, N. Bhuvanesh, *Macromolecules* **2008**, *41*, 3493.
[159] H. Thomas, T. P. Spaniol, J. Okuda, *Angew. Chem., Int. Ed.* **2006**, *45*, 7818.
[160] A. J. Chmura, D. M. Cousins, M. G. Davidson, M. D. Jones, M. D. Lunn, M. F. Mahon, *Dalton Trans.* **2008**, 1437.
[161] A. J. Chmura, M. G. Davidson, C. J. Frankis, M. D. Jones, M. D. Lunn, *Chem. Commun.* **2008**, 1293.
[162] C. Alonso-Moreno, A. Garces, L. F. Sanchez-Barba, M. Fajardo, J. Fernandez-Baeza, A. Otero, A. Lara-Sanchez, A. Antinolo, L. Broomfield, M. I. Lopez-Solera, A. M. Rodriguez, *Organometallics* **2008**, *27*, 1310.
[163] X. Pang, X. Chen, X. Zhuang, X. Jing, *J. Polym. Sci., Part A: Polym. Chem.* **2007**, *46*, 643.
[164] A. Pietrangelo, M. A. Hillmyer, W. B. Tolman, *Chem. Commun.* **2009**, 2736.
[165] A. P. Dove, V. C. Gibson, E. L. Marshall, A. J. P. White, D. J. Williams, *Chem. Commun.* **2001**, 283.
[166] S. Gambarotta, F. Arena, C. Floriani, P. F. Zanazzis, *J. Am. Chem. Soc.* **1982**, *104*, 5082.
[167] B. Beguin, B. Denise, R. P. A. Sneeden, *J. Organomet. Chem.* **1981**, *208*, C18.

[168] H. Inoue, Y. Sasaki, H. Hashimoto, H. Izumida, *Chem. Commun.* **1975**, 718.
[169] P. Haynes, L. H. Slaugh, J. F. Kohnle, *Tetrahedron Lett.* **1970**, *5*, 365.
[170] D. H. Gibson, *Chem. Rev.* **1996**, *96*, 2063.
[171] D. Walther, M. Ruben, S. Rau, *Coord. Chem. Rev.* **1999**, *182*, 67.
[172] P. Braunstein, D. Matt, D. Nobel, *Chem. Rev.* **1988**, *88*, 747.
[173] L. R. Sita, J. R. Babcock, R. Xi, *J. Am. Chem. Soc.* **1996**, *118*, 10912.
[174] C. Chung-Cheng, L. Min-Chun, C. Tsu-Hsin, P. Shie-Ming, L. Gene-Hsiang, *Angew. Chem., Int. Ed.* **2005**, *44*, 7418.
[175] H. Phull, D. Alberti, I. Korobkov, S. Gambarotta, P. H. M. Budzelaar, *Angew. Chem., Int. Ed.* **2006**, *45*, 5331.
[176] S. C. Bart, C. Anthon, F. W. Heinemann, E. Bill, N. M. Edelstein, K. Meyer, *J. Am. Chem. Soc.* **2008**, *130*, 12536.
[177] D. J. Brunelle, *ACS Symp. Ser.* **2005**, *898*, 1.
[178] S. Inoue, H. Koinuma, T. Tsuruta, *J. Polym. Sci. Part B: Polym. Lett.* **1969**, *7*, 287.
[179] W. Kuran, T. Listo, *Macromol. Chem. Phys.* **1994**, *195*, 1011.
[180] D. J. Darensbourg, M. W. Holtcamp, *Macromolecules* **1995**, *28*, 7577.
[181] D. J. Darensbourg, M. W. Holtcamp, G. E. Struck, M. S. Zimmer, S. A. Niezgoda, P. Rainey, J. B. Robertson, J. D. Draper, J. H. Reibenspies, *J. Am. Chem. Soc.* **1999**, *121*, 107−116.
[182] G. W. Coates, D. R. Moore, M. Cheng, E. B. Lobkovsky, *Angew. Chem., Int. Ed.* **2002**, *41*, 2599.
[183] G. W. Coates, D. R. Moore, *Angew. Chem., Int. Ed.* **2004**, *43*, 6618.
[184] P. Gorecki, W. Kuran, *J. Polym. Sci. Part C* **1985**, *23*, 299.
[185] D. J. Darensbourg, *Chem. Rev.* **2007**, *107*, 2388.
[186] D. J. Darensbourg, M. W. Holtcamp, *Coord. Chem. Rev.* **1996**, *153*, 155.
[187] D. J. Darensbourg, R. M. Mackiewicz, A. L. Phelps, D. R. Billodeaux, *Acc. Chem. Res.* **2004**, *37*, 836.
[188] E. J. Beckman, *Science* **1999**, *283*, 946.
[189] S. Inoue, *Chemtech* **1976**, *6*, 588.
[190] M. S. Super, E. J. Beckman, *Trends Polym. Sci.* **1997**, *5*, 236.
[191] D. V. Vitanova, F. Hampel, K. C. Hultzsch, *J. Organomet. Chem.* **2005**, *690*, 5182.
[192] S. Mang, A. I. Cooper, M. E. Colclough, N. Chauhan, A. B. Holmes, *Macromolecules* **2000**, *33*, 303.
[193] D. J. Darensbourg, J. C. Yarbrough, *J. Am. Chem. Soc.* **2002**, *124*, 6335.
[194] D. J. Darensbourg, J. L. Rodgers, C. C. Fang, *Inorg. Chem.* **2003**, *42*, 4498.
[195] D. J. Darensbourg, J. C. Yarbrough, C. Ortiz, C. C. Fang, *J. Am. Chem. Soc.* **2003**, *125*, 7586.
[196] R. Eberhardt, M. Allmendinger, B. Rieger, *Macromol. Rapid Commun.* **2003**, *24*, 194.
[197] D.-Y. Rao, B. Li, R. Zhang, H. Wang, X.-B. Lu, *Inorg. Chem.* **2009**, *48*, 2830.
[198] D. J. Darensbourg, A. I. Moncada, *Inorg. Chem.* **2008**, *47*, 10000.
[199] H. Sugimoto, H. Ohshima, S. Inoue, *J. Polym. Sci., Part A: Polym. Chem.* **2003**, *41*, 3549.

[200] F. Jutz, J.-D. Grunwaldt, A. Baiker, *J. Mol. Catal. A* **2008**, *279*, 94.
[201] M. L. Man, K. C. Lam, W. N. Sit, S. M. Ng, Z. Zhou, Z. Lin, C. P. Lau, *Chem. Eur. J.* **2006**, *12*, 1004.
[202] A. Sibaouih, P. Ryan, K. V. Axenov, M. R. Sundberg, M. Leskelae, T. Repo, *J. Mol. Catal. A* **2009**, *312*, 87.
[203] X.-B. Lu, L. Shi, Y.-M. Wang, R. Zhang, Y.-J. Zhang, X.-J. Peng, Z.-C. Zhang, B. Li, *J. Am. Chem. Soc.* **2006**, *128*, 1664.
[204] K. Nakano, T. Kamada, K. Nozaki, *Angew. Chem., Int. Ed.* **2006**, *45*, 7274.
[205] X.-B. Lu, Y. Wang, *Angew. Chem., Int. Ed.* **2004**, *43*, 3574.
[206] W.-M. Ren, Z.-W. Liu, Y.-Q. Wen, R. Zhang, X.-B. Lu, *J. Am. Chem. Soc.* **2009**, *131*, 11509.
[207] M. F. Pilz, C. Limberg, B. B. Lazarov, K. C. Hultzsch, B. Ziemer, *Organometallics* **2007**, *26*, 3668.
[208] K. Mori, Y. Mitani, T. Hara, T. Mizugaki, K. Ebitani, K. Kaneda, *Chem. Commun.* **2005**, 3331.
[209] D. R. Moore, M. Cheng, E. B. Lobkovsky, G. W. Coates, *J. Am. Chem. Soc.* **2003**, *125*, 11911.
[210] H. S. Kim, J. J. Kim, S. D. Lee, M. S. Lah, D. Moon, H. G. Jang, *Chem. Eur. J.* **2003**, *9*, 678.
[211] R. Eberhardt, M. Allmendinger, G. A. Luinstra, B. Rieger, *Organometallics* **2003**, *22*, 211.
[212] Z. Liu, M. Torrent, K. Morokuma, *Organometallics* **2002**, *21*, 1056.
[213] D. J. Darensbourg, J. R. Wildeson, J. C. Yarbrough, *Inorg. Chem.* **2002**, *41*, 973.
[214] H. S. Kim, J. J. Kim, B. G. Lee, O. S. Jung, H. G. Jang, S. O. Kang, *Angew. Chem., Int. Ed.* **2000**, *39*, 4096.
[215] D. J. Darensbourg, M. S. Zimmer, P. Rainey, D. L. Larkins, *Inorg. Chem.* **2000**, *39*, 1578.
[216] D. J. Darensbourg, M. S. Zimmer, *Macromolecules* **1999**, *32*, 2137.
[217] J. Darensbourg, S. A. Niezgoda, J. D. Draper, J. H. Reibenspies, *J. Am. Chem. Soc.* **1998**, *120*, 4690.
[218] D. J. Darensbourg, M. W. Holtcamp, B. Khandelwal, K. K. Klausmeyer, J. H. Reibenspies, *J. Am. Chem. Soc.* **1995**, *117*, 538.
[219] G. A. Luinstra, G. R. Haas, F. Molnar, V. Bernhart, R. Eberhardt, B. Rieger, *Chem. Eur. J.* **2005**, *11*, 6298.
[220] T. Aida, M. Ishikawa, S. Inoue, *Macromolecules* **1986**, *19*, 8.
[221] D. J. Darensbourg, P. Rainey, J. Yarbrough, *Inorg. Chem.* **2001**, *40*, 986.
[222] Z. Qin, C. M. Thomas, S. Lee, G. W. Coates, *Angew. Chem., Int. Ed.* **2003**, *42*, 5484.

Chapter 2: Synthesis of M^{III} complexes

2.1 Synthesis and characterisation of proligands HL^R

2.1.1 Introduction

Interest in the co-ordination chemistry of phosphoryl donor ligands has largely involved monodentate donors, although several examples of homoleptic multidentate phosphoryl compounds and their metal complexes have been documented. There is a surprising dearth of published material concerning heterodentate compounds containing one or more P=O functionalities, and the majority have been reported only in recent years.[1] Phosphoryl oxygens are moderately basic and, although tolerant of a whole range of metal oxidation states, are most suited to high-valent metals. Our interest in P=O donors comes from a desire to synthesise anionic chiral heterobidentate compounds capable of forming stable well-defined metal complexes. Several groups already shown an interest in similar ligands but mainly synthesised aryl derivatives in the *tert*-butyl position and in the R group position.[2-5]

2.1.2 Synthesis of proligands *rac*-HL^R

The ring opening of *rac*-3,3-dimethyl-epoxybutane with R_2PH (R = *tert*-butyl (^{t}Bu), Phenyl (Ph) or C_6H_3-3,5-Me (Ar)) in the presence of ^{n}BuLi followed by oxidation with H_2O_2 afforded the target ligand precursor $\mathbf{HL^{tBu}}$, $\mathbf{HL^{Ph}}$ and $\mathbf{HL^{Ar}}$ (in 58 %, 82 %, 64 % respectively), (Scheme 2.1).

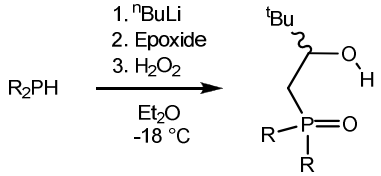

Scheme 2.1: Synthesis of proligands HL^{tBu}, HL^{Ph} and HL^{Ar}

The ligand preparation (Scheme 2.1) is based on a modification of the literature by Cross *et al.*,[2, 3] and was first synthesised by previous PhD students (Dr. R. P. Blaudeck for *rac*-HL^{tBu} and Dr. M. I. Ali for *rac*-HL^{Ph}).[7-9]

To improve the low yielding previous steps of the synthesis of HL^{R} (where numerous by-products were formed), the first step has been changed for the synthesis of **HL^{Ar}**. ArMgBr was reacted with an aminochlorophosphine and treated with HCl to make pure Ar_2PCl, which was isolated as viscous yellow oil in 93 %. A single resonance in the $^{31}P\{^{1}H\}$ NMR spectrum at 86 ppm provides strong evidence of purity and is consistent with values provided in the literature for ArPCl (where Ar = C_6H_3-Me-3,5).[10, 11]. The general synthesis of HL^{Ar} is shown in Scheme 2.2 and was first synthesised by a project student (Mr. S. E. Gorringe).[12]

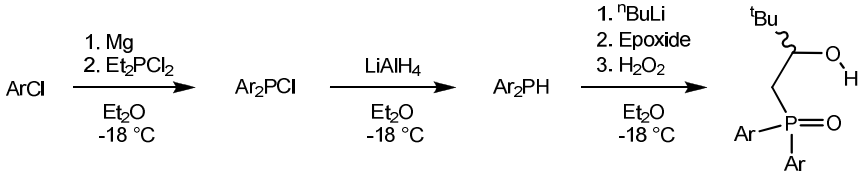

Scheme 2.2: New synthesis of proligand HL^{Ar}

The same procedure has been used to synthesise $HL^{Ar,Ph}$ but in this case *rac*-styrene oxide was used instead of *rac*-3,3-dimethyl-epoxybutane to afford a colourless solid in 73 % yield.

2.1.3 Synthesis of Group 1 metal salts of the proligands.

A variety of routes were tried to synthesise potassium or lithium salts (KL^{R} or LiL^{R}) from proligands HL^{R}. The bases used were KN", $KO^{t}Bu$, KH and $^{n}BuLi$.

All deprotonation reactions with the potassium bases afforded an intractable mixture of products. The reaction of HL^{R} with $^{n}BuLi$, at -78 °C in THF, afforded a solution (that changed from colourless to red and back to colourless), (Equation 2.1). The $^{31}P\{^{1}H\}$ NMR spectrum contains one resonance at 39.9 ppm and the ^{7}Li NMR

spectrum contains a doublet at 0.6 ppm with a coupling constant of $^2J_{PLi}$ = 42.1 Hz, all consistent with the formulation of a colourless solid, **LiL^{Ph}.**

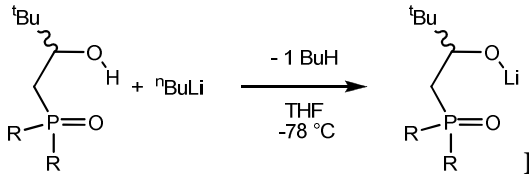

Eq. 2.1

This compound has been shown to be stable at room temperature in the solid state and at cold temperature in solution over-night but decomposed after few hours in solution at room temperature.

2.2 Synthesis and characterisation of *rac*-$M(L^R)_3$ complexes

2.2.1 Introduction

In the search for new asymmetric catalysts, chiral C_3-symmetric complexes are emerging as interesting competitor systems to the ubiquitous C_2-symmetric systems. Trivalent lanthanide cations are obvious candidates for the development of catalysts with three-fold symmetry. However, the lability and the weak coordination geometry preferences of Ln^{III} centres make the synthesis of enantiopure lanthanide coordination compounds a difficult goal. One approach involves the coordination of three enantiopure C_2-symmetric biaryl ligands to make a homochiral LnL_3 complex.[13-15] The most successful asymmetric and bifunctional lanthanide-based catalysts are based on $Li_3[Ln(L)_3]$ (L = chiral enantiopure 1,1'-binaphtholate, binolate). This latter class includes, to our knowledge, the only example of spontaneous resolution of three molecules of a racemic ligand at a lanthanide centre to date; the reaction of $YN"_3$ with *rac*-NaHbinol affords an equal mixture of the heterobimetallic *RRR*- and *SSS*- $Na_3[Y(binol)_3]$ complexes (**A**, Figure 2.1). However, all other lanthanide/alkali metal combinations give different combinations of *RRS-/SSR*- complexes.[16]

Another approach is to use pre-resolved, chiral polydentate ligands such as C_3-symmetric *tris*(oxazoline) adducts (**B**, Figure 2.1).[17] A few examples of ligand self-recognition based solely on chirality exist in transition metal chemistry and have helped define the requirements for ligand self-recognition: ligands must be rigid, sized to fit the correct number around the metal centre (here 2 or 3), project chirality and assemble to generate a more compact structure than a heterochiral ligand would.[18] The binding of lanthanides of different sizes inside the chiral nonaazamacrocycles, L, made by Lisowski *et al.* has been shown to generate enantiopure helical complexes of the form LnL, (**C**, Figure 2.1). For example, while the (*M*)-helical complex is the kinetic product formed with the all-*R*-enantiomer of the macrocycle, both (*M*)- and (*P*)-helical complexes are formed over time and are favoured for early and late lanthanides respectively (Figure 2.1).[19]

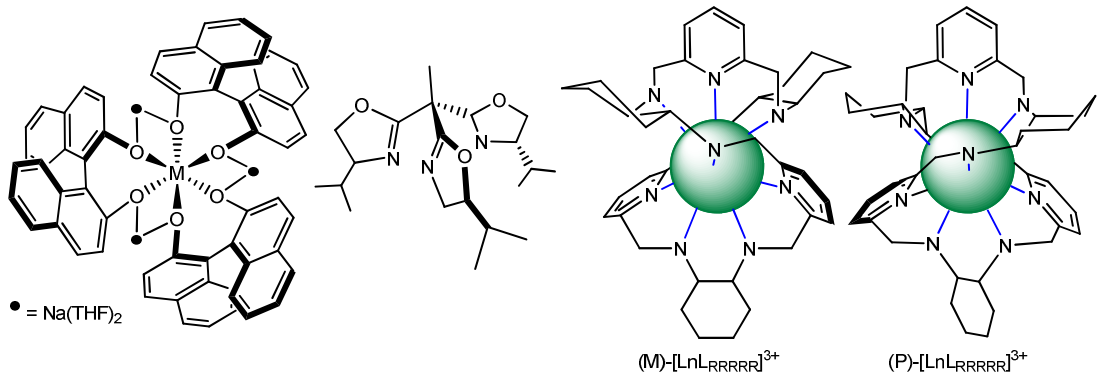

Figure 2.1: Aspinall's *RRR*-$Na_3[Y(binol)_3](THF)_6$ complex, **A**, Gade's *tris* (oxazoline) ligand, **B** and Lisowski's (*M*) and (*P*)-helical complexes, **C**.

2.2.2 Synthesis of *rac*-$M(L^R)_3$ complexes

Treatment of three equivalents of HL^R with one equivalent of $M\{N(SiMe_3)_2\}_3$ ($MN"_3$ and where M = Sc, In, Lu, Y, Bi, and La) in THF at -78 °C affords ***rac*-$M(L^R)_3$** in good yield (75-90 %) (Equation 2.2). Lanthanide complexes $Ln(L^{tBu})_3$ (where Ln = Y, Er, Eu and Yb) were first synthesised by Dr. R. P Blaudeck.[6-8, 20]

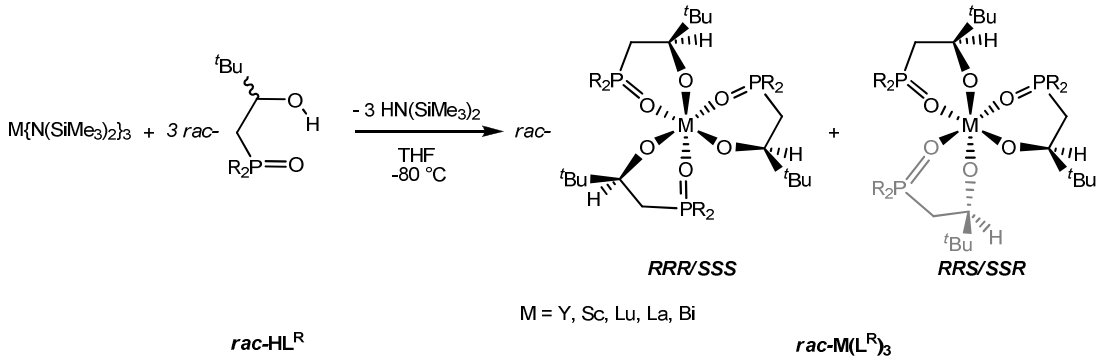

Eq. 2.2

rac-$M(L^R)_3$ denotes $M(L^R)_3$ made from HL^R and represents a mixture of *RRR*-$M(L^R)_3$/*SSS*-$M(L^R)_3$ mixed with *RRS*-$M(L^R)_3$/*SSR*-$M(L^R)_3$. The latter *RRS*-$M(L^R)_3$/*SSR*-$M(L^R)_3$ can be regarded as an impurity of the synthesis of *rac*-$M(L^R)_3$ complexes because the desirable mixture is only *RRR*-$Ln(L^R)_3$/*SSS*-$Ln(L^R)_3$, a direct result of the ligand self-recognition. In this thesis, the diastereomeric index (DI) will represent the percentage of *RRR/SSS*-$M(L^R)_3$ in the complexes $M(L^R)_3$.

2.2.3 NMR spectral characterisation of *rac*-$M(L^R)_3$ complexes

The easiest way to measure the diastereomeric index of the complex is by integration of the NMR spectra of ***rac*-$M(L^R)_3$** complexes. Table 2.1 shows the homochiral purity achieved for each metal.

Table 2.1: Comparison between the diastereomeric index of the complexes $M(L^R)_3$

M	Sc		In		Lu		Y			Bi		La
R=	^{t}Bu	Ph	^{t}Bu	Ph	^{t}Bu	Ph	^{t}Bu	Ph	Ar	^{t}Bu	Ph	^{t}Bu
RRR/SSS	55	90	95	75	65	65	80	50	75	30	20	40
RRS/SSR	45	10	5	25	35	35	20	50	25	70	80	60

Comparison of diastereomeric index of the complexes *rac*-$M(L^R)_3$ is clarified by selected $^{31}P\{^1H\}$ NMR spectra (Figure 2.2). It is possible to distinguish important features; firstly, despite changing the size of the metal, it is not possible to find the perfect metal-ligand combination to obtain 100 % *rac*-$M(L^{tBu})_3$ (Figure 2.2 a) and the

best diastereomeric index was attained for ***rac*-In(L^{tBu})$_3$** (however other geometric complicating factors are observed which will be discussed later in, see section 2.2.5); secondly, the homochiral purity for *rac*-M(L^R)$_3$ increases with a decrease in metallic radius (Figure 2.2 b).

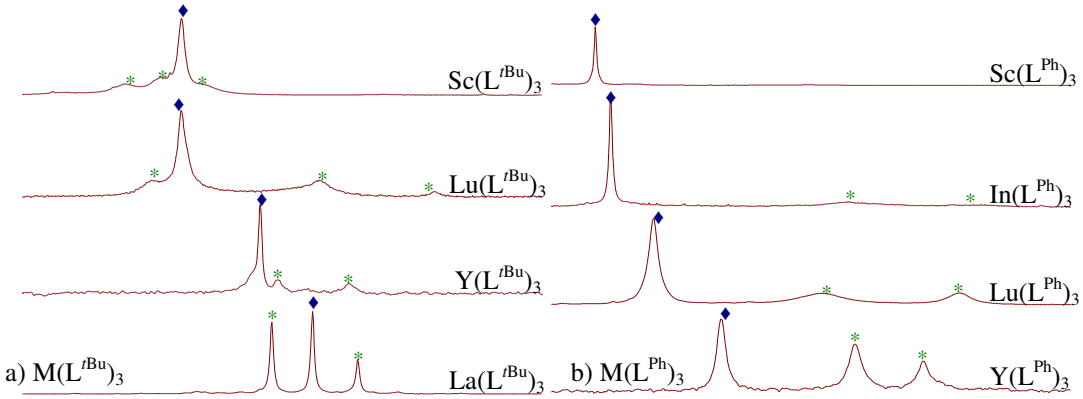

Figure 2.2: $^{31}P\{^1H\}$ NMR spectra of various *rac*-M(L^R)$_3$ in d_6-benzene, a) *rac*-M(L^{tBu})$_3$ and b) *rac*-M(L^{Ph})$_3$. ♦ denotes *RRR/SSS*-M(L^R)$_3$, * denotes *RRS/SSR*-M(L^R)$_3$.

Comparison with the literature show that Aspinall *et al.* reported a homochiral purity of 100 % *RRR/SSS*-Na_3[Y(binol)$_3$] but that any other metallic combinations afforded low percentages of homochirality.[13] However, most of the complexes ***rac*-M(L^R)$_3$** show good diastereomeric index (above 75 % in most cases) and moreover only at a single lanthanide centre.

Only bismuth and lanthanum complexes have very low amounts of the homochiral isomer (below 40 %). This is due to the large size of the metal (r(Bi^{3+}) = 1.030 Å and r(La^{3+}) = 1.032 Å) shows the limits of the ligand self-recognition. Varying the reaction temperature (between -78 °C and room temperature), the solvent or dilution did not improve the diastereomeric index of the resulting complexes.

All *rac*-M(L^R)$_3$ complexes have been isolated as colourless solids in yield of 75 % (*rac*-Sc(L^{tBu})$_3$), 47 % (*rac*-In(L^{tBu})$_3$), 94 % (*rac*-Lu(L^{tBu})$_3$), 90 % (*rac*-Y(L^{tBu})$_3$), 17% (*rac*-Bi(L^{tBu})$_3$), 64 % (*rac*-La(L^{tBu})$_3$), 70 % (*rac*-Sc(L^{Ph})$_3$), 76 % (*rac*-In(L^{Ph})$_3$), 76 % (*rac*-Lu(L^{Ph})$_3$), 91 % (*rac*-Y(L^{Ph})$_3$) and 87 % (*rac*-Y(L^{Ar})$_3$).

The effect of the ionic radius on the extent of the diastereomeric index of the complexes *rac*-M(L^{Ph})$_3$ is summarised in Figure 2.3.

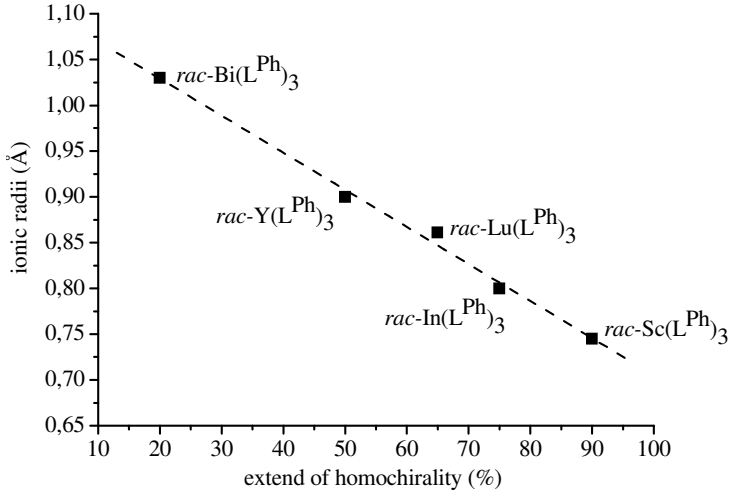

Figure 2.3: Ionic radius (Å) versus extent of the homochirality of *rac*-M(L^{Ph})$_3$.

2.2.4 NMR spectral characterisation of *rac*-Y(L^{R})$_3$ complexes

In order to have a diamagnetic comparison with the lanthanides previously reported in our group, the yttrium complexes have been the most investigated during the course of this work.

The ^{1}H and ^{31}P{^{1}H} NMR spectra of ***R*-Y(L^{tBu})$_3$** show a single ligand environment consistent with a single C_3-symmetric *RRR*-Y(L^{tBu})$_3$ complex (Figure 2.4 a) and d)).

Spectra of solutions of ***rac*-Y(L^{tBu})$_3$** contain 80 % of this homochiral isomer (as a mixture of *RRR*- and *SSS*-Y(L^{tBu})$_3$) and an additional, minor set of resonances which correspond to the diastereomer, *RRS-/SSR*-Y(L^{tBu})$_3$, present in about 20 % of the total yield (Figure 2.4 c) and f)).

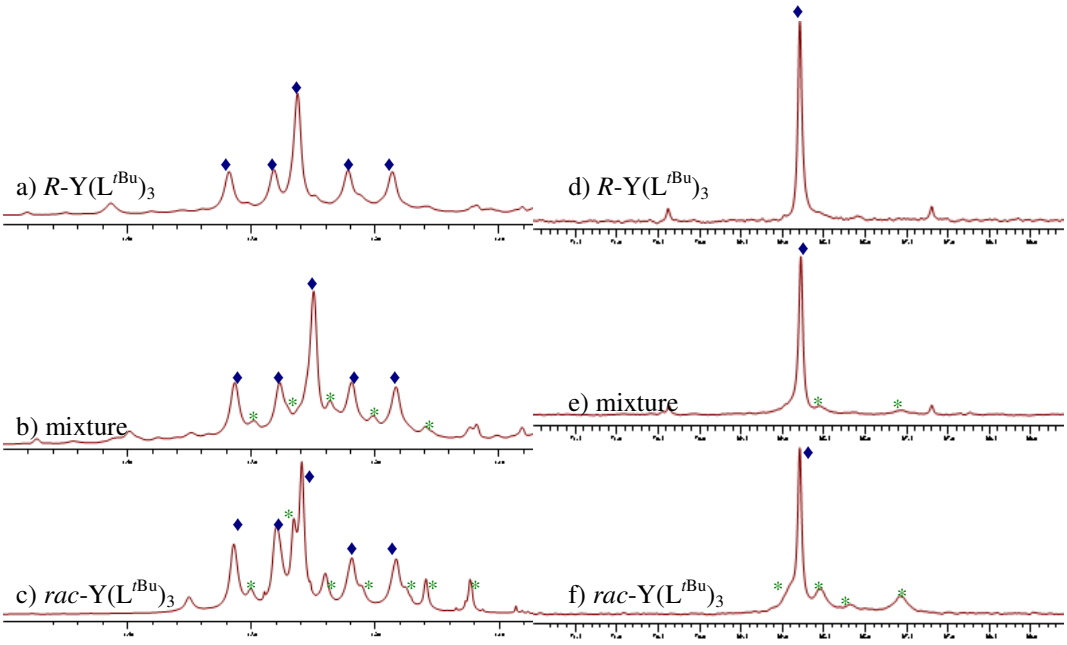

Figure 2.4: ^{1}H (*tert*-butyl region) and $^{31}P\{^{1}H\}$ NMR spectra of *rac*-$Y(L^{tBu})_3$ and *R*-$Y(L^{tBu})_3$ (d_6-benzene), a) ^{1}H: *R*-$Y(L^{tBu})_3$, b) ^{1}H: 50 % of *R*-$Y(L^{tBu})_3$ and 50 % of *rac*-$Y(L^{tBu})_3$, c) ^{1}H: *rac*-$Y(L^{tBu})_3$, d) $^{31}P\{^{1}H\}$: *R*-$Y(L^{tBu})_3$, e) $^{31}P\{^{1}H\}$: 50 % of *R*-$Y(L^{tBu})_3$ and 50 % of *rac*-$Y(L^{tBu})_3$ and f) $^{31}P\{^{1}H\}$: *rac*-$Y(L^{tBu})_3$. ♦ denotes *RRR/SSS* $Y(L^{tBu})_3$, * denotes *RRS/SSR* $Y(L^{tBu})_3$.

Spectra of ***rac*-$Y(L^{Ph})_3$** contain only 50 % of *RRR*- and *SSS*-$Y(L^{Ph})_3$) (Figure 2.5 a) and c)), and 50 % of *RRS/SSR*-$Y(L^{Ph})_3$. NMR spectra representing enantiopure ***R*-$Y(L^{Ph})_3$** are also shown (Figure 2.5 b) and d)).

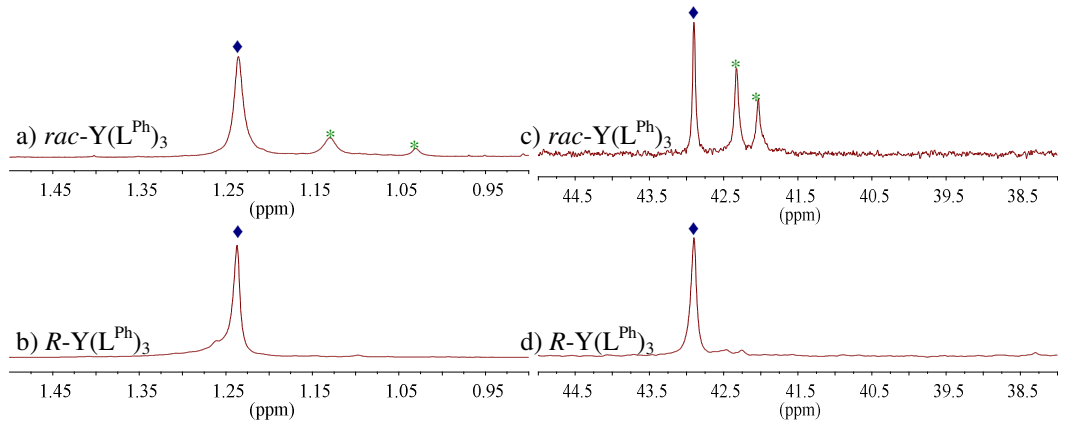

Figure 2.5: ^{1}H (*tert*-butyl region) and $^{31}P\{^{1}H\}$ NMR spectra of *rac*-$Y(L^{Ph})_3$ and *R*-$Y(L^{Ph})_3$ (d_6-benzene), a) ^{1}H: *rac*-$Y(L^{Ph})_3$, b) ^{1}H: *R*-$Y(L^{Ph})_3$, c) $^{31}P\{^{1}H\}$: *rac*-$Y(L^{Ph})_3$

and d) $^{31}P\{^{1}H\}$ of *R*-$Y(L^{Ph})_3$. ♦ denotes *RRR/SSS*-$Y(L^{Ph})_3$, * denotes *RRS/SSR*-$Y(L^{Ph})_3$.

A protonolysis reaction between one equivalent of $YN"_3$ and three equivalents of the aryl ligand, *rac*-HL^{Ar}, at room temperature in d_6-benzene gave *rac*-$Y(L^{Ar})_3$ in 75 % homochiral purity. This is increased from 50 % for the *rac*-$Y(L^{Ph})_3$ in accordance with increased bulk of the aryl group (Figure 2.6).

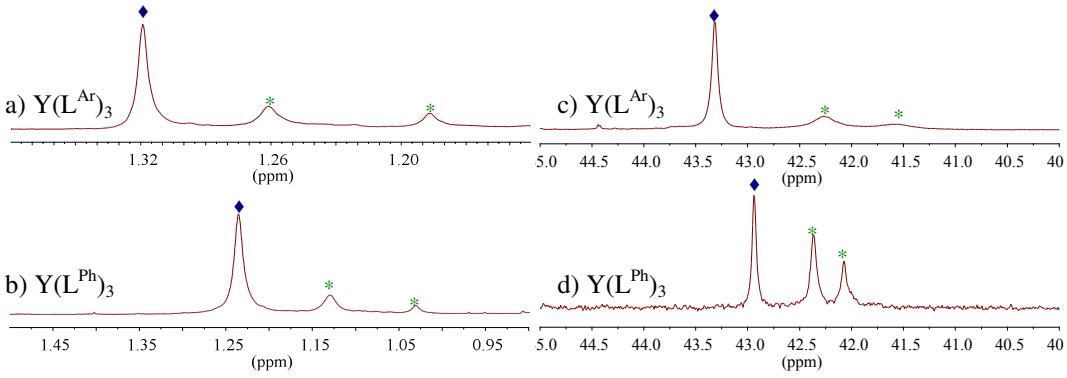

Figure 2.6: ^{1}H (*tert*-butyl region) and $^{31}P\{^{1}H\}$ NMR spectra of *rac*-$Y(L^{Ph})_3$ and *rac*-$Y(L^{Ar})_3$ (d_6-benzene), a) ^{1}H: *rac*-$Y(L^{Ar})_3$, b) ^{1}H: *rac*-$Y(L^{Ph})_3$, c) $^{31}P\{^{1}H\}$ *rac*-$Y(L^{Ar})_3$, and d) $^{31}P\{^{1}H\}$: *rac*-$Y(L^{Ph})_3$. ♦ denotes *RRR/SSS*-$Y(L^{R})_3$, * denotes *RRS/SSR*-$Y(L^{R})_3$

A reaction using one equivalent of $YN"_3$ and three equivalents of *rac*-$HL^{Ar,Ph}$ at room temperature in d_6-benzene was also investigated (Equation 2.3).

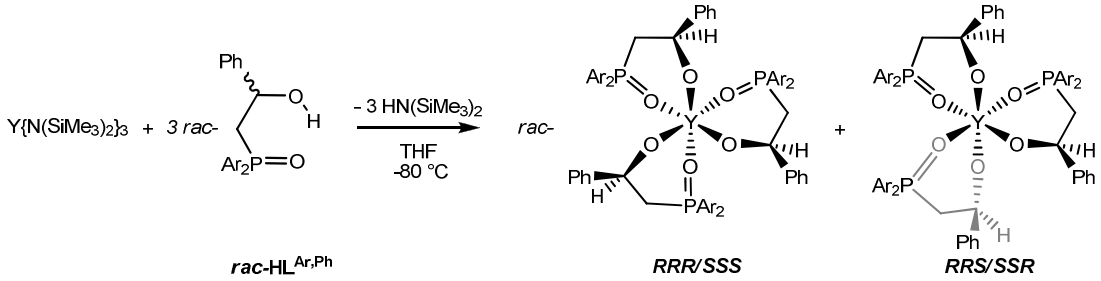

Eq. 2.3

The extent of homochiral purity of *rac*-$Y(L^{Ar,Ph})_3$ is around 60 % which is higher than for *rac*-$Y(L^{Ph})_3$ (showing the impact of the methyl group on the aryl group) but lower than for *rac*-$Y(L^{Ar})_3$ (showing the importance of the bulky *tert*-butyl group on the asymmetric group).

These results indicate that the best ligand for yttrium should have a *tert*-butyl group on the asymmetric carbon and bulky substituent on the aryl group (maybe *tert*-butyl instead of methyl).

2.2.5 Displacements reactions

The reactivity of *rac*-Y(L^{Ph})$_3$ with a series of neutral donor molecules, considered suitable competitors for the bound PO group of L^{Ph}, was also studied. *rac*-Y(L^{Ph})$_3$ was reacted with one equivalent of each donor, D (D = Me_3PO and ^{t}BuCN), in d_6-benzene and in a THF/d_6-benzene mixture (Equation 2.4).

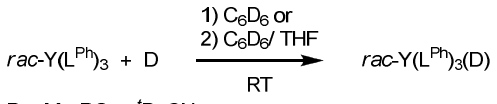

Eq. 2.4

The reactions in only d_6-benzene solution and d_6-benzene/THF solution did not show any changes in ^{1}H and ^{31}P{^{1}H} NMR spectra for either donor, D.

2.2.6 NMR spectral characterisation of *rac*-In(L^{tBu})$_3$ complexes

The reaction of one equivalent of InN"$_3$ with three equivalents *rac*-HL^{tBu} at -78 °C did not afford the desired product *rac*-In(L^{tBu})$_3$ but instead (L^{tBu})$_2$InN" was isolated. On heating the reaction mixture (80 °C, seven days) ***rac*-In(L^{tBu})$_3$** was afforded after work-up (Equation 2.5).

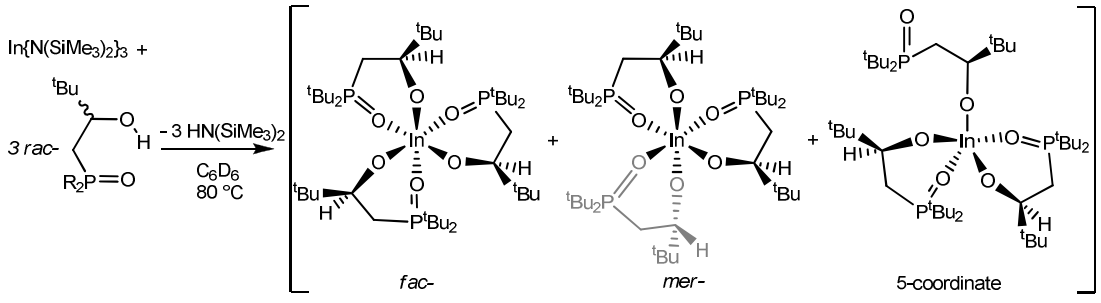

Eq. 2.5

The NMR spectra of solutions of analytically pure *rac*-In(L^{tBu})$_3$ in d_6-benzene at room temperature display multiple resonances in the *tert*-butyl region of the ^{1}H NMR

spectrum and in the $^{31}P\{^{1}H\}$ NMR spectrum, indicating that a mixture of compounds with different arrangements of the three ligands around the metal is present (Figure 2.7).

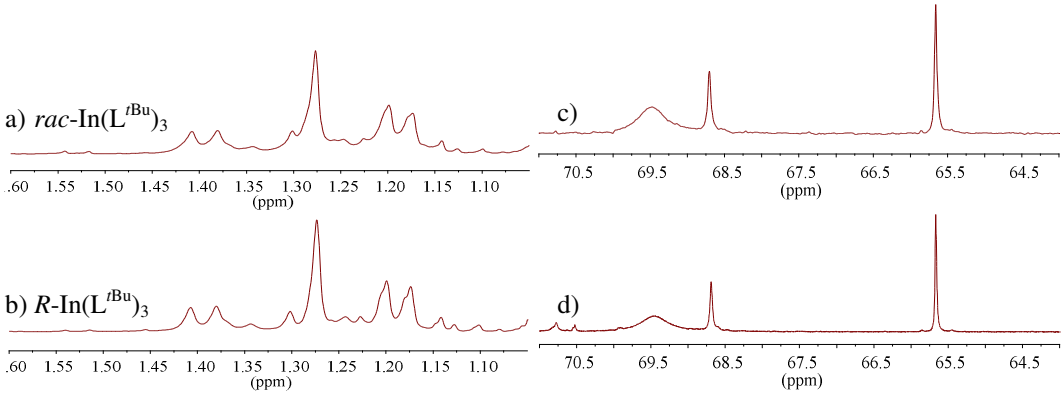

Figure 2.7: ^{1}H (*tert*-butyl region) and $^{31}P\{^{1}H\}$ NMR spectra of *rac*-In(L^{tBu})$_3$ and *R*-In(L^{tBu})$_3$ (d_8-toluene), a) ^{1}H: *rac*-In(L^{tBu})$_3$, b) ^{1}H: *R*- In(L^{tBu})$_3$, c) $^{31}P\{^{1}H\}$: *rac*-In(L^{tBu})$_3$ and d) $^{31}P\{^{1}H\}$: *R*- In(L^{tBu})$_3$.

It is proposed that these are *fac*- and *mer*- six coordinate isomers and a five-coordinate isomer of *rac*-In(L^{tBu})$_3$, in which one phosphine oxide group remains uncoordinated), Equation 2.5.

A variable temperature ^{1}H and $^{31}P\{^{1}H\}$ NMR spectroscopic study of *rac*-In(L^{tBu})$_3$ in d_8-toluene was undertaken. A stackplot showing the variation with temperature of the $^{31}P\{^{1}H\}$ NMR spectra of *rac*-In(L^{tBu})$_3$ is shown (Figure 2.8). At low temperature (238 K), the $^{31}P\{^{1}H\}$ NMR spectrum shows four sharp resonances in the region 65-70 ppm (with an integration ratio of 3 : 3 : 2 : 3). At 298 K, they have coalesced to three resonances with an integration ratio of 6 : 2 : 3 which then remain essentially unchanged up to 338 K. This confirms the presence of different geometric isomers. The lower frequency resonance (65.5 ppm) is tentatively assigned as the pendant PO group of a monodentate ligand because the resonance is close to the one representating the proligand *rac*-HL^{tBu} (63.7 ppm).

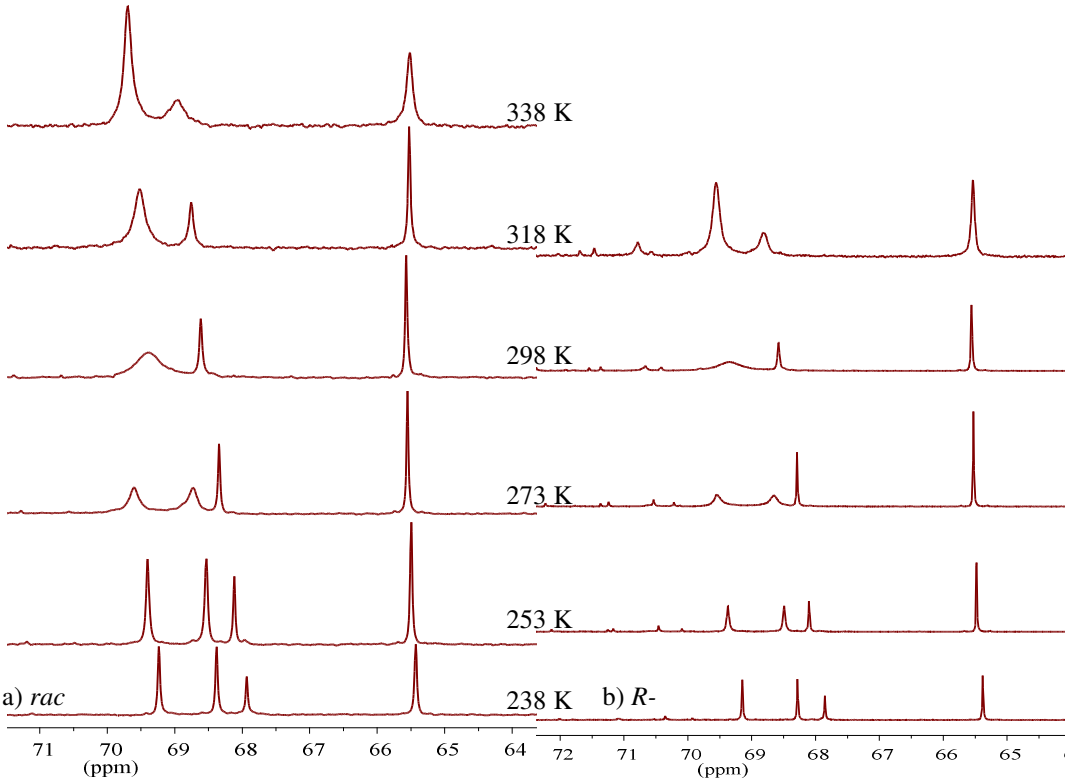

Figure 2.8: Variable temperature $^{31}P\{^{1}H\}$ NMR spectra (d_8-toluene) of a) *rac*-In(L^{tBu})$_3$ and b) *R*-In(L^{tBu})$_3$.

A stackplot showing the variation with temperature of the ^{1}H NMR spectra of *rac*-In(L^{tBu})$_3$ is shown in Figure 2.9 (the C*H* region has been expanded for clarity).

We have been unsuccessful in obtaining ^{115}In NMR spectra of solutions of *rac*-In(L^{tBu})$_3$, possibly due to its fluxional behaviour in this system and the high quadrupole moment of indium (I = 9/2).

The FTIR spectra in the solid state and solution are more informative than the NMR spectra of *rac*-In(L^{tBu})$_3$, since it is possible to see both coordinated P=O (υ = 1106 cm^{-1}) and uncoordinated P=O (υ = 1065 cm^{-1}) in the solid state spectrum (nujol mull) and a coordinated P=O (υ = 1107 cm^{-1}) and uncoordinated P=O (υ=1077 cm-^{1}) in solution (non-coordinating toluene solution) which implies the presence of the five-coordinate isomer of *rac*-In(L^{tBu})$_3$.

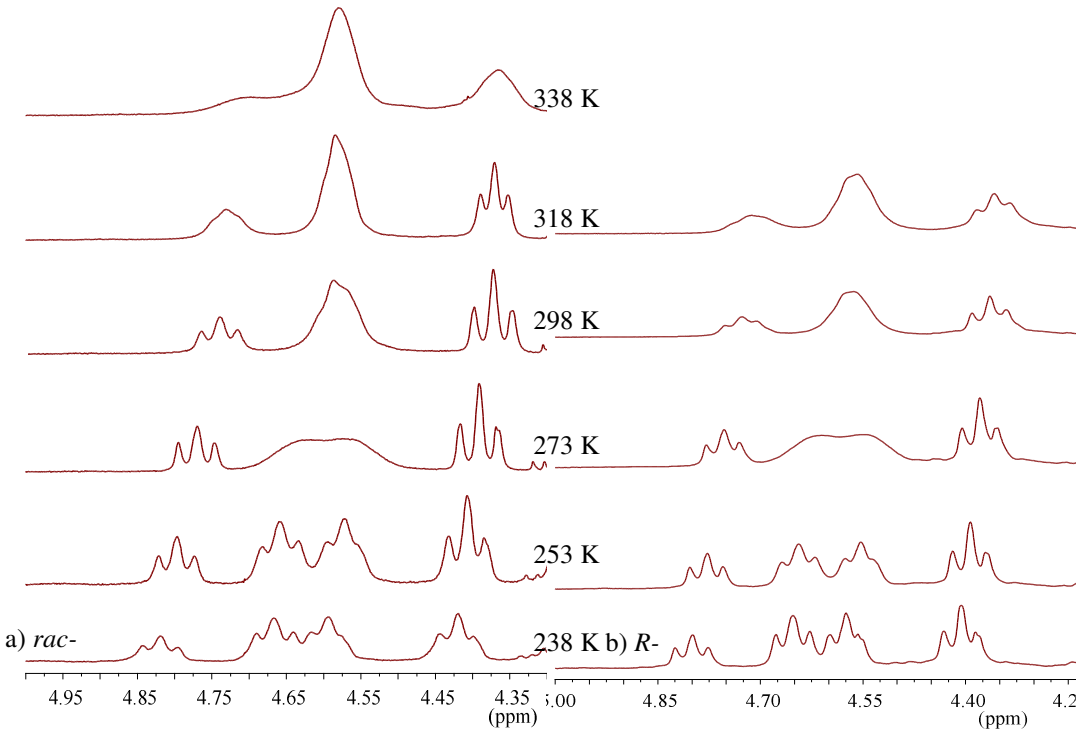

Figure 2.9: Variable temperature ^{1}H NMR spectra (expanded CH region) d_8-toluene of a) *rac*-In(L^{tBu})$_3$ and b) *R*-In(L^{tBu})$_3$.

As Figure 2.8 and 2.9 show, both *rac*-In(L^{tBu})$_3$ and *R*-In(L^{tBu})$_3$ have similar $^{31}P\{^{1}H\}$ and ^{1}H NMR spectra from 238 K to 338 K.

2.2.7 Crystals structures of complexes *rac*-M(L^{R})$_3$ complexes

Although NMR spectroscopy is the best quantitative way to find the ratio of homochiral purity, the 'impurity' was previously seen as a disorder component of one ligand in the single crystal structures of both Eu(L^{tBu})$_3$ and Er(L^{tBu})$_3$. Continuing this study by single crystal X-Ray diffraction proved of much interest.[7]

Colourless crystals of complexes ***rac*-Y(L^{Ph})$_3$** and ***rac*-Y(L^{Ar})$_3$** suitable for a single crystal X-ray diffraction study were grown from a DME solution and a DME/hexanes solution respectively. The molecular structures are depicted in Figure

2.10. The configuration of the molecules shown is Y(*R*-L^{Ph})$_3$ and Y(*S*-L^{Ar})$_3$. The homochirality is crystallographically imposed by C_3-symmetry in both crystals.

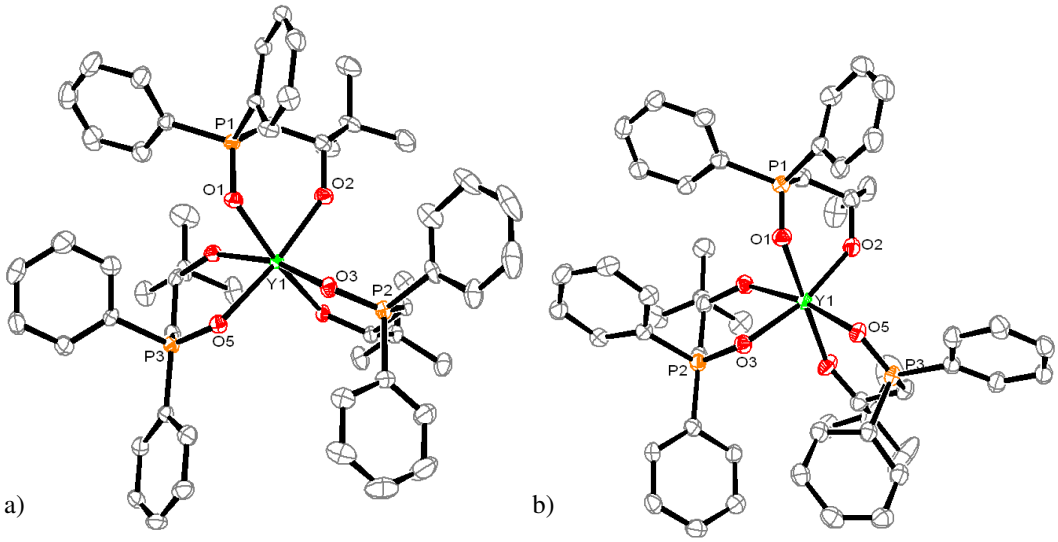

Figure 2.10: Displacement ellipsoid drawing of a) Y(*R*-L^{Ph})$_3$ and b) Y(*S*-L^{Ar})$_3$, 50 % probability ellipsoids. Lattice solvent, all hydrogen atoms and methyl group on the aryl ring of Y(*S*-L^{Ar})$_3$ omitted for clarity. Average distances (Å): (*rac*-Y(L^{Ph})$_3$) Y-OR 2.146, Y-OP 2.349 and (*rac*-Y(L^{Ar})$_3$) Y-OR 2.145, Y-OP 2.352. Selected angles (°): (*rac*-Y(L^{Ph})$_3$) O1-Y-O2 80.25(10), O1-Y-O3 88.75(10), O1-Y-O5 86.15(9), and (*rac*-Y(L^{Ar})$_3$) O1-Y-O2 81.07(8), O1-Y-O3 82.60(7), O1-Y-O5 88.78(7)

The coordination geometry of the yttrium metal in *rac*-Y(L^{R})$_3$ complexes is octahedral. The Y-alkoxy-O bonds are very short with average values of Y-OR (2.146 Å) for *rac*-Y(L^{Ph})$_3$ and Y-OR (2.145 Å) for *rac*-Y(L^{Ar})$_3$, in comparison the average Y-OR bond distances reported by Aspinall *et al*. are 2.24 Å in Li$_3$[Y(*R*-binol)$_3$].6 THF.[21]

The Y-OP average bond distance in *rac*-Y(L^{R})$_3$ is within the literature range for a Y^{III}-OP bond (2.266-2.381 Å).

The molecular structures drawn as space filling plots are shown in Figure 2.11 for *RRR*-Y(L^{tBu})$_3$, *RRR*-Y(L^{Ph})$_3$ and *SSS*-Y(L^{Ar})$_3$. Looking down the formal C_3 axis that trisects the three yttrium-alkoxide bonds, it is easiest to see how the packing is

disrupted by the incorporation of the methyl group on the aryl ring, in c). The distortion in c) is also visible by looking at the opposite side of the molecule along the C_3 axis. Thus, it appears that the homochiral product really is the most densely packed, as would be required in a ligand self-recognition process (Figure 2 a)).

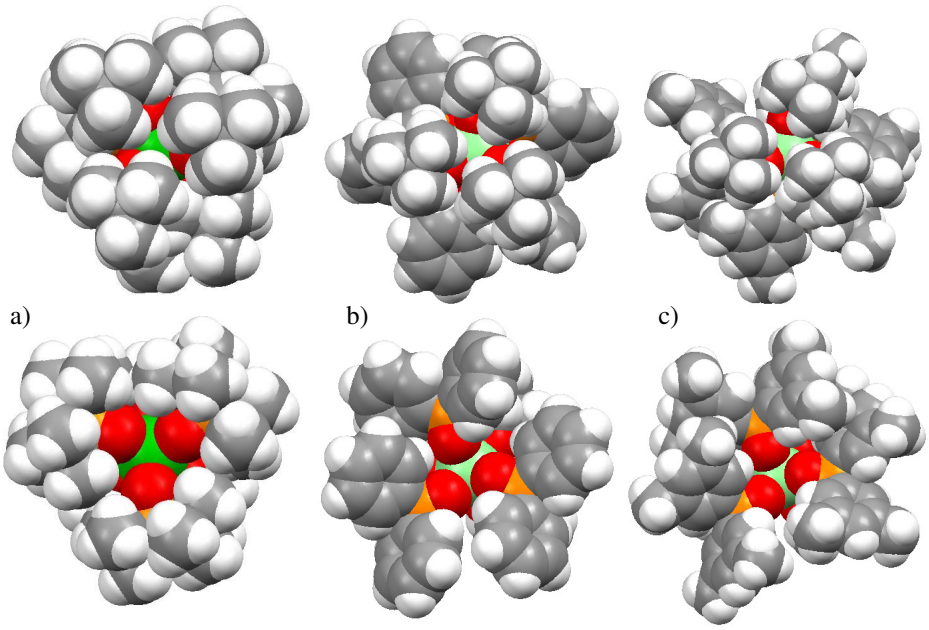

Figure 2.11: Space filling drawings of the molecular structures viewed from above the plane of the three alkoxides (above) and above the plane of the phosphine oxides (below) for (a) *RRR*-Y(L^{tBu})$_3$, (b) *RRR*-Y(L^{Ph})$_3$ and (c) *SSS*-Y(L^{Ar})$_3$. Yttrium is coloured green, oxygen red, phosphorus orange, carbon grey, hydrogen white.

Table 2.2 contains the distances and average distances of Y-OR and Y-OP bonds, for the structures of *RRR*-Y(L^{tBu})$_3$, *RRR*-Y(L^{Ph})$_3$ and *SSS*-Y(L^{Ar})$_3$. The Y-OR distances are the same within the 3σ criterion for all complexes, which is expected as the coordinating moiety does not change the steric profile. However, the range of average Y-OP distances is larger and the Y-OR distances for each complex are no longer statistically equivalent. The range is largest for *rac*-Y(L^{Ph})$_3$ demonstrating the poorest fit of ligands around the metal centre (confirming results in Table 2.1).

The average Y-OP distance with *RRR*-Y(L^{tBu})$_3$ (2.375 Å) is longer than the other two complexes average distances for *RRR*-Y(L^{Ph})$_3$ and *SSS*-Y(L^{Ar})$_3$ (2.349 Å and 2.352 Å respectively).

Table 2.2: Comparison of Y-O distances in *RRR*-Y(L^{tBu})$_3$, *RRR*-Y(L^{Ph})$_3$, and *RRR*-Y(L^{Ar})$_3$

Distance (Å)	*RRR*-Y(L^{tBu})$_3$	*RRR*-Y(L^{Ph})$_3$	*RRR*-Y(L^{Ar})$_3$
Y-OR	2.151(2)	2.145(3)	2.140(2)
	2.143(2)	2.154(3)	2.152(2)
	2.151(2)	2.139(3)	2.145(2)
Average Y-OR	2.148	2.146	2.145
Y-OP	2.379(2)	2.369(3)	2.290(4)
	2.376(2)	2.319(3)	2.322(4)
	2.369(2)	2.358(3)	2.327(4)
Average Y-OP	2.375	2.349	2.352
Average Y-O	2.262	2.248	2.248

Colourless crystals of complexes ***rac*-Bi(L^{tBu})$_3$** and ***rac*-Lu(L^{Ph})$_3$** suitable for a single crystal X-ray diffraction study were grown from a cooled hexanes solution and a cooled DME/THF/hexanes solution respectively. The molecular structures are depicted in Figure 2.12. The configuration of the molecules shown is Bi(*R*-L^{tBu})$_3$ and Lu(*S*-L^{Ph})$_3$. The homochirality is crystallographically imposed by C_3-symmetry in both crystals.

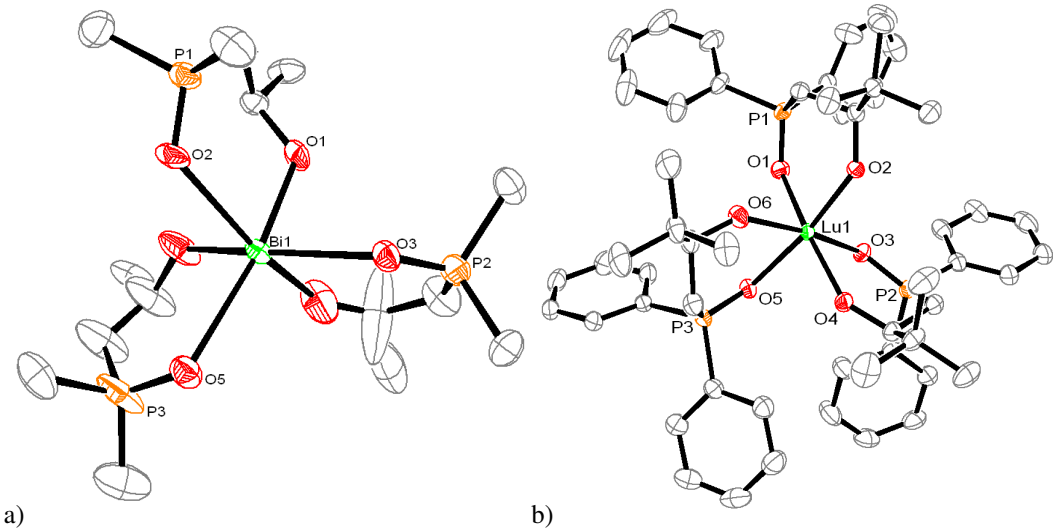

a) b)

Figure 2.12: Displacement ellipsoid drawing of a) Bi(*R*-L^{tBu})$_3$ and b) Lu(*S*-L^{Ph})$_3$, 50% probability ellipsoids. Lattice solvent and all hydrogen atoms omitted for

clarity. Average distances (Å): (*rac*-Bi(L^{tBu})$_3$) Bi-OR 2.110, Bi-OP 2.707 and (*rac*-Lu(L^{Ph})$_3$) Lu-OR 2.110, Lu-OP 2.306. Selected angles (°): (*rac*-Bi(L^{tBu})$_3$) O1-Bi-O2 77.3(2), O1-Bi-O3 82.5(2), O1-Bi-O5 91.7(3), and (*rac*-Lu(L^{Ph})$_3$) O1-Lu-O2 85.70(7), O1-Lu-O3 82.14(6), O1-Lu-O5 87.22(6)

The remarkable features of the *rac*-Bi(L^{tBu})$_3$ are the bond lengths and these are collated and compared with the bond lengths of *rac*-Y(L^{tBu})$_3$ in Table 2.3.

Table 2.3: Comparison of M-O distances in *RRR*-Y(L^{tBu})$_3$, *RRR*-Bi(L^{tBu})$_3$.

Distance (Å)	*RRR*-Y(L^{tBu})$_3$	*RRR*-Bi(L^{tBu})$_3$
M-OR	2.151(2)	2.118(8)
	2.143(2)	2.110(7)
	2.151(2)	2.102(8)
Average M-OR	2.148	2.110
M-OP	2.379(2)	2.694(7)
	2.376(2)	2.712(7)
	2.369(2)	2.716(7)
Average M-OP	2.375	2.707
Average M-O	2.262	2.409

The average M-OR distance is slightly smaller for Bi-OR than for *rac*-Y(L^{tBu})$_3$ (Bi-OR 2.110 Å < Y-OR 2.148 Å respectively) but Tondello *et al.* obtained a dramatically larger average Bi-OR bond distance of 2.32 Å in Bi(acac)$_3$ which shows a better packing here.[22]

However, the average M-OP distance is larger for Bi-OP (Bi-OP 2.707 Å > Y-OP 2.375 Å) which is related to an increasing average O-M-O bite angle of the ligand L (O-Bi-O 77.7 < O-Y-O 82.0°); an effect of the stereochemically active lone pair of the bismuth. Mehring *et al*. reported a 9-coordinate bismuth complex with two chelating ligands (^{i}PrO)$_2$(O)PCH$_2$P(O)(O^{i}Pr)$_2$, two bidentate nitrate ligands and one monodentate nitrate ligand. The average Bi-OP distance is 2.467 Å and the average O-Bi-O bite angle of their ligand is 78.9°. These values are similar to those in

bismuth halide adducts $[BiX_3\{(^iPrO)_2(O)PCH_2P(O)(O^iPr)_2\}]_2$; the Bi-OP average distance (2.467 Å) is far smaller than for *rac*-Bi(L^{tBu})$_3$ (2.707 Å) showing the stereochemically active bismuth lone pair has a greater effect in 6-coordinate than in a 9-coordinate complex.[23, 31-32]

Both complexes *rac*-Y(L^{Ph})$_3$ and *rac*-Lu(L^{Ph})$_3$ are isostructural but it is possible to notice some differences in their bond lengths which are collated in Table 2.4.

Table 2.4: Comparison of M-O distances in *RRR*-Y(L^{Ph})$_3$, *RRR*-Lu(L^{Ph})$_3$.

Distance (Å)	*RRR*-Y(L^{Ph})$_3$	*RRR*-Lu(L^{Ph})$_3$
M-OR	2.145(3)	2.120(16)
	2.154(3)	2.108(19)
	2.139(3)	2.103(17)
Average M-OR	2.146	2.110
M-OP	2.369(3)	2.279(18)
	2.319(3)	2.313(18)
	2.358(3)	2.326(18)
Average M-OP	2.349	2.306

In both cases, the average Lu-O bond distance (Lu-OR 2.110 Å and Lu-OP 2.306 Å) are shorter than thoses for Y-O (Y-OR 2.146 Å and Y-OP 2.349 Å) respectively showing a better packing for *rac*-Lu(L^{Ph})$_3$ in according with the smaller ionic radii for lutetium ($r(Lu^{3+})$ = 0.861 Å and $r(Y^{3+})$ = 0.900 Å).

Walsh *et al*. reported a binolate derivative where the structure of $Li_3(DMEDA)_3(BINOLate)_3Lu$ consists of a 6-coordinate distorted octahedral lutetium centre with an average Lu-OR bond distance of 2.204 Å. This is far longer than in *rac*-Lu(L^{Ph})$_3$ showing poorer packing around the lutetium.[33]

Three different batches of crystals of *rac*-In(L^{tBu})$_3$ suitable for a single crystal X-ray diffraction study were isolated from concentrated DME solution (*mer-RRR*-

In(L^{tBu})$_3$) or different mixtures of hexanes/DME solutions (one afforded *mer-RRR*-In(L^{tBu})$_3$ and one afforded *fac-RRR*-In(L^{tBu})$_3$) (Figure 2.13).

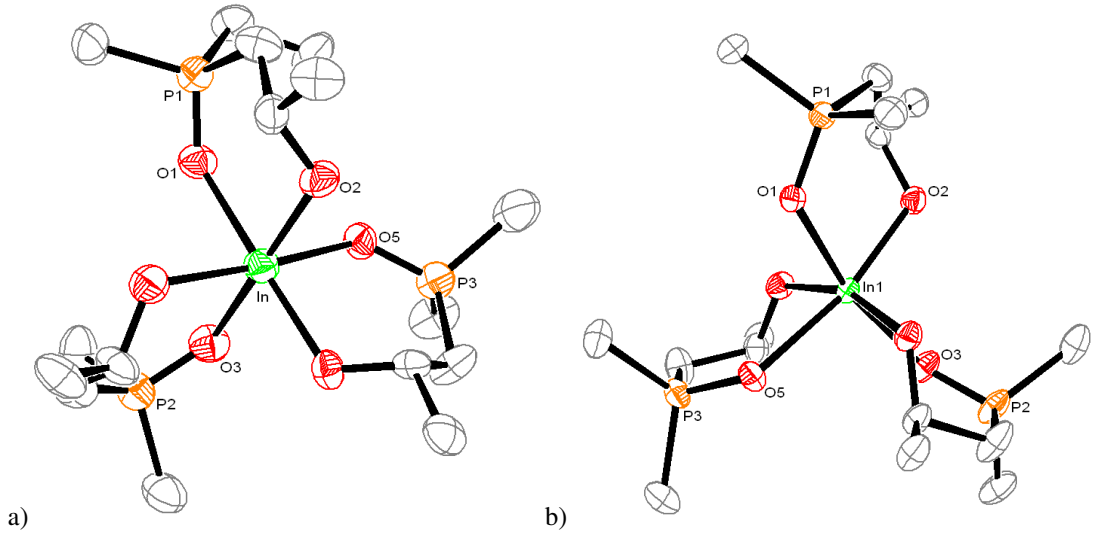

Figure 2.13: Displacement ellipsoid drawings of *rac*-In(L^{tBu})$_3$ a) homochiral *fac-RRR*-In(L^{tBu})$_3$ and b) *mer-RRR*-In(L^{tBu})$_3$, 50 % probability ellipsoids. The *tert*-butyl groups and all hydrogen atoms except those at the chiral carbon atoms are omitted. Selected distances (Å): (for *fac-rac*-In(L^{tBu})$_3$) In1-O5 2.268(9), In1-O3: 2.274(9), In1-O1: 2.265(9); (for *mer-rac*-In(L^{tBu})$_3$) In1-O5 2.3333(16), In1-O3: 2.2707(17), In1-O1: 2.2768(16); and angles (°): (for *fac-rac*-In(L^{tBu})$_3$) O3-In1-O1: 89.9(3), O6-In1-O2: 99.1(3), O2-In1-O4: 101.1(4), O4-In1-O5: 169.1(4), O5-In1-O6: 85.7(3); (for *mer-rac*-In(L^{tBu})$_3$) O3-In1-O1: 166.24(6), O6-In1-O2: 95.68(7), O2-In1-O4: 102.65(7), O4-In1-O5: 83.20(6), O5-In1-O6: 80.24(6).

The *fac-RRR*-In(L^{tBu})$_3$ molecular structure is C_3-symmetric with octahedral co-ordination about the metal centre (Figure 2.14 a)). However, in *mer-RRR*-In(L^{tBu})$_3$, one of the ligands points in the opposite direction with respect to the other two others

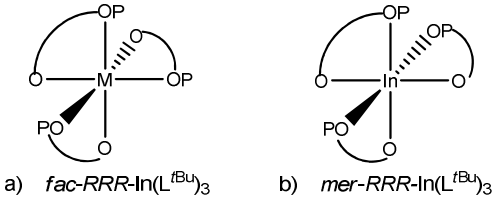

Figure 2.14: Drawing of molecular structures a) *rac*-In(L^{tBu})$_3$ *fac*- configuration, b) *rac*-In(L^{tBu})$_3$ with the *mer*- configuration.

Interestingly, the only significant difference in the coordinated ligand geometries is that In-OP in the 'inverted ligand' is longer than the two other In-OP bond lengths (compare In-O5 2.3333(16) Å with In-O1 2.2768(16) Å and In1-O3 2.2707(17) Å). This is shown in Table 2.5.

Table 2.5: Metal oxygen distances in *fac-rac*-In(L^{tBu})$_3$ and the *mer-rac*-In(L^{tBu})$_3$ (shadowed)

Distances (Å)	ligand 1	ligand 2	'inverted ligand'	ligand 1	ligand 2	ligand 3
In-OP	2.2768(16)	2.2707(17)	2.3333(16)	2.268(9)	2.274(9)	2.265(9)
In-OR	2.0864(16)	2.0656(16)	2.0611(16)	2.077(9)	2.073(9)	2.074(9)
O-P	1.5106(17)	1.5120(18)	1.5084(17)	1.487(10)	1.512(10)	1.499(10)
O-R	1.385(3)	1.393(3)	1.399(3)	1.366(17)	1.400(17)	1.411(16)
P-C	1.816(3)	1.816(3)	1.805(3)	1.802(14)	1.820(15)	1.819(15)
C-C	1.556(3)	1.552(3)	1.551(3)	1.572(18)	1.46(2)	1.51(2)

Neumuller *et al*. showed that in Li_3[In(*R*-binol)$_3$].6 THF the average In-OR bond distance is 2.13 Å and for Li_3[In(*R*-binol)$_3$] 3 DME is 2.14 Å,[24, 25] which is higher than the average In-OR bond distances of *rac*-In(L^{tBu})$_3$ (2.07 Å) demonstrating a better packing in *rac*-In(L^{tBu})$_3$.

Space filling plots of the molecular structures are shown in Figure 2.15 for a) *RRR*-Y(L^{tBu})$_3$, b) *fac-RRR*-In(L^{tBu})$_3$ and c) *mer-RRR*-In(L^{tBu})$_3$.

Looking down the formal C_3 axis that trisects the three alkoxides, it is easiest to see how the packing is disrupted by the inversion in one ligand in c). The distortion in c) is also visible by looking at the opposite side of the molecule along the C_3 axis. Thus, it appears once again that the homochiral products are the most densely packed, as would be required in a ligand self-recognition process in a) and b).

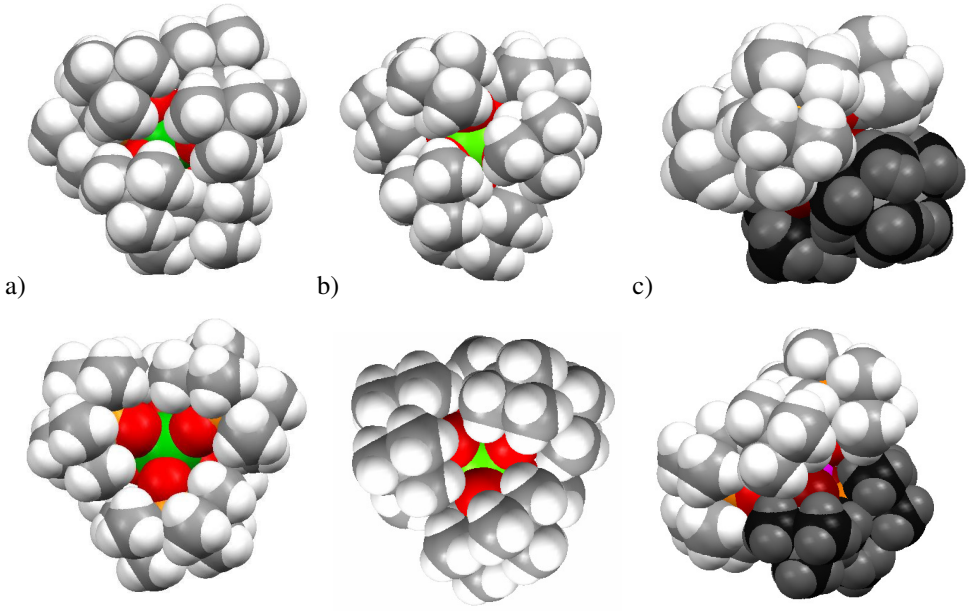

Figure 2.15: Space filling drawings of the molecular structures viewed from above the plane of the three alkoxides (above) and above the plane of the phosphine oxides (below) for a) *fac- RRR*-Y(L^{tBu})$_3$, b) *fac- RRR*-In(L^{tBu})$_3$ and c) *mer- RRR*-In(L^{tBu})$_3$. Metal is coloured green, oxygen red, phosphorus orange, carbon grey, hydrogen white. The atoms of the 'inverted ligand' configuration are drawn in a darker colours.

2.3 Synthesis of $(L^R)_2MX$

2.3.1 Introduction

If the mechanism of formation of the homochiral C_3-symmetric system allows ligand redistribution to occur as the ligands L^R are introduced, then a dynamic redistribution of the *R*- and *S*-L^R isomers between the heteroleptic intermediates $(L^R)MN"_2$, $(L^R)_2MN"$ and uncomplexed ligand *rac*-HL^R might be anticipated to allow the most densely packed complex – *i.e.* the homochiral complex - to form as a thermodynamic product.

It is generally agreed that protonolysis reactions of $LnN"_3$ proceed *via* an associative mechanism.[26] The slow rate of the formation of *rac*-$M(L^R)_3$ led to the complexes of $(L^R)MN"_2$ and $(L^R)_2MN"$ being targeted; in order to identify whether the steric bulk and chirality of less substituted $M(L^R)_n$ (n = 1 or 2) complexes could

afford some stereochemical control over the subsequent protonolysis reactions with HL^R or whether a dynamic equilibrium could be set up that demonstrated a thermodynamic control over ligand coordination.

2.3.2 Synthesis of amido $(L^R)_2MN''$ complexes

2.3.2.1 Synthesis and NMR spectral characterisation of $(L^R)_2MN''$

Treatment of MN''_3 (M = In or Y) with two equivalents of *rac*-HL^R (R = ^{t}Bu or Ph) in THF at -78 °C afforded **$(L^R)_2MN''$** in good yield (75-90 %), as a mixture of diastereomers (Equation 2.6).

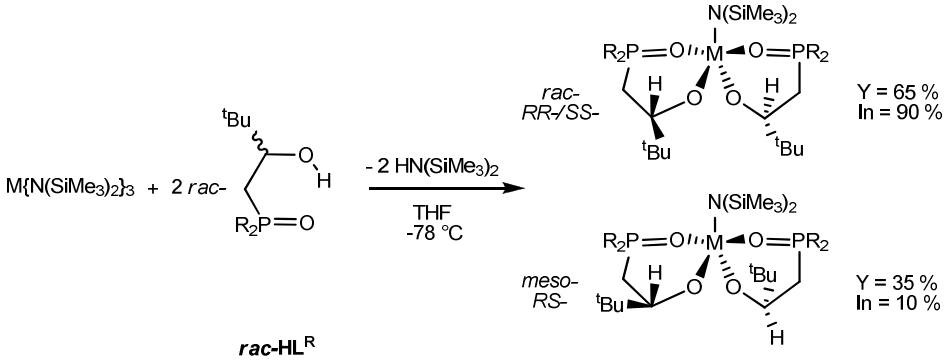

Eq. 2.6

A reaction between YN''_3 and two equivalents of *rac*-HL^{tBu} or *R*-HL^{tBu} at -78 °C was stirred for 1 hour, dried under vacuum at -78 °C then was worked up at room temperature to afford diastereomers of the complex $(L^{tBu})_2YN''$ or *RR*-$(L^{tBu})_2YN''$ respectively. The complex $(L^{tBu})_2YN''$ was isolated as colourless solid in a yield of 71 %. The ^1H and $^{31}P\{^1H\}$ NMR spectra of solutions of *RR*-$(L^{tBu})_2YN''$ show a single ligand environment for *RR*-$(L^{tBu})_2YN''$. NMR spectra of solutions of $(L^{tBu})_2YN''$ show the same resonances assigned as homochiral isomers *RR*-$(L^{tBu})_2YN''$ and *SS*-$(L^{tBu})_2YN''$; this component of the mixture comprising approximately 65 % of the product. The remaining 35 % of the total yield is the *meso*-diastereoisomer *RS*-$(L^{tBu})_2YN''$.

A variable temperature ^1H and ^{31}P NMR spectroscopic study of $(L^{tBu})_2YN''$ in d_8-toluene was undertaken. A stackplot of the data collected is shown in Figure 2.16. At

low temperature (253 K), the $^{31}P\{^{1}H\}$ NMR spectrum shows two broad resonances in the region 70-71 ppm (with an integration ratio of 65 : 35) which remain essentially unchanged up to 323 K. In the ^{1}H NMR spectra, it is possible to see a broadening of the resonances as the temperature is decreased from 323 K to 253 K where it became difficult to distinguish between *rac*- or *meso*-$(L^{tBu})_2YN"$.

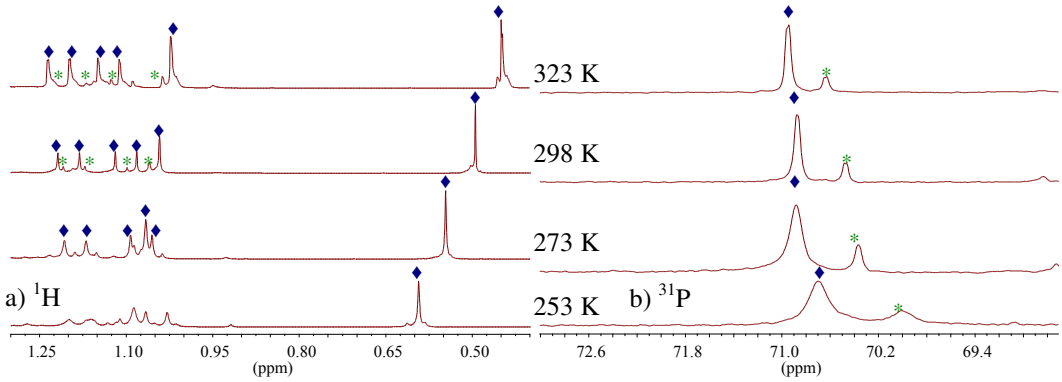

Figure 2.16: Variable temperature ^{1}H (expanded methyl region) and $^{31}P\{^{1}H\}$ NMR spectra (in d_8-toluene) of $(L^{tBu})_2YN"$ a) ^{1}H NMR and b) $^{31}P\{^{1}H\}$ NMR. ♦ denotes homochiral *RR/SS*-$(L^{tBu})_2YN"$, * denotes meso *RS*-$(L^{tBu})_2YN"$

A set of NMR-scale reactions was carried out in which $YN"_3$ was treated with one, two or three equivalents of *rac*-HL^{tBu}, or *R*-HL^{tBu}, in d_6-benzene at room temperature. In each case, the distribution of products (mono, *bis*, and *tris*-L^{tBu} adducts) and the ratio of enantiomers or diastereomers, if applicable, recorded. The mixtures were then heated to reflux until no further change was observed (this was found to be between 48 and 96 hours in each case), and both the distribution and stereochemical ratio of the products were again measured. All data were obtained by measurement of the chemical shifts and integrals in the ^{1}H and $^{31}P\{^{1}H\}$ NMR spectra of the solutions. No precipitation of any material was observed in any of the experiments. The data are summarised in Table 2.6.

Notably, it is almost impossible to isolate pure $(L^{tBu})YN"_2$; the addition of one or two equivalents of *rac*-HL^{tBu} (*i.e.* a 50:50 mixture of *R*-HL^{tBu} and *S*-HL^{tBu}) affords significant quantities of *rac*-$Y(L^{tBu})_3$ immediately (with $YN"_3$ and HN" as byproducts) and only after heating does a further comproportionation reaction occur between the $Y(L^{tBu})_3$ and remaining $YN"_3$ to form significant quantities of

$(L^{tBu})_2YN''$ (*i.e.* $(R\text{-}L^{tBu})_2YN''$, $(S\text{-}L^{tBu})_2YN''$) and *meso*-$(R\text{-}L^{tBu})(S\text{-}L^{tBu})YN''$) as the predominant product. However, the reaction is not very clean. The best route to $(L^{tBu})_2YN''$ is *via* the low temperature addition of two equivalents of HL^{tBu} to YN''_3. The analogous NMR scale reaction between YN''_3 and two equivalents of *R*-HL^{tBu} cleanly affords $(R\text{-}L^{tBu})_2YN''$.

Comparison of Table 2.6, Entry 3 with Entry 6 and Entry 5 with Entry 7, shows no significant effect on the reaction outcome with either two or three equivalents of *rac*-HL^{tBu} upon changing the reaction solvent from d_6-benzene to THF.

When YN''_3 is treated with *rac*-HL^{tBu} to afford $(L^{tBu})_2YN''$ there is a modest degree of ligand self-recognition (Entries 3, 6, and 8), affording approximately a 60 : 40 ratio of homochiral $(L^{tBu})_2YN''$: *meso*-$(L^{tBu})_2YN''$.

Finally, entry 10 is the most important result in this section, confirming that the bound ligand L^{tBu} is exchangeable with another equivalent of protonated ligand HL^{tBu} in solution. This experiment, described in Equation 2.7, shows that the optical purity of the enantiopure *RRR*-$Y(L^{tBu})_3$ is lowered upon treatment with *rac*-HL^{tBu}, as small quantities of *RRS*-$Y(L^{tBu})_3$ are formed. Knowing that the ligand is inert to epimerisation under these conditions (Entry 2), this confirms that the formation of the predominantly homochiral $Y(L^{tBu})_3$ complexes is under thermodynamic control.

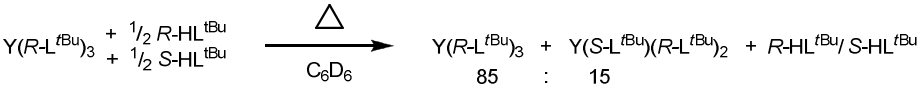

Eq. 2.7

A reaction between InN''_3 and two equivalents of *rac*-HL^{tBu} at -78 °C was allowed to warm up to room temperature over 16 hours to afford diastereomers of the complex **$(L^{tBu})_2InN''$**, isolated as a colourless solid in yield of 70 %. Enantiopure *R*-HL^{tBu} was also used in the synthesis of diastereomerically pure *RR*-$(L^{tBu})_2InN''$.

.

Table 2.6: Compositional and stereochemical product mixtures for the reactions of $YN"_3$ to make, $(L^{tBu})YN"_2$, $(L^{tBu})_2YN"$ and $Y(L^{tBu})_3$

				number of coordinated L^{tBu}			stereochemical ratios for $(L^{tBu})_2$ adducts			stereochemical ratios for $(L^{tBu})_3$ adducts		
Entry	Eq. and stereo.[a] of HL	T Start (ºC)	Solv-ent	Initial Ratio YL_1:YL_2:YL_3[b]	Ratio after Heating YL_1:YL_2:YL_3[b]	Ratio after recryst YL_1:YL_2:YL_3[b]	Initial Ratio *RR*/*RS*-[c]	Ratio after heating for 96 h, 80 ºC *RR*/*RS*-[c]	Ratio after recryst. *RR*/*RS*-[c]	Initial Ratio *RRR*/*RRS*-[d]	Ratio after Heating for 96 h, 80 ºC *RRR*/*RRS*-[d]	Ratio after recryst. *RRR*/*RRS*-[d]
1	1 *rac*-	+ 25	C_6D_6	5 / 15 / 80	20 / 80 / 0	--	65 / 35	55 / 45	--	60 / 40	0 / 0	--
2	1 *R*-	+ 25	C_6D_6	5 / 5 / 90	15 / 15 / 70	--	100 / 0	100 / 0	--	100 / 0	100 / 0	--
3	2 *rac*-	+ 25	C_6D_6	5 / 10 / 85	5 / 45 / 50	--	65 / 35	60 / 40	--	60 / 40	55 / 45	--
4	2 *R*-	+ 25	C_6D_6	2 / 1 / 97	10 / 15 / 75	--	100 / 0	100 / 0	--	100 / 0	100 / 0	--
5	3 *rac*-	+ 25	C_6D_6	0 / 2 / 98	0 / 10 / 90	--	--	--	--	60 / 40	60 / 40	--
6	2 *rac*-	+ 25	THF	5 / 10 / 85	5 /10 / 85	--	60 / 40	60 / 40	--	55 / 45	55 / 45	--
7	3 *rac*-	+ 25	THF	0 / 0 / 100	0 / 0 / 100	--	--	--	--	60 / 40	60 / 40	--
8	2 *rac*-	-78	THF	5 / 40 / 55	--	0 / 90 / 10	60 / 40	--	75 / 25	55 / 45	--	60 / 40
9	3 *rac*-	-78	THF	--	--	0 / 100 / 0	--	--	85 / 15	--	--	--
10[e]	3 *R*- + 1 *rac*[e]	+ 25	C_6D_6	0 / 0 / 100	0 / 0 / 100	--	--	--	--	100 / 0	85 / 15	--

a: stereo. = stereoisomer of HL^{tBu} used (*rac* = racemic); b: YL_1:YL_2:YL_3 = $Y(L^{tBu})N"_2$: $Y(L^{tBu})_2N"$: $Y(L^{tBu})_3$; c: for *bis*(L^{tBu}) adducts; d: for *tris*(L^{tBu}) adducts; e: see Equation 2.7; a reaction between $Y(R\text{-}L^{tBu})_3$ + *rac*-HL^{tBu}.

The ^{1}H and $^{31}P\{^{1}H\}$ NMR spectra of solutions of *RR*-$(L^{tBu})_2InN''$ show a single ligand environment for *RR*-$(L^{tBu})_2InN''$ (Figure 2.17). NMR spectra of solutions of $(L^{tBu})_2InN''$ show the same resonances for the homochiral isomers *RR*-$(L^{tBu})_2InN''$ and *SS*-$(L^{tBu})_2InN''$; this component of the mixture comprises approximately 90 % of the product. The remaining 10 % of the total yield is the *meso*-diastereoisomer *RS*-$(L^{tBu})_2InN''$.

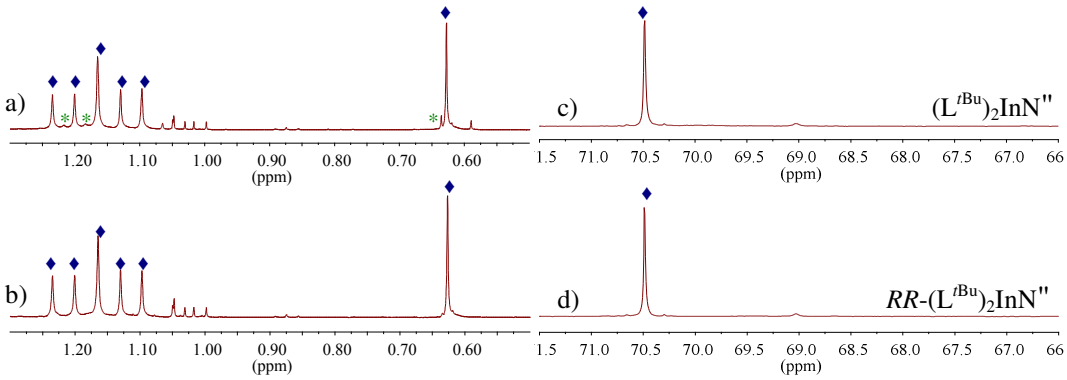

Figure 2.17: ^{1}H (expanded methyl region) and $^{31}P\{^{1}H\}$ NMR spectra (d_6-benzene), a) ^{1}H: $(L^{tBu})_2InN''$, b) ^{1}H: *RR*-$(L^{tBu})_2InN''$, c) $^{31}P\{^{1}H\}$: $(L^{tBu})_2InN''$ and d) $^{31}P\{^{1}H\}$: *RR*-$(L^{tBu})_2InN''$. ♦ denotes *RR/SS*-$(L^{tBu})_2InN''$, * denotes *RS*-$(L^{tBu})_2InN''$

A reaction between InN''_3 and two equivalents of *rac*-HL^{Ph} at room temperature afforded the colourless solid **$(L^{Ph})_2InN''$** in yield of 91 %. The $^{31}P\{^{1}H\}$ NMR spectrum shows a major resonance at 47.0 ppm and a minor resonance at 43.6 ppm (with a ratio major : minor of 85 : 15); diagnostic features in the ^{1}H NMR spectrum are the *tert*-butyl group at 1.05 ppm and -$SiMe_3$ group at 0.78 ppm.

An analogous reaction between one equivalent of LuN''_3 and two equivalents of *rac*-HL^{tBu} at room temperature was worked up after 16 hours and affords diastereomers of the complex $(L^{tBu})_2LuN''$ as a colourless solid in yield of 26 %. The ^{1}H and $^{31}P\{^{1}H\}$ NMR spectra of solutions of $(L^{tBu})_2LuN''$ are shown in Figure 2.18 and show a homochiral purity of 75 % with the remaining 25 % consisting of the impurity *RS*-$(L^{tBu})_2LuN''$.

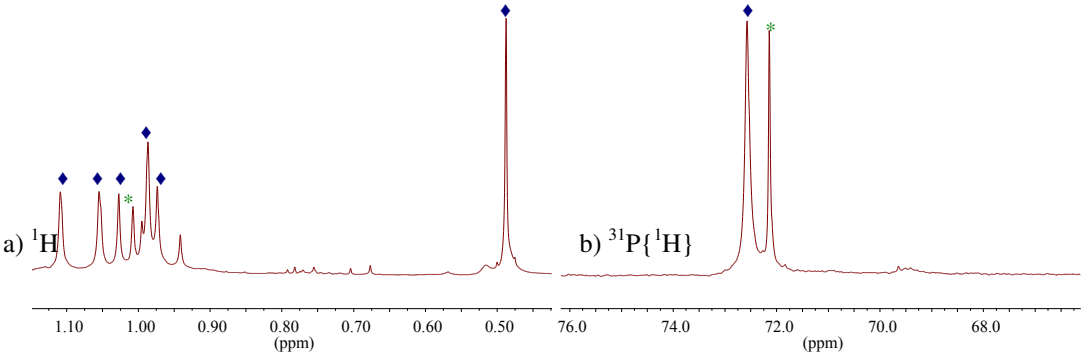

Figure 2.18: ^{1}H (expanded methyl region) and ^{31}P{^{1}H} NMR spectra of $(L^{tBu})_2$LuN" (d_6-benzene), a) ^{1}H: $(L^{tBu})_2$LuN" and b) ^{31}P{^{1}H}: $(L^{tBu})_2$LuN". ♦ denotes *RR/SS*-$(L^{tBu})_2$LuN", * denotes *RS*-$(L^{tBu})_2$LuN"

To avoid the thermodynamically favoured *rac*-Y$(L^{tBu})_3$ the synthesis of **$(L^{tBu})_2$YN"** was stopped after 1 hour at -78 °C. However, the synthesis of **$(L^{tBu})_2$LuN"** can be carried out at room temperature and for 16 hours, with a higher diastereomeric index for $(L^{tBu})_2$LuN" over $(L^{tBu})_2$YN" (75 % of *RR/SS*-$(L^{tBu})_2$LuN" > 65 % of *RR/SS*-$(L^{tBu})_2$YN"). These results show the influence of the radii on the thermodynamics of the ligand self recognition ($r(Lu^{3+})$ = 0.86 Å and $r(Y^{3+})$ = 0.90 Å).

The effect of the ionic radius on the extent of the diastereomeric index of the complexes **$(L^{tBu})_2$MN"** is shown in Figure 2.19.

The linear relationship between ionic radius and complex diastereomeric index is clear. As the ionic radius decreases, the diastereomeric index increases. This simple relationship was not observed for *rac*-M$(L^{tBu})_3$; this show that the steric bulk of the ligand is also very important.

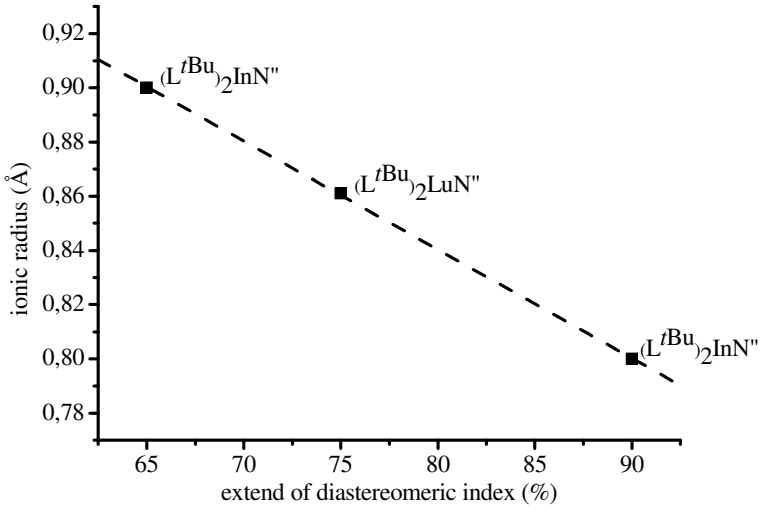

Figure 2.19: Ionic radius (Å) versus extend of the diastereomeric index of $(L^{tBu})_2MN"$.

2.3.2.2 Synthesis and characterisation of $(L^R)_2M(NPh_2)$

The reaction of one equivalent of $(L^{tBu})InN"$ with one equivalent of $HNPh_2$ in d_6-benzene at 80 °C over 3 days afforded colourless compound **$(L^{tBu})_2In(NPh_2)$** in a yield of 68 %. An alternative synthesis involved reaction between one equivalent of $InN"_3$, two equivalents of *rac*-HL^{tBu} and one equivalent of $HNPh_2$ heated at 80 °C in d_6-benzene for 16 hours (Scheme 2.3).

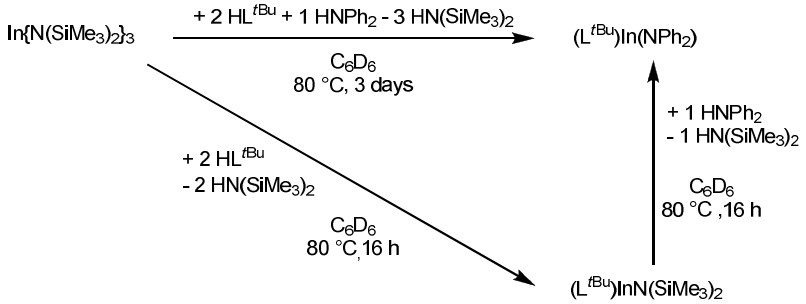

Scheme 2.3: Reactions of $InN"_3$ to afford $(L^{tBu})_2In(NPh_2)$.

The ^1H and $^{31}P\{^1H\}$ NMR spectra of solutions of **$(L^{tBu})_2In(NPh_2)$** show resonances assigned as the homochiral isomers *RR*-$(L^{tBu})_2In(NPh_2)$ and *SS*-$(L^{tBu})_2In(NPh_2)$; this

component of the mixture comprising approximately 80 % of the product. The remaining 20 % of the total yield is the *meso*- diastereoisomer *RS*-$(L^{tBu})_2In(NPh_2)$ (Figure 2.20).

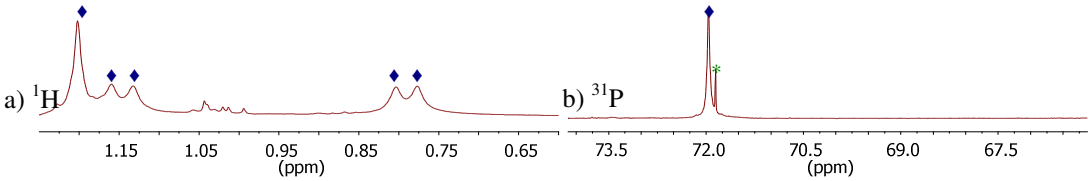

Figure 2.20: ^{1}H and ^{31}P{^{1}H} NMR spectra of $(L^{tBu})_2In(NPh_2)$ (d_6-benzene), a) ^{1}H: $(L^{tBu})_2In(NPh_2)$ and b) ^{31}P{^{1}H}: $(L^{tBu})_2In(NPh_2)$. ♦ denotes *RR/SS*-$(L^{tBu})_2In(NPh_2)$, * denotes *RS*-$(L^{tBu})_2In(NPh_2)$.

2.3.2.3 Crystals structures of amido $(L^R)_2MX$ complexes

Crystals of complexes **$(L^{tBu})_2$YN"** and **$(L^{tBu})_2$InN"** suitable for a single crystal X-ray diffraction study were grown from hexanes solutions; the complexes are isostructural. Both an end-on view (looking down the amido group towards the metal) and a side-on view of the molecular structures are shown in Figure 2.21.

The configuration of the molecules shown is (*R*-$L^{tBu})_2$MN" and the homochirality is imposed by a crystallographic two-fold rotational symmetry.

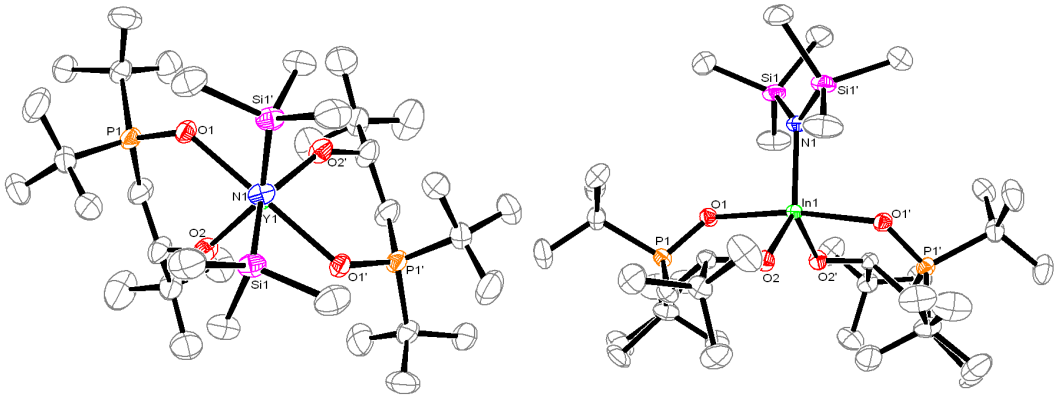

Figure 2.21: Displacement ellipsoid drawing of (*R*-$L^{tBu})_2$YN" (end-on, above) and (*R*-$L^{tBu})_2$InN" (side on, below), 50 % probability ellipsoids. Lattice solvent and all hydrogen atoms omitted for clarity. Selected distances (Å): (for $(L^{tBu})_2$YN) for Y1-OR 2.098, Y1-OP 2.294, Y1-N1 2.297; (for $(L^{tBu})_2$YN) In1-OR 2.0604(13), In1-OP 2.2337(13), In1-N1 2.101(2). Selected angles (°): (for $(L^{tBu})_2$YN) O1-Y1-O1'

175.07(14), O2-Y1-O2' 113.34(16), O2-Y1-N1 123.33(8), N1-Y1-O1 92.47(7), O2-Y1-O1 95.54(10); (for $(L^{tBu})_2InN$) O1-In1-O1' 170.38(7), O2-In1-O2' 111.40(8), O2-In1-N1 124.30(4), N1-In1-O1 94.81(4), O2-In1-O1 86.50(5).

The metal cations in molecules of **$(L^{tBu})_2YN''$** and **$(L^{tBu})_2InN''$** have a distorted trigonal bipyramidal geometry, with the sterically demanding $^tBu_2PO$ groups opposite to each other and two *tert*-butyl groups of the chiral carbon atom facing down and away from each other, generating a rotational symmetry axis as was observed in the C_3-symmetric *rac*-$M(L^{tBu})_3$ structures. The O-M-O angle formed by the two phosphine oxide ligands is close to linear (O1-Y1-O1' 175.1°, O1-In1-O1' 170.38°). The amido-nitrogen and the two alkoxide-oxygens form a trigonal plane, with angles close to 120° (O2-Y1-N1 123.3°, O2-Y1-O2' 113.3°, O2-In1-N1 124.30°, O2-In1-O2' 111.40°). The M-O bond lengths in $(L^{tBu})_2YN''$ are significantly shorter than the corresponding bonds in *rac*-$Y(L^{tBu})_3$ (in brackets), Y1-OR 2.098 (2.148) Å and Y1-OP 2.294 (2.375) Å, in accordance with the lower coordination number.

In comparison with the literature, the Y-N bond length (2.297(4) Å) is very short showing more compact system. Zi *et al.* reported a bond length of 2.447(11) Å in $[(R)\text{-}C_{20}H_{12}(NCHC_4H_3N)_2]YN\text{-}(SiMe_3)_2(THF)$ and Lee *et al*. published a bond length of 2.338(11) Å in Y[4,13-Diaza-18-crown-6][$N(SiMe_3)_2$].[27, 28]

Colourless crystals of complex **$(L^{tBu})_2In(NPh_2)$** suitable for a single crystal X-Ray diffraction study were grown from evaporation of a DME/hexanes solution.

The molecular structure is depicted in Figure 2.22. The configuration of the molecule shown is $(R\text{-}(L^{tBu})_2In(NPh_2)$.

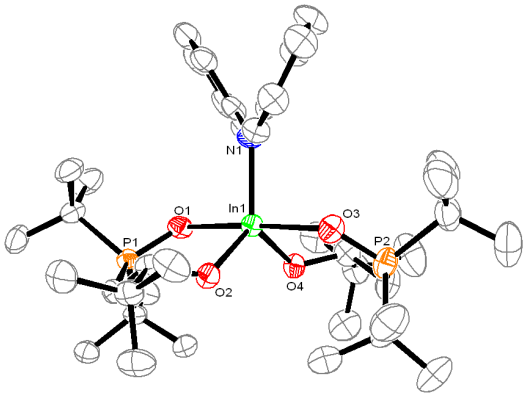

Figure 2.22: Displacement ellipsoid drawing of $(L^{tBu})_2In(NPh_2)$, 50 % probability ellipsoids. All hydrogen atoms are omitted for clarity. Selected distances (Å) and angles (º): In1-O1: 2.174(3), In1-O2: 2.038(3)), In1-N1: 2.114(4). O3-In1-O1: 176.24(12), O2-In1-O4: 115.47(13), O4-In1-N1 122.73(14), N1-In1-O2: 121.79(11).

The metal centre shows a distorted trigonal bipyramidal geometry, with the sterically demanding $(^tBu)_2PO$ groups opposite to each other. The apical group occupies one equatorial site, the other two being occupied by the alkoxide groups of the ligand. The O-M-O angle formed by the two phosphine oxide ligating groups is close to linear (O3-In1-O1 176.24° for $(L^{tBu})_2In(NPh_2)$). The apical group (N1) and the two alkoxide-oxygens (O1 and O3) form a trigonal plane, with angles close to 120° (O2-In1-O4 115.47°, O4-In1-N1 122.73°, O2-In1-N1 121.79°).

2.3.3 Synthesis and characterisation of aryloxo or alkoxo $(L^R)_2MX$

2.3.3.1 Synthesis and NMR spectral characterisation of $(L^R)_2Y(OAr)$

The lability of the ligand L^{tBu} in **$(L^{tBu})_2$MN"** prompted the investigation into finding a suitably large ancillary ligand, **X**, that could improve the ligand self-recognition process in $(L^{tBu})_2MX$ adducts. In a survey for lanthanide compounds that assigns a 'ligand effective radius' to a ligand by the Van der Waals sphere size of its component atoms, the di-*tert*-butylaryloxo ligand is slightly larger than silylamido ligand having 'steric coordination numbers' of 2.41 and 2.17 respectively.[29]

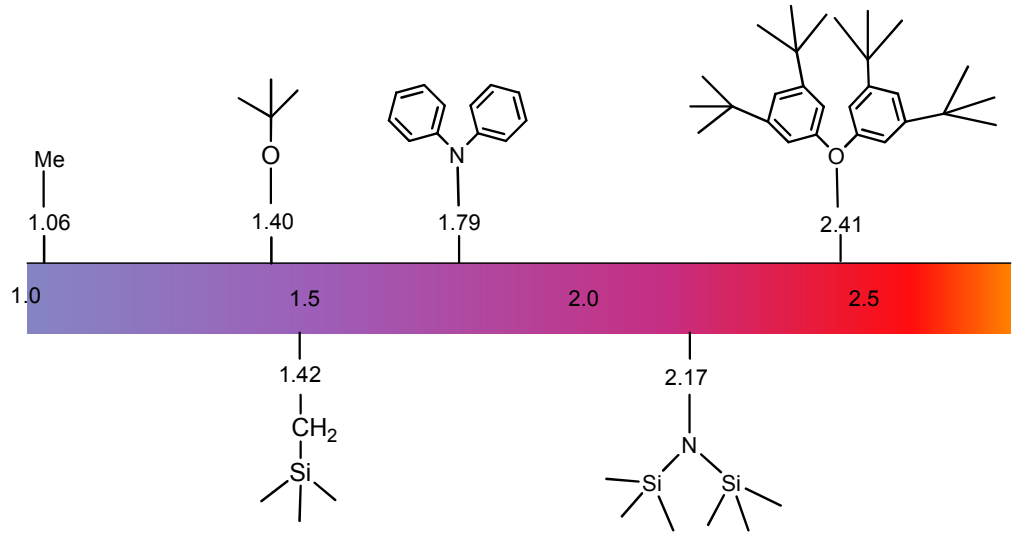

Figure 2.23: Chart of 'ligand effective radius' predicted per Marçalo *et al*.

Therefore, we studied four different synthetic routes to the target complex $(L^{tBu})_2Y(OAr)$ (Ar = 2,6-^{t}Bu-C_6H_3) (Scheme 2.4).

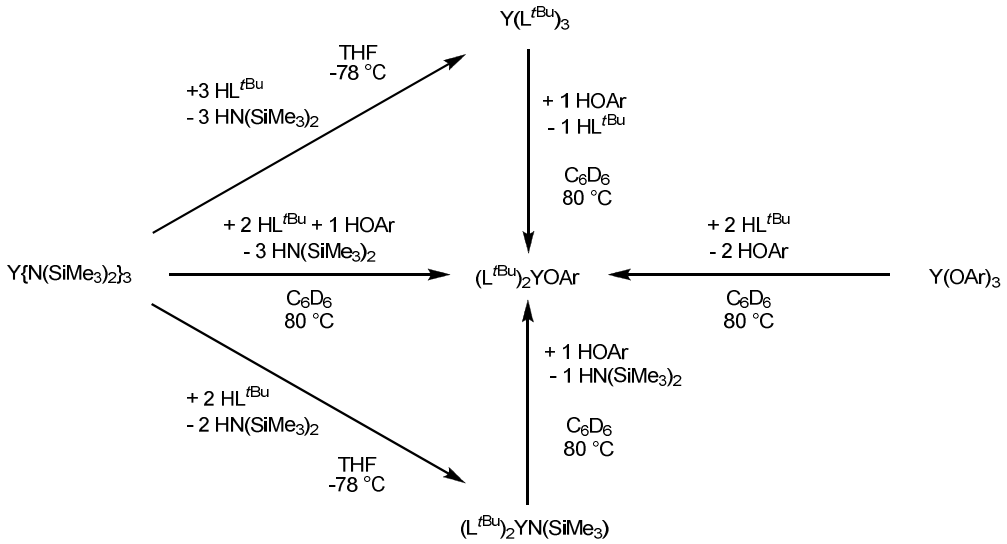

Scheme 2.4: Reactions of YN"$_3$ and Y(OAr)$_3$ to afford $(L^{tBu})_2Y(OAr)$

In all four routes, the extent of the homochirality of the product **$(L^{tBu})_2Y(OAr)$** is close to 85 %, suggesting that this a good combination of ligands for allowing the self-recognition of two L^{tBu} ligands into the *RR*/*SS*-diastereomers. Reactions of HOAr with $(L^{tBu})_2Y$- and $Y(L^{tBu})_3$ derivatives that were of 65 and 75 % homochiral

purity yielded $(L^{tBu})_2Y(OAr)$; products which were shown by NMR spectroscopy to be 85 % homochiral $(L^{tBu})_2Y(OAr)$. The data are summarised in Table 2.7.

Table 2.7: Summary of the stereochemical outcomes of the different synthetic routes to **$(L^{tBu})_2Y(OAr)$**.

Entry	YL_n starting material	Initial ratio *RR-SS/RS*	Initial ratio *RRR-SSS/RRS*	Final Ratio *RR-SS/RS*
1	$(L^{tBu})_2YN''$	65 / 35	--	85 / 15
2	$Y(L^{tBu})_3$	--	80 / 20	85 / 15
3	YN''_3	--	--	85 / 15
4	$Y(OAr)_3$	--	--	85 / 15

These data are clarified by the $^{31}P\{^1H\}$ NMR spectra which show the improvement of the homochiral purity in the complex **$(L^{tBu})_2Y(OAr)$** (Figure 2.24).

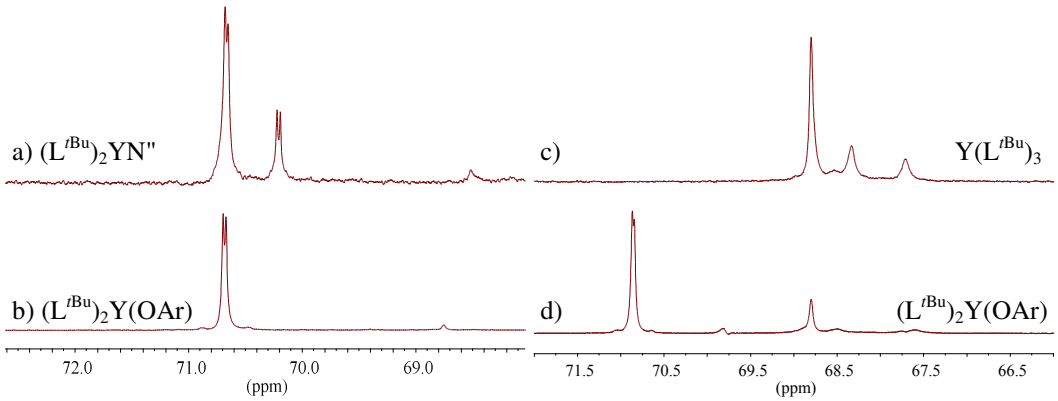

Figure 2.24: $^{31}P\{^1H\}$ NMR spectra illustrating Table 2.7, Entry 1 (a and b) and Entry 2 (c and d); a) $(L^{tBu})_2YN''$ and b) $(L^{tBu})_2Y(OAr)$, c) $Y(L^{tBu})_3$ and d) $(L^{tBu})_2Y(OAr)$.

These data provide further confirmation that the formation of homochiral lanthanide L^{tBu} adducts is under thermodynamic control and the homochiral arrangement of the L^{tBu} ligands affords the most stable conformation.

2.3.3.2 Synthesis and NMR spectral characterisation of $(L^R)_2In(OAr)$.

Heating a mixture of $(L^{tBu})_2InN''$ and one equivalent of ArOH at 80 °C for 16 hours afforded the complex $(L^{tBu})_2In(OAr)$ (Ar = 2,6-^{t}Bu-C_6H_3) after workup (Equation 2.8).

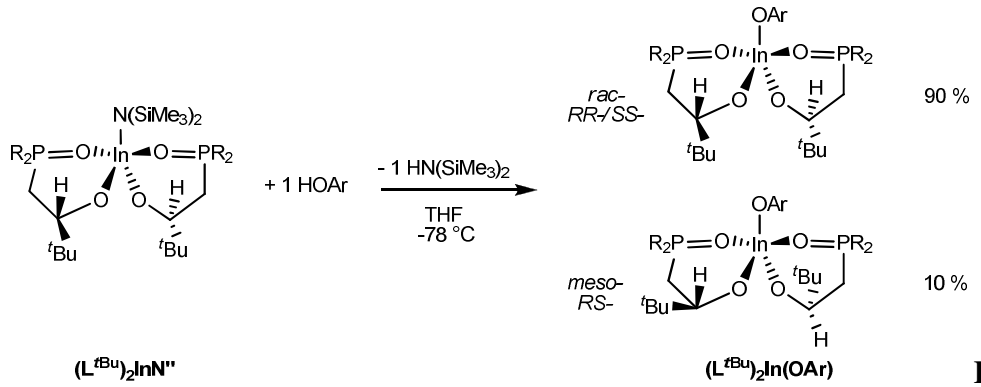

Eq. 2.8

The ^1H and $^{31}P\{^1H\}$ NMR spectra of $(L^{tBu})_2In(OAr)$ in d_6-benzene at room temperature display a single set of resonances for the *tert*-butyl groups, indicating that both ligands are equivalent. Comparison with spectra of *RR*-$(L^{tBu})_2In(OAr)$, made from *R*-HL^{tBu} show that 90 % of the sample is the homochiral *RR/SS*-$(L^{tBu})_2In(OAr)$ (Figure 2.25).

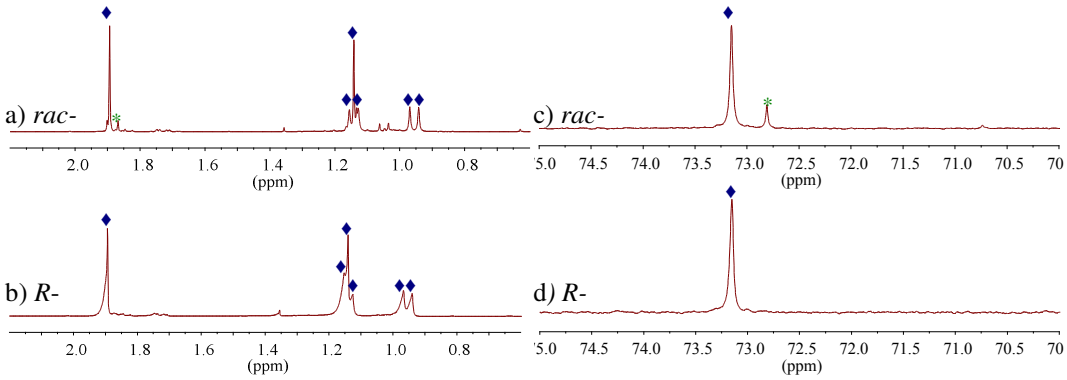

Figure 2.25: ^1H (expanded methyl region) and $^{31}P\{^1H\}$ NMR spectra of $(L^{tBu})_2In(OAr)$ and *R*-$(L^{tBu})_2In(OAr)$ (d_6-benzene), a) ^1H: $(L^{tBu})_2In(OAr)$, b) ^1H: *R*-$(L^{tBu})_2In(OAr)$, c) $^{31}P\{^1H\}$: $(L^{tBu})_2In(OAr)$ and d) $^{31}P\{^1H\}$: *R*-$(L^{tBu})_2In(OAr)$. ♦ denotes *RR/SS*-$(L^{tBu})_2In(OAr)$, * denotes *RS*-$(L^{tBu})_2In(OAr)$.

2.3.3.3 Synthesis and NMR spectral characterisation of $(L^R)_2In(OR')$

Reactions of $(L^{tBu})_2InN''$ with various alcohol R'OH (R' = ^{t}Bu, Bz, or $CH(CH_3)CO_2C(^tBu)$) were carried out for 16 hours at 80 °C in d_6-benzene (Equation 2.9).

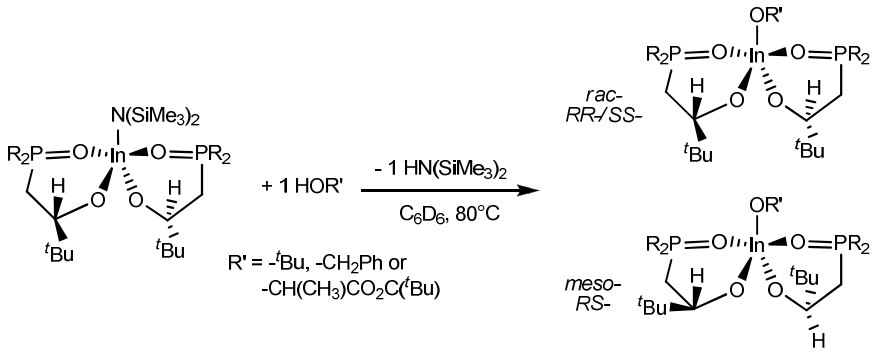

Eq. 2.9

Despite numerous attempts, the reaction of $(L^{tBu})_2InN''$ with one equivalent of benzyl alcohol only afforded decomposition products.

In an attempt to make an analogue of the initiating complex involved in the lactide polymerisation, a reaction between $(L^{tBu})_2InN''$ and *R-tert*-butyl lactate ($HOCH(CH_3)CO_2C(^tBu)$) was carried out but afforded no isolable products.

However, the reaction of $(L^{tBu})_2InN''$ with one equivalent of *tert*-butanol afforded the colourless solid **$(L^{tBu})_2In(O^tBu)$**. The ^1H and $^{31}P\{^1H\}$ NMR spectra of $(L^{tBu})_2In(O^tBu)$ shows resonances assigned to the homochiral isomers *RR/SS*-$(L^{tBu})_2In(O^tBu)$; this component of the mixture comprising approximately 90 % of the product (Figure 2.26).

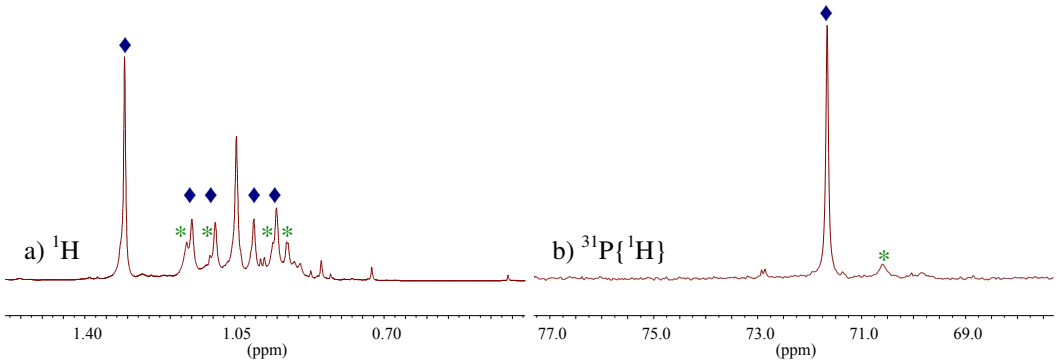

Figure 2.26: ^{1}H (methyl region) and ^{31}P{^{1}H} NMR spectra of $(L^{tBu})_2In(O^tBu)$ (d_6-benzene), a) ^{1}H: $(L^{tBu})_2In(O^tBu)$ and b) ^{31}P{^{1}H}: $(L^{tBu})_2In(O^tBu)$.

The reaction of one equivalent of $In(O^iPr)_3$ with two equivalents of *rac*-HL^{tBu} in d_6-benzene at 80 °C for 16 hours afforded mainly proligand *rac*-HL^{tBu}. There was a new resonance at 71 ppm in ^{31}P{^{1}H} NMR spectrum (region of $(L^{tBu})_2InX$ complexes). The solution was heated at 80 °C for several days but showed no further changes in the NMR spectrum, indicating that **$(L^{tBu})_2In(O^iPr)$** was not formed.

2.3.3.4 X-Ray crystal structures of aryloxo or alkoxo $(L^R)_2MX$ complexes

Colourless crystals of complexes **$(L^{tBu})_2Y(OAr)$** and **$(L^{tBu})_2In(OAr)$** suitable for a single crystal X-Ray diffraction study were grown from a hexanes solution. The molecular structures are depicted in Figure 2.27.

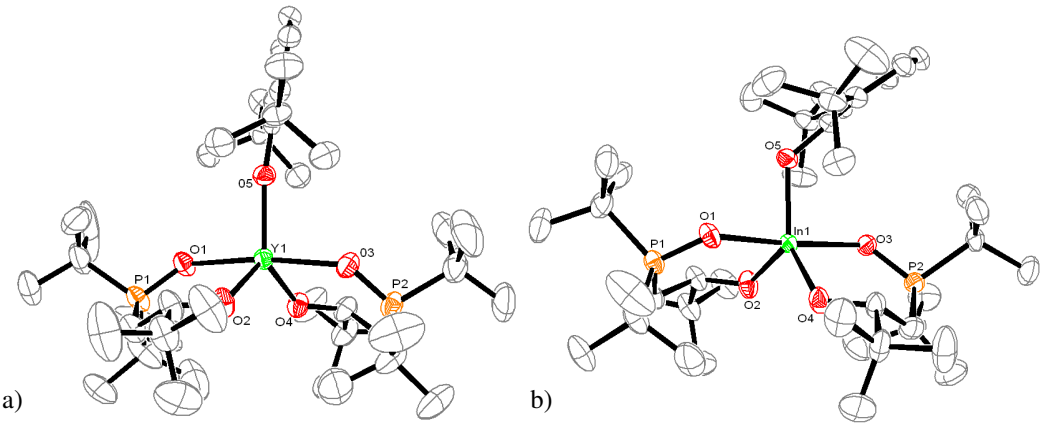

Figure 2.27: Displacement ellipsoid drawing of a) $(L^{tBu})_2Y(OAr)$ and b) $(L^{tBu})_2In(OAr)$, 50 % probability ellipsoids. All hydrogen atoms are omitted.

Selected distances (Å): (for $(L^{tBu})_2Y(OAr)$) Y1-O1: 2.264(3), Y1-O2: 2.108(3)), Y1-O5: 2.135(3); (for $(L^{tBu})_2In(OAr)$) In1-O1: 2.193(2), In1-O2: 2.037(2), In1-O5: 2.072(2); Selected angles (º): (for $(L^{tBu})_2Y(OAr)$) O3-Y1-O1: 172.25(10), O2-Y1-O4: 114.09(12), O4-Y1-O5: 125.83(11), O5-Y1-O2: 120.09(11), C29-O5-Y1: 171.6(2); (for $(L^{tBu})_2In(OAr)$) O3-In1-O1: 173.29(10), O2-In1-O4: 107.75(13), O4-In1-O5: 132.14(12).

The metal centre in each complex shows a distorted trigonal bipyramidal geometry, with the sterically demanding $^tBu_2PO$ groups opposite to each other in axial sites. The apical group occupies one equatorial site, the other two being occupied by the alkoxide groups of the ligand. The O-M-O angle formed by the two phosphine oxide ligating groups is close to linear in both (O3-Y1-O1 172.25° for $(L^{tBu})_2Y(OAr)$, O3-In1-O1 173.29° for $(L^{tBu})_2In(OAr)$).

The apical group and the two alkoxide-oxygens form a trigonal plane in each complex, with angles close to 120° (O2-Y1-O4 114.09°, O4-Y1-O5 125.83°, O2-Y1-O5 120.09° for $(L^{tBu})_2Y(OAr)$, O2-In1-O4 107.75°, O4-In1-O5 132.14°, O5-In1-O2 119.67° for $(L^{tBu})_2In(OAr)$). The aryloxide ligand is bent by a very large angle (C29-O5-In1: 129.3(2)º) for $(L^{tBu})_2In(OAr)$ compared to the angle in $(L^{tBu})_2Y(OAr)$ (C29-O5-Y1: 171.6(2)º). Space filling plots are shown in Figure 2.28.

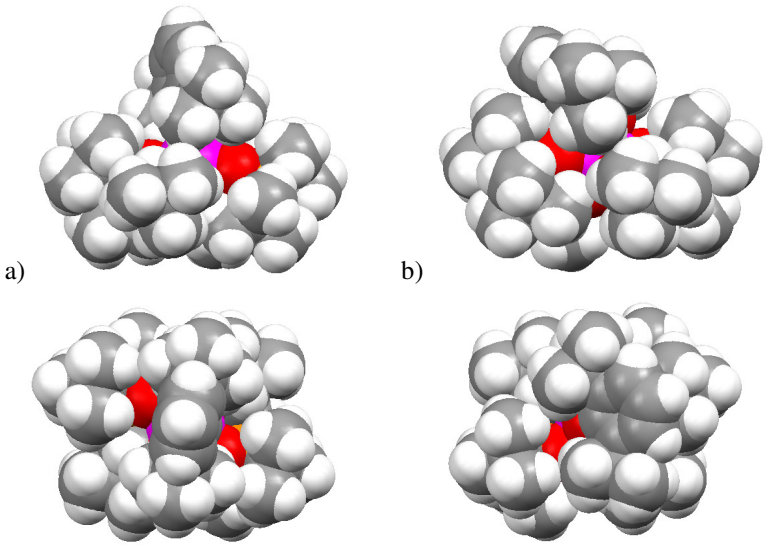

Figure 2.28: Space filling drawings of the molecular structures viewed from above the plane of the three alkoxides (above) and above the plane of the phosphine oxides

(below) for a) $(L^{tBu})_2Y(OAr)$, b) $(L^{tBu})_2In(OAr)$. Metal is coloured pink, oxygen red, phosphorus orange, carbon grey, hydrogen white.

2.3.4 Synthesis and characterisation of alkylo $(L^R)_2MX$ complexes

The reaction of $In(CH_2SiMe_3)_3$ and two equivalents of *rac*-HL^{tBu} in d_6-benzene at 80 °C for 16 hours afforded a mixture of **$(L^{tBu})_2In(CH_2SiMe_3)$** and **$(L^{tBu})In(CH_2SiMe_3)_2$** with a ratio of 75 : 25 respectively (Figure 2.29). Heating the solution at 80 °C over 5 days shows no further change and it was not possible to isolate pure $(L^{tBu})_2In(CH_2SiMe_3)$.

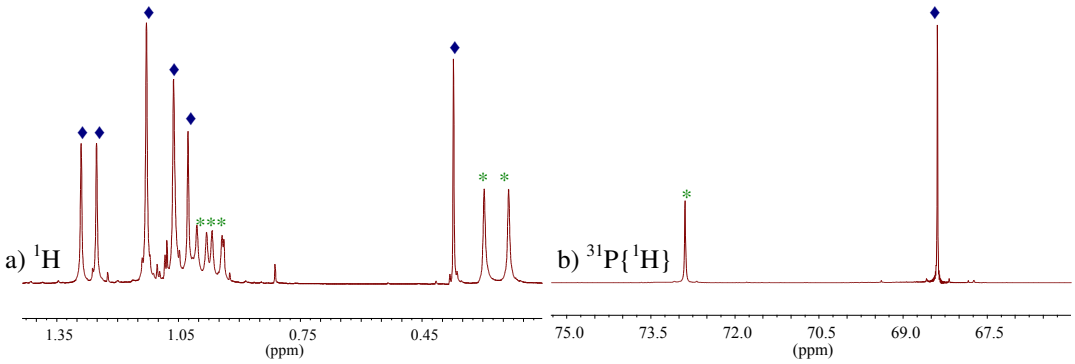

Figure 2.29: ^{1}H (expanded methyl region) and ^{31}P{^{1}H} NMR spectra of a mixture of $(L^{tBu})_2In(CH_2SiMe_3)$ and $(L^{tBu})In(CH_2SiMe_3)_2$ (d_6-benzene), a) ^{1}H and b) ^{31}P{^{1}H}. ♦ denotes $(L^{tBu})_2In(CH_2SiMe_3)$ and * denotes $(L^{tBu})In(CH_2SiMe_3)_2$

The reaction of one equivalent of $In(CH_2SiMe_3)_3$ and two equivalents of *rac*-HL^{Ph} in d_6-benzene at 80 °C for 16 hours afforded a mixture of starting materials and new products, which could not be isolated or identified.

2.3.5 Other reactions using $(L^R)_2MX$

The reaction of one equivalent of $(L^{tBu})_2InN"$ with one equivalent of $Eu(fod)_3$, acting as chiral agent, in d_6-benzene at 80 °C for 16 hours resulted in decomposition products.

The reaction of one equivalent of $(L^{tBu})_2InN''$ with one equivalent of 9-BBN (9-borabicyclo[3.3.1]nonane) in d_6-benzene at 80 °C for 16 hours reacted to form new products which decomposed and could not be isolated.

2.4 Synthesis of $(L^R)MX_2$

Reaction of MX_3 (X = $N(SiMe_3)_2$, Me or CH_2SiMe_3) with one equivalent of *rac*-HL^R afforded $(L^R)MX_2$ (Equation 2.10).

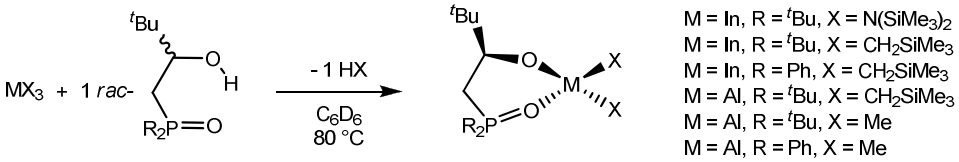

rac-HL^{tBu} $(L^{tBu})MX_2$ **Eq. 2.10**

2.4.1 Synthesis of $(L^{tBu})InX_2$

The reaction of InN''_3 with *rac*-HL^{tBu} in THF at -78 °C for one hour afforded $(L^{tBu})InN''_2$ as the major product (Figure 2.30).

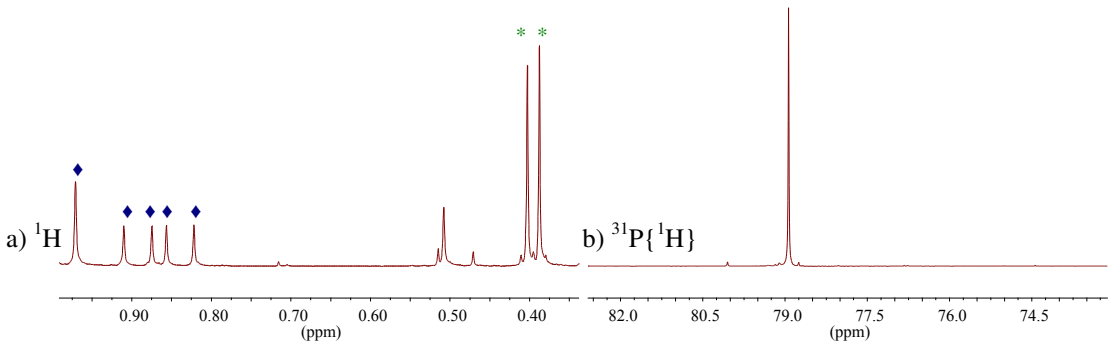

Figure 2.30: ^1H (expanded methyl region) and $^{31}P\{^1H\}$ NMR spectra of $(L^{tBu})InN''_2$ (d_6-benzene, a) ^1H, and b) $^{31}P\{^1H\}$, ♦ denotes ^{t}Bu group and * denotes Me group

It has not been possible to totally purify this product due to the constant presence of $(L^{tBu})_2InN''$ or InN''_3 in the mixture, which confirms that $(L^{tBu})_2InN''$ is the thermodynamic product as shown earlier (see section 2.3.2.1).

The reaction of $In(CH_2SiMe_3)_3$ with *rac*-HL^{tBu} in d_6-benzene at 80 °C for 16 hours afforded $(L^{tBu})In(CH_3SiMe_3)_2$ as a colourless solid (Figure 2.31).

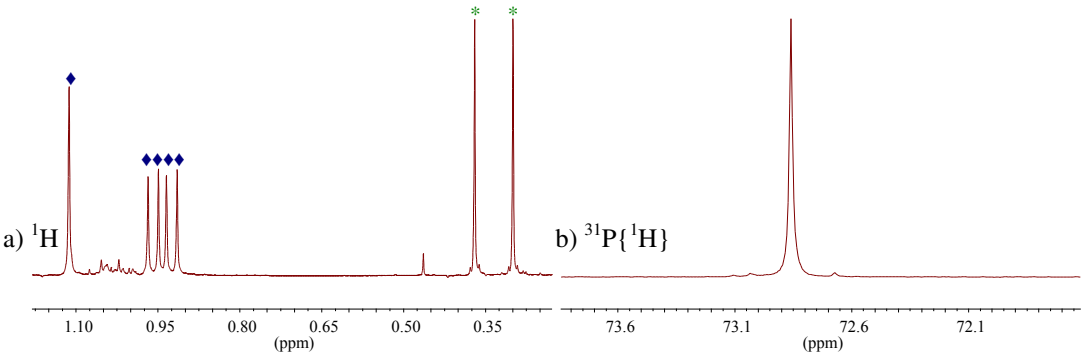

Figure 2.31: ^{1}H (expanded methyl region) and ^{31}P{^{1}H} NMR spectra of $(L^{tBu})In(CH_3SiMe_3)_2$ (d_6-benzene), a) ^{1}H and b) ^{31}P{^{1}H}. ♦ denotes ^{t}Bu group and * denotes Me group

2.4.2 Synthesis of $(L^R)AlX_2$

The reaction of $Al(CH_2SiMe_3)_3$ with *rac*-HL^{tBu} in d_6-benzene at 80 °C for 16 hours afforded $(L^{tBu})Al(CH_3SiMe_3)_2$ as a colourless solid (Figure 2.32).

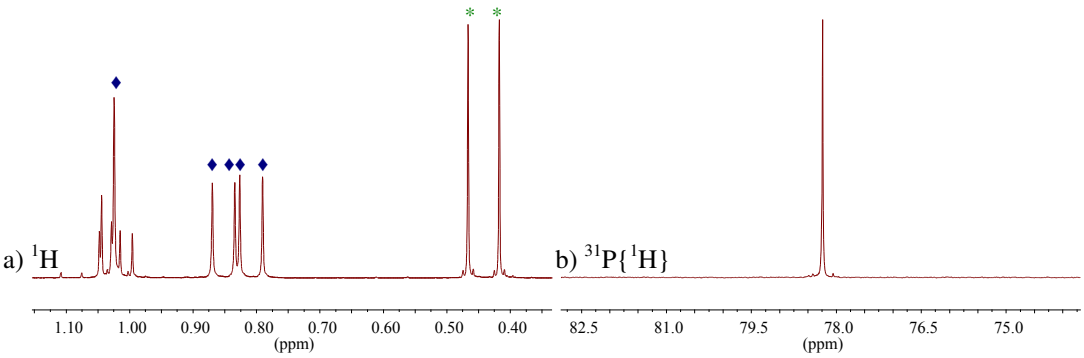

Figure 2.32: ^{1}H (expanded methyl region) and ^{31}P{^{1}H} NMR spectra of $(L^{tBu})Al(CH_3SiMe_3)_2$ (d_6-benzene), a) ^{1}H and b) ^{31}P{^{1}H}. ♦ denotes ^{t}Bu group and * denotes Me group

The reaction of $AlMe_3$ with *rac*-HL^R (R = ^{t}Bu or Ph) in d_6-benzene at 80 °C for 16 hours afforded $(L^R)Al(Me_3)_2$. The ^{1}H NMR spectra is consistent with a single ligand environment and two methyl groups. The ^{31}P{^{1}H} NMR spectra shows a singlet

resonance at 78.9 ppm for $(L^{tBu})AlMe_2$ and 51.0 ppm for $(L^{Ph})AlMe_2$. Mass spectrometry for $(L^{Ph})AlMe_2$ confirmed this result with a fragment peak of 100 % at m/z = 343 corresponding to $[M\text{-}Me]^+$.

Heating the solution of $(L^{Ph})AlMe_2$ in d_6-benzene over a period of 13 days at 80 °C resulted in the growth of a doublet in the $^{31}P\{^1H\}$ NMR spectrum at 40.0 ppm and a decrease of the singlet at 51.1 ppm; similarly, in the ^1H NMR spectrum, the doublet around -0.1 ppm (corresponding to methyl group in $(L^{Ph})AlMe_2$) decreases to be replaced by a singlet around 0.35 ppm (methyl group in $(L^{Ph})_2AlMe$). This compound was tentatively assigned to be $(L^{Ph})_2AlMe$.

A single crystal X-Ray diffraction study of $(L^{Ph})AlMe_2$ is shown in Figure 2.33 (crystals were grown by Dr. L. Postigo).

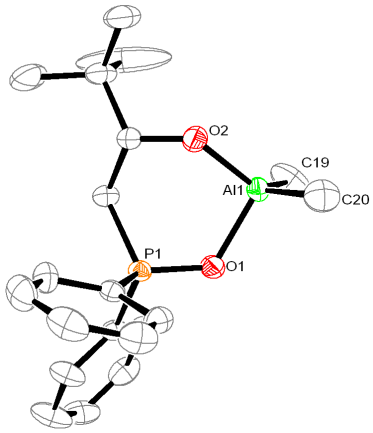

Figure 2.33: Displacement ellipsoid drawing of $(L^{Ph})AlMe_2$, 50 % probability ellipsoids. Lattice solvent and all hydrogen atoms omitted for clarity. Selected distances (Å) and angles (°): Al1-O1 1.865(2), Al1-O2 1.766(7), Al1-C19 1.951(3); and O2-Al1-O1 98.1(2), O1-Al1-C19 104.15(11), O2-Al1-C19 123.4(5).

The aluminium cation is in a tetrahedral geometry with O2-Al1-C19 angle close to 120° (123.4(5)°). The observed bond lengths of $(L^{Ph})AlMe_2$ are shorter than that reported by Pietrzykowski *et al*. (bond lengths give in brackets) where the aluminium complex is an dimer with bridging oxygens $[Me_2Al(\mu\text{-}OCH(Me)CH_2OtBu)]_2$; Al1-C19 1.951(3) Å (1.959(3) Å) and Al1-O2 1.766(7) Å (1.8298(17) Å).[30] Henderson

et al. also published an dimeric aluminium complex $[Al_4\text{-}(CH_3)_6(\mu^3\text{-}O)_2(\mu\text{-}\{Ph_2P(O)\}_2CH)_2]$.THF where the average Al-OP bond length is 1.777 and is smaller that Al1-O1 (1.865(2) Å).

2.5 Reactions of CO_2 using $(L^R)_2InX$

2.5.1 General background on CO_2 fixation with indium complexes

One of the first indications that CO_2 could be activated by indium was reported in the mid 1970s by Weidlein *et al.*, with the cleavage of one M-C bond in MR_3 by gaseous CO_2 (M = Al, Ga, In; R = Me, Et) to give $[R_2MOC(O)R]_n$ (M = Ga or In, n = 2; M = Al, n =3).[158] In the 1980s, Guilard *et al.* reported the insertion of CO_2 into the In-C bond of methylindium^{III} porphyrins, **D** (Equation 2.11), upon irradiation by visible light in dry benzene-pyridine media, leading to stable acetato complexes; reactions which were studied in more depth recently.[159, 160]

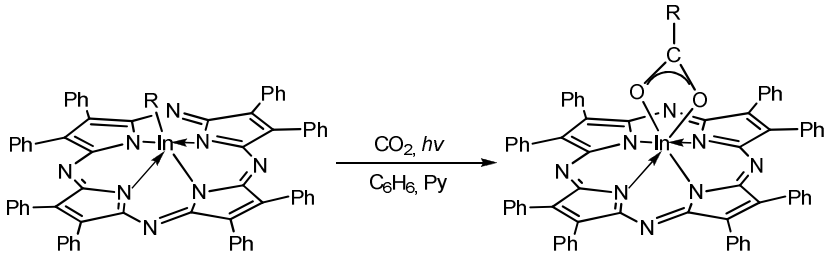

D **Eq 2.11**

2.5.2 CO_2 insertion in $(L^{tBu})_2InN''$

Heating a solution of $(L^{tBu})_2InN''$ with CO_2 at 80 °C for 16 hours did not afford the anticipated complex, $(L^{tBu})_2In(CO_2)N''$, a product of direct single insertion into the amide bond. After work-up, colourless solid crystalline $(L^{tBu})_2In(OSiMe_3)$ was isolated in a yield of 79 % (Scheme 2.5).

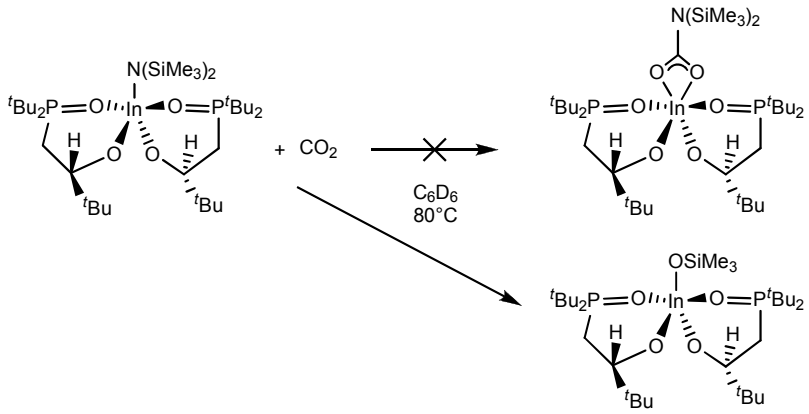

Scheme 2.5: Synthesis of $(L^{tBu})_2In(OSiMe_3)$

^1H and $^{31}P\{^1H\}$ NMR spectra of $(L^{tBu})_2In(OSiMe_3)$ are shown in Figure 2.34.

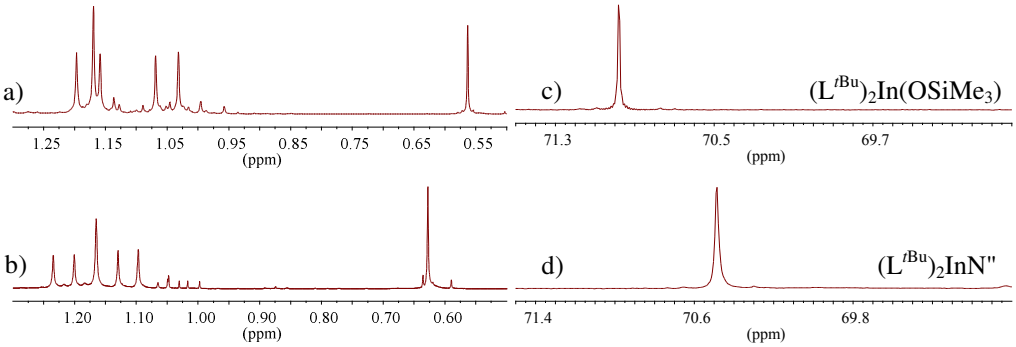

Figure 2.34: ^1H (expanded Me region) and $^{31}P\{^1H\}$ NMR spectra of $(L^{tBu})_2In(OSiMe_3)$ and $(L^{tBu})_2InN"$ (d_6-benzene), a) ^1H: $(L^{tBu})_2In(OSiMe_3)$ b) ^1H: $(L^{tBu})_2InN"$, c) $^{31}P\{^1H\}$: $(L^{tBu})_2In(OSiMe_3)$ and d) $^{31}P\{^1H\}$: $(L^{tBu})_2InN"$

The driving force of the reaction is likely to be the formation and release of the stable isocyanate, R-NCO. A mechanism for the reaction is suggested in Figure 2.35.

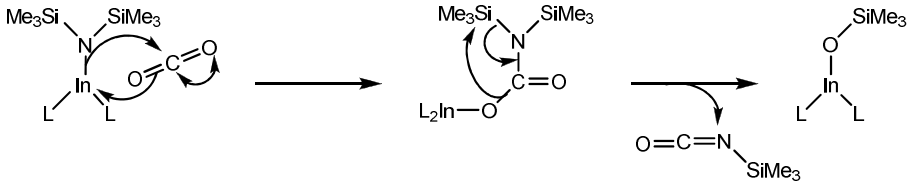

Figure 2.35: Proposed mechanism for the synthesis of $(L^{tBu})_2In(OSiMe_3)$

Enantiopure *R*-HL^{tBu} was also used in the synthesis of diastereomerically pure *RR*-$(L^{tBu})_2In(OSiMe_3)$. The ^1H and $^{31}P\{^1H\}$ NMR spectra of solutions of *RR*-$(L^{tBu})_2In(OSiMe_3)$ show a single ligand environment for *RR*-$(L^{tBu})_2In(OSiMe_3)$. NMR spectra of solutions of $(L^{tBu})_2In(OSiMe_3)$ show the same resonances assigned as the homochiral isomers *RR/SS*-$(L^{tBu})_2In(OSiMe_3)$ comprising 90 % of the product.

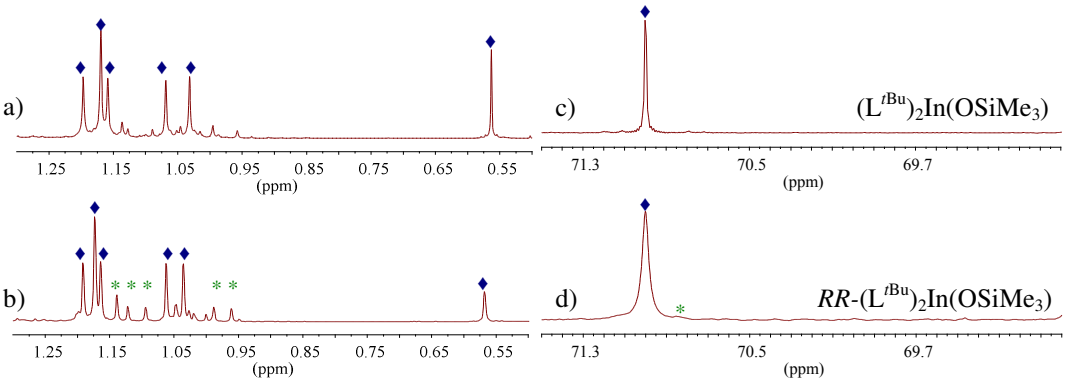

Figure 2.36: ^1H (Me region) and $^{31}P\{^1H\}$ NMR spectra of $(L^{tBu})_2In(OSiMe_3)$ and *R*-$(L^{tBu})_2In(OSiMe_3)$ (d_6-benzene), a) ^1H: $(L^{tBu})_2In(OSiMe_3)$, b) ^1H: *R*-$(L^{tBu})_2In(OSiMe_3)$, c) ^{31}P: of $(L^{tBu})_2In(OSiMe_3)$, and d) ^{31}P: *R*-$(L^{tBu})_2In(OSiMe_3)$. ♦ denotes *RR/SS*-$(L^{tBu})_2In(OSiMe_3)$, * denotes *RS*-$(L^{tBu})_2In(OSiMe_3)$

Colourless crystals of complex $(L^{tBu})_2In(OSiMe_3)$ suitable for a single crystal X-Ray diffraction study were grown from a hexanes solution. The molecular structures are depicted in Figure 2.37. The configuration of the molecule shown is *R*-$(L^{tBu})_2In(OSiMe_3)$.

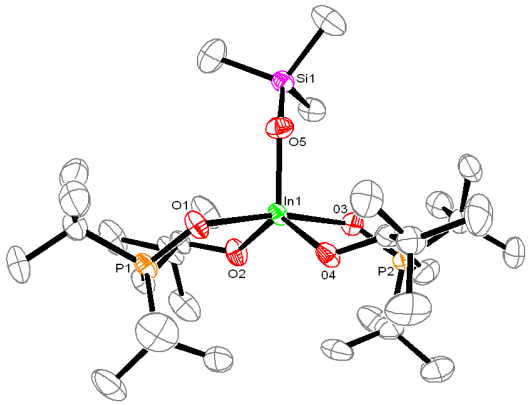

Figure 2.37: Displacement ellipsoid drawing of $(L^{tBu})_2In(OSiMe_3)$, 50 % probability ellipsoids. All hydrogen atoms are omitted. Selected distances (Å) and angles (°):

In1-O1: 2.202(3), In1-O2: 2.034(3)), In1-O5: 2.017(3), C29-Si1: 1.871(6), O5-Si1: 2.017(3). O3-In1-O1: 167.41(11), O2-In1-O4: 126.06(13), O4-In1-O5: 113.86(13), O5-In1-O2: 119.99(11), Si1-O5-In1: 134.04(19).

The metal center in complex $(L^{tBu})_2In(OSiMe_3)$ shows a distorted trigonal bipyramidal geometry, with the sterically demanding $^tBu_2PO$ groups opposite to each other in axial sites. The apical group occupies one equatorial site, the other two being occupied by the alkoxide groups of the ligand. The O-M-O angle formed by the two phosphine oxide ligating group is close to linear (O3-In1-O1 167.41).

The apical group and the two alkoxide-oxygens form a trigonal plane, with angles close to 120° (O2-In1-O4 126.06°, O4-In1-O5 113.86°, O2-In1-O5 119.99° for $(L^{tBu})_2In(OSiMe_3)$. The siloxane ligand is bent by a very large angle (Si1-O5-In1: 134.04(19)º) similar to that for $(L^{tBu})_2In(OAr)$ (C29-O5-In1: 129.3(2)º).

2.5.3 CO_2 insertion in $(L^{tBu})_2In(NPh_2)$

In an effort to further understand the reactivity of CO_2 into In−N amido bonds, the reactivity of $(L^{tBu})_2In(NPh_2)$ with CO_2 was also investigated (Equation 2.12).

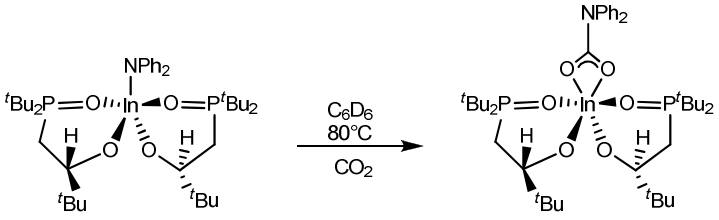

Eq. 2.12

The ^1H and $^{31}P\{^1H\}$ NMR spectra of solutions of $(L^{tBu})_2In(O_2CNPh_2)$ show resonances assigned as 95 % of the homochiral product, *RR/SS*-$(L^{tBu})_2In(O_2CNPh_2)$, and 5 % of *RS*-$(L^{tBu})_2In(O_2CNPh_2)$. This indicates that insertion of CO_2 in $(L^{tBu})_2In(NPh_2)$ increases the resulting homochiral purity ($(L^{tBu})_2In(NPh_2)$ has a purity of 80 %) (Figure 2.38).

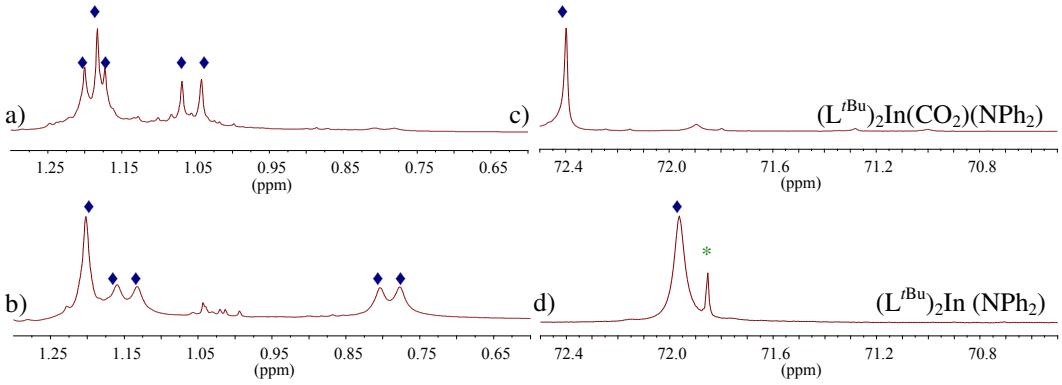

Figure 2.38: ^{1}H and $^{31}P\{^{1}H\}$ NMR spectra of $(L^{tBu})_2In(O_2CNPh_2)$ and $(L^{tBu})_2In(NPh_2)$ (d_6-benzene), a) ^{1}H: $(L^{tBu})_2In(O_2CNPh_2)$, b) ^{1}H: $(L^{tBu})_2In(NPh_2)$, c) $^{31}P\{^{1}H\}$: $(L^{tBu})_2In(O_2CNPh_2)$ and d) $^{31}P\{^{1}H\}$: $(L^{tBu})_2In(NPh_2)$, ♦ denotes *RR/SS* homochiral and denotes **RS*- meso

Colourless crystals of complex $(L^{tBu})_2In(O_2CNPh_2)$ suitable for a single crystal X-Ray diffraction study were grown from evaporation of a DME/hexanes solution.

The molecular structure is depicted in Figure 2.39. The configuration of the molecules shown is *S*-$(L^{tBu})_2In(O_2CNPh_2)$.

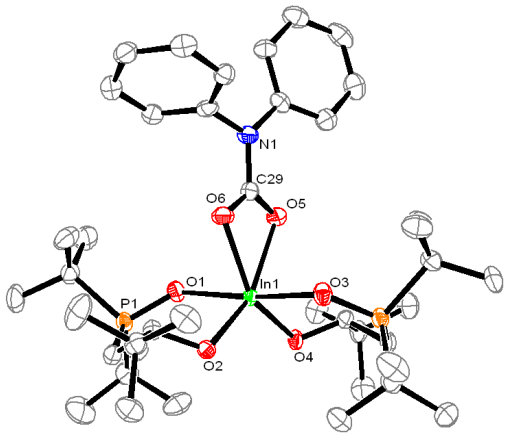

Figure 2.39: Displacement ellipsoid drawing of $(L^{tBu})_2In(O_2CNPh_2)$ 50 % probability ellipsoids. All hydrogen atoms are omitted. Selected distances (Å) and angles (º) for $(L^{tBu})_2In(O_2CNPh_2)$: In1-O1: 2.218(10), In1-O2: 2.045(9), In1-O5: 2.252(9), In1-O6: 2.305 (11); O3-In1-O1: 171.9(9), O2-In1-O4: 110.5(4), O6-C29-O5: 122.1(14), O6-C29-N1: 115.3, O6-In1-O5: 57.6(4)

The coordination geometry of the metal in $(L^{tBu})_2In(O_2CNPh_2)$ complex is distorted octahedral with the angle of O3-In1-O1 close to 180º (171.9(9) º). The bond lengths of In1-OP (2.218(10) Å) and In1-OR (2.045(9) Å) are longer than those in $(L^{tBu})_2In(NPh_2)$, 2.174(3) Å and 2.038(3) Å respectively.

2.6 Conclusion

In conclusion, the racemic phosphine oxide-alkoxide ligand *rac*-HL^R (where R = ^{t}Bu, Ph or Ar) is resolved into the enantiomer *RRR/SSS*-$M(L^R)_3$ complexes of trivalent cations, Sc^{III}, Lu^{III}, Y^{III}, In^{III}, Bi^{III}, or La^{III} to afford a racemic mixture of homochiral C_3–symmetric $M(L^R)_3$ complexes with varying amounts of diastereomeric index (55 % for *rac*-$Sc(L^{tBu})_3$, 90 % for *rac*-$Sc(L^{Ph})_3$, 100 % for *rac*-$In(L^{tBu})_3$, 75 % for *rac*-$In(L^{Ph})_3$, 65 % for *rac*-$Lu(L^{tBu})_3$, 65 % for *rac*-$Lu(L^{Ph})_3$, 80 % for *rac*-$Y(L^{tBu})_3$, 60 % for *rac*-$Y(L^{Ph})_3$, 75 % for *rac*-$Y(L^{Ar})_3$, 30 % for *rac*-$Bi(L^{tBu})_3$, 20 % for *rac*-$Bi(L^{Ph})_3$, 40 % for *rac*-$La(L^{tBu})_3$).

It has been shown that this resolution is under thermodynamic control and driven by a ligand self-recognition process. The isolation of *bis*(L^R) adducts $(L^R)_2MX$ in which the third anion X is large (where X = $N(SiMe_3)_2$ or O-C_3H_6-^{t}Bu-2,6), has also shown that homochiral $(L^R)_2$ complexes can be isolated but less easily as $M(L^R)_3$ are the thermodynamic product.

Complexes $(L^R)_2MX$ (where M = Al or In and X = $N(SiMe_3)_2$, CH_2SiMe_3 or Me) have been synthesised.

Reaction of CO_2 with a In-N (amide) have been proposed for the complexes $(L^{tBu})_2In\{N(SiMe_3)_2\}$ and $(L^{tBu})_2M(NPh_2)$.

[1] R. S. Tanke, E. M. Holt, R. H. Crabtree, *Inorg. Chem.* **2002**, *30*, 1714.
[2] R. J. Cross, L. J. Farrugia, P. D. Newman, R. D. Peacock, D. Stirling, *J. Chem. Soc., Dalton Trans.* **1996**, 1637.
[3] R. J. Cross, P. D. Newman, R. D. Peacock, D. Stirling, *J. Mol. Cat. A* **1999**, *144*, 273.
[4] D. G. Genov, R. A. Kresinski, J. C. Tebby, *J. Org. Chem.* **1998**, *63*, 2574.
[5] Y. G. Shermolovich, A. V. Solov'ev, N. P. Kolesnik, L. N. Markovskii, *Zh. Obshch. Khim.* **1989**, *59*, 523.
[6] P. Arnold, (The University of Nottingham, UK). Application: WO 2007/148136 A2, **2007**, p. 51pp.
[7] P. L. Arnold, J.-C. Buffet, R. P. Blaudeck, S. Sujecki, A. J. Blake, C. Wilson, *Angew. Chem., Int. Ed.* **2008**, *47*, 6033.
[8] R. P. Blaudeck, *PhD Thesis* **2007***,* University of Nottingham.
[9] M. I. Ali, *PhD Thesis* **2009,** University of Edinburgh.
[10] A. L. Casalnuovo, T. V. RajanBabu, T. A. Ayers, T. H. Warren, *J. Am. Chem. Soc.* **2002**, *116*, 9869.
[11] L. A. van der Veen, P. C. J. Kamer, P. W. N. M. van Leeuwen, *Organometallics* **1999**, *18*, 4765.
[12] S. E. Gorringe, *MSc Thesis* **2009***,* University of Edinburgh.
[13] H. C. Aspinall, *Chem. Rev.* **2002**, *102*, 1807.
[14] M. Shibasaki, H. Sasai, T. Arai, *Angew. Chem., Int. Ed.* **1997**, *36*, 1236.
[15] M. Shibasaki, H. Sasai, T. Arai, T. Lida, *Pure Appl. Chem.* **1998**, *70*, 1027.
[16] H. C. Aspinall, J. F. Bickley, J. L. M. Dwyer, N. Greeves, R. V. Kelly, A. Steiner, *Organometallics* **2000**, *19*, 5416.
[17] L. H. Gade, S. Bellemin-Laponnaz, *Chem. Eur. J.* **2008**, *14*, 4142.
[18] M. A. Masood, J. E. Eric, T. D. P. Stack, *Angew. Chem., Int. Ed.* **1998**, *37*, 928.
[19] J. Gregolinski, P. Starynowicz, K. T. Hua, J. L. Lunkley, G. Muller, J. Lisowski, *J. Am. Chem. Soc.* **2008**, *130*, 17761.
[20] P. L. Arnold, J.-C. Buffet, R. P. Blaudeck, S. Sujecki, C. Wilson, *Chem. Eur. J.* **2009**, *15*, 8241.
[21] H. C. Aspinall, J. L. M. Dwyer, N. Greeves, A. Steiner, *Organometallics* **1999**, *18*, 1366.
[22] L. Armelao, G. Bandoli, M. Casarin, G. Depaoli, E. Tondello, A. Vittadini, *Inorg. Chim. Acta* **1998**, *275-276*, 340.
[23] M. Mehring, C. Low, M. Schurmann, F. Uhlig, K. Jurkschat, B. Mahieu, *Organometallics* **2000**, *19*, 4613.
[24] S. Chitsaz, B. Neumuller, *Organometallics* **2001**, *20*, 2338.
[25] J. Pauls, S. Chitsaz, B. Neumüller, *Z. Anorg. Allg. Chem.* **2000**, *626*, 2028.
[26] J. Eppinger, M. Spiegler, W. Hieringer, W. A. Herrmann, R. Anwander, *J. Am. Chem. Soc.* **2000**, *122*, 3080.
[27] Q. Wang, L. Xiang, H. Song, G. Zi, *Inorg. Chem.* **2008**, *47*, 4319.
[28] L. Lee, D. J. Berg, G. W. Bushnell, *Inorg. Chem.* **1994**, *33*, 5302.
[29] J. Marçalo, A. P. De Matos, *Polyhedron* **1989**, *8*, 2431.

[30] A. Pietrzykowski, T. Skrok, S. Pasynkiewicz, M. Brzoska-Mizgalski, J. Zachara, R. Anulewicz-Ostrowska, K. Suwinska, L. B. Jerzykiewicz, *Inorg. Chim. Acta* **2002**, *334*, 385.
[31] M. Mehring, C. Low, M. Schurmann, F. Uhlig, K. Jurkschat, B. Mahieu, *Organometallics* **2000**, *19*, 4613
[32] D. Mansfeld, M. Mehring, M. Schurmann, *Inorg. Chim. Acta* **2003**, *348*, 82
[33] A. J. Wooten, P. J. Carroll, P. J. Walsh, *J. Am. Chem. Soc.* **2008***, 130*, 7407

Chapter 3: Polymerisation using M^{III} complexes

3.1 Introduction

The conversion of a racemic mixture of lactide monomer into a racemic mixture of two homochiral lactide polymers presents a suitable challenge for the complexes described in Chapter 2. The physical properties of polylactides are strongly dependent on their stereochemical composition; melting and glass-transition temperatures have been used to characterise the stereoregularity of polylactides. When independently-made poly[(*R*)-(lactic acid)] and poly[(*S*)-(lactic acid)] are mixed, the chains co-crystallise to form a stereocomplex with a melting point of up to 230 °C (50 °C higher than simple poly[(*S*)-(lactic acid)]).[1, 2] Stereoregular crystalline polylactides retain their mechanical properties near melting point and thus have higher usable temperatures than amorphous atactic polymers. High-melting polylactides are attractive targets for a wide variety of new applications, provided their preparation is achievable through efficient and inexpensive processes.

A one-pot catalytic process in which a racemic mixture of a chiral catalyst polymerises *R,R*-lactide and *S,S*-lactide monomers separately into two enantiomerically-pure isotactic polymer chains, which can then mix to form a stereocomplex, is an important goal.[3] Currently, highly selective single-site catalysts based on the Al-salen framework have been shown to form predominantly stereoblock polylactide, in which the long alternating chains of ~~(~~RRRRRR~~)~~$_n$ and ~~(~~SSSSSS~~)~~$_n$ PLA subsequently form stereocomplex PLA with a melting point up to 196 °C.[4-7] Both single-site [LLn(OR)] and homoleptic [$Ln(OR)_3$] lanthanide alkoxides have previously been shown to be excellent initiators for the synthesis of PLA, but normally produce heterotactic polymer.[8, 9]

It is of interest to identify if the *rac*-$M(L^R)_3$, $(L^R)_2MX$ and $(L^R)MX_2$ complexes can firstly act as stereoselective initiators, and secondly, can provide the correct environment for tacticity control of the polymerisation reaction.

3.2 Polymerisation of *rac*-lactide using *rac*-M(L^R)$_3$

3.2.1 Polymerisation of *rac*-lactide using *rac*-Y(L^{tBu})$_3$

Previously published polylactide synthesised using complexes *rac*-Ln(L^{tBu})$_3$ (M = Y and Er),[10] showed that, even at -18 ºC, polymerisation is rapid (50 % of monomer consumed in 4 minutes) and controlled. The polymer weights were high (above 150 000 g/mol at full conversion) and the polydispersities (PDI) of the polymers were narrow (1.2-1.4). The most notable property of these polymers was their high crystallinity and stereoregularity (around 70-80 %) but none of the polymerisations resulted in polymer crystallinity above 80 %; a property thought to result in very high melting points.

A new series of polymerisations have been carried out in order to increase the stereoregularity of the polymers produced. Complex *rac*-Y(L^{tBu})$_3$ was tested further as an initiator for the polymerisation of *rac*-lactide (Equation 3.1).

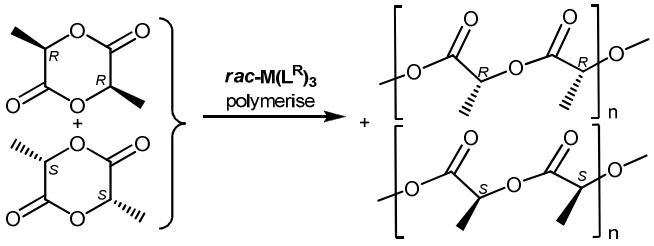

Eq. 3.1

A solution of *rac*-Y(L^{tBu})$_3$, in DCM, was added to a solution of *rac*-lactide in DCM; the polymerisation conditions and results are collated in Table 3.1.

Table 3.1: Polymerisation data of *rac*-lactide using *rac*-Y(L^{tBu})$_3$

Entry	Cat:Monomer:Solvent ratio (mole)[b]	T / °C	Time / min	Conv.[c] / %	Pi[d]
1[a]	1 : 1212 : 10 000	- 18	10	90	0.81
2[a]	1 : 606 : 10 000	- 18	8	90	0.78
3	1 : 100 : 10 000	- 18	6	> 99	> 99
4	1 : 100 : 10 000	- 10	3	> 99	> 99

a: previous published results[10]; b: solvent = DCM; c: conversion of LA monomer (($[LA]_0$-[LA])/$[LA]_0$); d: Probability of forming a new *i* dyad, determined by ^{1}H NMR spectroscopy.[11]

At -18 °C, all polymerisations are rapid and high conversion is attained in less than 10 minutes. The time of polymerisation decreases as the monomer : solvent ratio does (1212 : 10 000, 10 minutes, Entry 1 and 100 : 10 000, 6 minutes, Entry 3) and is inversely proportional to the temperature of polymerisation (-18 °C, 10 minutes, Entry 3 and -10 °C, 3 minutes, Entry 4).

The data suggest that the catalyst : monomer ratio (1212 : 10 000, Entry 1 and 606 : 10 000, Entry 2, results obtained by Dr. R. Blaudeck) does not affect the isotacticity. However, an increase in the dilution of the polymerisation results in an dramatic increase in the isotacticity of the polylactide (1212 : 10 000, *iii* = 81 %, Entry 1 and 100 : 10 000, *iii* > 99 %, Entry 3). Therefore high dilution conditions in this system is a requirement to obtain high isotacticity.

The formation of a predominantly isotactic polymer, *i.e.* polymerisation of the *R*- and *S*-lactide monomers in parallel, is confirmed by ^{1}H and $^{13}C\{^{1}H\}$ NMR spectroscopy.

The proton decoupled $^{1}H\{^{1}H\}$ NMR spectrum of an isotactic polymer chain should look like that of poly-*S*-lactide or poly-*R*-lactide, with a single C*H*Me resonance (if the chains are infinitely long). If the polymerisation is less selective, or transesterification becomes a competing reaction at higher conversions, the original stereochemical control will be lost and will show the different C*H* environments.

Figure 3.1 a) shows the methine region of $^{1}H\{^{1}H\}$ NMR spectra of the polymer obtained using *rac*-Y(L^{tBu})$_3$ (Entry 1, *iii* = 81 %, result previously obtained by Dr. R. Blaudeck).

Figure 3.1 b) (Entry 3, *iii* > 99 %) and Figure 3.1 c) (Entry 4, *iii* > 99 %) show the dominance of the *iii* tetrad in the polymer made recently by *rac*-Y(L^{tBu})$_3$ from *rac*-lactide at complete conversion. This confirms the stereospecific control of the polymerisation of *D*- and *L*-lactide into separate, isotactic chains.

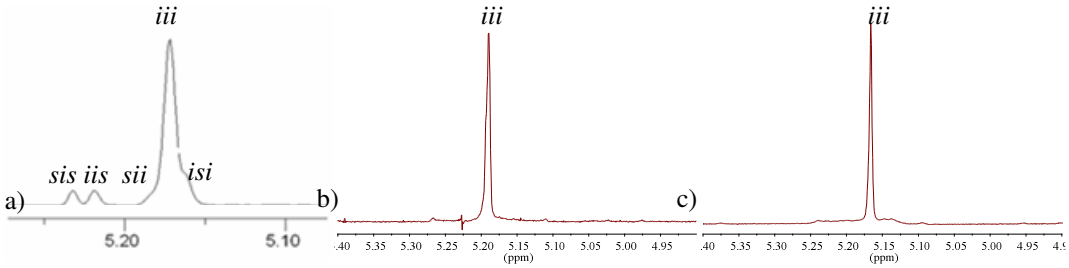

Figure 3.1: Methine region of homonuclear decoupled ^{1}H NMR spectra of isotactic PLA, Table 3.1 a) Entry 1, *iii* = 81 %, with tetrad resonances arising from insertion errors assigned, b) Entry 3, *iii* > 99 %, c) Entry 4, *iii* > 99 %.

The most desirable tetrad represents isotactic polymer (*iii*) with the smaller tetrad resonances characteristic of the polymer defects. The ratio of the defect sizes should be 1 : 2 : 1 : 1 corresponding to *iis* : *isi* : *sis* : *sii*. This ratio is only possible for a chain of the stereochemical composition -*RRRRRRSSRRRRRR*- (and *vice versa*) containing single insertion defects. This type of polymer is most able to form stereocomplex upon annealing and so the formation of high melting polymers may be possible for this system. If the polymer chains were stereoblock, of the form *RRRRRRSSSSSSRRRRRR*-, the ratio of defect resonances should be 1 : 1 : 1 corresponding to *iis* : *isi* : *sii*, with the *sis* resonance absent. This type of polymer reflects a lower degree of stereocontrol and is not observed for this system. Although it is still possible to form a stereocomplex from such a polymer, it is less likely.

Analysis of the kinetics of the reaction suggest that no transesterifications occurred (Figure 3.2). In Figure 3.2 a) (polymerisation conditions: 1 : 100 : 10 000, -18 °C, Entry 3) and Figure 3.2 b) (1 : 100 : 10 000, -10 °C, Entry 4), the ^{1}H NMR spectra show that the polylactide attains full conversion only after 15 and 20 seconds respectively. Temperature has an effect on the tacticity; new resonances, characteristic of traces of polymer defects are visible from 1.5 minutes onwards as shown in Figure 3.2 b) (-10 °C, Entry 4, Table 3.1) but even after 10 minutes, the polylactide synthesis remains controlled, shown in Figure 3.2 a) (-18 °C, Entry 3, Table 3.1). This shows that greater tacticity control is possible at lower temperature.

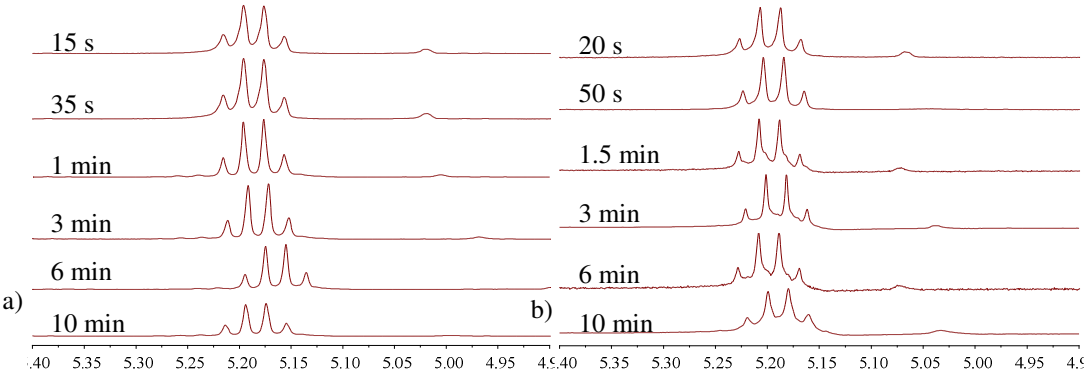

Figure 3.2: Kinetics of the polymerisation of *rac*-lactide using *rac*-Y(L^{tBu})$_3$. Methine region of ^{1}H NMR spectra of polymerisation using conditions as in a) Table 3.1 Entry 3, -18 °C b) Table 3.1 Entry 4, -10 °C.

A study of various molecular weights of the polylactides synthesised from *rac*-Y(L^{tBu})$_3$ are collated in Table 3.2.

Table 3.2: Polymerisation data of *rac*-lactide using *rac*-Y(L^{tBu})$_3$

Entry	Cat:monomer: solvent ratio	T / °C	Time / min	Conv.[c] / %	$M_{n,exp}$[d] g/mol	$M_{n,theo}$[e] g/mol	M_w/M_n[f]
1	1 : 2421 : 10 000[b]	- 20	6	> 99	145 000	349 196	1.95
2	1 : 1211 : 10000[a]	- 20	6	> 99	87 000	174 598	1.27
3	1 : 605 : 10000[a]	- 20	6	> 99	104 500	87 299	1.22

a: solvent = THF; b: solvent = DCM; c: conversion of LA monomer (($[LA]_0$-[LA])/$[LA]_0$); d: measured by GPC, values based on polystyrene standards, weight corrected by multiplication by 0.58 [Mark-Houwink equation]; e: Molecular weight theoretical calculated using $M_{n,\ theo}$ = Conv. × [Mono]/[Cat] × M_{Mono}; f: polydispersity index (M_w/M_n), PDI, measured by GPC.

The main feature of Table 3.2 is the dramatic decrease of the polydispersity with decreasing monomer : solvent ratio (PDI = 1.95 with 2421 : 10 000, Entry 1) and (PDI = 1.22 with 605 : 10 000, Entry 3).

These results show that the polymerisation is faster and the molecular weights are higher than those reported by Tolman *et al.*. Here, with a catalyst : monomer ratio of 1 : 150, the polymerisation with a dimeric yttrium alkoxide complex needed 48 hours

to attain 88 % conversion with M_n of 20 900 g/mol.[12] These results are similar to those published by Duda *et al.* using yttrium *tris*-isopropoxyethoxide and by Tolman *et al.* using a Y^{III} complex of *N,-bis*(trimethylsilyl)benzamidinate (**A**, Figure 3.3), M_n (20000 - 40 000), PDI (1.2 - 1.5).[13, 14]

However, Carpentier *et al.* reported $[Box]_2Y[N(SiHMe_2)_2]$ (**B**, Figure 3.3) which polymerised *rac*-lactide with catalyst : monomer ratio of 1 : 1000 (M_n of 144 000 g/mol and PDI of 1.24) and with a catalyst : monomer ratio of 1 : 2000 (M_n of 273 600 g/mol and PDI of 1.37).[15]

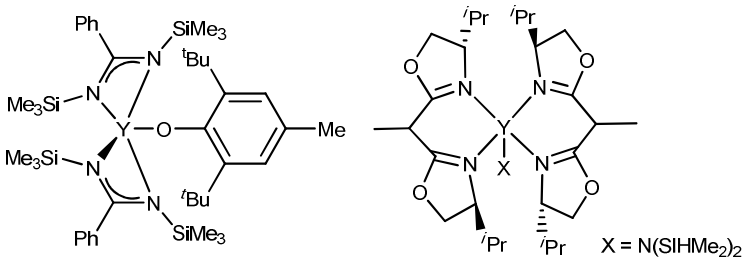

A **B**

Figure 3.3: Y^{III} *N,*-bis(trimethylsilyl)benzamidinate **A**, $[Box]_2Y[N(SiHMe_2)_2]$ **B**

The GPC traces of polymerisation of *rac*-lactide using *rac*-$Y(L^{tBu})_3$ showed a poor control of the polymerisation under Table 3.2 conditions, confirming the importance of high dilution of the *rac*-lactide in dichloromethane (Figure 3.4).

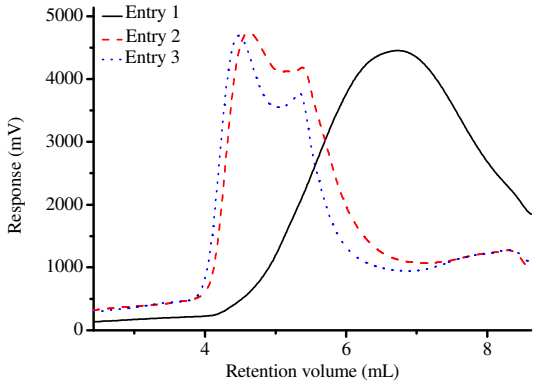

Figure 3.4: GPC chromatogram traces of polylactide synthesised using *rac*-$Y(L^{tBu})_3$, Table 3.2, Entry 1-3.

3.2.2 Polymerisation of *rac*-lactide using *rac*-Y(L^{Ph}) and *rac*-Y(L^{Ar})

The ligands around the yttrium centre were varied in order to understand how changes in stereoelectronics and homochiral purity of the rac-Y(L^R)$_3$ complex affects the isotacticity of the resultant polymerisations.

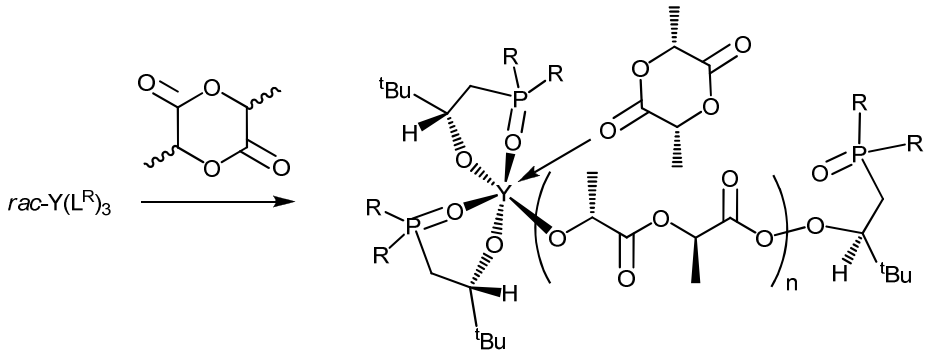

Figure 3.5: Coordination-insertion mechanism using *rac*-Y(L^R)$_3$

The data of the polymerisation study of *rac*-lactide using *rac*-Y(L^{Ph})$_3$ or *rac*-Y(L^{Ar})$_3$ are collated in Table 3.3.

Table 3.3: Polymerisation data of *rac*-lactide using *rac*-Y(L^{Ph})$_3$ and *rac*-Y(L^{Ar})$_3$

Entry	Cat:Monomer:Solvent ratio	T / °C	Time / min	Conv.[e] / %	Pi[f]
1[a]	1 : 100 : 10 000[c]	- 40	10	> 99	> 0.99
2[a]	1 : 100 : 10 000[c]	- 20	3	> 99	0.94
3[a]	1 : 100 : 10 000[c]	- 20	6	> 99	0.92
4[a]	1 : 100 : 10 000[c]	- 18	6	> 99	> 0.99
5[a]	1 : 200 : 10 000[c]	- 10	3	83	0.93
6[a]	1 : 1358 : 1 000[d]	0	1	> 99	0.74 (h)[g]
7[a]	1 : 679 : 1 000[d]	0	1	> 99	0.63 (h)[g]
8[a]	1 : 200 : 10 000[d]	0	0.5	> 99	atactic
9[a]	1 : 200 : 10 000[d]	0	1	> 99	0.40
10[a]	1 : 1377 : 1 000[d]	25	2	> 99	atactic
11[b]	1 : 1611 : 1 000[d]	25	1	> 99	atactic

a: using *rac*-Y(L^{Ph})$_3$; b: using *rac*-Y(L^{Ar})$_3$; c: solvent = DCM; d: solvent = THF, e: conversion of LA monomer (([LA]$_0$-[LA])/[LA]$_0$); f: Probability of forming a new *i* dyad; g: heterotactic.

The time required for complete conversion of 100 or 200 equivalents of lactide for all of the initiators, was less than 10 minutes. These times compare with the fastest yttrium initiators in the literature.[16-19] However, caution should be applied on analysing such rapid polymerisations using single point kinetic data as the precise end-point is difficult to determine.[20-24] It is possible to obtain very high isotacticity using each *rac*-$Y(L^R)_3$; comparison with the literature shows that Carpentier *et al.* reported 71 % *iso*-tactic enriched PLA from an enantiopure single-site Y^{III} initiator with a bulky C_2-symmetric diamido ligand (catalyst : monomer ratio of 1 : 200).[19]

At equivalent catalyst : monomer : solvent ratios, an increase in temperature results in a decrease in the polymerisation time needed to attain full conversion but a similar very high isotacticity (Table 3.3, Entry 1 to 5), (Figure 3.5).

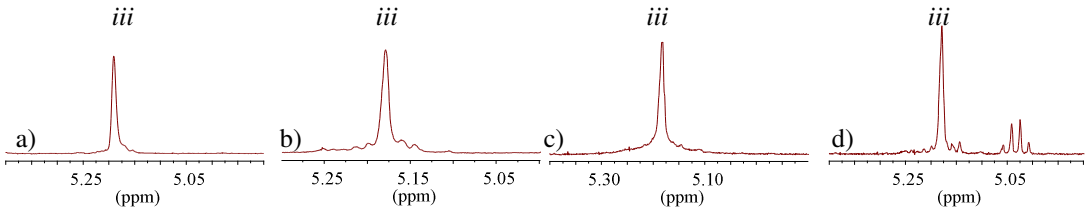

Figure 3.6: Methine region of homonuclear decoupled ^{1}H NMR spectra of isotactic PLA, Table 3.3 a) Entry 1, b) Entry 3, c) Entry 4, d) Entry 5.

A change in the solvent from dichloromethane to THF has a dramatic effect on the control of the polymerisation (Figure 3.7).

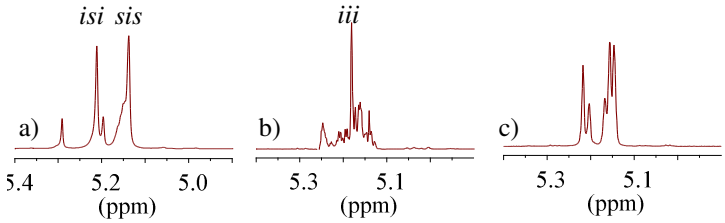

Figure 3.7: Methine region of homonuclear decoupled ^{1}H NMR spectra of Table 3.3 a) heterotactic PLA, Entry 7, b) atactic PLA, Entry 9, c) atactic PLA, Entry 11.

Even at low temperature and a monomer : solvent ratio of 1358 : 1 000, the system showed a tendency to heterotacticity (*isi/sis* = 74 %) in THF (Table 3.3, Entry 6). At

0 °C, with a catalyst : monomer : solvent ratio of 1 : 200 : 10 000, in THF, full conversion is attained after 30 seconds to afford a colourless polymer with $M_{n,exp}$ of 48 000 g/mol and a PDI of 1.24 (Table 3.3, Entry 8); after 1 minute, $M_{n,exp}$ of 45 000 g/mol and a PDI of 1.10 (Table 3.3, Entry 9). In the same condition, but at room temperature, after 2 minutes, $M_{n,exp}$ of 43 000 g/mol and a PDI of 1.30 (Table 3.3, Entry 10). Williams *et al.* published very similar value of heterotacticity using *bis*(thiophosphinic amine) yttrium complex (**C**, Figure 3.8), *isi/sis* of 0.69-0.79.[25]

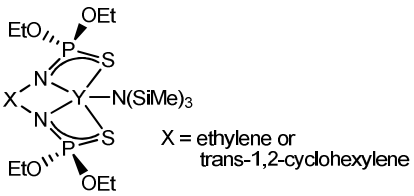

C

Figure 3.8: Bis(thiophosphinic amine) yttrium complex, **C**

Similarly, at low temperature and with a high dilution (monomer : solvent ratio of 200 : 10 000), the polymerisations in THF are poorly controlled in comparison to those in DCM (*iii* = 40 % for Entry 9 and *iii* = 93 % for Entry 5)

Polymerisation of *rac*-lactide using *rac*-$Y(L^{Ar})_3$, with a catalyst : monomer : ratio of 1 : 100 : 1 000, at room temperature in THF, forms an atactic colourless polymer with $M_{n,exp}$ of 80 000 g/mol and a PDI of 1.42 (Table 3.3, Entry 11).

Even at -40 °C, the polymerisation is rapid in DCM and appears to be living in nature. Approximately half of the monomer is consumed after 3 minutes and full conversion is reached after 10 minutes (Table 3.3, Entry 1).

The ^{1}H NMR spectroscopic studies show that the polymerisation using *rac*-$Y(L^{Ph})_3$ is controlled as there is a linear variation of ln(1/(1-conversion)) *vs* time (Figure 3.9 a).

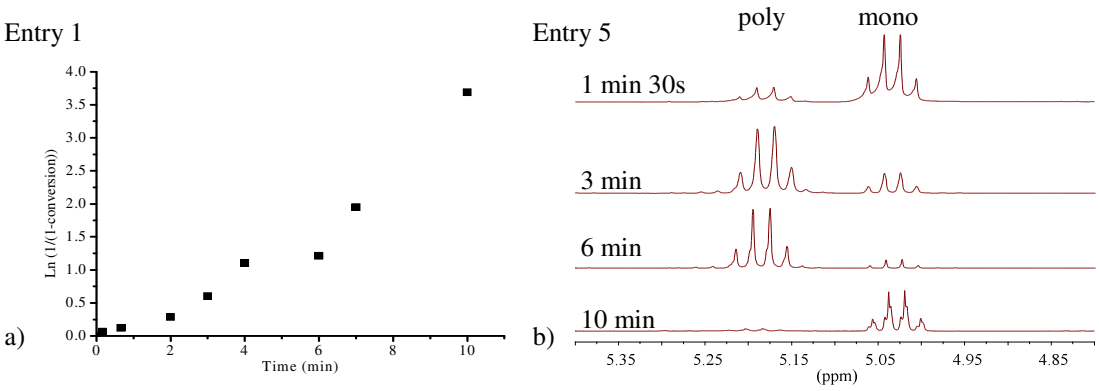

Figure 3.9: Polymerisation kinetics of *rac*-Y(L^{Ph})$_3$, a) Ln(1/(1-conversion)) *vs* time, Table 3.3, Entry 1, -40 °C b) methine region of ^{1}H NMR spectrum, Table 3.3, Entry 5, - 10 °C.

A kinetic study on the polymerisation conditions of Entry 1 and Entry 5 in Table 3.3 shows the importance of the temperature on the control of the polymerisation. The noticeable difference is after 6 minutes; there is a depolymerisation at -10 °C (Table 3.3, Entry 5, Figure 3.9 b)) but not at -40 °C (Table 3.3, Entry 1, Figure 3.9a). This enlighten the problem of living polymerisation, Carpentier *et al.* showed that yttrium alkoxide complexes had the potential to be labile to alcohol exchange; the growing species of lactide polymerisation was a metal-alkoxide and so the alcohol behaves as a reversible chain transfer agent, creating a living ROP of lactide.[16, 26-28]

The polylactides synthesised using *rac*-Y(L^{tBu})$_3$ do not show evidence of depolymerisation and just small quantities of transesterification (Figure 3.2). After two years of storage, all the polylactides show degradation.

The polymerisation kinetics show that the size of the ligand is important for the control of the polymerisation. In the case of *rac*-Y(L^{tBu})$_3$ (the highest homochiral purity) the polymerisation is slightly slower than when using *rac*-Y(L^{Ph})$_3$ (the lowest homochiral purity) but no transesterifications were observed (Figure 3.2). However, depolymerisations occurred after 10 minutes using *rac*-Y(L^{Ph})$_3$ in the same conditions (Figure 3.9).

3.2.3 Copolymerisation of lactide and glycolide by *rac*-Y(L^{Ph})$_3$

Polyglycolide (PGL) is the simplest linear polyester[29] and possesses good mechanical strength; most lactide polymers used for medical applications are copolymers of polylactide and glycolide, in which the glycolide is added to decrease the degradation rate.[30]

When, a DCM solution of *rac*-Y(L^{Ph})$_3$ was added to a vigorously stirred solution of glycolide (catalyst : monomer : solvent = 1 : 150 : 10000) in DCM at -40 °C, colourless polyglycolide instantly precipitated out of solution (Equation 3.2).

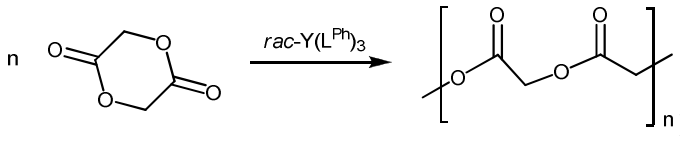

Eq. 3.2

The ^{1}H NMR spectra in d_6-DMSO show polyglycolide but no GPC characterisation has been possible due to poor solubility in THF. Polyglycolide with a molecular weight of above 20 000 g/mol is insoluble in most organic solvents.

An attempt to produce a lactide-glycolide copolymer was made with a catalyst : lactide : solvent ratio of 1 : 100 : 10 000 and a lactide : glycolide ratio of 1 : 3.5, (Equation 3.3).

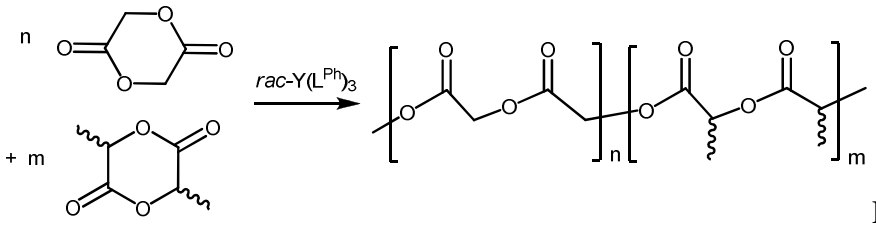

Eq. 3.3

The ^{1}H NMR spectra (in d_6-DMSO) after 1.5, 3, 6 and 10 minutes indicate copolymerisation between lactide-glycolide, with the same integrations which reveals that full conversion of both monomers is attained instantly. No GPC characterisation has been possible due to the solubility problem.

3.2.4 Polymerisation of *rac*-lactide using other *rac*-$M(L^R)_3$

3.2.4.1 Polymerisation of *rac*-lactide using *rac*-$In(L^{tBu})_3$

A solution of 5 mg of catalyst (*rac*-$In(L^{tBu})_3$, 5.6 μmol) in 1 g of DCM was added to a solution of *rac*-lactide (0.5 or 1 g according to Table Entry) which was dissolved in 49 g of DCM. The data from a series of polymerisation of *rac*-lactide by *rac*-$In(L^{tBu})_3$ are collated in Table 3.4.

Table 3.4 Polymerisation data of *rac*-lactide using *rac*-$In(L^{tBu})_3$

Entry	Cat:monomer: solvent ratio	T / °C	Time / h	Conv.[c] / %	$M_{n,exp}$[d] g/mol	$M_{n,\,theo}$[e] g/mol	M_w/M_n[f]	Pi[g]
1	1 : 100 : 500[a]	25	16	95	44 500	86 508	2.08	-
2	1 : 100 : 10000[b]	25	2.5	56	51 000	50 913	1.66	0.63
3	1 : 100 : 10000[b]	25	16	83	120 500	75 893	1.25	0.52
4	1 : 200 : 10000[b]	25	0.17	2	-	-	-	-
5	1 : 200 : 10000[b]	25	0.5	9	26 500	16 594	1.46	0.30
6	1 : 200 : 10000[b]	25	1	21	39 500	39 501	1.23	0.38
7	1 : 200 : 10000[b]	25	4	42	139 000	76 115	1.28	0.44
8	1 : 200 : 10000[b]	25	8	45	147 000	81 706	1.30	0.47
9	1 : 200 : 10000[b]	25	16	99	236 000	174 467	1.28	0.54
10	1 : 400 : 10000[b]	25	16	78	243 000	280 474	1.43	-
11	1 : 400 : 10000[b]	25	40	91	282 500	332 420	1.43	0.36

a: solvent = THF; b: solvent = DCM; c: conversion of LA monomer (($[LA]_0$-[LA])/$[LA]_0$); d: measured by GPC, values based on polystyrene standards, weight corrected by multiplication by 0.58 [Mark-Houwink equation] e: Molecular weight theoretical $M_{n,\,theo}$ = Conv. × [Mono]/[Cat] × M_{Mono}; f: polydispersity index (M_w/M_n), PDI, measured by GPC; g: Probability of forming a new *i* dyad.

At room temperature, with a monomer : catalyst ratio of 200 : 1, full conversion is attained after 16 hours to afford a polymer with $M_{n,\,exp}$ of 236 000 g/mol, $M_{n,\,theo}$ of 174 467 g/mol and a PDI of 1.28 (Table 3.4, Entry 9).

The polymerisation is slightly slower with a monomer : catalyst ratio of 400 : 1; a conversion of 78 % is attained after 16 hours to afford a polymer with $M_{n,\,exp}$ of 243 000 g/mol, $M_{n,\,theo}$ of 280 474 g/mol and a PDI of 1.43 (Table 3.4, Entry 10).

The GPC chromatogram traces are not very clean and have shoulders on the major peaks at low conversion (Table 3.4, Entries 4-6) but these disappear at high conversion (Table 3.4, Entries 7-9) (Figure 3.10 a).

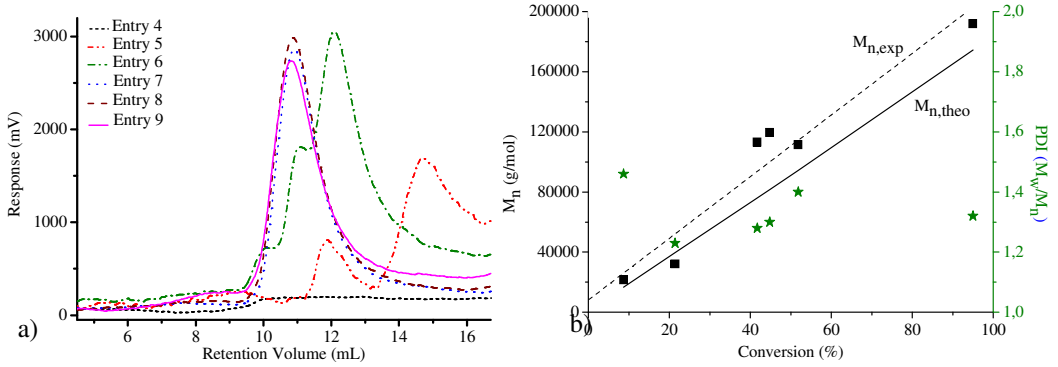

Figure 3.10: Series of polymerisations of *rac*-lactide by *rac*-In(L^{tBu})$_3$, Table 3.4, Entry 4-9: a) GPC chromatogram traces b) Plot of M_n and polydispersity (M_w/M_n) as a function of *rac*-lactide conversion

The experimental molecular weights are close to the theoretical molecular weights and there is linear relationship between them and the conversion. This dependence, and the low polydispersities measured indicate controlled propagation characteristics of these polymerisations (Figure 3.10 b).

Compared with the indium initiators reported by Mehrkhodavandi *et al.*, Okuda *et al.* and Tolman *et al.*, the polylactide polymers made here have similar PDI values (around 1.1-1.5) and polymer molecular weights (20 000-40 000 g/mol); however, Tolman *et al.* reported highly heterotactic PLA (0.90).[31-33]

A stackplot of the GPC chromatogram traces to show the effect on polymerisation of the catalyst : monomer : solvent ratio is plotted in Figure 3.11.

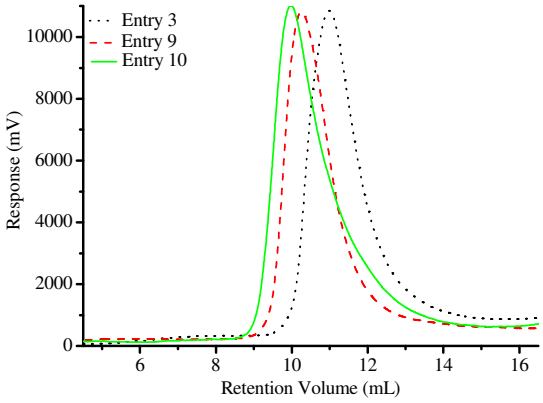

Figure 3.11: GPC chromatogram traces for catalyst : monomer ratio ratios of 1 : 100 (Entry 3), 1 : 200 (Entry 9) and 1 : 400 (Entry 10) according to Table 3.4.

The data show how the molecular weight increases with increasing monomer : catalyst ratio; 100 : 1 ($M_{n,\,exp}$ of 120 500 g/mol), 200 : 1 ($M_{n,\,exp}$ of 236 000 g/mol) and 400 : 1 ($M_{n,\,exp}$ of 282 500 g/mol) (Table 3.4, Entry 3, 9 and 11).

Analysis of the ^{1}H NMR spectra of the polymers show that they display a reasonable degree of isotacticity (*iii*) from 50 to 63 % (Figure 3.12a, *iii* of 63 %; Entry 2 and Figure 3.12b, *iii* of 53 %, Entry 9). For comparison a ^{1}H NMR spectrum of polylactide synthesised using *rac*-Y(L^{tBu})$_3$ is included (Figure 3.12c, *iii* of 99.0 %, Table 3.1, Entry 3).[2, 34]

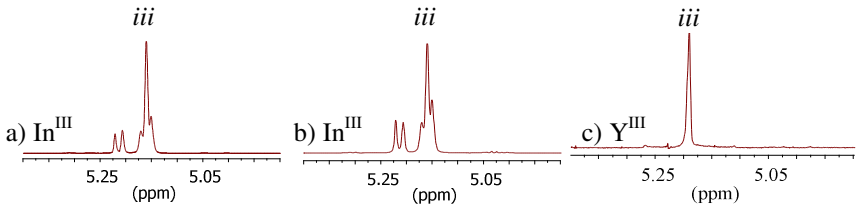

Figure 3.12: Methine region of homonuclear decoupled ^{1}H NMR spectra of isotactic PLA made by a) *rac*-In(L^{tBu})$_3$ (Table 3.4, Entry 2), b) *rac*-In(L^{tBu})$_3$ (Table 3.4, Entry 9) with tetrad resonances arising from insertion errors, c) *rac*-Y(L^{tBu})$_3$ (Table 3.1, Entry 3).

The tacticity is better controlled with *rac*-Y(L^{tBu})$_3$ than with *rac*-In(L^{tBu})$_3$ due to a more rapid polymerisation and less competitive transesterifications.

3.2.4.2 Polymerisations of *rac*-lactide using *rac*-M(L^{Ph})$_3$

A solution of catalyst *rac*-M(L^{Ph})$_3$ in DCM was added to a solution of *rac*-lactide which was dissolved in DCM (according to Table Entry). The data are collated in Table 3.5.

Table 3.5: Polymerisation data of *rac*-lactide using *rac*-M(L^{Ph})$_3$

Entry	Cat:monomer: solvent ratio	T / °C	Time / min	Conv.[f] / %	$M_{n,exp}$[g] g/mol	$M_{n,\,theo}$[h] g/mol	M_w/M_n[i]
1[a]	1 : 658 : 1000[d]	25	1	> 99.0	40 000	94 898	1.49
2[a]	1 : 1316 : 1000[d]	25	1	> 99.0	64 000	189 796	1.46
3[a]	1 : 200 : 1000[d]	0	6	> 99.0	60 500	57 672	1.27
4[b]	1 : 200 : 10000[e]	0	0.15	> 99.0	25 000	28 836	1.03
5[b]	1 : 200 : 10000[e]	0	0.15	>99.0	29 000	28 836	1.05
6[c]	1 : 1412 : 1000[d]	25	1	3	-	-	-
7[c]	1 : 1412 : 1000[d]	25	3	9	-	-	-

a: *rac*-Sc(L^{Ph})$_3$; b. *rac*-Lu(L^{Ph})$_3$; c: *rac*-In(L^{Ph})$_3$; d: solvent = THF; e: solvent = DCM; f: conversion of LA monomer (([LA]$_0$-[LA])/[LA]$_0$); g: measured by GPC, values based on polystyrene standards, weight corrected by multiplication by 0.58 [Mark-Houwink equation]; h: theoretical molecular weight calculated using $M_{n,\,theo} = Conv. \times [Mono]/[Cat] \times M_{Mono}$; i: PDI ($M_w/M_n$), measured by GPC.

At room temperature, using *rac*-Sc(L^{Ph})$_3$, with a catalyst : monomer : solvent ratio of 1 : 658 : 1000 or 1 : 1316 : 1000, full conversion is attained after 1 minute to afford a polymer with $M_{n,\,exp}$ of 40 000 g/mol, $M_{n,\,theo}$ of 94 898 g/mol and a PDI of 1.49 (Table 3.5, Entry 1) and $M_{n,\,exp}$ of 64 000 g/mol, $M_{n,\,theo}$ of 189 796 g/mol and a PDI of 1.46 respectively (Table 3.5, Entry 2.). A decrease in the catalyst : monomer : ratio to 1 : 200 :1000 and a lower temperature (0 °C) resulted in better control of the polymerisation with $M_{n,\,exp}$ of 60 500 g/mol, $M_{n,\,theo}$ of 57 672 g/mol and a PDI of 1.27 (Table 3.4, Entry 3). Full conversion is attained after 6 minutes in this case. Compared with the dithiaalkanediyl-bridged *bis*(phenolato) scandium initiator reported by Okuda *et al.* (**D**, Figure 3.13) the polylactide polymers made there have

similar molecular weights (20 000-60 000 g/mol); however, their PDI values varied more greatly 1.1-1.9.[9, 35]

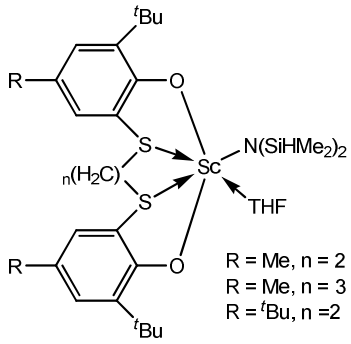

D

Figure 3.13: Dithiaalkanediyl-bridged bis(phenolato) scandium, **D**

At room temperature, the polymerisation of *rac*-lactide using *rac*-In(L^{Ph})$_3$ is very slow, only 9 percent of conversion is attained after 3 minutes. The preliminary results show tacticity control with a *iii* tetrad of 60 %.

At 0 °C, using *rac*-Lu(L^{Ph})$_3$, with a catalyst : monomer : solvent ratio of 1 : 200 : 10000, full conversion is attained after 15 seconds to afford a polymer with $M_{n,\,exp}$ of 29 000 g/mol, $M_{n,\,theo}$ of 28 836 g/mol and a PDI of 1.05 (Table 3.4, Entry 5) showing a very good control of the polymerisation with a high isotacticity *iii* of 0.91 (Figure 3.14).

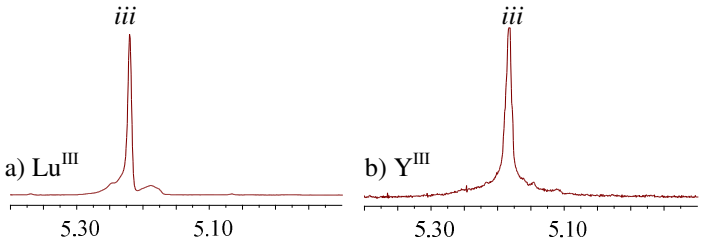

Figure 3.14: Methine region of homonuclear decoupled ^{1}H NMR spectra of isotactic PLA made by a) *rac*-Lu(L^{Ph})$_3$, Table 3.5, Entry 6, b) *rac*-Y(L^{Ph})$_3$, Table 3.3, Entry 4.

In the literature, lutetium initiators have been used to polymerise *L*-lactide with a slow rate of polymerisation (several hours to polymerise the monomer at room temperature).[18, 23, 36, 37] However, some examples of polymerisation of *rac*-lactide

with lutetium initiators afforded polylactides with very high heterotacticity[26, 38, 39] or atacticity.[40]

Compared with the literature, *rac*-Lu(L^{Ph})$_3$ is quicker than any other reported lutetium initiators. Furthermore, it is the first example where the resulting polylactide has a very high isotacticity when synthesised from *rac*-lactide.

3.3 Polymerisation of polar monomers using $(L^R)_2MX$

It is of interest to explore if the complexes $(L^R)_2MX$, are capable of controlling polymer synthesis by ROP (Equation 3.4).

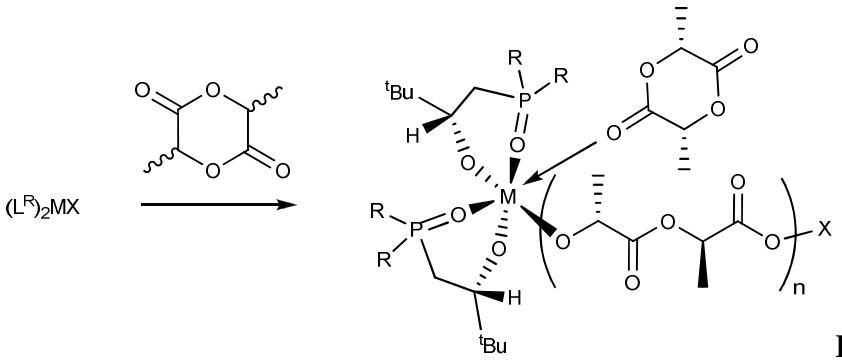

Eq. 3.4

If the insertion of the monomer *rac*-lactide is occurring in the metal-ancillary group bond (M-X), it would be possible for polymerisation control as the $[(L^R)_2M]$- group should be sufficiently asymmetric to allow stereoselective monomer insertion. This was previously shown to be the mechanism for polymerisation using *rac*-M(L^R)$_3$.

3.3.1 Polymerisation of *rac*-lactide using amido $(L^R)_2MX$

3.3.1.1 Polymerisation using $(L^{tBu})_2InN''$

The complex $(L^{tBu})_2InN''$ was tested as an initiator for the polymerisation of *rac*-lactide (Equation 3.5).

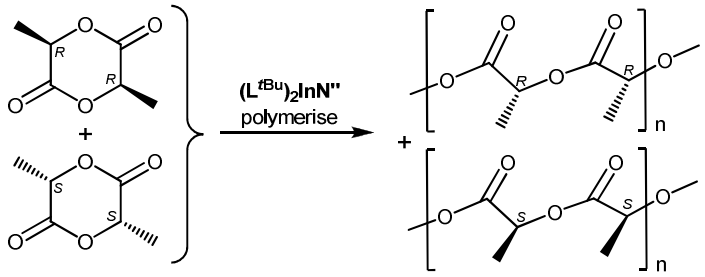

Eq. 3.5

For a series of polymerisations, solution of $(L^{tBu})_2InN"$ was added to a vigorously stirred solution of *rac*-lactide at room temperature. The conditions and results are collated in Table 3.6.

Table 3.6: Polymerisation data of *rac*-lactide by $(L^{tBu})_2InN"$

Entry	Cat:monomer: solvent ratio	T /°C	Time / h	Conv.[c] / %	$M_{n,exp}$[d] g/mol	$M_{n,\ theo}$[e] g/mol	M_w/M_n[f]	Pi[g]
1	1 : 100 : 1000[a]	25	16	95	64 000	76 727	1.63	-
2	1 : 200 : 1000[a]	25	1	7	5 000	11 509	1.08	-
3	1 : 200 : 1000[a]	25	2	14	19 000	23 498	1.18	atactic
4	1 : 200 : 1000[a]	25	4	20	28 000	32 929	1.12	0.39
5	1 : 200 : 1000[a]	25	6	25	34 500	41 081	1.10	0.37
6	1 : 200 : 1000[a]	25	8	26	39 500	42 679	1.11	0.37
7	1 : 200 : 1000[a]	25	24	56	38 000	90 314	1.26	atactic
8	1 : 200 : 1000[b]	25	16	> 99	120 500	159 049	1.56	0.35
9	1 : 200 : 10000[b]	25	16	25	37 000	41 081	1.96	atactic
10	1 : 200 : 10000[b]	25	24	28	81 000	45 077	1.48	atactic
11	1 : 200 : 10000[b]	25	48	52	46 500	83 601	1.87	

a: solvent = THF; b: solvent = DCM; c: conversion of LA monomer ($([LA]_0-[LA])/[LA]_0$); d: measured by GPC, values based on polystyrene standards, weight corrected by multiplication by 0.58 [Mark-Houwink equation]; e: Molecular weight theoretical calculated using $M_{n,\ theo}$ = Conv. × [Mono]/[Cat] × M_{Mono}; f: polydispersity index (M_w/M_n), PDI, measured by GPC. g: Probability of forming a new *i* dyad.

At room temperature, with a catalyst : monomer : solvent ratio of 1 : 200: 1000 (Table 3.6, Entry 6), the polymerisation is slow; a conversion of 26 % is attained after 8 hours but the molecular weight is very good (39 500 g/mol), and the PDI excellent (1.11). The PDI remains low until 57 % of conversion (Table 3.6, Entry 7), by which point it has increased to 1.26. The use of DCM rather than THF as the solvent for the polymerisation reaction increases the rate; full conversion is attained after 16 hours but with a considerably higher $M_{n,exp}$ of 120 500 g/mol and a poor PDI of 1.56 (Table 3.6, Entry 8). Compared with the indium initiator reported by Mehrkhodavandi *et al.*[31] the polylactide polymers made here have similar PDI values (1.1-1.5) and molecular weights (20 000-40 000 g/mol).

A solution of 15 mg of $(L^{tBu})_2InN''$ in THF was added to a solution of 150 mg *rac*-lactide in THF and the mixture was stirred overnight and controlled by NMR. The sample was then evaporated, filtered through a pad of silica gel 60 and dried to constant weight. Mass spectral analysis of the polymer indicates that each chain is terminated by a $-N(SiMe_3)_2$ group.

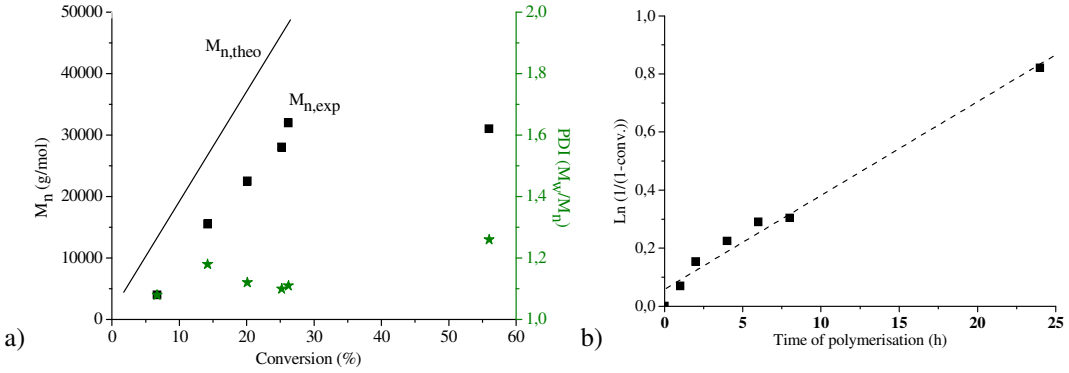

Figure 3.15: Series of polymerisations of *rac*-lactide by $(L^{tBu})_2InN''$: a) Plot of PLA M_n and polydispersity (M_w/M_n) as a function of *rac*-lactide conversion. b) Kinetic plots of the *rac*-lactide conversion versus reaction time

Entries 2 to 6 (Table 3.6) show the linear relationship between M_n and increasing monomer conversion (plotted in Figure 3.15) and the good correlation with the

theoretical molecular weight, calculated assuming that the polymer chain growth occurs from a single ligand site at the metal.

The influence of the stereochemical purity of the catalyst was also investigated in the polymerisation of *SS*-lactide (*L*-Lactide) by $(L^{tBu})_2InN"$ and *RR*-$(L^{tBu})_2InN"$. Complex *RR*-$(L^{tBu})_2InN"$ polymerises *SS*-lactide faster than $(L^{tBu})_2InN"$, demonstrating that the *RR*-$(L^{tBu})_2InN"$ complex favours the insertion of the *SS*-lactide. The PDI of polymer made by $(L^{tBu})_2InN"$ is 2.81 in comparison to *RR*-$(L^{tBu})_2InN"$ with 1.13 (Table 3.7, Entries 1 and 2). For $(L^{tBu})_2InN"$, the monomer *SS*-lactide is polymerised first by *RR*-$(L^{tBu})_2InN"$ and then by *SS*-$(L^{tBu})_2InN"$, This gives a multimodal polymer molecular distribution and a large PDI.[10]

Table 3.7: Polymerisation data of *SS*-Lactide using $(L^{tBu})_2InN"$ and *RR*-$(L^{tBu})_2InN"$.

Entry	Cat:monomer: solvent ratio	T / °C	Time / h	Conv.[b] / %	$M_{n,exp}$[c] g/mol	$M_{n,\ theo}$[d] g/mol	M_w/M_n[e]
1	1: 100 : 1000[a]	25	16	91	26 500	73 290	2.81
2	1: 100 : 1000[a]	25	16	> 99	63 500	90 011	1.13

a: solvent = DCM; b: conversion of LA monomer (($[LA]_0$-[LA])/$[LA]_0$); c: measured by GPC, values based on polystyrene standards, weight corrected by multiplication by 0.58 [Mark-Houwink equation]; d: Molecular weight theoretical calculated using $M_{n,\ theo}$ = Conv. × [Mono]/[Cat] × M_{Mono}; e: polydispersity index (M_w/M_n), PDI, measured by GPC.

The stereochemical microstructure of the resultant PLA was determined by inspection of the methine region of $^{13}C\{^1H\}$ NMR spectra (Figure 3.16).

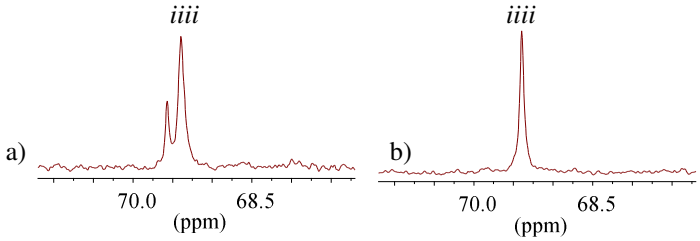

Fiigure 3.16: $^{13}C\{^1H\}$ NMR spectra of poly-*L*-lactide, Table 3.7 made using a) $(L^{tBu})_2InN"$, Entry 1, b) *RR*-$(L^{tBu})_2InN"$, Entry 2.

The spectral data show that the poly-*L*-lactide synthesised using the enantiopure *RR*-$(L^{tBu})_2InN''$ has a better control (Figure 3.16 b) than the one synthesised by the racemic $(L^{tBu})_2InN''$ (Figure 3.16 a), confirming the results obtained with the GPC chromatogram traces.

3.3.1.2 Polymerisation of *rac*-lactide using $(L^{tBu})_2In(NPh_2)$

The complex $(L^{tBu})_2In(NPh_2)$ was tested as an initiator for the polymerisation of *rac*-lactide in THF. Conditions and results are collated in Table 3.8.

Table 3.8: Polymerisation of *rac*-lactide using $(L^{tBu})_2In(NPh_2)$

Entry	Cat:monomer: solvent ratio	T / °C	Time / min	Conv.[a] / %	$M_{n,exp}$[b] g/mol	$M_{n,\ theo}$[c] g/mol	M_w/M_n[d]
1	1 : 1229 : 1000	25	2	-	-	-	-
2	1 : 1229 : 1000	25	13	0.63	63 000	113 370	1.40
3	1 : 1229 : 1000	25	23	0.90	63 000	159 426	1.56
4	1 : 1229 : 1000	25	35	> 0.99	38 000	177 140	1.94
5	1 : 1229 : 1000	25	960	> 0.99	126 000	177 140	1.32

a: conversion of LA monomer $(([LA]_0-[LA])/[LA]_0)$; b: measured by GPC, values based on polystyrene standards, weight corrected by multiplication by 0.58 [Mark-Houwink equation]; c: Molecular weight theoretical calculated using $M_{n,\ theo}$ = Conv. × [Mono]/[Cat] × M_{Mono}; d: polydispersity index (M_w/M_n), PDI, measured by GPC.

At room temperature, with a catalyst : monomer : solvent ratio of 1 : 1229: 1000, 90 % conversion is attained after 23 minutes to afford a polymer with $M_{n,\ exp}$ of 63 000 g/mol, $M_{n,\ theo}$ of 113 370 g/mol and a PDI of 1.56 (Table 3.8, Entry 3). Another attempt showed that polymerisation carried out for 16 hours under the same condition affords a polymer with $M_{n,\ exp}$ of 126 000 g/mol, $M_{n,\ theo}$ of 177 140 g/mol and a PDI of 1.32 (Table 3.8, Entry 5). These results (in comparison with Table 3.6) show that it is apparently easier to insert *rac*-lactide into an In-NPh_2 bond that into an In-$N(SiMe_3)_2$, probably due to the higher polarisability of the bond in the latter case.

The GPC chromatogram traces confirm poor control of the polymerisation of *rac*-lactide using $(L^{tBu})_2In(NPh_2)$ (Entry 1-Entry 5, Table 3.8). The results are shown in Figure 3.17.

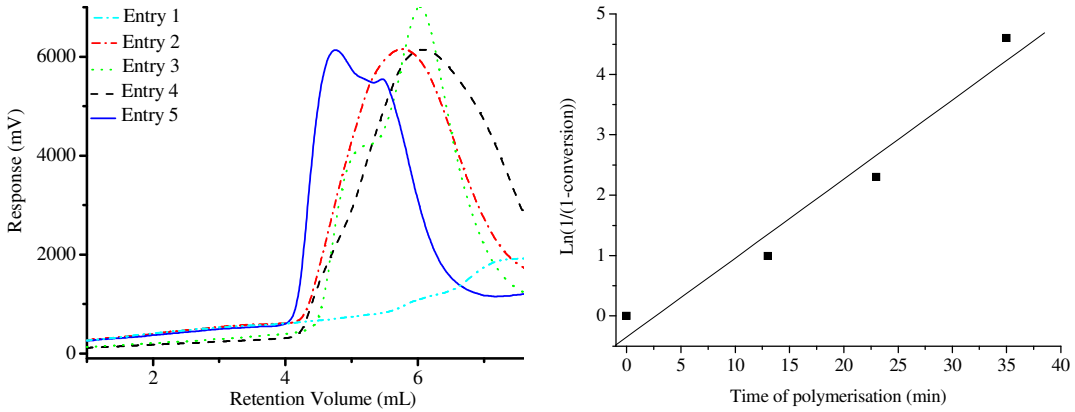

Figure 3.17: Polymerisation data for *rac*-lactide synthesised by $(L^{tBu})_2In(NPh_2)$: a) GPC chromatogram traces b) Kinetic plots of the *rac*-lactide conversion *vs* reaction time

The $^1H\{^1H\}$ NMR spectra of the polylactides synthesised using $(L^{tBu})_2In(NPh_2)$ resulted in atactic polymers (Figure 3.18).

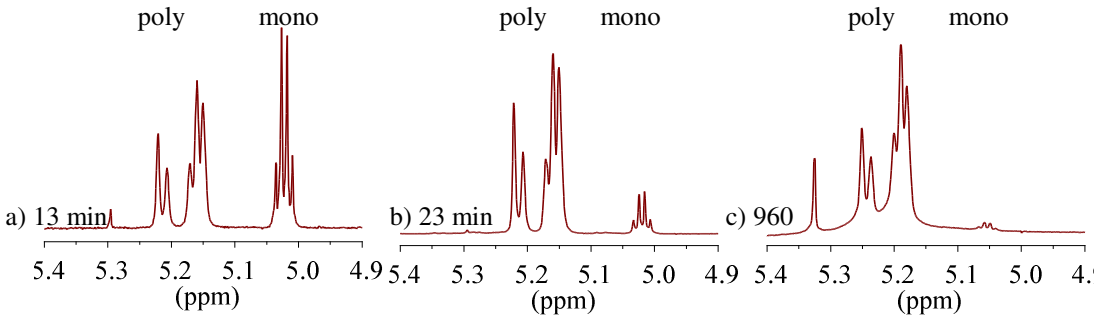

Figure 3.18: Methine region of homonuclear decoupled ^1H NMR spectra of isotactic PLA Table 3.8 a) Entry 2, b) Entry 3 with tetrad resonances arising from insertion errors and c) Entry 5.

These kinetic studies show a better control for the polymerisations using $(L^{tBu})_2InN"$ than those using $(L^{tBu})_2In(NPh_2)$ but slower.

3.3.2 Polymerisation of *rac*-lactide using alkoxide $(L^R)_2MX$

3.3.2.1 Polymerisation using $(L^{tBu})_2M(OR)$

The data from a series of polymerisations of *rac*-lactide by the $(L^{tBu})_2M(OR)$ (where R = OC_6H_3-^{t}Bu-2,6 or O^{t}Bu) initiators are collated in Table 3.9.

Table 3.9: Polymerisation data of *rac*-lactide using $(L^{tBu})_2Y(OAr)$

Entry	Cat:monomer: solvent ratio	T / °C	Time / min	Conv.[f] / %	$M_{n,\,exp}$[g] g/mol	$M_{n,\,theo}$[h] g/mol	M_w/M_n[i]
1[a]	1 : 1134: 5000[d]	25	5	> 99.0	70 000	171 262	1.53
2[a]	1 : 1134 : 5000[d]	0	30	> 99.0	283 000	171 262	1.28
3[a]	1 : 2267 : 5000[d]	0	12	99.0	273 500	342 524	1.29
4[a]	1 : 567 : 5000[d]	- 20	360	50.0	24 500	40 861	1.32
5[b]	1 :1106 :10000[e]	25	960	42	105 000	71 169	1.66
6[c]	1 : 1229 : 1000[d]	25	960	> 99.0	128 000	145 346	1.32

a: $(L^{tBu})_2Y(OAr)$; b: $(L^{tBu})_2In(OAr)$; c: $(L^{tBu})_2In(O^tBu)$; d: solvent = DCM; e: solvent = THF; f: conversion of LA monomer (($[LA]_0$-[LA])/$[LA]_0$); g. measured by GPC, values based on polystyrene standards, weight corrected by multiplication by 0.58 [Mark-Houwink equation]; h: molecular weight calculated using $M_{n,\,theo}$ = Conv. × [Mono]/[Cat] × M_{Mono}; i: PDI, measured by GPC.

At room temperature, the polymerisation of *rac*-lactide using $(L^{tBu})_2Y(OAr)$ is very rapid; full conversion is attained after only 5 minutes to afford a polymer with a molecular weight of 70 000 g/mol and a PDI of 1.53 (Table 3.9, Entry 1). As expected, polymerisation runs at lower temperatures are slower. Even at 0 °C, using $(L^{tBu})_2Y(OAr)$ with a monomer : catalyst ratio of 400 : 1, the polymerisation is rapid and controlled. After 12 minutes, the polymerisation is complete and polymer with a molecular weight of 273 500 g/mol and a PDI of 1.29 is formed (Table 3.9, Entry 3). Polymerisation at -20 °C resulted in a conversion of 50 % after 6 hours to give a polymer with a molecular weight of 24 500 g/mol and a PDI of 1.32 (Table 3.9, Entry 4).

Changing yttrium to indium in $(L^{tBu})_2M(OAr)$ dramatically decreases the rate of the polymerisation. At room temperature, full conversion is attained after 5 minutes using $(L^{tBu})_2Y(OAr)$, but only 42 % of conversion is attained after 16 hours with $(L^{tBu})_2In(OAr)$ (Table 3.9, Entry 1 and Entry 5). However, the control of the molecular weights and polydispersities are comparable (PDI of 1.53 for yttrium and 1.66 for indium).

Changing the OR group from aryloxide (-OAr, 2,6-di-*tert*-butylphenyl) to an alkoxide (-O^{t}Bu) increases the rate of the polymerisation. At room temperature, after 16 hours, full conversion is attained using $(L^{tBu})_2In(O^tBu)$ with a molecular weight of 128 000 g/mol and a PDI of 1.32 (Table 3.9, Entry 6).

These results are in agreement with the literature, showing the insertion of *rac*-lactide to a metal-alkoxide bond is easier than to a metal-aryloxide bond.[41-43]

A study of these polymers show a reasonable degree of crystallinity and stereoregularity. Analysis of the ^{1}H NMR spectra of the polymers show the isotacticity *iii* of 40-50 % (Figure 3.19).

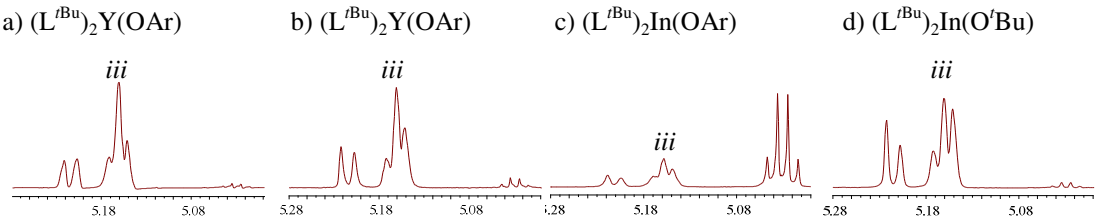

Figure 3.19: Methine region of homonuclear decoupled ^{1}H NMR spectra of isotactic PLA Table 3.9, made using a) $(L^{tBu})_2Y(OAr)$ and Entry 1, b) $(L^{tBu})_2Y(OAr)$ and Entry 4, c) $(L^{tBu})_2In(OAr)$ and Entry 5 and d) $(L^{tBu})_2In(O^tBu)$ and Entry 6, with tetrad resonances arising from insertion errors

3.3.2.2 Polymerisation of ε-caprolactone using $(L^{tBu})_2Y(OAr)$

The cyclic monomer ε-caprolactone (εCL) is polymerised to polycaprolactone (PCL) by a coordination-insertion mechanism similar to the ROP of lactide and glycolide (Equation 3.6).

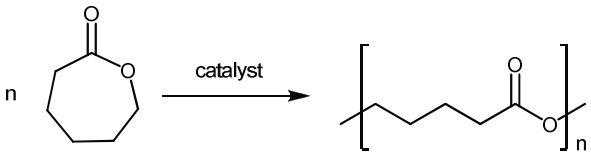

Eq. 3.6

Among the most active catalysts reported to date are $(Sc[(CH_2SiMe_3)_2(THF)][2\text{-}(2,4,6\text{-}Me_3C_6H_2N{=}CH)(6\text{-}Bu^t)C_6H_3OH]$ (**E**, Figure 3.20),[44] polymerising neat ε-caprolactone (catalyst : monomer = 1 : 110) at 0 °C within 1 minute with quantitative conversion. The obtained polymer had an M_w of 71 000 g/mol and a PDI of 2.9. The high PDI was caused by transesterification reactions, which led to oily oligomeric products if the reaction time was increased. Lanthanide complexes, like 2,6-dimethylphenolate adducts ($[Ln(ODMP)_3]$ (**F**, Figure 3.20),[45] are active initiators for the ROP of ε-caprolactone in solution. The activity decreases with decreasing radius of the lanthanide; the highest activity was found for La (100 % conversion, 60 °C, toluene, M_n of 56 000 g/mol) whilst Er and Y initiators produced only moderate molecular weight polymers (M_n of 16 000 g/mol). Various Al complexes have also been reported as initiators.[46, 47] Polymer formed using Al complexes $((CH_3CH_2CH_2)N\text{-}(CH_2\text{-}2\text{-}HO\text{-}3,5\text{-}C_6H_2(^tBu)_2)_2]$ (**G**, Figure 3.20)[48] is of moderate molecular weight (10 000-20 000 g/mol) with a very good PDI (1.05-1.1).

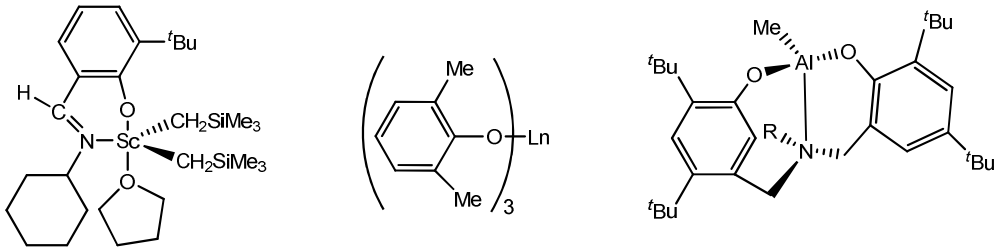

E **F** **G**

Figure 3.20: Catalysts for ε-caprolactone polymerisation **E**, **F** and **G**

For comparison, the reactivity of $(L^{tBu})_2Y(OAr)$ as an initiator for PCL synthesis was investigated. A solution of $(L^{tBu})_2Y(OAr)$ in toluene was added to a solution of ε-caprolactone in toluene and heated to 80 °C. Quenching of the reaction after 16 hours afforded a colourless polymer which has a molecular weight of 18 500 g/mol and a PDI of 1.54. Compared with the initiators reported in the literature,[2, 44, 46-48] the PCL made here have good PDI values but the polymer molecular weights are moderate (Figure 3.21).

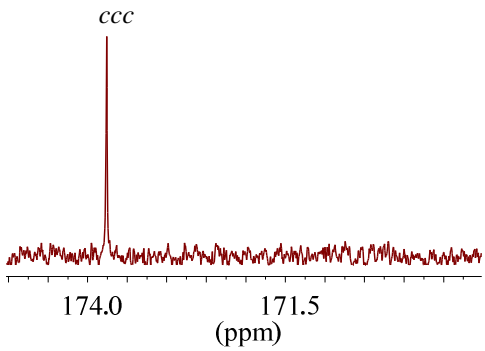

Figure 3.21: $^{13}C\{^1H\}$ NMR spectrum (showing the carbonyl region) of PCL made using $(L^{tBu})_2Y(OAr)$ as initiator, $M_{n,\,exp}$ = 18 500 g/mol, PDI = 1.54, *c* represents ε-caprolactone dyad

3.3.2.3 Copolymerisation of lactide and ε-caprolactone using $(L^{tBu})_2Y(OAr)$

The copolymerisation of lactide and ε-caprolactone by $(L^{tBu})_2Y(OAr)$ was also studied (Equation 3.7).

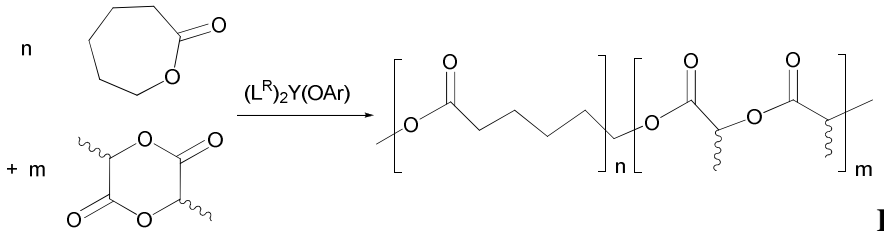

Eq. 3.7

Heating a toluene solution of 10 mg of $(L^{tBu})_2Y(OAr)$, 1 g of ε-caprolactone and 0.5 g *rac*-lactide at 80 °C for 16 hours afforded a colourless copolymer. After work-

up, the polymeric product was shown to have a molecular weight of 34 500 g/mol and a PDI of 1.64.

To confirm the copolymeric nature of the ε-caprolactone/*rac*-lactide material, the $^{13}C\{^1H\}$ NMR spectrum was analysed (Figure 3.22).[49, 50] It reveals the presence of copolymer with long chains of poly(ε-caprolactone) through the resonance at 173.9 ppm. The carbonyl signals due to longer poly(lactide) sequences (169.5 ppm) are virtually absent. The resonance at 171.2 ppm, which corresponds to the heterotetrad *clc* shows the enchainment of one monomer of ε-caprolactone and one of *rac*-lactide.

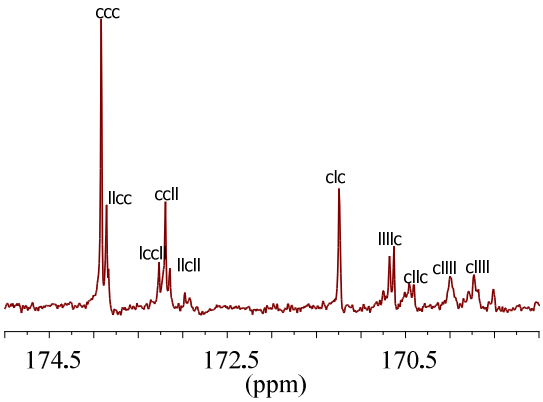

Figure 3.22: $^{13}C\{^1H\}$ NMR spectrum of the copolymer of *rac*-lactide and ε-caprolactone made using $(L^{tBu})_2Y(OAr)$; $M_{n,\ exp}$ = 34 500 g/mol, PDI = 1.64; *c* represents ε-caprolactone dyad, *l* represents *rac*-lactide dyad

3.4 Polymerisation of polar monomers using $(L^R)MX_2$

Ring opening polymerisation of lactide using a complex $(L)MMe_2$ have recently been explored; a series of Al complexes containing phenoxy-imine ligands, of the type $Me_2Al[O\text{-}2\text{-}^tBu\text{-}6\text{-}(RN{=}CH)C_6H_3]$ (**H**, Figure 3.23), polymerise *rac*-lactide (catalyst : monomer ratio of 1 : 100) at 80 °C with M_n varying between 10 000-20 000 g/mol and with a PDI below 1.2 were first introduced by Iwasa et *al.*.[51-54] Their studies have been extended by Pappalardo *et al.* by variation of the R groups and applications to copolymerisation with ε -caprolactone.[55]

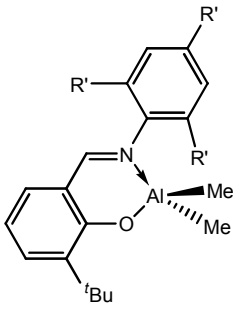

R' = Me, ^{t}Bu, cyclohexyl, adamantyl, Ph, 2,6-$Me_2C_6H_3$, 2,6-$^i Pr_2C_6H_3$, 2,4,6-$Me_3C_6H_2$, 2,4,6-$^t Bu_3C_6H_2$ or C_6F_5

H

Figure 3.23: Al complexes containing phenoxy-imine ligands, **H**

3.4.1 Polymerisation of *rac*-lactide using $(L^R)AlMe_2$

The complex $(L^{tBu})AlMe_2$ was examined for polymerisation activity with *rac*-lactide (catalyst : monomer ratio of 1 : 50). The polymerisations were carried out in toluene at 100 °C with benzyl alcohol as co-initiator (such polymerisations did not work without a co-initiator). From the polymerisation data, it is apparent than the aluminium complex shows a conversion > 90 % but with large polydispersities (1.7-1.9) and low molecular weights (around 1000-2000 g/mol).

Polymerisation of *rac*-lactide using $(L^{tBu})AlMe_2$ at 140 °C, in melt, with a catalyst : monomer : solvent ratio of 1 : 2 : 0 (and with benzyl alcohol as co-initiator) showed full conversion is attained after 16 hours (Figure 3.24).

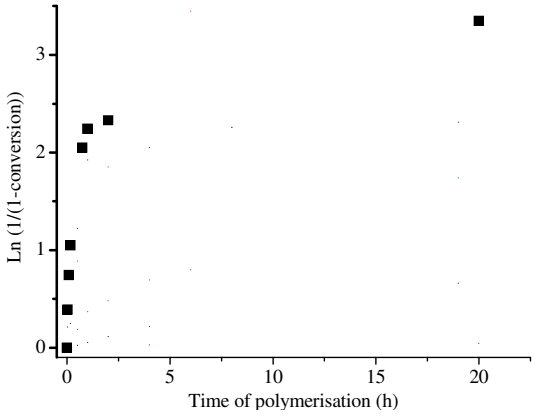

Figure 3.24: Plot of the conversion of *rac*-lactide over time for $(L^{tBu})AlMe_2$.

3.4.2 Copolymerisation of glycolide and lactide by $(L^{Ph})AlMe_2$

Copolymerisation of *rac*-lactide and glycolide using $(L^{Ph})AlMe_2$ at 140 °C in a melt polymerisation with a catalyst : lactide : solvent ratio of 1 : 50 : 0 and a lactide : glycolide ratio of 1 : 4 showed the formation of a colourless precipitate instantly which was not soluble in common solvents. This is indicative of polyglycolide but unfortunately not of a copolymer of glycolide and lactide.

3.5 Copolymerisation of CO_2 and epoxides

3.5.1 Polymerisation of propylene oxide using $(L^{tBu})_2InX$

The polymerisation of propylene oxide using $(L^{tBu})_2InN"$ or $(L^{tBu})_2In(NPh_2)$ at room temperature, neat or in solution in toluene, affords colourless poly(propylene oxide) (Equation 3.8).

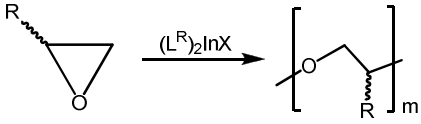

Eq. 3.8

At room temperature, with a catalyst : monomer : ratio of 1 : 1134 : 5000, using $(L^{tBu})_2In(NPh_2)$, full conversion is attained after 5 minutes to afford a polymer with a molecular weight of 70 000 g/mol and a PDI of 1.53.

3.5.2 Copolymerisation CO_2 and epoxide using $(L^{tBu})_2In(NPh_2)$

The reaction of coupling between carbon dioxide and an epoxide should afford polycarbonates, Equation 3.9.

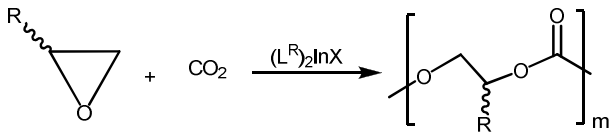

Eq. 3.9

Copolymerisation of carbon dioxide and epoxide showed very little activities, only 0.4 % of carbonate linkages are present in the copolymer CO_2 and propylene oxide.

3.6 Conclusion

Rac-M(L^R)$_3$ (where M = Sc, Lu, In, or Y and R = ^{t}Bu, Ph or Ar) complexes, (L^R)$_2$MX (where M = In or Y, R = ^{t}Bu or Ph and X = N(SiMe$_3$)$_2$, NPh$_2$, O^{t}Bu) complexes and (L^R)MX$_2$ (where M = Al, R = ^{t}Bu or Ph and X = Me) are excellent initiators for the polymerisation of a range of cyclic esters to form polymers including poly(lactide), poly(ε-caprolactone) and its copolymer with lactide.

The *rac*-M(L^R)$_3$ complexes are also highly active catalysts for the polymerisation of glycolide. However, the polymerisation of this monomer is too fast to produce good copolymers of glycolide and lactide.

Initial attempts to copolymerise carbon dioxide and epoxide have been successful but with very low carbonate linkages.

[1] Y. Ikada, K. Jamshidi, H. Tsuji, S. H. Hyon, *Macromolecules* **1987**, *20*, 904.
[2] J. Zhang, K. Tashiro, H. Tsuji, A. J. Domb, *Macromolecules* **2007**, *40*, 1049.
[3] H. Tsuji, *Macromol. Bio.* **2005**, *5*, 569.
[4] T. M. Ovitt, G. W. Coates, *J. Am. Chem. Soc.* **2002**, *124*, 1316.
[5] C. P. Radano, G. L. Baker, M. R. Smith, *J. Am. Chem. Soc* **2000**, *122*, 1552.
[6] N. Spassky, M. Wisniewski, C. Pluta, A. Le Borgne, *Macromol. Chem. Phys.* **1996**, *197*, 2627.
[7] Z. Zhong, P. J. Dijkstra, J. Feijen, *J. Am. Chem. Soc* **2003**, *125*, 11291.
[8] N. Spassky, V. Simic, M. S. Montaudo, L. G. Hubert-Pfalzgraf, *Macromol. Chem. Phys.* **2000**, *201*, 2432.
[9] H. Ma, T. P. Spaniol, J. Okuda, *Angew. Chem., Int. Ed.* **2006**, *45*, 7818.
[10] P. L. Arnold, J.-C. Buffet, R. P. Blaudeck, S. Sujecki, A. J. Blake, C. Wilson, *Angew. Chem., Int. Ed.* **2008**, *47*, 6033.
[11] J. Coudane, C. Ustariz-Peyret, G. Schwach, M. Vert, *J. Polym. Sci. Part A: Polym. Chem.* **1997**, *35*, 1651.
[12] B. M. Chamberlain, B. A. Jazdzewski, M. Pink, M. A. Hillmyer, W. B. Tolman, *Macromolecules* **2000**, *33*, 3970.
[13] V. Simic, V. Girardon, N. Spassky, L. G. Hubert-Pfalzgraf, A. Duda, *Polym. Deg. Stab.* **1998**, *59*, 227.
[14] K. B. Aubrecht, K. Chang, M. A. Hillmyer, W. B. Tolman, *J. Polym. Sci. Part A: Polym. Chem.* **2001**, *39*, 284.
[15] A. Alaaeddine, A. Amgoune, C. M. Thomas, S. Dagorne, S. Bellemin-Laponnaz, J.-F. Carpentier, *Eur. J. Inorg. Chem.* **2006**, *2006*, 3652.
[16] A. Amgoune, C. M. Thomas, J.-F. Carpentier, *Macromol. Rapid Commun.* **2007**, *28*, 693.
[17] A. Amgoune, C. M. Thomas, T. Roisnel, J.-F. Carpentier, *Chem. Eur. J.* **2006**, *12*, 169.
[18] W. Miao, S. Li, H. Zhang, D. Cui, Y. Wang, B. Huang, *J. Organomet. Chem.* **2007**, *692*, 4828.
[19] R. Heck, E. Schulz, J. Collin, J.-F. Carpentier, *J. Mol. Cat. A* **2007**, *268*, 163.
[20] R. H. Platel, A. J. P. White, C. K. Williams, *Inorg. Chem.* **2008**, *47*, 6840.
[21] W. M. Stevels, M. J. K. Ankone, P. J. Dijkstra, J. Feijen, *Macromolecules* **1996**, *29*, 6132.
[22] C.-X. Cai, A. Amgoune, C. W. Lehmann, J.-F. Carpentier, *Chem. Commun.* **2004**, 330.
[23] H. Ma, J. Okuda, *Macromolecules* **2005**, *38*, 2665.
[24] L. M. Hodgson, A. J. P. White, C. K. Williams, *J. Polym. Sci. Part A: Polym. Chem.* **2006**, *44*, 6646.
[25] L. M. Hodgson, R. H. Platel, A. J. P. White, C. K. Williams, *Macromolecules* **2008**, *41*, 8603.
[26] N. Ajellal, D. M. Lyubov, A. Mikhail, A. Sinenkov, G. K. Fukin, V. Anton. Cherkasov, C. M. Thomas, J.-F. Carpentier, A. A. Trifonov, *Chem. Eur. J.* **2008**, *14*, 5440.
[27] T. V. Mahrova, G. K. Fukin, A. V. Cherkasov, A. A. Trifonov, N. Ajellal, J.-F. Carpentier, *Inorg. Chem.* **2009**, *48*, 4258.

[28] E. Grunova, E. Kirillov, T. Roisnel, J.-F. Carpentier, *Organometallics* **2008**, *27*, 5691.
[29] D. K. Gilding, A. M. Reed, *Polymer* **1979**, *20*, 1459.
[30] A.-C. Albertsson, M. Ryner, K. Stridsberg, in *Controlled Ring-Opening Polymerization: Polymers with designed Macromolecular Architecture, Vol. 157*, **2002**, p. 41.
[31] A. F. Douglas, B. O. Patrick, P. Mehrkhodavandi, *Angew. Chem., Int. Ed.* **2008**, *47*, 2290.
[32] I. Peckermann, A. Kapelski, T. P. Spaniol, J. Okuda, *Inorg. Chem.* **2009**, *48*, 5526.
[33] A. Pietrangelo, M. A. Hillmyer, W. B. Tolman, *Chem. Commun.* **2009**, 2736.
[34] Y. Fan, H. Nishida, Y. Shirai, Y. Tokiwa, T. Endo, *Polym. Deg. Stab.* **2004**, *86*, 197.
[35] H. Ma, T. P. Spaniol, J. Okuda, *Dalton Trans.* **2003**, 4770.
[36] Y. Luo, X. Wang, J. Chen, C. Luo, Y. Zhang, Y. Yao, *J. Organomet. Chem.* **2009**, *694*, 1289.
[37] M. Konkol, T. P. Spaniol, M. Kondracka, J. Okuda, *Dalton Trans.* **2007**, 4095.
[38] H. Ma, T. P. Spaniol, J. Okuda, *Inorg. Chem.* **2008**, *47*, 3328.
[39] X. Liu, X. Shang, T. Tang, N. Hu, F. Pei, D. Cui, X. Chen, X. Jing, *Organometallics* **2007**, *26*, 2747.
[40] B. Liu, D. Cui, J. Ma, X. Chen, X. Jing, *Chem. Eur. J.* **2007**, *13*, 834.
[41] M. Cheng, A. B. Attygalle, E. B. Lobkovsky, G. W. Coates, *J. Am. Chem. Soc.* **1999**, *121*, 11583.
[42] M. H. Chisholm, J. Gallucci, K. Phomphrai, *Inorg. Chem.* **2002**, *41*, 2785.
[43] M. H. Chisholm, J. C. Gallucci, K. Phomphrai, *Inorg. Chem.* **2004**, *43*, 6717.
[44] A. Lara-Sanchez, A. Rodriguez, D. L. Hughes, M. Schormann, M. Bochmann, *J. Organomet. Chem.* **2002**, *663*, 63.
[45] L. Zhang, C. Yu, Z. Shen, *Polym. Bull.* **2003**, *51*, 47.
[46] B.-T. Ko, C.-C. Lin, *Macromolecules* **1999**, *32*, 8296.
[47] L. M. Alcazar-Roman, B. J. O'Keefe, M. A. Hillmyer, W. B. Tolman, *Dalton Trans.* **2003**, 3082.
[48] C.-T. Chen, C.-A. Huang, B.-H. Huang, *Macromolecules* **2004**, *37*, 7968.
[49] J. Kasperczyk, M. Bero, *Makromol. Chem.* **1993**, *194*, 913.
[50] M. Florczak, A. Duda, *Angew. Chem., Int. Ed.* **2008**, *47*, 9088.
[51] N. Iwasa, M. Fujiki, K. Nomura, *J. Mol. Cat. A* **2008**, *292*, 67.
[52] N. Iwasa, S. Katao, J. Liu, M. Fujiki, Y. Furukawa, K. Nomura, *Organometallics* **2009**, *28*, 2179.
[53] N. Iwasa, J. Liu, K. Nomura, *Cat. Commun.***2008**, *9*, 1148.
[54] J. Liu, N. Iwasa, K. Nomura, *Dalton Trans.* **2008**, 3978.
[55] D. Pappalardo, L. Annunziata, C. Pellecchia, *Macromolecules* **2009**, *42*, 6056.
[56] G. W. Coates, D. R. Moore, *Angew. Chem., Int. Ed.* **2004**, *43*, 6618.
[57] D. J. Darensbourg, *Chem. Rev.* **2007**, *107*, 2388.

Chapter 4: Synthesis of $M(L^R)_2$ complexes and their use as polymerisation initiators

4.1 Introduction

While there has been significant progress with stereoselective group 3 and 13 initiators,[1-5] calcium, magnesium and zinc hold the most promise for industrial application owing to their low cost, remarkably high activities and minimal toxicity. Several such catalyst systems which exhibit good stereochemical control have revealed two unique, and possibly competing, mechanisms: chain-end control and enantiomorphic site-control.[6]

4.2 Synthesis and characterisations of $M(L^R)_2$

4.2.1 General synthesis of $M(L^{tBu})_2$

Treatment of two equivalents of *rac*-HL^{tBu} with one equivalent of $M\{N(SiMe_3)_2\}_2$ (MN''_2 and where M = Ca, Zn and Sn) in THF at low temperature (-78 °C) affords $M(L^{tBu})_2$ in very good yield (85-95 %) (Equation 4.1).

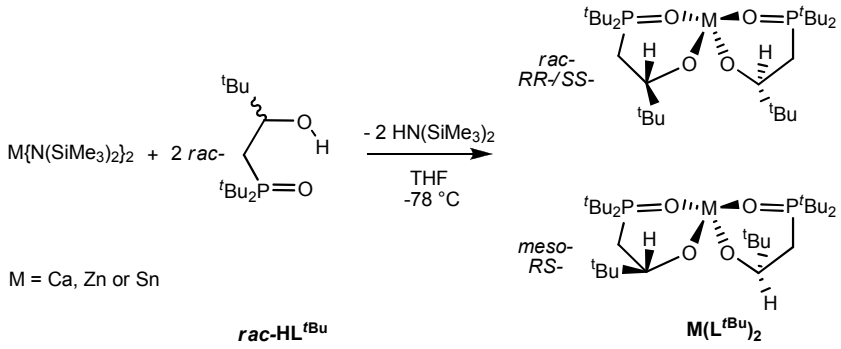

Eq 4.1

$M(L^{tBu})_2$ (M = Ca, Zn, and Sn) comprises a mixture of *RR*-$M(L^{tBu})_2$/*SS*-$M(L^{tBu})_2$ (*rac*-$M(L^{tBu})_2$) and *RS*-$M(L^{tBu})_2$ (*meso*-$M(L^{tBu})_2$). For a given metal, diastereomeric index is most readily measured by integration of the NMR spectra of $M(L^{tBu})_2$ complexes. The diagnostic resonances in the ^1H NMR spectra are two doublets (^{t}Bu-H coupling to P) and a singlet (^{t}Bu-H) for the group on the chiral carbon.

4.2.2 NMR characterisation of $M(L^{tBu})_2$

The reaction of $CaN"_2(THF)_2$ with one equivalent of *rac*-HL^{tBu} at -78 °C for 16 hours led, after work-up, to a colourless solid of $Ca(L^{tBu})_2$ in 64 % yield. The ^1H and $^{31}P\{^1H\}$ NMR spectra are consistent with a single ligand environment and contain approximately 90 % of *RR/SS*-$Ca(L^{tBu})_2$ and 10 % of *RS*-$Ca(L^{tBu})_2$ (Figure 4.1).

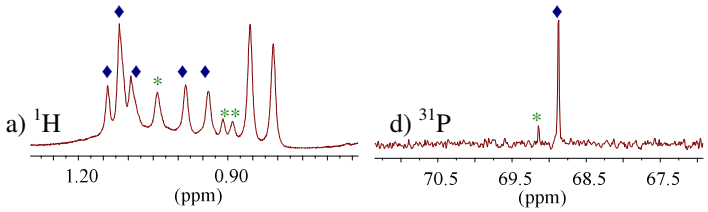

Figure 4.1: $^{31}P\{^1H\}$ and ^1H (*tert*-butyl region) NMR spectra of $Ca(L^{tBu})_2$ (d_6-benzene) a) ^1H and b) $^{31}P\{^1H\}$. ♦ denotes *rac*-$Ca(L^{tBu})_2$, * denotes *RS*-$Ca(L^{tBu})_2$

The complex $Zn(L^{tBu})_2$ was isolated as a colourless solid with a yield of 70 %. The ^1H and $^{31}P\{^1H\}$ NMR spectra of $Zn(L^{tBu})_2$ contain approximately 75 % of *RR/SS*-$Zn(L^{tBu})_2$ and 25% of *RS*-$Zn(L^{tBu})_2$ (Figure 4.2).

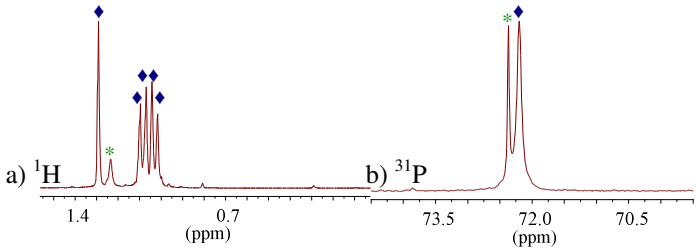

Figure 4.2: $^{31}P\{^1H\}$ and ^1H (*tert*-butyl region) NMR spectra of $Zn(L^{tBu})$ (d_6-benzene): a) ^1H and b) $^{31}P\{^1H\}$. ♦ denotes *rac*-$Zn(L^{tBu})_2$, * denotes *RS*-$Zn(L^{tBu})_2$.

The complex $Sn(L^{tBu})_2$ was isolated as a colourless solid in 71 % yield. The ^1H and $^{31}P\{^1H\}$ NMR spectra of *RR*-$Sn(L^{tBu})_2$ show a single ligand environment (Figure 4.3 b) and d)). Spectra of $Sn(L^{tBu})_2$ indicate 100 % diastereomeric index (a mixture of *RR-/SS*-$Sn(L^{tBu})_2$) are shown in Figure 4.3 a) and c). The coupling constant $^2J_{SnP}$ is 255.6 Hz.

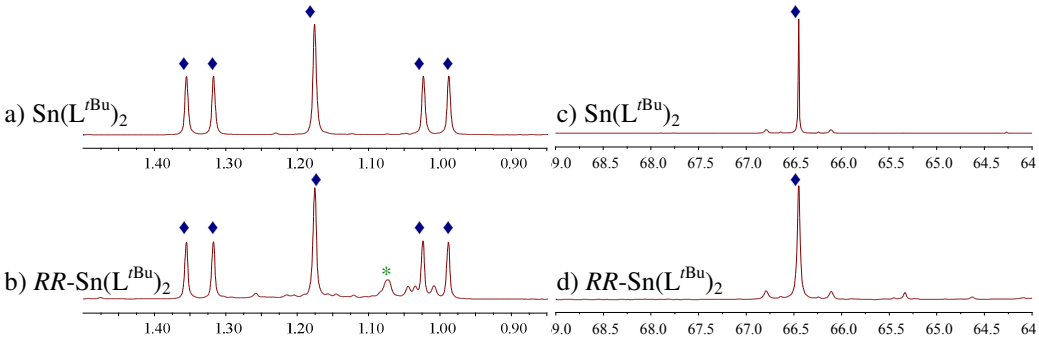

Figure 4.3: ^{1}H (*tert*-butyl region) and $^{31}P\{^{1}H\}$ NMR spectra of Sn(L^{tBu})$_2$ and *RR*-Sn(L^{tBu})$_2$ (d_6-benzene), a) ^{1}H: Sn(L^{tBu})$_2$, b) ^{1}H: *RR*-Sn(L^{tBu})$_2$, c) $^{31}P\{^{1}H\}$: Sn(L^{tBu})$_2$ and d) $^{31}P\{^{1}H\}$: *RR*-Sn(L^{tBu})$_2$. ♦ denotes *rac*-Sn(L^{tBu})$_2$, * denotes some impurities in *RR*-Sn(L^{tBu})$_2$

Several attempts have been made to synthesise Mg(L^{tBu}); the reaction of MgN"$_2$(THF)$_2$ with two equivalents on *rac*-HL^{tBu} in THF or d_6-benzene at different temperatures (-78, 25 and 80 °C) for 16 hours (Scheme 4.1) led to intractable mixtures of products possibly due to the small size and Lewis acidity of the magnesium cation. A similar result was obtained for the reaction of (L^{tBu})Mg(OAr) (where Ar = 2,6-^{t}Bu-C$_6$H$_3$) with one equivalent of *rac*-HL^{tBu} in d_6-benzene at 25 °C for 16 hours (Scheme 4.1).

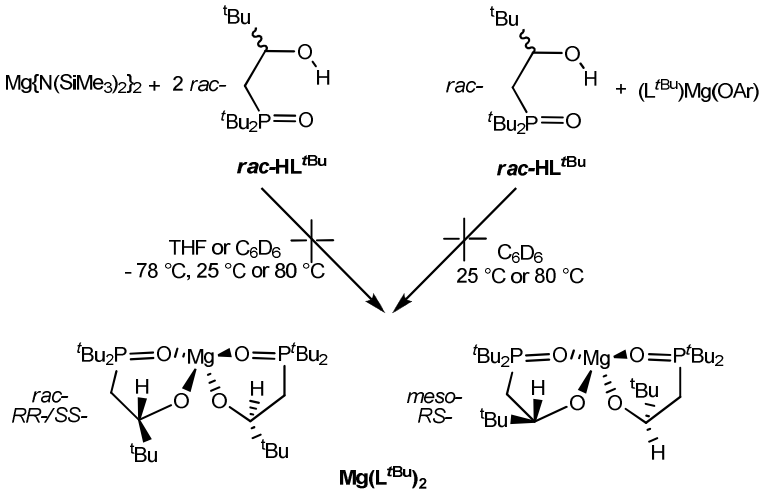

Scheme 4.1: Attempted reaction for the synthesis of Mg(L^{tBu})$_2$ complex.

4.2.3 X-Ray crystallography of $M(L^{tBu})_2$

Colourless crystals of complexes **$Zn(L^{tBu})_2$** and **$Sn(L^{tBu})_2$** suitable for a single crystal X-ray diffraction study were grown from a cooled (- 20 °C) hexanes solution. The molecular structures are depicted in Figure 4.4. The configuration of the molecules shown is *RR*-$Zn(L^{tBu})_2$ and *RR*-$Sn(L^{tBu})_2$.

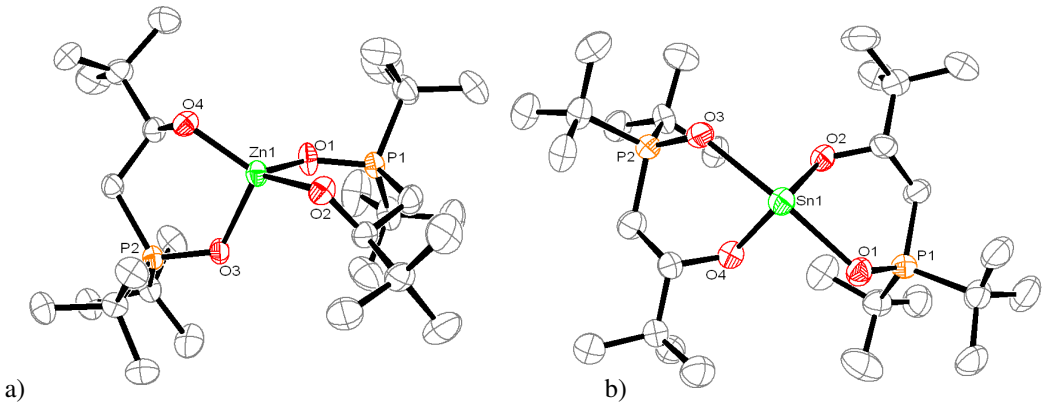

Figure 4.4: Displacement ellipsoid drawing of $M(L^{tBu})_2$, a) $Zn(L^{tBu})_2$ and b) $Sn(L^{tBu})_2$, 50 % probability ellipsoids. Lattice solvent and all hydrogen atoms omitted for clarity. Selected distances (Å): (for $Zn(L^{tBu})_2$): Zn1-O1 2.0272(18), Zn1-O2 1.8729(18), Zn1-O3 2.0269(18) and Zn1-O4 1.8719(18); (for $Sn(L^{tBu})_2$): Sn1-O1 2.370(4), Sn1-O2 2.054(4), Sn1-O3 2.374(4) and Sn1-O4 2.042(5); selected angles (°): (for $Zn(L^{tBu})_2$): O1-Zn1-O4 113.46(8), O1-Zn1-O2 98.76(8), O2-Zn1-O3 111.93(9) and O3-Zn1-O4 98.87(8); (for $Sn(L^{tBu})_2$): O1-Sn1-O2 79.60(14), O1-Sn1-O3 154.40(13), O2-Sn1-O4 95.79(16);

The metal cation in **$Zn(L^{tBu})_2$** has a distorted tetrahedral geometry. The distortion is due to the bulkiness of the *tert*-butyl group. As a result it is possible to see that the dihedral angles between O1–Zn–O2 (98.76(8)°) and O3–Zn–O4 (98.87(8)°) planes are small, and that the angles O1-Zn1-O4 (113.46(8)°) and O2-Zn1-O3 (111.93(9)°) deviate from the theoretical 109°. The Zn-OP average bond distance (2.027 Å) is in the higher part of the literature range (1.949 – 2.031 Å).[7-11] The average bond distances in $Zn(L^{tBu})_2$ are significantly shorter than in the tin analogue; Zn-OP (2.027

Å) *vs* Sn-OP (2.372 Å) and Zn-OR (1.873 Å) *vs* Sn-OR (2.048 Å) in agreement with the smaller ionic radius for the zinc cation ($r(Zn^{2+})$ = 0.69 Å and $r(Sn^{2+})$ = 1.12 Å).

The metal cation in **$Sn(L^{tBu})_2$** has a distorted sawhorse geometry. The O1-Sn-O3 angle formed by the two O donors of the sterically demanding phosphine oxide ligands is 154.4(13)°. Most of the complexes with a tin-phosphine oxide bond in the literature feature Sn^{IV} centres but Ionkin *et al.* reported a very similar Sn^{II} compound with two CF_3 groups on C1 instead of a *tert*-butyl group, $Sn[OC(CF_3)_2CH_2P(O)^tBu_2]_2$, **A**.[12, 13] The Sn−OR bonds in $Sn(L^{tBu})_2$ are shorter than in **A** (2.054(4) Å and 2.042(5) Å for $Sn(L^{tBu})_2$ *vs* 2.0987(18) Å and 2.1051(17) Å for **A**). The Sn-OP bonds in $Sn(L^{tBu})_2$ (2.370(4) Å and 2.374(4) Å) are longer than those in **A** (2.293(2) and 2.298(2) Å). The phosphoryl groups in $Sn(L^{tBu})_2$ remain double bonded at (P=O of 1.505(4) Å and 1.502(4) Å). These bond lengths are typical of double bonds.[14, 15]

4.2.4 General synthesis of $[M(L^{Ar})_2]_2$

Treatment of two equivalents of *rac*-HL^{Ar} (where Ar = Ph or 3,5-Me-C_6H_3) with one equivalent of $M\{N(SiMe_3)_2\}_2$ ($MN"_2$ and where M = Mg, Co, Zn and Sn) in d_6-benzene at 80 °C affords $[M(L^{Ar})_2]_2$ in reasonable yield (55-75 %) (Equation 4.2).

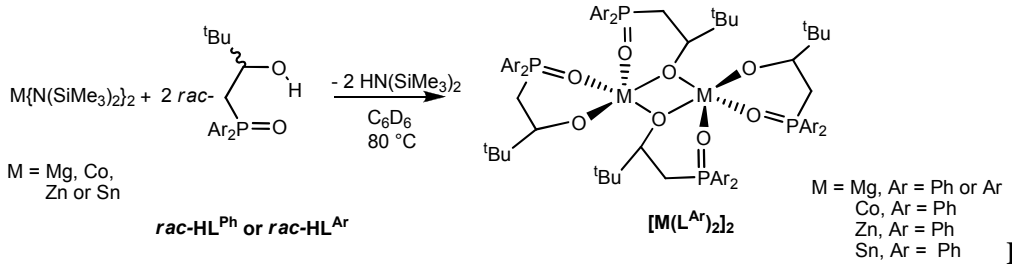

Eq 4.2

4.2.5 NMR characterisation of $[M(L^{Ar})_2]_2$

The complex $[Mg(L^{Ph})_2]_2$ was isolated as a colourless solid with a yield of 45 %. The ^1H and $^{31}P\{^1H\}$ NMR spectra of $[Mg(L^{Ph})_2]_2$ contain two sets of bound ligand resonances (indicating inequivalent ligand environments in a dimeric structure), at 40.2 and 40.4 ppm in the $^{31}P\{^1H\}$ NMR spectrum and at 1.1 and 1.2 ppm in the ^1H

NMR spectrum (Figure 4.5). It has been possible to obtain a single crystal of $[Mg(L^{Ar})_2]_2$ for X-Ray diffraction but no clean NMR spectra have been obtained.

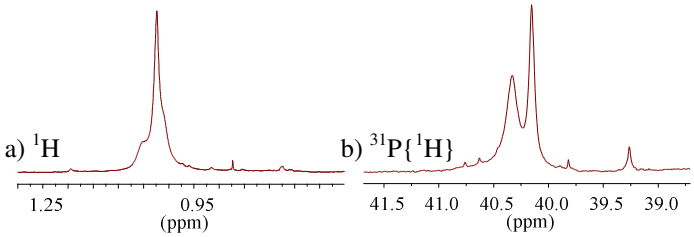

Figure 4.5: $^{31}P\{^{1}H\}$ and ^{1}H (*tert*-butyl region) NMR spectra of $[Mg(L^{Ph})_2]_2$ (d_6-benzene) a) ^{1}H and b) $^{31}P\{^{1}H\}$

The complex $[Co(L^{Ph})_2]_2$ was isolated as a purple solid with a yield of 88 %; the NMR spectra were paramagnetic. The ^{1}H NMR spectrum contains broad and overlapping resonances in the range of -40 to 60 ppm so they can not be counted and assigned with confidence. The ^{31}P NMR spectrum contains a very broad resonance at 27 ppm.

Several attempts have been made to synthesise $[Zn(L^{Ph})_2]_2$ but it has not been possible to isolate a pure product.

The complex $[Sn(L^{Ph})_2]_2$ was isolated as a colourless solid in 62 % yield. The ^{1}H and $^{31}P\{^{1}H\}$ NMR spectra of $[Mg(L^{Ph})_2]_2$ contain two sets of bound ligand resonances, at 37.6 and 38.6 ppm in the $^{31}P\{^{1}H\}$ NMR spectrum and at 0.9 and 0.95 ppm in the ^{1}H NMR spectrum (Figure 4.6). It is possible to see the tin satellites around the phosphorus resonances in Figure 4.6 b); the coupling constants $^{2}J_{SnP}$ are 198.0 Hz and 241.2 Hz.

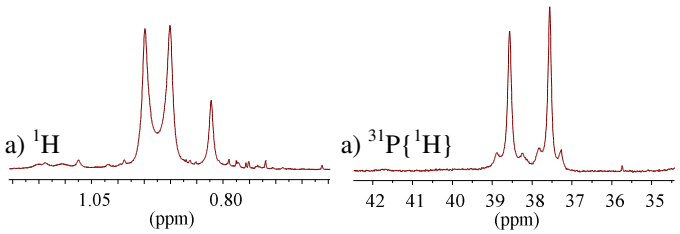

Figure 4.6: $^{31}P\{^{1}H\}$ and ^{1}H (*tert*-butyl region) NMR spectra of $[Sn(L^{Ph})_2]_2$ (d_6-benzene) a) ^{1}H and b) $^{31}P\{^{1}H\}$

4.2.6 X-Ray crystallography of $[M(L^{Ar})_2]_2$

Colourless crystals of complex **$[Mg(L^{Ar})_2]_2$** and purple crystals of complex **$[Co(L^{Ph})_2]_2$** suitable for a single crystal X-ray diffraction study were grown from a cooled DME/hexanes and hexanes solution respectively (Figure 4.7).

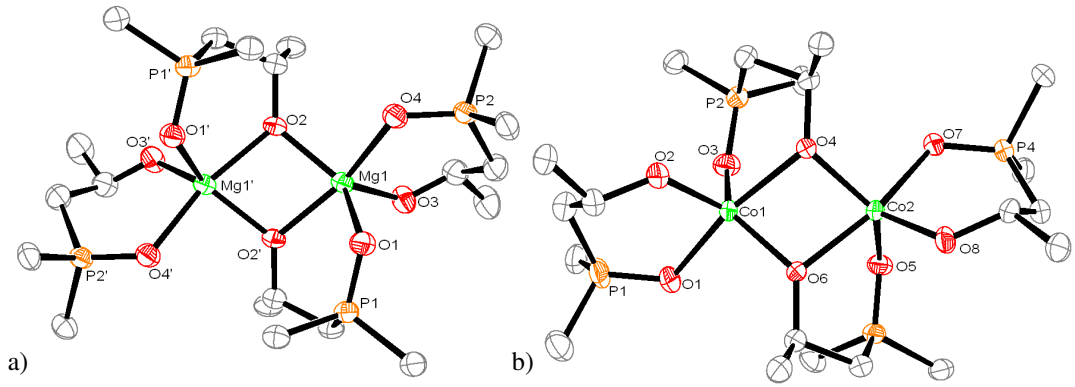

Figure 4.7: Displacement ellipsoid drawing of a) $[Mg(L^{Ar})_2]_2$, and b) $[Co(L^{Ph})_2]_2$, 50 % probability ellipsoids. Lattice solvent, aryl groups, phenyl groups, *tert*-butyl groups and all hydrogen atoms omitted for clarity. Selected distances (Å): (for $[Mg(L^{Ar})_2]_2$): Mg1-O1 2.096(3), Mg1-O2 2.047(3), Mg1-O3 1.930(3) and Mg1-O4 2.072(3); (for $[Co(L^{Ph})_2]_2$): Co1-O1 2.159(3), Co1-O2 1.918(4), Co1-O3 2.109(3) and Co1-O4 2.094(3); and selected angles (°): (for $[Mg(L^{Ar})_2]_2$): O1-Mg-O2 130.03(12), O1-Mg1-O3 103.38(13) and O2-Mg1-O3 106.31(12); (for $[Co(L^{Ph})_2]_2$): O1-Co-O2 94.74(15), O1-Co1-O3 85.71(13) and O2-Co1-O3 108.76(15)

The metal cations in the both dimeric **$[Mg(L^{Ar})_2]_2$** and **$[Co(L^{Ph})_2]_2$** structures have distorted square pyramidal geometries. Around one metal is a normally bound ligand in a bidentate fashion. A second ligand is bound by the phosphoryl oxygen donor and bridges across to the other metal centre by the alkoxy oxygen donor. In both complexes, the sum of the angles forming the square pyramidal base is close to 360°; $[Mg(L^{Ar})_2]_2$ (369.8°) and $[Co(L^{Ph})_2]_2$ (370.1°). Both metals have similar radii (5-coordinate), $r(Mg^{2+})$ = 0.66 Å and $r(Co^{2+})$ = 0.67 Å, which is demonstrated by similar M-M bond distances (3.044 Å for Co and 3.082 Å for Mg) and by similar M-O-M angles (97.65° for Co and 99.56° for Mg).

Jones *et al*. reported a compound $(C_{36}H_{30}NP_2)[Mg_2(C_2H_3O_2)(C_5H_7O_2)_4]\cdot H_2O$ (**B**, Figure 4.8) where four acetylacetonate groups are binding with two magnesium, a molecule of water and a molecule of acetate. The average Mg-OR bond distance is 2.052 Å, longer than in $[Mg(L^{Ar})_2]_2$ (1.930 Å).[16] However, the Mg-OP average bond distance (2.084 Å) is higher than reported in the literature (1.940 Å).[17, 18]

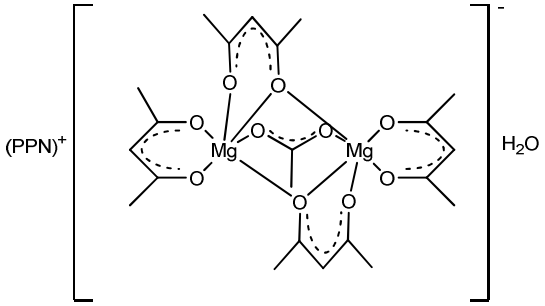

B

Figure 4.8: Acetylacetonate magnesium dimer complex, **B**

In $[Co_2(acac)_4(H_2O)_2]$, which has two bridging acac-O atoms, where the Co-O(bridging) average bond distance is 2.058 Å which is similar to that in $[Co(L^{Ph})_2]_2$ (2.022 Å). The Co-OR average bond distances in $[Co(L^{Ph})_2]_2$ are smaller (1.917 Å vs 2.049 Å).[19] The Co-OP average bond distance (1.961 - 2.150 Å) is in the higher part of the literature range (1.949 - 2.031 Å).[20-23]

4.2.7 Synthesis and characterisation of $[\{Co(L^{Ph})_2\}\{L^{Ph}Co(O_2CL^{Ph})\}]$

A solution of $[Co(L^{Ph})_2]_2$ stored in hexane in a Schlenk for a period of 11 months led to the formation of a new complex with bound CO_2 from adventitious air present. The CO_2 inserted in the cobalt-alkoxide bond to afford purple crystals characterised as $[\{Co(L^{Ph})_2\}\{L^{Ph}Co(O_2CL^{Ph})\}]$ but with no recorded yield (Equation 4.3).

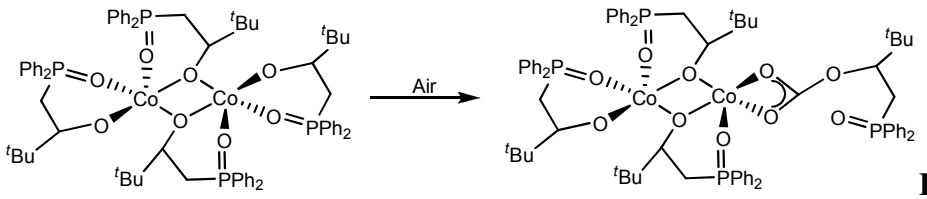

Eq. 4.3

The NMR spectra were paramagnetic, the ^1H NMR spectrum contains broad and overlapping resonances in the range of -40 to 60 ppm and so they can not be counted

or assigned with confidence. The ^{31}P NMR spectrum contains a very broad resonance at 34 ppm which is slightly shifted from the resonance at 27 ppm for $[Co(L^{Ph})_2]_2$.

Purple crystals of complex $[\{Co(L^{Ph})_2\}\{L^{Ph}Co(O_2CL^{Ph})\}]$ suitable for a single crystal X-ray diffraction study were grown from a cooled hexanes solution. The molecular structure is depicted in Figure 4.9.

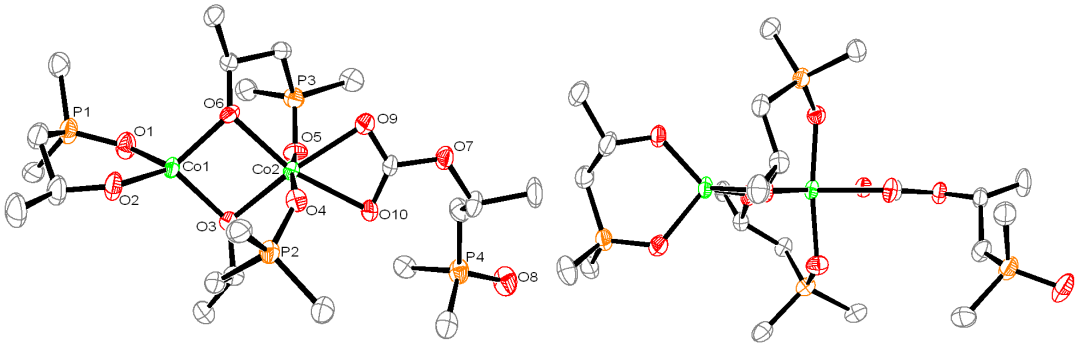

Figure 4.9: Displacement ellipsoid drawing of $[\{Co(L^{Ph})_2\}\{L^{Ph}Co(O_2CL^{Ph})\}]$ a) top view and b) side-on view, 50 % probability ellipsoids. Lattice solvent and all hydrogen atoms omitted for clarity. Selected distances (Å): Co1-O1 2.037(6), Co1-O2 1.906(6), Co1-O3 1.962(5), Co1-O6 1.948(5), Co2-O4 2.068(6), Co2-O9 2.148(5) and Co2-O10 2.203(5) and selected angles (°): O1-Co1-O2 98.9(2), O1-Co1-O3 118.9(3) and O9-Co2-O10 60.9(2).

The geometry around the Co1 metal is distorted tetragonal. The angle between O1–Co1–O2 (98.9(2)°) is small and the angles O1-Co1-O6 (107.4(2)°) and O2-Co1-O3 (117.6(2)°) deviate from the theoretical 109°. Co2 has a distorted octahedral geometry with the angles O6-Co2-O10 (164.4(2)°) and O3-Co2-O9 (173.6(2)°) in the equatorial plane and O5-Co2-O4 on the axial axis close to linear. The change in structure and symmetry does not affect the bond distances or angles between $[Co(L^{Ph})_2]_2$ and $[Co(L^{Ph})_2]_2(CO_2)]$. For example, the average Co-O-Co angle is very similar in both cases (97.65° and 95.25° respectively). There is no example of CO_2 inserted into a Co^{II} centre complex currently reported in the literature.

4.3 Synthesis and characterisation of $(L^R)MX$

4.3.1 Synthesis and characterisation of $(L^{tBu})MgN''$

Treatment of HL^{tBu} with MgN''_2 at -78 °C in THF afforded a mixture of compounds including $(L^{tBu})MgN''$ identified by ^1H NMR spectroscopy (Equation 4.4).

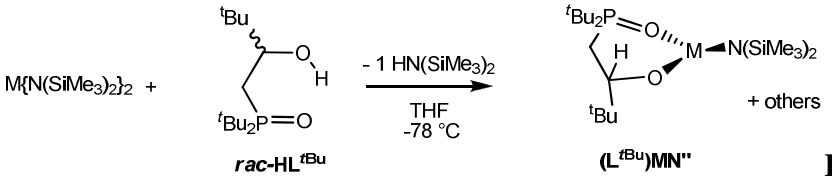

rac-HL^{tBu} $(L^{tBu})MN''$ **Eq. 4.4**

Despite several attempts, the reactions always gave a intractable mixture of compounds alongside $(L^{tBu})MgN''$. This route was not pursued further.

4.3.2 Synthesis and characterisation of $(L^{tBu})Mg(OAr)$

Treatment of HL^{tBu} and HOAr (HOAr = 2,6-^{t}Bu-C_6H_3) with MgN''_2 at 25 °C in THF afforded a colourless compound characterised as $(L^{tBu})Mg(OAr)$ (Equation 4.5).

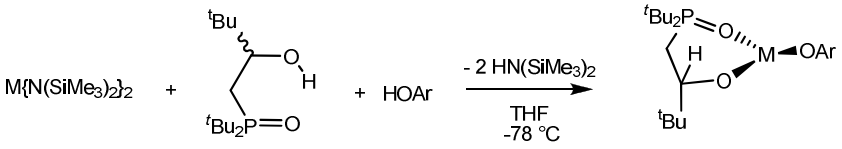

rac-HL^{tBu} $(L^{tBu})M(OAr)$ **Eq. 4.5**

Complex **$(L^{tBu})Mg(OAr)$** was isolated in a yield of 81 % as a colourless solid, the $^{31}P\{^1H\}$ NMR spectrum contains a single resonance at 74.5 ppm. The mass spectrum results shows m/z (7.2 %) = 489.4 $[(L^{tBu})Mg(OAr)]^+$.

4.4 Synthesis and characterisation of $[(HL^R)_2MCl].Cl$

4.4.1 General synthesis of $[(HL^R)_2MCl].Cl$

Treatment of two equivalents of *rac*-HL^R with MCl_2 (M = Mg or Zn and R = ^{t}Bu or Ph) in toluene at 80 °C affords $[(HL^R)_2MCl].Cl$ in yields of 70 - 90 % (Equation 4.6).

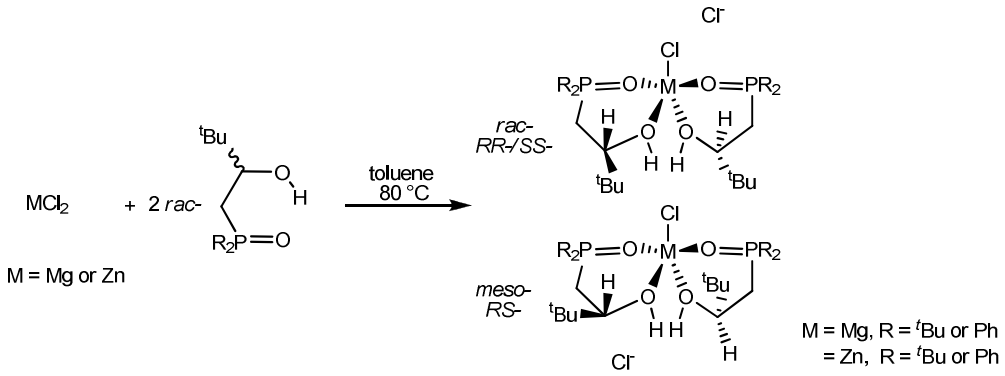

Eq 4.6

4.4.2 NMR and mass spectrometry characterisation of $[(HL^R)_2MgCl].Cl$

The complex **$[(HL^R)_2MgCl].Cl$** was isolated in 70 % yield as a colourless solid. The $^{31}P\{^1H\}$ NMR spectrum contains two resonances (70.0 and 70.6 pm) (Figure 4.10 b)) and ^1H NMR spectrum contains a broad singlet at 5.22 ppm (O*H*) (the mass spectrum shows m/z at (11.5 %) = 582.6 [M - HCl] and m/z (7.1 %) = 546.6 [M– 2 HCl]).

The complex **$[(HL^R)_2MgCl].Cl$** was isolated in a yield of 76 % as a colourless solid. The $^{31}P\{^1H\}$ NMR spectrum contains two resonances (32.0 and 35.3 pm) (Figure 4.10 d)). The resonance for the O*H* is significantly shifted from 5.22 ppm ($[(HL^{tBu})_2MgCl].Cl$) to 3.65 ppm ($[(HL^{Ph})_2MgCl].Cl$), The mass spectrometric analysis shows m/z (8.49 %) = 663.1 [M - HCl].

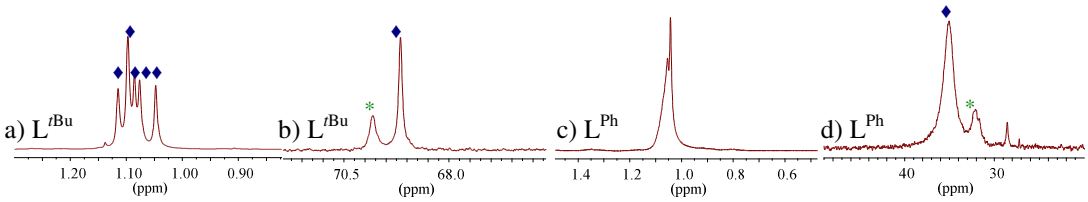

Figure 4.10: $^{31}P\{^{1}H\}$ and ^{1}H (*tert*-butyl region) NMR spectra (d_6-benzene) a) ^{1}H: $[(HL^{tBu})_2MgCl].Cl$, b) $^{31}P\{^{1}H\}$: $[(HL^{tBu})_2MgCl].Cl$, c) ^{1}H: $[(HL^{Ph})_2MgCl].Cl$ and d) $^{31}P\{^{1}H\}$: $[(HL^{Ph})_2MgCl].Cl$. ♦ denotes *RR/SS*-$[(HL^{R})_2MgCl].Cl$, * denotes *RS*-$[(HL^{R})_2MgCl].Cl$

The ^{1}H and $^{31}P\{^{1}H\}$ NMR spectra of $[(HL^{R})_2MgCl].Cl$ show that there is 75 % of *RR/SS*-$[(HL^{tBu})_2MgCl].Cl$ (25 % of *RS*-$[(HL^{tBu})_2MgCl].Cl$) and 85 % of *rac*-$[(HL^{Ph})_2MgCl].Cl$ (15 % of *RS*-$[(HL^{Ph})_2MgCl].Cl$).

4.4.3 X-Ray spectroscopic study of $[(HL^{tBu})_2MgCl].Cl$

Colourless crystals of complexes **$[(HL^{tBu})_2MgCl].Cl$** and **$[(HL^{tBu})_2Mg(OH_2)].2Cl$** suitable for a single crystal X-ray diffraction study were grown from a cooled hexanes and wet d_1-chloroform solution respectively The molecular structures are depicted in Figure 4.11. The configuration of the molecules shown is *RS*-$[(HL^{tBu})_2MgCl].Cl$ and *SS*-$[(HL^{tBu})_2Mg(OH_2)].2Cl$

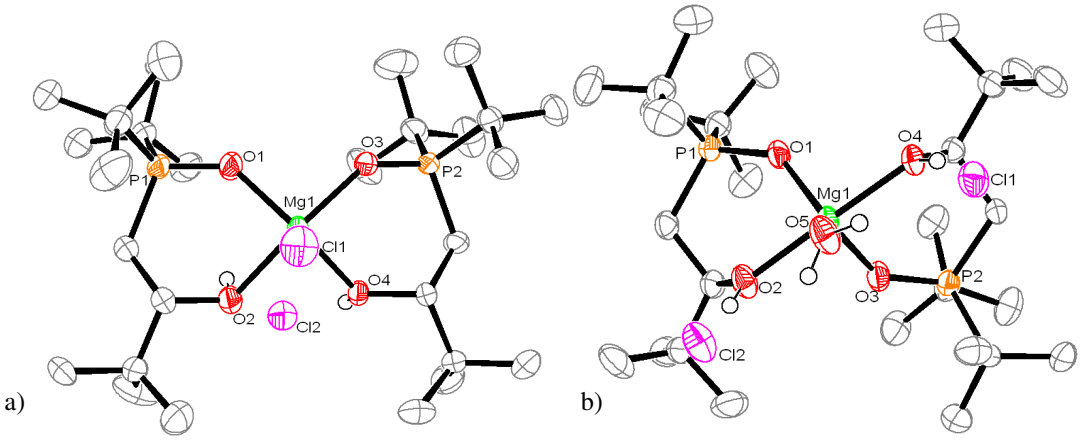

Figure 4.11: Displacement ellipsoid drawing of a) $[(HL^{tBu})_2MgCl].Cl$ and b) $[(HL^{tBu})_2Mg(OH_2)].2Cl$, 50 % probability ellipsoids. Lattice solvent and all hydrogen

atoms except OH and H_2O atoms omitted for clarity. Selected distances (Å): for ([$(HL^{tBu})_2$MgCl].Cl): Mg1-O1 1.941(5), Mg1-O2 2.108(5) and Mg1-Cl1 2.316(3); for ([$(HL^{tBu})_2Mg(OH_2)$].2Cl) Mg1-O1 1.950(2), Mg1-O2 2.048(3), Mg1-O3 1.959(3) and Mg1-O4 2.076(3). Selected angles (°): for (([$(HL^{tBu})_2$MgCl].Cl): O1-Mg1-O2 86.0(2), O1-Mg1-O3 91.4(2), O1-Mg1-Cl2 109.65(19); for ([$(HL^{tBu})_2Mg(OH_2)$] .2Cl): O1-Mg1-O2 87.96(11), O1-Mg1-O3 110.81(11) and O1-Mg1-O5 126.39(12).

The metal cation in each molecular structure, [$(HL^{tBu})_2$MgCl].Cl and [$(HL^{tBu})_2Mg(OH_2)$].2Cl, has a distorted square pyramidal geometry with O1, O2, O3 and O4 forming the square plane base.

Kontturi *et al.* and Jokiniemi *et al.* reported 6-coordinate magnesium complexes $[MgCl_2C(PO_3Et)_2(H_2O)_3]_n$, **C**, and $[Mg(CH_3PO_3CCl_2PO_2NC_4H_8O)(H_2O)_3]_n$, **D**, (Figure 4.12) respectively. The average Mg-OH_2 bond distances are 2.118 Å (in **C**) and 2.144 Å (in **D**). The Mg-OP average bond distances are 2.064 Å (in **C**) and 2.078 Å (in **D**); which is higher than those in [$(HL^{tBu})_2Mg(OH_2)$].2Cl with an Mg-OH_2 bond distance of 1.971(3) Å and an average Mg-OP bond distance of 1.955 Å reflecting the decrease in coordination number.[24, 25]

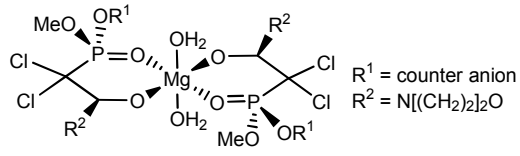

D

Figure 4.12: Structure of $[Mg(CH_3PO_3CCl_2PO_2NC_4H_8O)(H_2O)_3]_n$, **D**

The molecular structures, drawn as space filling plots, are shown in Figure 4.13 for a) $(HL^{tBu})_2MgCl_2$ and c) [$(HL^{tBu})_2Mg(OH_2)$].2Cl. Looking down the formal axis that bisects the two magnesium-alkoxide bonds, it is easiest to see how the packing is disrupted by the chloride/water-magnesium bond in both cases in Figure 4.13 a). It is possible to observe hydrogen bonding between the free chloride and the hydrogen of the alkoxide oxygen and of the water molecule creating a compact structure (Figure

4.13 b)). Thus, it appears that $[(HL^{tBu})_2Mg(OH_2)].2Cl$ is the most densely packed, as would be required in a ligand self-recognition process in Figure 4.13 c).

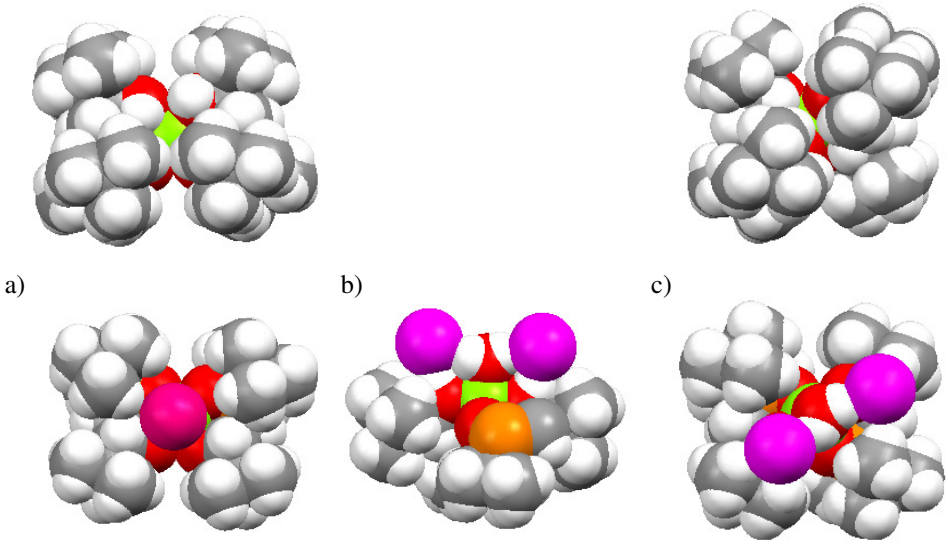

Figure 4.13: Space filling drawings of the molecular structures viewed from above the plane of the two alkoxides (above) and above the plane of the phosphine oxides (below) for a) $(HL^{tBu})_2MgCl_2$ and c) $[(HL^{tBu})_2Mg(OH_2)].2Cl$. Metal is coloured green, oxygen red, phosphorus orange, chloride magenta, carbon grey and hydrogen white.

Complex **$[(HL^{tBu})_2ZnCl].Cl$** was isolated in a yield of 82 % as a colourless solid; the $^{31}P\{^1H\}$ NMR spectrum contains one resonance at 72.6 pm (Figure 4.14 b)), and the ^1H NMR spectrum contains a broad singlet at 4.63 ppm (O*H*). The mass spectrum shows the molecular ion m/z (10.5 %) = 623.0 [M - HCl] and m/z (7.1 %) = 587.0 [M – 2 HCl].

Complex **$[(HL^{Ph})_2ZnCl].Cl$** was isolated in a yield of 85 % as a colourless solid; the $^{31}P\{^1H\}$ NMR spectrum contains one resonance at 41.6 pm (Figure 4.14 d)) and the ^1H NMR spectrum contains a broad singlet at 4.95 ppm (O*H*). The mass spectrum shows m/z (7.3 %) = 667.4 [(M – 2 HCl].

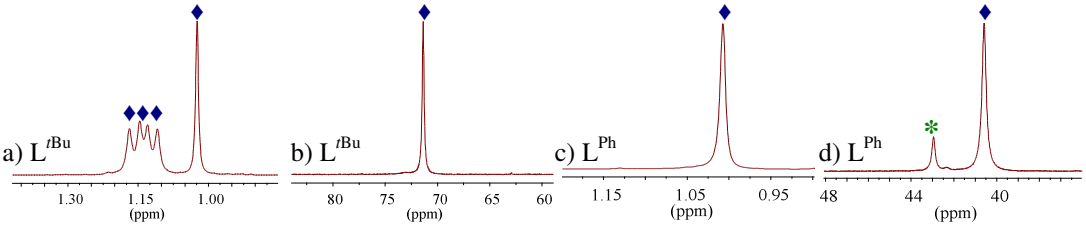

Figure 4.14: $^{31}P\{^{1}H\}$ and ^{1}H (*tert*-butyl region) NMR spectra (d_6-benzene) a) ^{1}H: $(HL^{tBu})_2ZnCl_2$, b) $^{31}P\{^{1}H\}$: $(HL^{tBu})_2ZnCl_2$, c) ^{1}H: $(HL^{Ph})_2ZnCl_2$ and d) $^{31}P\{^{1}H\}$: $(HL^{Ph})_2ZnCl_2$. ♦ denotes *rac*-$(HL^{R})_2ZnCl_2$, * denotes *RS*-$(HL^{R})_2ZnCl_2$

The ^{1}H and $^{31}P\{^{1}H\}$ NMR spectra of $(HL^{R})_2ZnCl_2$ show that there is 100 % of *rac*-$(HL^{tBu})_2ZnCl_2$ and 90 % of *rac*-$(HL^{Ph})_2ZnCl_2$ (10 % of $(HL^{Ph})_2ZnCl_2$); there is an improvement in diastereomeric index with the increase of the steric bulk of the ligand around the zinc centre.

A colourless single tablet of complex **$(HL^{tBu})ZnCl_2$** was grown from a d_6-benzene solution which was not representative of the bulk sample. The molecular structure is depicted in Figure 4.15.

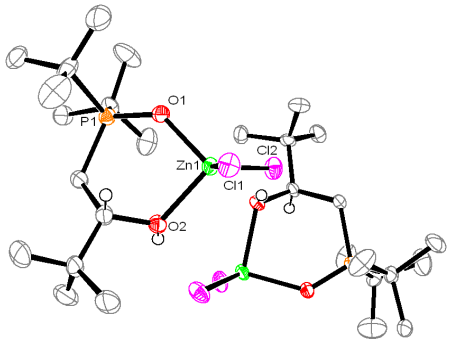

Figure 4.15: Crystal structure of $(HL^{tBu})ZnCl_2$, 50 % probability ellipsoids. All lattice solvents, *tert*-butyl group and all hydrogen atoms except CH and OH omitted. Selected distances (Å): Zn1-O1 1.951(4), Zn1-O2 2.058(4) and Zn1-Cl1 2.2021(14). Selected angles (°) O1-Zn1-O2 91.68(15) and O1-Zn1-Cl1 112.31(12).

Both enantiomers, ***R*-$(HL^{tBu})ZnCl_2$** and ***S*-$(HL^{tBu})ZnCl_2$,** are present in the asymmetric unit. The metal cation has distorted tetrahedral geometry. The distortion is due to the steric bulk of the *tert*-butyl group. As a result, the bond angles O1-Zn1-

Cl2 (111.70(12)°) and O2-Zn1-Cl1 (106.75(12)°) deviate from the theoretical 109°. The Zn-OR average bond distances are significantly longer than in $Zn(L^{tBu})_2$ (2.051 Å and 1.873 Å respectively). The average Zn-OP bond distances are similar (1.955 Å and 2.027 Å respectively).

4.4.4 Synthesis and characterisation of $(HL^R)_2SnCl_2$

Treatment of two equivalents of *rac*-HL^R with $SnCl_2$ in toluene at 80 °C for 16 hours affords $(HL^R)_2SnCl_2$ in good yield (> 80 %) (Equation. 4.7).

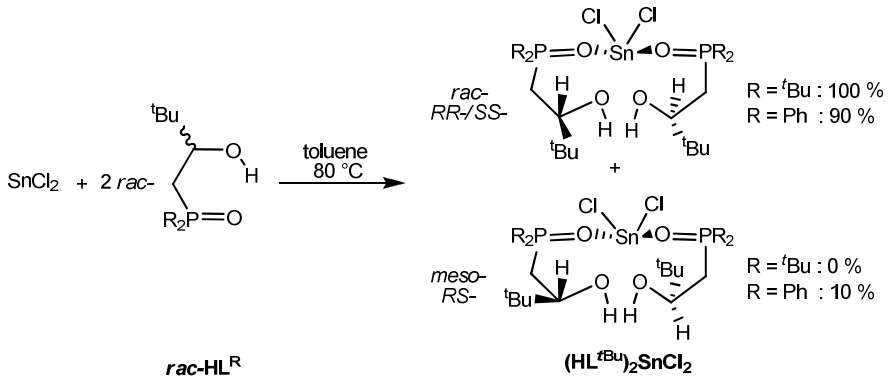

Eq 4.7

Complex $\mathbf{(HL^{tBu})_2SnCl_2}$ was isolated in a yield of 81 % as a colourless solid. The $^{31}P\{^1H\}$ NMR spectrum contains one resonance at 70.2 pm (Figure 4.16 b)) and the ^1H NMR spectrum contains a broad singlet at 4.93 ppm (OH). The mass spectrum shows m/z (39.1 %) = 677.3 [M - HCl], m/z (29.8 %) = 640.3 [M– 2 HCl].

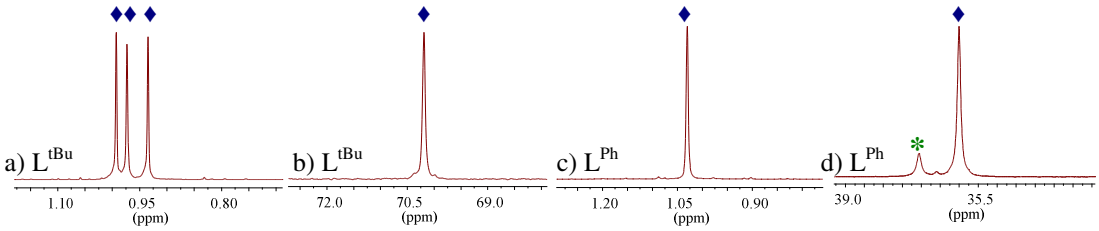

Figure 4.16: $^{31}P\{^1H\}$ and ^1H (*tert*-butyl region) NMR spectra (d_6-benzene) a) ^1H: $(HL^{tBu})_2SnCl_2$, b) $^{31}P\{^1H\}$: $(HL^{tBu})_2SnCl_2$, c) ^1H: $(HL^{Ph})_2SnCl_2$ and d) $^{31}P\{^1H\}$: $(HL^{Ph})_2SnCl_2$. ♦ denotes *rac*-$(HL^R)_2SnCl_2$, * denotes *RS*-$(HL^R)_2SnCl_2$

Complex $\mathbf{(HL^{Ph})_2SnCl_2}$ was isolated in a yield of 89 % as a colourless solid. The $^{31}P\{^1H\}$ NMR spectrum contains one resonance at 36.7 pm (Figure 4.16 d)) and the

^{1}H NMR spectrum contains a broad singlet at 4.61 ppm (O*H*). The mass spectrum shows m/z (30.3 %) = 721.0 [M – 2 HCl].

The ^{1}H and ^{31}P{^{1}H} NMR spectra of $(HL^{R})_2SnCl_2$ show that there is 100 % of *rac*-$(HL^{tBu})_2SnCl_2$ and 90 % of *rac*-$(HL^{Ph})_2SnCl_2$ (10 % of $(HL^{Ph})_2SnCl_2$). This shows an improvement in diastereomeric index as the steric bulk of the ligand around the tin centre increases.

Colourless crystals of complex **$(HL^{tBu})_2SnCl_2$** suitable for a single crystal X-ray diffraction study were grown from a cooled hexanes solution; the molecular structure is depicted in Figure 4.17. It was not possible to locate the hydrogen atom on the alcohol oxygen.

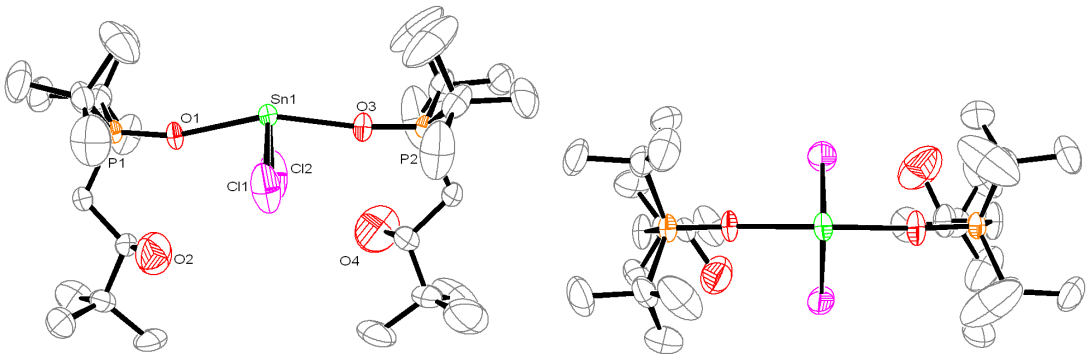

Figure 4.17: Displacement ellipsoid drawing of $(HL^{tBu})_2SnCl_2$ a) top view and b) side view, 50 % probability ellipsoids. Lattice solvent and all hydrogen atoms omitted for clarity. Selected distances (Å): Sn1-O1 2.328(4), Sn1-O3 2.313(5) and Sn1-Cl1 2.442(2). Selected angles (°): O1-Sn1-O3 160.53(19) and O1-Sn1-Cl1 82.92(15)

The metal cation in the molecule **$(HL^{tBu})_2SnCl_2$** has a distorted sawhorse geometry. The O1-Sn-O3 angle formed by the two sterically demanding phosphine oxide ligands deviates from linearity (160.53(19)°) and this is undoubtedly, due to the stereochemically active lone pair of Sn^{II}. Mehring *et al.* reported the Sn^{II} complex $\{\{2,6\text{-}[P(O)(OEt)_2]_2\text{-}4\text{-}^{t}Bu\text{-}C_6H_2\}SnCl(\mu\text{-}S)\}_2$ (**E**, Figure 4.18) The average Sn-OP bond distance in $(HL^{tBu})_2SnCl_2$ (2.328 Å) is longer than that in **E** (2.263 Å).[26]

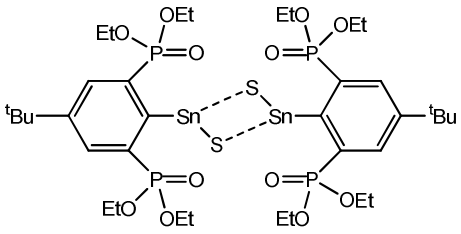

E

Figure 4.18: {{2,6-[P(O)(OEt)$_2$]$_2$-4-*tert*-Bu-C$_6$H$_2$}SnCl(μ-S)}$_2$, **E**

The average Sn-Cl bond distance (2.437 Å) is within the literature range for a Sn^{II}-Cl bond (2.436-2.500 Å).[27, 28] The Sn-OP average bond distance in (HL^{tBu})SnCl$_2$ are slightly shorter than in Sn(L^{tBu})$_2$ (2.321 Å and 2.372 Å respectively).

4.4.5 Deprotonation reaction of (HL^{tBu})$_2$MCl$_2$

4.4.5.1 Deprotonation reactions using DABCO

To a solution of (HL^{tBu})$_2$MCl$_2$ (where M = Mg or Sn) in toluene was added three equivalents of DABCO (1,4-diazabicyclo[2.2.2]octane) in toluene at -78 °C, this was left to warm up to room temperature and then stirred for 16 hours. The reaction was left to settle down to afford white solid and colourless solution; after filtration the solution was dried under vacuum to afford colourless glue. The NMR spectroscopy shows intractable mixtures of compounds (Equation 4.8).

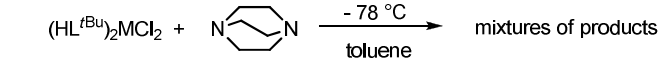

M = Mg or Sn **Eq. 4.8**

4.4.5.2 Deprotonation reaction using LiN"

To a solution of **(HL^{tBu})$_2$SnCl$_2$** in *d*$_6$-benzene was added two equivalents of LiN" in C$_6$D$_6$ at room temperature, the reaction was heated for 16 hours at 80 °C, the NMR spectroscopy shows an intractable mixture of compounds (Equation 4.9).

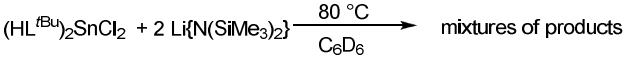

Eq. 4.9

4.5 Polymerisation of *rac*-lactide using M^{II} complexes

4.5.1 Polymerisation of *rac*-lactide using $M(L^R)_2$

A solution of 10 mg of catalyst $M(L^R)_2$ in DCM or toluene was added to a solution of 0.5 g of *rac*-lactide which was dissolved in DCM or toluene according to the Table Entry (Equation 4.10).

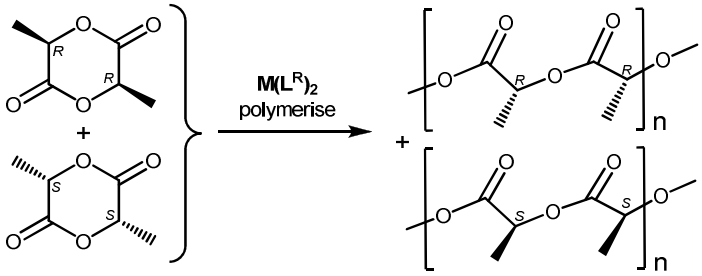

rac-lactide *isotactic chains of PLA* **Eq. 4.10**

The series of conditions and results of the polymerisation of *rac*-lactide by $Zn(L^{tBu})_2$ or $Sn(L^{tBu})_2$ are collated in Table 4.1.

Table 4.1: Polymerisation data of *rac*-lactide using $Zn(L^{tBu})_2$ or $Sn(L^{tBu})_2$

Metal/ Entry	Cat:monomer :solvent ratio	T /°C	Time / h	Conv.[c] / %	$M_{n,\,exp}$[d] g/mol	$M_{n,\,theo}$[e] g/mol	PDI[f] M_w/M_n
Zn / 1	1 : 100 : 1000[a]	25	0.17	> 99	41 500	58 541	1.75
Sn / 2	1 : 100 : 1000[a]	25	16	15	7 500	10 380	1.18
Zn / 3	1 : 200 : 10000[a]	25	16	98	82 000	115 327	1.42
Sn / 4	1 : 200 : 1000[b]	60	16	93	65 000	60 098	1.53

a: DCM; b: toluene; c: conversion of LA monomer (($[LA]_0$-[LA])/$[LA]_0$); d: measured by GPC, weight corrected by multiplication by 0.58; e: molecular weight theoretical calc. using $M_{n,\,theo}$ = Conv. × [Mono]/[Cat] × M_{Mono}; f: polydispersity index (M_w/M_n), PDI, measured by GPC.

At 25 °C, the polymerisation using $Zn(L^{tBu})_2$ with a catalyst : monomer : solvent ratio of 1 : 100 : 1 000 is rapid as full conversion is attained after 10 minutes with $M_{n,exp}$ of 41 500 g/mol and a polydispersity (PDI) of 1.75 (Entry 1, Table 4.1). A change in the monomer : solvent ratio from 100 : 1 000 to 200 : 10 000 decreases the

rate of the polymerisation; conversion is 98 % after 16 hours with PDI of 1.42 and M_n,exp of 82 000 g/mol (Entry 3). The fastest zinc-alkoxide initiator published was by Tolman *et al.* with a mononuclear zinc complex (**F**, Figure 4.19). The results were similar to Entry 1 but with a catalyst : monomer ratio of 1 : 650 (M_n of 67 000 g/mol and PDI of 1.42).[29]

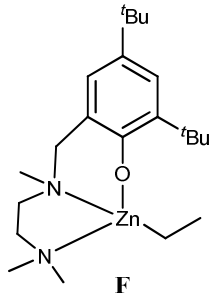

F

Figure 4.19: Phenoxy zinc alkoxide, **F**

In contrast, at 25 °C, the polymerisation using Sn(L^{tBu}) is slow; only 15 % of conversion is attained after 16 hours in CH_2Cl_2, with a $M_{n,exp}$ of 7 500 g/mol and PDI of 1.18 (Entry 2). Increasing the temperature from 25 °C to 60 °C increases the rate of polymerisation and 93 % conversion is attained after 16 hours but the PDI also rises from 1.18 to 1.53 (Entry 4).

Most of the tin complexes in the literature use a co-initiator, in similar experimental conditions to Entry 4. Hillmyer *et al*. reported a mixture of benzyl alcohol and [$L^{SiMe2PhSn}(OCPh_3)$] (**G**, Figure 4.20) which gives a polylactide with a molecular weight of 30 000 g/mol and a PDI of 1.30; Kricheldorf *et al*. published a cyclic tin alkoxide, in $CHCl_3$, which needed 71 hours for only 78 % of conversion but with a PDI of 1.10 and a molecular weight of 39 000 g/mol.[30-32]

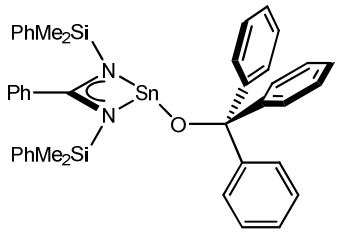

G

Figure 4.20: Monomeric Sn^{II} alkoxide complex of bulky amidinate ligand, **G**

The complex **Ca(L^{Ph})$_2$** was examined for polymerisation activity with *rac*-lactide with a catalyst : monomer ratio of 1 : 50. The polymerisations were carried out in bulk at 140 °C with benzyl alcohol as co-initiator. From the polymerisation data, it is apparent than the calcium complex shows, at full conversion (> 95 %), a narrow PDI (1.2-1.3) but low molecular weights (around 1000-2000 g/mol). The conversion *vs* the time of polymerisation using **Ca(L^{Ph})$_2$** is shown in Figure 4.21 b).

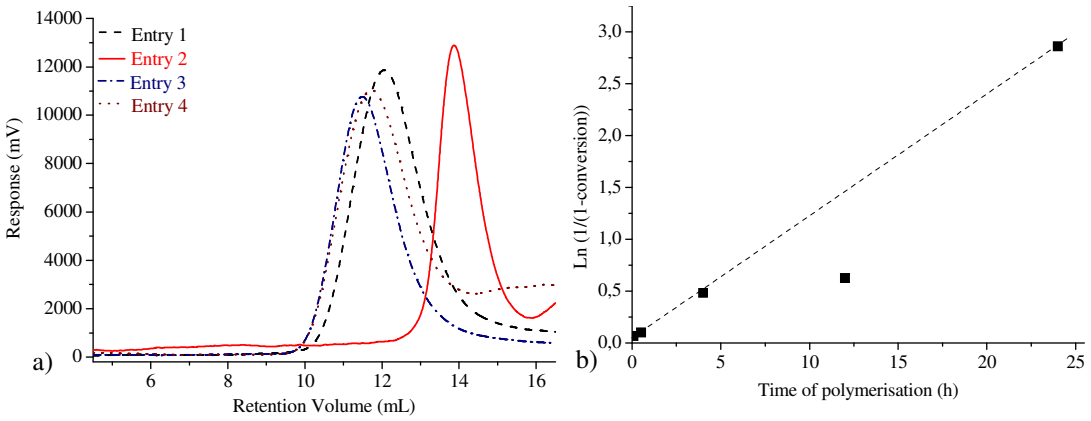

Figure 4.21: Polymerisation data for *rac*-lactide by M(L^{R})$_2$ a) GPC chromatogram traces for polylactides synthesised by Sn(L^{tBu})$_2$ and Zn(L^{tBu})$_2$, entries correspond to Table 4.1 b) Kinetic plots of the *rac*-lactide conversion *vs* reaction time by Ca(L^{Ph})$_2$

Figure 4.22 shows the methine region of $^{13}C\{^{1}H\}$ NMR spectra of the polymers produced using Ca(L^{Ph})$_2$ at 140 °C with benzyl alcohol.

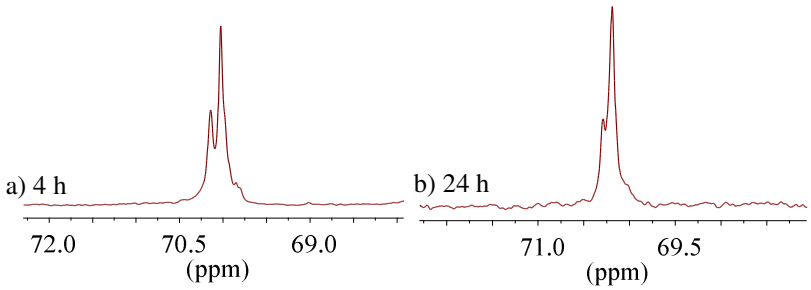

Figure 4.22: Methine region of ^{13}C NMR spectra of the polymerisation of *rac*-lactide using a mixture of Ca(L^{Ph})$_2$/benzyl alcohol a) PLA, after 4 hours, *iii* = 45 % and b) PLA, after 24 hours, *iii* = 55 %

There is a reasonable proportion of isotactic polymer, with the *iii* resonance integrated to 55 % of the total C*H* resonance after 24 hours of polymerisation.

Compared with literature, these calcium complexes showed similar polydispersities but lower molecular weights, Darensbourg *et al.* reported tridentate Schiff base calcium complexes (**H**, Figure 4.23), which polymerise *rac*-lactide with M_n from 60 000 to 100 000 g/mol and PDIs below 1.05.[33]

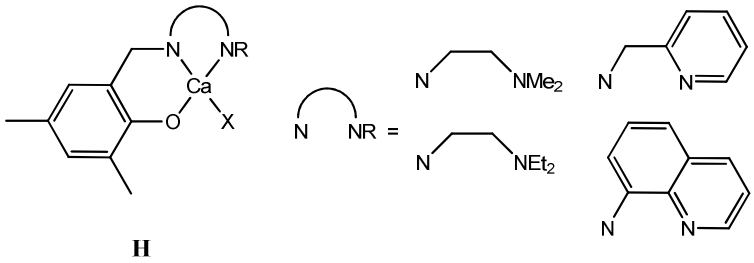

H

Figure 4.23: Calcium complexes with tridentate Schiff base ligands, **H**

4.5.2 Polymerisation of *rac*-lactide using $(HL^R)_2MCl_2$

For polymerisations in solution; a solution of 10 mg of catalyst $(HL^R)_2MCl_2$ in toluene was added to a solution of 0.5 g of *rac*-lactide in toluene and heated to 60 °C (with benzyl alcohol as co-initiator) or 100 °C (without co-initiator) (Figure 4.24).

For polymerisations in melt conditions; the catalyst $(HL^R)_2MCl_2$ (10 mg) was added to a mixture of *rac*-lactide (0.5 g) and benzyl alcohol before being heated to 140 °C.

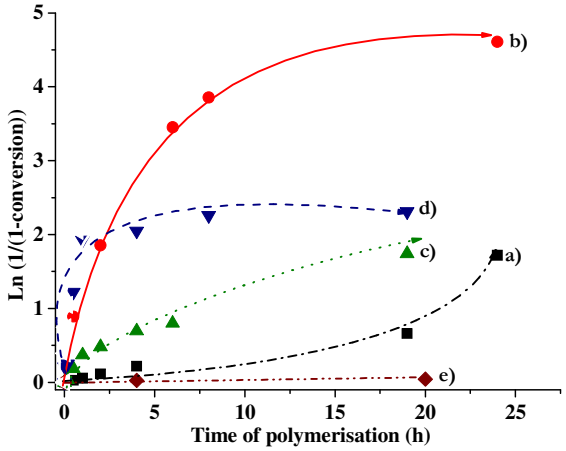

Figure 4.24: Kinetic plots of the *rac*-lactide conversion *vs* reaction time for a) 60 °C, $(HL^{Ph})_2SnCl_2$ with BzOH b) 100 °C, $(HL^{Ph})_2SnCl_2$ with BzOH c) 60 °C,

$(HL^{tBu})_2SnCl_2$ with BzOH d) 100 °C, $(HL^{tBu})_2SnCl_2$ with BzOH and e) 100 °C, $(HL^{tBu})_2SnCl_2$ without BzOH

The kinetic studies show that the polymerisation of *rac*-lactide by $(HL^{R})_2SnCl_2$ is faster with $(HL^{Ph})_2SnCl_2$ than with $(HL^{tBu})_2SnCl_2$, in agreement with the rates found for *rac*-$Y(L^{R})_3$. As expected, the polymerisation is faster with a co-initiator and at a higher temperature.

To confirm that *rac*-HL^{R} does not polymerise *rac*-lactide, the proligand was treated with benzyl alcohol which was subsequently used in the attempted polymerisation of *rac*-lactide; the ^1H NMR spectrum shows no polymerisation after 24 hours at 140 °C.

Despite the use of a co-initiator to improve the rates of the polymerisation, the reactions were slow. So, the polymerisations of *rac*-lactide were then carried out as melts at 140 °C, using benzyl alcohol as co-initiator (Table 4.2).

Table 4.2: Polymerisation data of *rac*-lactide using $[(HL^{R})_2MCl_2$.

Entry	Catalyst/ Metal	Cat:monomer: initiator ratio	T / °C	time / h	Conv.[a] / %	$M_{n, exp}$[b] g/mol	$M_{n, theo}$[c] g/mol	PDI[d] M_w/M_n
1	Mg	1:50:1	140	24	89	5 300	6 416	1.61
2	Mg	1:50:1	140	24	95	4 500	6 848	1.88
3	Zn	1:50:1	140	24	55	1 100	3965	2.33
4	Zn	1:50:1	140	24	97	1 300	6 992	1.42
5	Sn	1:50:1	140	24	69	4 400	4 974	1.19
6	Sn	1:50:1	140	24	55	1 100	3 964	2.33
7	$Sn(oct)_2$	1:50:1	140	24	24	700	1 730	1.13

a: conversion of LA monomer ($([LA]_0$-$[LA])/[LA]_0$), calculated by ^1H NMR; b: measured by GPC, values based on polystyrene standards and corrected by multiplication by 0.57 (Mark-Houwink law); c. Molecular weight theo calc. using $M_{n, theo}$ = Conv. × [Mono]/[Cat] × M_{Mono} d. polydispersity index (M_w/M_n), PDI, measured by GPC.

The polymerisations using **$(HL^R)_2MgCl_2$** shows the best results; high molecular weight (M_n of 15 000 - 20 000 g/mol) although the polydispersities are not narrow (PDI of 1.6 - 1.8). Also, the kinetic traces show a living nature with a linear relationship between M_n and conversion, PDI decreases with an increasing conversion.

At 2 % catalyst loading, the polymerisations using **$(HL^R)_2ZnCl_2$** are slow, the molecular weights are low (below 2000 g/mol) and the polydispersities fluctuate between 1.3 - 2.

Compared with the magnesium and zinc complexes from the literature (benzyl alcohol as co-initiator), the polymers have similar molecular weights (10 000 - 30 000 g/mol) but the PDI are lower than those reported (below 1.5).[34-39]

The polymerisation data using **$(HL^R)_2SnCl_2$** are difficult to interpret and inconsistent; generally the polymerisation rates were slow and the molecular weights low. However, under the same conditions, the polymerisations using **$Sn(oct)_2$** were slower than $(HL^R)_2SnCl_2$.

The GPC chromatogram in Figure 4.25 shows that the polymerisations of *rac*-lactide using $(HL^{tBu})_2MgCl_2$ and $(HL^{Ph})_2MgCl_2$ have the highest molecular weight, and that formed using $(HL^{tBu})_2SnCl_2$ has the most narrow polydispersity.

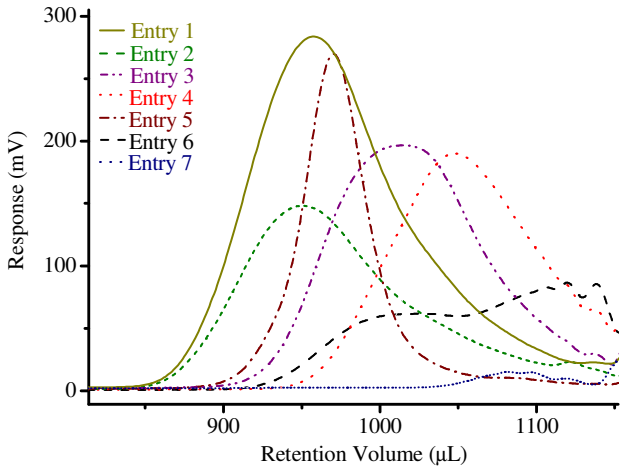

Figure 4.25: GPC chromatogram traces of the polymerisation of *rac*-lactide by $(HL^R)MCl_2$ and $Sn(oct)_2$, Entry 1 - Entry 7, Table 4.2

The polymerisation data of *rac*-lactide using (HL^{tBu})$MgCl_2$ at 140 °C with benzyl alcohol as co-initiator are collated in Table 4.3.

Table 4.3: Polymerisation data of *rac*-lactide using (HL^{tBu})$MgCl_2$

Entry	Cat:monomer: initiator ratio	T / °C	time / h	Conv.[a] / %	$M_{n, exp}$[b] g/mol	$M_{n, theo}$[c] g/mol	PDI[d] M_w/M_n
1	1 : 50 : 1	140	0.5	6	900	433	1.07
2	1 : 50 : 1	140	2	20	6 500	1 441	1.15
3	1 : 50 : 1	140	6	77	13 000	5 550	1.32
4	1 : 50 : 1	140	15	88	14 500	6 344	1.35
5	1 : 50 : 1	140	24	92	13 500	6 632	1.38
6	1 : 100 : 1	140	0.5	3	900	433	1.08
7	1 : 100 : 1	140	2	12	8 000	1 730	1.11
8	1 : 100 : 1	140	6	17	8 000	2 451	1.14
9	1 : 100 : 1	140	15	88	10 000	12 500	1.39
10	1 : 100 : 1	140	24	95	20 000	13 697	1.38
11	1 : 200 : 1	140	0.5	2	1 000	577	1.18
12	1 : 200 : 1	140	2	19	6 500	5 500	1.07
13	1 : 200 : 1	140	6	91	12 500	26 240	1.32
14	1 : 200 : 1	140	15	94	20 000	27 106	1.38
15	1 : 200 : 1	140	24	97	4 000	27 971	1.49

a: conversion of LA monomer (($[LA]_0$-[LA])/$[LA]_0$), calculated by ^1H NMR; b: measured by GPC, values based on polystyrene standards and corrected by multiplication by 0.57 (Mark-Houwink law); c. Molecular weight theo calc. using M_{th} = Conv. × [Mono]/[Cat] × M_{Mono} d. polydispersity index (M_w/M_n), PDI, measured by GPC.

Table 4.3 shows that (HL^{tBu})$MgCl_2$ polymerises *rac*-lactide with a reasonable rate; 90 % conversion is attained in each polymerisation within 24 hours at 140 °C

(varying the initiator : monomer ratio 1 : 50, 1 :100 or 1 :200.). All the PDI are between 1.1 - 1.4 and the experimental molecular weights are close to the theoretical.

The polymerisations with a initiator : monomer ratio of 1 : 50 and 1 : 200 show transesterifications at high conversion (Table 4.3, Entry 5 and Entry 15), in contrast with the polymerisation with a initiator : monomer ratio of 1 : 100 which does not.

The tacticity of the polymers formed using $(HL^{tBu})_2MgCl_2$ as an initiator have been studied. The NMR spectra of samples of *rac*-lactide, at 89 % monomer conversion, show a isotacticty *iii* of 35 %.

Despite the poor tacticity of the polymer, Figure 4.26 shows that the polymerisation of *rac*-lactide by $(HL^{tBu})_2MgCl_2$ and benzyl alcohol is controlled.

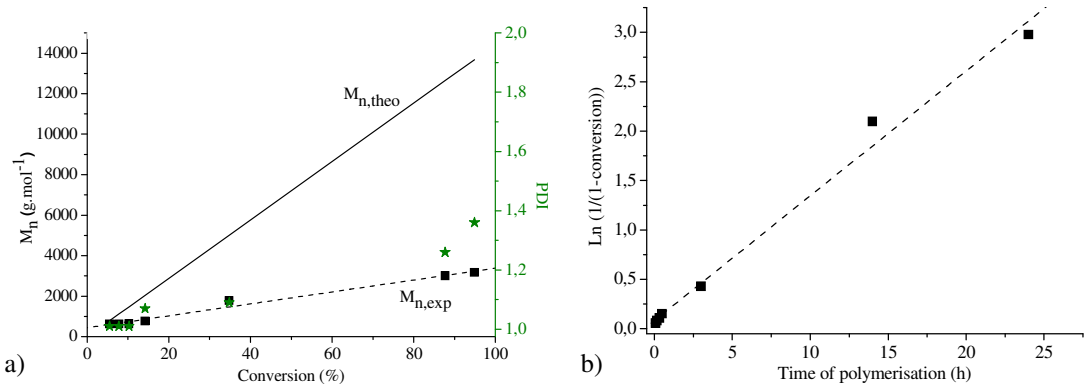

Figure 4.26: Polymerisation data for *rac*-lactide by $(HL^{tBu})_2MgCl_2$: a) Plot of PLA M_n and polydispersity (M_w/M_n) as a function of *rac*-lactide conversion b) Kinetic plots of the *rac*-lactide conversion *vs* reaction time

The GPC data and ^1H NMR spectra show a linear variation between $M_{n,exp}$ vs. conversion (despite being below $M_{n,theo}$) and between Ln(1/(1-conversion)) and the time of polymerisation. The PDI remained below 1.4 throughout the polymerisation.

These results are similar to previous observations made by Chisholm *et al.* on magnesium alkoxides [(BDI)Mg(O^{t}Bu)(THF)] (**I**, Figure 4.27), and [(η^3-*tris*pyrazolylborate))MgOR] (**J**, Figure 4.27), producing polymer with molecular weights ranging from 6 000-20 000 g/mol and PDI values of 1.1-1.3.[35, 40-42]

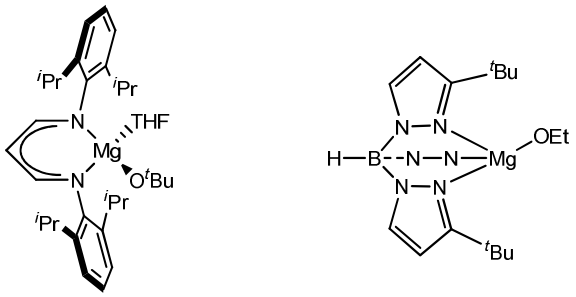

I **J**

Figure 4.27: Alkoxide magnesium complexes, **I** and **J**

4.5.3 Copolymerisation of *L*-lactide and glycolide

For the copolymerisation of *L*-lactide and glycolide, the catalyst $(HL^{R})_2MCl_2$, was dissolved in a melting mixture of *L*-lactide and glycolide at 140 °C and then the co-initiator (benzyl alcohol) was added (Equation 4.11).

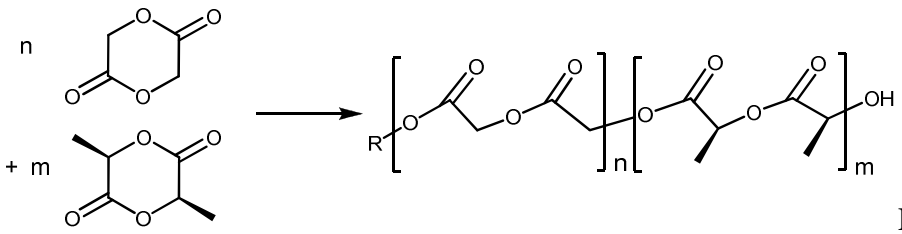

Eq. 4.11

To understand the kinetics of copolymerisation, variables were systematically altered and the effects recorded: metal (Mg, Zn, Sn), the ligand (L^{tBu}, L^{Ph} or octanoate), the polymerisation time (5 minutes - 96 hours), the feed composition (from 100 % of *L*-lactide to 100 % of glycolide) and the temperature (140 or 180 °C). The initial conditions were: 140 °C, 96 hours, lactide : glycolide ratio of 4 : 1 and catalyst : lactide ratio of 1 : 50.

4.5.3.1 Influence of the feed composition

The lactide : glycolide ratio has been varied from pure *L*-lactide to pure glycolide while maintaining temperature at 140 °C (melt polymerisation) for 96 hours using $(HL^{tBu})ZnCl_2$ and co-initiator (benzyl alcohol) (Table 4.4).

Table 4.4: Copolymerisation data of *L*-lactide/glycolide using $(HL^{tBu})_2ZnCl_2$..

Entry	Cat : lactide ratio	lactide : glycolide ratio	T / °C	time / h	Conv.[a] lac / %	Conv[b] gly / %	Initial lactide feed / %	Final lactide[c] / %
1	0 : 0	0 : 1	140	96	> 99	> 99	0	0
2	1 :50	1 : 4	140	96	> 99	> 99	20	23
3	1: 50	2 : 3	140	96	> 99	> 99	40	35
4	1 : 50	3 : 2	140	96	> 99	> 99	60	57
5	1 : 50	4 : 1	140	96	> 99	> 99	80	59
6	1 : 50	1 : 0	140	96	> 99	> 99	100	100

a: conversion of LA monomer (($[LA]_0$-[LA])/$[LA]_0$), calculated by ^{1}H NMR; b: conversion of G monomer (($[G]_0$-[G])/$[G]_0$), calculated by ^{1}H NMR; c: calculated by ^{1}H NMR.

Full conversion, in glycolide and in lactide, is attained in each copolymerisation of *L*-lactide/glycolide using $(HL^{tBu})ZnCl_2$. The final composition is similar to the initial feed in each Entry except Entry 5 (initial lactide feed = 80 % and lactide final composition = 59 %) which demonstrates stability in the final copolymer with the proportion lactide : glycolide of 3 : 2 despite an increase in initial lactide feed.

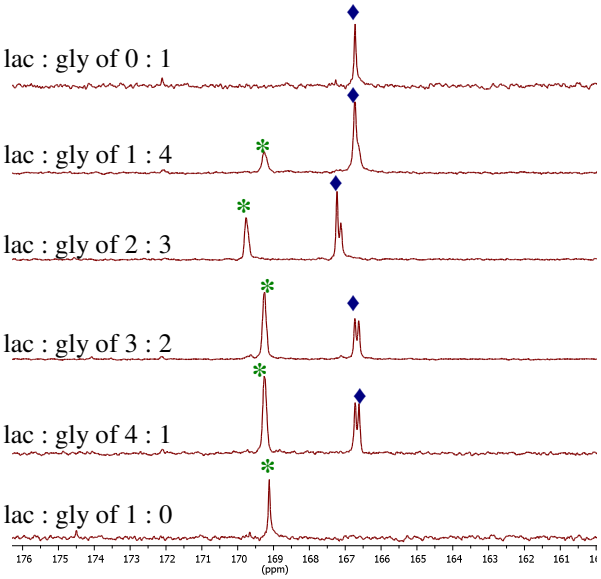

Figure 4.28: $^{13}C\{^1H\}$ NMR spectra (carbonyl region) of the copolymer *L*-lactide/glycolide at variation feed composition. ♦ glycolide, * lactide

4.5.3.2 Kinetic study using $(HL^{Ph})_2ZnCl_2$

Various times of copolymerisation were then examined at 140 °C, using a initiator : lactide ratio of 1 : 50, a lactide : glycolide ratio of 3 : 2 and using the initiator $(HL^{Ph})_2ZnCl_2$ and co-initiator (benzyl alcohol) (Table 4.5).

Table 4.5: Copolymerisation data of the *L*-Lactide/glycolide using $(HL^{Ph})_2ZnCl_2$

Entry	Cat:lactide ratio	lactide: glyco. ratio	T / °C	time / h	Conv. lac[a] / %	Conv. gly[b] / %	$M_{n,\,exp}$[c] g/mol	$M_{n,\,theo}$[d] g/mol	PDI[e] M_w/M_n
1	1 : 50	3 : 2	140	0.08	7	6	400	734	1.06
2	1 : 50	3 : 2	140	0.5	19	67	700	3946	1.11
3	1 : 50	3 : 2	140	1.5	56	> 99	-	7 836	-
4	1 : 50	3 : 2	140	8	63	> 99	800	8 338	1.30
5	1 : 50	3 : 2	140	16	80	> 99	-	9 559	-
6	1 : 50	3 : 2	140	24	86	> 99	800	9 989	1.57
7	1 : 50	3 : 2	140	48	90	> 99	1 100	10 277	1.67
8	1 : 50	3 : 2	140	72	93	> 99	2 000	10 493	1.60
9	1 : 50	3 : 2	140	96	95	> 99	5 000	10 636	1.52
10	1 : 50	3 : 2	140	120	98	> 99	-	10 852	-

a: conversion of LA monomer (($[LA]_0$-[LA])/$[LA]_0$), calculated by ^{1}H NMR; n: conversion of G monomer (($[G]_0$-[G])/$[G]_0$), calculated by ^{1}H NMR c: measured by GPC, values based on polystyrene standards and corrected by multiplication by 0.57 (Mark-Houwink law); d. Molecular weight theoretical calc. using $M_{n,\,theo} = (x_{LA} \times conv._{LA} \times M_{LA} + x_G \times conv._G \times M_G) \times ([LA]_0/[Cat]_0 + [G]_0/[Cat]_0)$ e. polydispersity index (M_w/M_n), PDI, measured by GPC

With an initiator : lactide ratio of 1 : 50 and a lactide : glycolide ratio of 3 : 2, copolymerisation is reasonably rapid, full conversion of glycolide is attained after 1 hour 30 minutes (Table 4.5, Entry 3) and 80 % of *L*-lactide after 16 hours (Table 4.5, Entry 5). As expected, glycolide is polymerised faster than *L*-lactide.

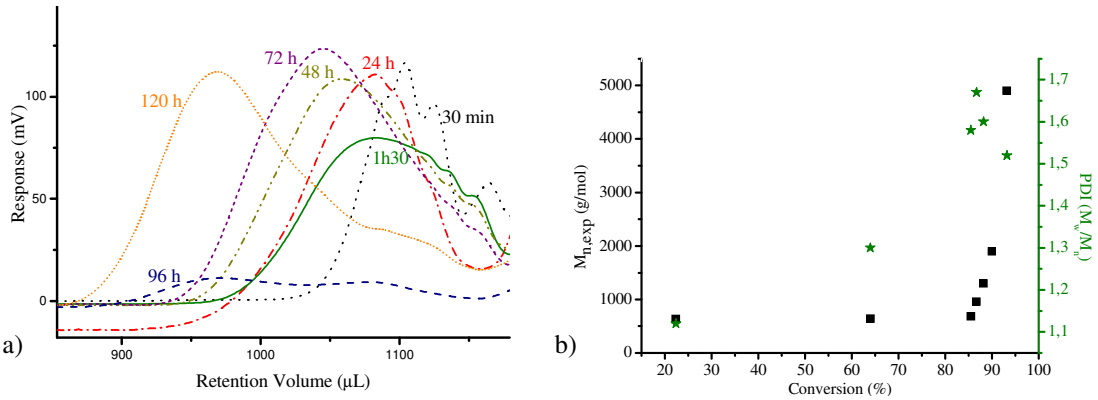

Figure 4.29: Series of polymerisations of *rac*-lactide by $(HL^{Ph})_2ZnCl_2$: a) GPC chromatogram traces and b) M_n and polydisersity (M_w/M_n) as a function of *rac*-lactide conversion

4.5.3.3 Influence of the ligand, metal

The copolymerisations were finally carried out at 140 °C, for 96 hours, with a initiator : lactide ratio of 1 : 50 and a lactide : glycolide ratio of 3 : 2 using different metal complexes. The results are collated in Table 4.6.

Table 4.6: Copolymerisation data of the *L*-lactide/glycolide

Entry	Catalyst	Cat : lactide ratio	lactide : glycolide ratio	T / °C	time / h	Conv.[a] lac / %	Conv[b] gly / %
1	$(HL^{Ph})_2ZnCl_2$	1 : 50	3 : 2	140	96	95	> 99
2	$(HL^{Ph})_2MgCl_2$	1 : 50	3 : 2	140	96	97	> 99
3	$(HL^{Ph})_2SnCl_2$	1 : 50	3 : 2	140	96	88	> 99
4	$(HL^{tBu})_2SnCl_2$	1 : 50	3 : 2	140	96	97	> 99
6	$Sn(oct)_2$	1 : 50	3 : 2	140	96	83	> 99

a: conversion of LA monomer (($[LA]_0$-[LA])/$[LA]_0$), calculated by ^{1}H NMR; b: conversion of G monomer (($[G]_0$-[G])/$[G]_0$), calculated by ^{1}H NMR; c: calculated by ^{1}H NMR.

After 96 hours, at 140 °C, with an initiator : lactide ratio of 1 : 50 and a lactide : glycolide ratio of 3 : 2, 97 % of conversion of *L*-Lactide is attained using $(HL^{Ph})_2MgCl_2$ (Table 4.6, Entry 2), 95 % using $(HL^{Ph})_2ZnCl$ (Table 4.6, Entry 1) and 88 % with $(HL^{Ph})_2SnCl_2$ (Table 4.6, Entry 3); showing that the magnesium complex is the fastest.

Under the same conditions, 97 % of conversion of *L*-lactide is attained using $(HL^{tBu})_2SnCl_2$ (Table 4.6, Entry 4), 88 % with $(HL^{Ph})_2SnCl_2$ (Table 4.6, Entry 3) and 83 % with $Sn(oct)_2$ (Table 4.6, Entry 5); the *tert*-butyl ligand complex is the fastest of the three. The ^1H NMR spectrum of the copolymerisation of *L*-lactide/glycolide also shows a better control of the polymerisation of *L*-lactide using the complex $(HL^{tBu})_2SnCl_2$ than $(HL^{Ph})_2SnCl_2$.

4.5.3.4 Conclusion on the kinetic of the copolymerisation

The most favourable feed composition was obtained with a lactide : glycolide ratio of 3 : 2.

As expected, the rate of the copolymerisation increases with increasing temperature.

The rate of the copolymerisation is also dependent on the ligand following the order ^tBu > Ph > octanoate and the metal following the order Mg > Zn > Sn.

In summary, the optimum combination for the copolymerisation of *L*-lactide and glycolide using $(HL^R)MCl_2$ should be: $(HL^{tBu})MgCl_2$, 140 °C, 24 hours, lactide : glycolide ratio of 3 : 2 and catalyst : lactide ratio of 1 : 50. This combination was therefore used in the microstructure studies of the synthesised copolymers.

4.5.3.5 Copolymer microstructure

Using the conditions described in section 4.1.1.4, copolymer microstructure was studied. The results are collated in Table 4.7.

Table 4.7: Copolymerisation data of the *L*-lactide/glycolide using $(HL^{tBu})_2MgCl_2$

Entry	Cat:lactide ratio	lac: gly ratio	T / °C	time / h	Conv. lac[a] / %	Conv. gly[b] / %	$M_{n,\,exp}$[c] g/mol	$M_{n,\,theo}$[d] g/mol	PDI[e] M_w/M_n
1	1 : 50	3 : 2	140	0.08	2	10	700	528	1.17
2	1 : 50	3 : 2	140	0.16	20	67	700	4 017	1.30
3	1 : 50	3 : 2	140	0.33	27	82	1 600	5 098	1.37
4	1 : 50	3 : 2	140	2	60	94	4 500	7 930	1.70
5	1 : 50	3 : 2	140	6	91	> 99	6 000	10 349	1.67
6	1 : 50	3 : 2	140	14	95	> 99	6 500	10 636	1.54
7	1 : 50	3 : 2	140	24	97	> 99	3 000	10 780	1.60

a: conversion of LA monomer (($[LA]_0$-[LA])/$[LA]_0$), calculated by ^{1}H NMR; n: conversion of G monomer (($[G]_0$-[G])/$[G]_0$), calculated by ^{1}H NMR c: measured by GPC, values based on polystyrene standards and corrected by multiplication by 0.57 (Mark-Houwink law); d. Molecular weight theo calc. using $M_{n,\,theo} = (x_{LA} \times conv._{LA} \times M_{LA} + x_G \times conv._G \times M_G) \times ([LA]_0/[Cat]_0 + [G]_0/[Cat]_0)$ e. polydispersity index (M_w/M_n), PDI, measured by GPC.

After 14 hours, 95 % of conversion of *L*-lactide is attained using $(HL^{tBu})_2MgCl_2$ with a molecular weight of 6 500 g/mol and a PDI of 1.54 (Table 4.7, Entry 6).

Kinetic plots of the *rac*-lactide conversion versus time shows, as predicted by theory, polymerisation is faster for the glycolide than for the *L*-lactide, and that 90 % of conversion is attained after only 5 minutes. The GPC data show a linear correlation between the molecular weight and degree of conversion. The PDI is below 1.7 for each copolymerisation (Figure 4.30 a)).

The kinetic results are shown as GPC chromatograms to demonstrate the dependence of the molecular weights with the conversion (Figure 4.30 b)).

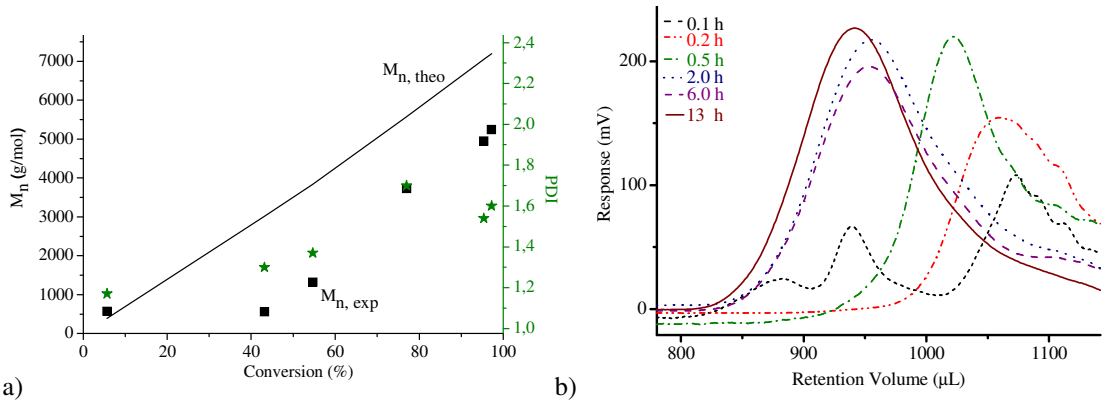

Figure 4.30: Polymerisation data for *rac*-lactide by $(HL^{tBu})_2MgCl_2$: a) Plot of PLA M_n and polydispersity (M_w/M_n) as a function of *rac*-lactide conversion and b) GPC chromatogram traces

Compared with the literature, these zinc and magnesium complexes show lower molecular weights (10 000 - 30 000 g/mol) and similar polydispersities (1.5 - 2.0) but less control of the copolymers microstructure.[43-45]

At the beginning of the polymerisation (after 6 hours), the ^1H NMR spectra of the copolymer product showed only –GGGGG- pentads (corresponding to six glycolide moieties) because the glycolide is polymerised faster than the *L*-lactide. With increasing time (14 hours), some –LLGGL- pentads emerged. After 14 hours, the presence of atactic tetrads (–GGLL–) were visible on the $^{13}C\{^1H\}$ NMR.

If the copolymerisation is less selective, no stereochemical control will be observed and the microstructure will show a different tacticity. By applying the probability theory to the estimation of copolymer sequence distribution we expected completely random copolymer with a 'blocking' tendency ($\chi < 1$).[46]

$$\chi = \frac{(r_A x + 2 + r_B/x)}{(r_A x + 1 + r_A r_B + r_B/x)} = 0.58$$

$r_A = r_L = 0.75$
$r_B = r_G = 11.75$
$x = [L]_0/[G]_0 = 1.5$

Figure 4.31: Probability theory of the estimation of the polymer sequence

4.6 Conclusions

In conclusion, the racemic phosphine oxide-alkoxide ligand HL^{tBu} is resolved into the diastereomeric *RR/SS*-$M(L^{tBu})_2$ complexes of the divalent cations, Ca^{II}, Zn^{II} and Sn^{II} to afford a racemic mixture of homochiral $M(L^{tBu})_2$ complexes with diastereomeric index of 90 %, 75 % and 100 % respectively. The complexes $[M(L^{Ph})_2]_2$ (where M = Mg^{II}, Co^{II} or Sn^{II}) have also been synthesised using HL^{Ph} and $[Mg(L^{Ar})_2]_2$ using HL^{Ar} (where Ar = 2,6-dimethylbenzene).

The complexes $(HL^{R})_2M(Cl)_2$ (where M = Mg^{II}, Zn^{II} or Sn^{II}) have been synthesised as protonated equivalents of $M(L^{R})_2$ using HL^{R} (where R = ^{t}Bu or Ph).

These complexes have provided a new class of initiators from the polymerisation of *rac*-lactide. The results have shown controlled polymerisations with various active catalysts and good isotacticity. A coordination-insertion mechanism is postulated; insertion taking place in the metal-alkoxide bond in $M(L^{R})_2$ and in the $(HL^{R})_2M(Cl)_2$/benzyl alcohol mixture. However, it is not clear yet which mechanism is taking place in the polymerisation of *rac*-lactide with $(HL^{R})_2M(Cl)_2$ without co-initiator.

The complexes $(HL^{R})_2MCl_2$ have given interesting results in the kinetic control of copolymerisation of *L*-lactide and glycolide.

[1] H. Ma, T. P. Spaniol, J. Okuda, *Angew. Chem., Int. Ed.* **2006**, *45*, 7818.
[2] A. Amgoune, C. M. Thomas, T. Roisnel, J.-F. Carpentier, *Chem. Eur. J.* **2006**, *12*, 169.
[3] T. M. Ovitt, G. W. Coates, *J. Am. Chem. Soc.* **2002**, *124*, 1316.
[4] P. Hormnirun, E. L. Marshall, V. C. Gibson, A. J. P. White, D. J. Williams, *J. Am. Chem. Soc.* **2004**, *126*, 2688.
[5] A. F. Douglas, B. O. Patrick, P. Mehrkhodavandi, *Angew. Chem., Int. Ed.* **2008**, *47*, 2290.
[6] M. H. Chisholm, N. J. Patmore, Z. Zhou, *Chem. Commun.* **2005**, 127.
[7] G. Kostina, A. Borodina, V. Emely'anova, D. Naumova, A. Virovetsa, M.-M. Rohmerb, A. Varnekb, *J. Mol. Struct.* **2007**, *837*, 63.
[8] P. Fernández, A. Sousa-Pedrares, J. Romero, J. A. García-Vázquez, A. Sousa, P. Pérez-Lourido, *Inorg. Chem.* **2008**, *47*, 2121.
[9] F. Fredoueil, M. Evain, D. Massiot, M. Bujoli-Doeuff, B. Bujoli, *J. Mater. Chem.* **2001**, *11*, 1106.
[10] F. Fredoueil, M. Evain, M. Bujoli-Doeuff, B. Bujoli, *Eur. J. Inorg. Chem.* **1999**, 1077.
[11] G. Borisov, S. G. Varbanov, L. M. Venanzi, A. Albinati, F. Demartin, *Inorg. Chem.* **1994**, *33*, 5430.
[12] A. S. Ionkin, W. J. Marshall, B. M. Fish, *Organometallics* **2006**, *25*, 4170.
[13] A. S. Ionkin, B. M. Fish, W. J. Marshall, (E. I. Du Pont de Nemours and Company, USA). Application: US, **2007**, p. 14 pp.
[14] M. Mehring, C. Low, M. Schurmann, F. Uhlig, K. Jurkschat, B. Mahieu, *Organometallics* **2000**, *19*, 4613.
[15] M. Mehring, D. Mansfeld, M. Schürmann, *Z. Anorg. Allg. Chem.* **2004**, *630*, 452.
[16] P. G. Jones, M. M. Alvarez-Falcon, *Acta Cryst.* **2003**, *E59*, m192.
[17] M. F. Davisa, W. Levason, R. Ratnani, G. Reid, M. Webster, *New J. Chem.* **2006**, *30*, 782.
[18] B. E. Kucera, M. M. Olmstead, R. S. Tankea, S. M. Kauzlarich, *Acta Cryst.* **2003**, *E59*, m359.
[19] M. McCann, S. Townsend, M. Devereux, V. McKee, B. Walker, *Polyhedron* **2001**, *20*, 2799.
[20] M. Fesslera, S. Ellera, C. Bachmanna, R. Gutmanna, B. Trettenbreina, H. Kopackaa, T. Muellerb, P. Brueggeller, *Dalton Trans.* **2009**, 1383.
[21] D. J. Harding, P. Harding, T. Thurakitseree, H. Adams, *Acta. Cryst.* **2007**, *E63*, m163.
[22] P. Pérez-Lourido, J. Romero, J. A. García-Vázquez, A. Sousa, J. Zubieta, K. Maresca, *Polyhedron* **1998**, *17*, 4457.
[23] S. M. Godfrey, D. G. Kelly, C. A. McAuliffe, R. G. Pritchard, *J. Chem. Soc., Dalton Trans.* **1995**, 1095.
[24] M. Kontturi, E. Vuokila-Laine, S. Peraniemi, T. T. Pakkanen, J. J. Vepsalainen, M. Ahlgren, *J. Chem. Soc., Dalton Trans.* **2002**, 1969.
[25] J. Jokiniemi, S. Peraniemi, J. J. Vepsalainen, M. Ahlgren, *CrystEngComm* **2008**, *10*, 1011.

[26] M. Mehring, C. Löw, M. Schürmann, F. Uhlig, K. Jurkschat, B. Mahieu, *Organometallics* **2000**, *19*, 4613.
[27] J. Martincov, R. Dostlov, L. Dostl, A. Rika, R. Jambo, *Organometallics* **2009**, *28*, 4823.
[28] R. S. Simons, L. Pu, M. M. Olmstead, P. P. Power, *Organometallics* **1997**, *16*, 1920.
[29] C. K. Williams, L. E. Breyfogle, S. K. Choi, W. Nam, V. G. Young, M. A. Hillmyer, W. B. Tolman, *J. Am. Chem. Soc.* **2003**, *125*, 11350.
[30] H. R. Kricheldorf, M. J. Jonté, M. Berl, *Makromol. Chem.* **1985**, *12*, 25.
[31] K. B. Aubrecht, M. A. Hillmyer, W. B. Tolman, *Macromolecules* **2002**, *35*, 644.
[32] M. Ryner, A. Finne, A.-C. Albertsson, H. R. Kricheldorf, *Macromolecules* **2001**, *34*, 7281.
[33] D. J. Darensbourg, W. Choi, C. P. Richers, *Macromolecules* **2007**, *40*, 3521.
[34] Y. Huang, W.-C. Hung, M.-Y. Liao, T.-E. Tsai, Y.-L. Peng, C.-C. Lin, *J. Polym. Sci., Part A: Polym. Chem.* **2009**, *47*, 2318.
[35] M. H. Chisholm, N. W. Eilerts, J. C. Huffman, S. S. Iyer, M. Pacold, K. Phomphrai, *J. Am. Chem. Soc.* **2000**, *122*, 11845.
[36] W.-C. Hung, C.-C. Lin, *Inorg. Chem.* **2008**, *48*, 728.
[37] J.-C. Wu, B.-H. Huang, M.-L. Hsueh, S.-L. Lai, C.-C. Lin, *Polymer* **2005**, *46*, 9784.
[38] M. H. Chisholm, J. Gallucci, K. Phomphrai, *Inorg. Chem.* **2002**, *41*, 2785.
[39] B. M. Chamberlain, M. Cheng, D. R. Moore, T. M. Ovitt, E. B. Lobkovsky, G. W. Coates, *J. Am. Chem. Soc.* **2001**, *123*, 3229.
[40] L. F. Sanchez-Barba, A. Garces, M. Fajardo, C. Alonso-Moreno, J. Fernandez-Baeza, A. Otero, A. Antinolo, J. Tejeda, A. Lara-Sanchez, M. I. Lopez-Solera, *Organometallics* **2007**, *26*, 6403.
[41] L. F. Sanchez-Barba, D. L. Hughes, S. M. Humphrey, M. Bochmann, *Organometallics* **2006**, *25*, 1012.
[42] M. H. Chisholm, J. C. Huffman, K. Phomphrai, *J. Chem. Soc., Dalton Trans.* **2001**, 222.
[43] J. Kasperczyk, *Polymer* **1996**, *37*, 201.
[44] A. Dumitrescu, B. Martin-Vaca, H. Gornitzka, J.-B. Cazaux, D. Bourissou, G. Bertrand, *Eur. J. Inorg. Chem.* **2002**, *2002*, 1948.
[45] C. A. Wheaton, P. G. Hayes, B. J. Ireland, *Dalton Trans.* **2009**, 4832.

Chapter 5: Experimental

5.1 Instrumentation and Reagents

5.1.1 Reagents

All manipulations were carried out using standard Schlenk techniques, or a Vacuum Atmosphere double glovebox, under an atmosphere of dry nitrogen. Pentane, hexane, toluene, diethyl ether, and THF were dried by passage through activated alumina towers and degassed before use. DME was distilled from potassium under an atmosphere of dry nitrogen. All solvents were stored over potassium mirrors (with the exception of THF and DME which were stored over activated 4 Å molecular sieves). Deuterated solvents were distilled from potassium, degassed by three freeze-pump-thaw cycles and stored under nitrogen.

The monomer ε-caprolactone (purchased from Sigma-Aldrich), *tert*-butanol (purchased from Sigma-Aldrich), benzyl alcohol (purchased from Alfa Aesar), were distilled from potassium, degassed by three freeze-pump-thaw cycles and stored under nitrogen. DABCO and LiN" purchased from Sigma Aldrich, was sublimed prior to use. The compounds $Al(CH_2SiMe_3)_3$, $In(CH_2SiMe_3)_3$ and $In(O^iPr)_3$ were obtained from Prof. Okuda's group and used as received. DABAL-Me was obtained from Prof. Woodward group and used as received. Trimethylaluminium was purchased from Sigma-Aldrich and used as received. Magnesium dichloride, tin dichloride and zinc chloride were dried using chlorotrimethylsilane and stored under dinitrogen. The epoxide 3,3-dimethyl-epoxybutane, purchased from Alfa Aesar, was distilled and stored over activated molecular sieves prior to use, *rac*-lactide was purchased from Alfa Aesar, recrystallised from hot toluene, washed with diethyl ether, and sublimed (10^{-4} torr, 110 °C) prior to use, 2,6-di-*tert*-butylphenol, purchased from Sigma Aldrich, was sublimed (10^{-4} torr, 80 °C) prior to use.

$MgN"_2THF_2$,[1] $CaN"_2THF_2$,[1] $CoN"_2THF_2$,[2] SnN",[3] $ZnN"_2$,[4] $InN"_3$[5] and $YN"_3$[6] were synthesised according to literature procedures.

5.1.2 NMR Spectroscopy

NMR spectra (^{1}H, $^{13}C\{^{1}H\}$ and $^{31}P\{^{1}H\}$) were recorded at 298 K on a Bruker DRX 400 spectrometer, operating frequency at 400.1 MHz (^{1}H), 100.6 MHz (^{13}C) and 161.9 (^{31}P) or on a Bruker ARX 250, DPX 360 or DMX 500, operating at 250.1, 360.1 or 500.1 (^{1}H), 63.0, 90.7 or 126.0 (^{13}C), and 101.3, 145.8 or 202.47 (^{31}P) MHz, respectively. Chemical shifts are quoted in ppm and are relative to external $SiMe_4$ or H_3PO_4.

5.1.3 Mass spectrometry

Mass spectra were, unless otherwise stated, run by Mr. Tony Hollingworth and Mr. Graham Coxhill on a VG autospec instrument in the University of Nottingham or by Dr. Ali Abdul-Sada in the University of Sussex.

5.1.4 Elemental analysis

Elemental microanalyses were determined by Mr. Stephen Boyer at London Metropolitan University.

5.1.5 Gel Permeation Chromatography

In Nottingham, molecular weight and molecular weight distribution of polymers were obtained by Gel Permeation Chromatography (PL-120, Polymer Labs) with an RI detector. The columns (30 cm PLgel Mixed-C, 2 in series) were eluted with THF and calibrated with polystyrene standards. In Edinburgh, Polymer molecular weight and molecular weight distributions were obtained by Gel Permeation Chromatography PLgel 5μm Mixed-C column (300 x 7.5 mm) from Polymer Laboratories on an Agilent 1100 HPLC. Data were analysed using ChemStation software. All calibration and analysis were performed at 35 °C and a flow rate of 1 mL / min. The obtained molecular weights for polylactide have been corrected using

the Mark-Houwink law[14]. The factor determined using the Mark-Houwink law for PLA and the used column is 0.577.

5.1.6 X-ray Crystallography

Single crystals were mounted on a glass fibre and transferred to a Bruker SMART APEX CCD diffractometer equipped with a graphite-monochromated Mo Kα radiation source (λ = 0.71073 Å) and omega scan measurement. Data were integrated using SAINT and absorption correction was performed with the program SADABS. Structure solution and refinement was carried out using the SIR 92 program, WinGX and the SHELXTL suite of programs, and graphics generated using Ortep. All non-hydrogen atoms were refined with anisotropic thermal parameters. Hydrogen atoms were placed using a 'riding model'.[7-9]

5.2 Synthetic Procedures described in Chapter 2

5.2.1 Preparation of $(^t\text{Bu})_2\text{P(O)CH}_2\text{CH}(^t\text{Bu})\text{OH}$, $\text{HL}^{t\text{Bu}}$

The procedure is the same as published except the reaction were carried out in ampoules with the addition of *n*-BuLi before the addition of the epoxide.[10, 11]

5.2.2 Preparation of $(\text{Ph})_2\text{P(O)CH}_2\text{CH}(^t\text{Bu})\text{OH}$, HL^{Ph}

The procedure is the same as published.[12]

5.2.3 Preparation of $(\text{Ar})_2\text{P(O)CH}_2\text{CH}(^t\text{Bu})\text{OH}$, HL^{Ar}

A three necked flask was fitted with a mechanical stirrer bar, reflux condenser and dropping funnel and charged with 1.5 equivalents of magnesium turnings (2.47 g, 102 mmol) in 40 mL of THF. Three small iodine crystals were also added to initiate

the reaction. One equivalent of 3,5-dimethylphenylbromide (12.5 g, 68 mmol) in 20 mL of THF was added dropwise via a dropping funnel. The reaction was highly exothermic and the colour of the mixture turned from clear to brown. After stirring at RT for 18 hours, the reaction yielded a clear brown liquid. Some solid was still observed at the bottom of the flask and it was thought that this was excess magnesium.

One equivalent of diethylphosphoramidousdichloride (4.73 g, 27.2 mmol) in 10 mL of THF was added to a schlenk and cooled to 0°C. ArMgBr was filtered dropwise into the schlenk containing the aminophosphine. Having completed the addition, a pale yellow solution resulted with a large amount of white precipitate ($MgBr_2$, $MgCl_2$). Having settled, the yellow liquid was filtered, concentrated under reduced pressure (10^{-2} mbar), and 30 mL of hexane was added. In a modification of the literature procedure, 4 equivalents of 2M HCl (54 mL, 109 mmol) were added dropwise to the mixture at 0°C. A white precipitate formed (amine by-product) and the reaction mixture was left to stir overnight at RT. Filtration and removal of all volatilities yielded 7.3 g (93%) of a viscous yellow oil.

In an ampoule, approximately 40 mL of THF was added to 2 equivalents of $LiAlH_4$ (1.9 g, 25 mmol) to create a grey suspension. One equivalent of Ar_2PCl (7.3 g, 25 mmol) in THF was added dropwise to the suspension at 0°C. The colour changed from grey to green and the mixture was left to stir overnight.

A 1.6M hexanes solution of 2 equivalents of *n*-BuLi (32 mL, 50 mmol) was added dropwise to a solution of Ar_2PH in THF at 0°C. A deep red colour resulted and the mixture was stirred overnight at RT. Two equivalents of 3,3-dimethyl-1,2-epoxybutane (3.0 g, 25 mmol) was added to the Ar_2PLi at 0°C, which subsequently turned yellow, and the solution was stirred at RT overnight. An excess of H_2O_2 was added which yielded a white solid. The product was dissolved in $CHCl_3$ and dried over anhydrous $MgSO_4$. Concentration and recrystallisation in hexane produced a colourless solid. Removal of all volatilities yielded $\mathbf{HL^{Ar,tBu}}$ in a 30% yield.

^{1}H-NMR δ($CHCl_3$): 0.85 (9 H, s, C-(CH_3)$_3$); 2.4 (12 H, d, C-(CH_3)$_4$); 3.6 (1 H, m, CH); 7.2-7.5 (6 H, m, P-Ar) [ppm].

$^{31}P\{^{1}H\}$-NMR $\delta(C_6D_6)$: 33.8 ppm.

Analysis Found: C 73.63 %, H 8.61; Calculated: C 73.72 %, H 8.72 %

5.2.4 Preparation of *R*-(*R*)$_2$P(O)CH$_2$CH(^{t}Bu)OH, *R*-HL^{R}

The procedure is the same as published except of the use of hexanediol as the reaction solvent instead of propanol to facilitate the purification by distillation.[11]

5.2.5 Attempted Preparation of KL$^{t\mathrm{Bu}}$

5.2.5.1 From KN"

In a NMR YT tube, one equivalent of HL$^{t\mathrm{Bu}}$ (20.0 mg, 0.076 mmol) and one equivalent of KN" (13.1 mg, 0.076 mmol) were dissolved in d_6-benzene (0.3 mL) and THF (0.2 mL) and were heated for 16 hours at 80 °C.

The ^{1}H and $^{31}P\{^{1}H\}$ NMR spectra after 10 minutes, 16 hours, and 40 hours show an intractable mixture of products.

5.2.5.2 From KO^{t}Bu

In a NMR YT tube, one equivalent of HL$^{t\mathrm{Bu}}$ (20.0 mg, 0.076 mmol) and one equivalent of KO^{t}Bu (8.6 mg, 0.076 mmol) were dissolved in d_6-benzene (0.3 mL) and THF (0.2 mL) and were heated for 16 hours at 80 °C.

The ^{1}H and $^{31}P\{^{1}H\}$ NMR spectra show after 10 minutes and after 3 days an intractable mixture of three different products (in $^{31}P\{^{1}H\}$ NMR, the resonances are at 61.0, 56.0 and 48 ppm).

5.2.5.3 From KH

In a NMR YT tube, one equivalent of HL$^{t\mathrm{Bu}}$ (20.0 mg, 0.076 mmol) and one equivalent of KH (3.05 mg, 0.076 mmol) were dissolved in 0.3 mL of d_6-benzene and 0.2 mL of THF and were heated for 16 hours at 80 °C.

The $^{31}P\{^{1}H\}$ NMR spectra shows after 10 minutes and after 3 days an intractable mixture of three different products.

5.2.6 Preparation of KL^{Ph}

5.2.6.1 From KN"

In a NMR YT tube, one equivalent of HL^{Ph} (20.0 mg, 0.066 mmol) and one equivalent of KN" (11.4 mg, 0.066 mmol) were dissolved in 0.3 mL of d_6-benzene and 0.2 mL of THF and were heated for 16 hours at 80 °C.

The ^{1}H and $^{31}P\{^{1}H\}$ NMR spectra after 10 min show traces of ligands and some impurities, and after 16 hours show an intractable mixture of products.

5.2.6.2 From KO^{t}Bu

In a NMR YT tube, one equivalent of HL^{Ph} (20.0 mg, 0.066 mmol) and one equivalent of KO^{t}Bu (7.4 mg, 0.066 mmol) were dissolved in 0.3 mL of d_6-benzene and 0.2 mL of THF and were heated for 16 hours at 80 °C.

The $^{31}P\{^{1}H\}$ NMR spectrum after 10 days show a major resonance at - 45 ppm.

5.2.6.3 From KH

In a NMR YT tube, one equivalent of HL^{Ph} (20.0 mg, 0.066 mmol) and one equivalent of KH (2.7 mg, 0.066 mmol) were dissolved in 0.3 mL of d_6-benzene and 0.2 mL of THF and were heated for 16 hours at 80 °C.

The $^{31}P\{^{1}H\}$ NMR spectrum after 10 minutes show resonances for decomposition products.

5.2.7 Preparation of LiL^{Ph}

A 1.6 M hexane solution of ^{n}BuLi (2.8 mL, 6.6 mmol) was added dropwise to a solution of HL^{Ph} in THF (2 g, 6.62 mmol, 10 mL) at -78 ºC via a dry ice/acetone bath and was stirred for 16 hours. The solution started colourless then dark orange, orange, yellow and finally colourless. After filtration by cannula, all volatile compounds were removed under reduced pressure and the residual solid was recrystallised in hexanes solution to afford colourless LiL^{Ph}.

^{1}H-NMR $\delta(C_6D_6)$: 2.6 – 2.9 (2H, m, CH_2); 4.3 – 4.4 (1H, m, CH); 6.9-7.2 (6 H, m, P-Ar); 7.5-8.1 (4 H, m, P-Ar) [ppm].

^{31}P{^{1}H}-NMR: $\delta(C_6D_6)$: 39.9 ppm.

^{7}Li-NMR $\delta(C_6D_6)$: 0.5-0.7 (d, $^{2}J_{PLi}$ = 42.1 Hz) ppm.

5.2.8 Preparation of *rac*-$Sc(L^{tBu})_3$

To a solution of $Sc\{N(SiMe_3)_2\}_3$ in THF (66.8 mg, 0.13 mmol, 2 mL) was added a solution of three equivalents of HL^{tBu} in THF (100 mg, 0.38 mmol, 10 mL) at -78 °C, and allowed to warm slowly to RT for 16 hours stirring. Volatiles were removed under reduced pressure and the residual solid recrystallised from hexanes to afford colourless ***rac*-Sc(L^{tBu})$_3$**. Yield 71 mg (75 %). Integration of the resonances in the spectra of bulk ***rac*-Sc(L^{tBu})$_3$** show that the *rac* isomer is the major isomer present with the minor identified as mixture of *RRS/SSR*-**Sc(L^{tBu})$_3$**, and the major : minor ratio is 55 : 45.

^{1}H-NMR $\delta(C_6D_6)$: major diastereomer (minor diastereomer in brackets); 4.70 (4.59, 4.36) (m, 3 H, CH); 1.9-1.7 (m, 6 H, CH_2); 1.31 (1.33) (d, 27 H, $^{2}J_{PH}$ = 13.7 Hz, P-^{t}Bu), 1.22 (1.23) (d, 27 H, $^{2}J_{PH}$ = 14.4 Hz, P-^{t}Bu); 1.17 (1.18) (s, 27 H, C-^{t}Bu) [ppm].

^{31}P{^{1}H}-NMR: $\delta(C_6D_6)$: 67.1 (67.6, 67.3 and 66.8 minor) ppm.

Analysis Found: C 60.79 %, H 10.82 %; Calculated: C 60.85; H 10.94.

5.2.9 Preparation of *rac*-Sc(L^{Ph})$_3$

To a solution of Sc{N(SiMe$_3$)$_2$}$_3$ in THF (174.0 mg, 0.33 mmol, 5 mL) was added a solution of three equivalents of HL^{Ph} in THF (300.0 mg, 0.99 mmol, 10 mL) at 78 °C, and allowed to warm slowly to RT for 16 hours with stirring. Volatiles were removed under reduced pressure and the residual solid recrystallised from a solution DME/hexanes to afford colourless ***rac*-Sc(L^{Ph})$_3$**. Yield 218.5 mg (70 %). Integration of the resonances in the spectra of bulk **Sc(L^{Ph})$_3$** show that the *rac* isomer is the major isomer present with the minor identified as mixture of *RRS/SSR*-**Sc(L^{Ph})$_3$**, and the major : minor ratio is 90 : 10. A similar reaction was carried out in d_6-benzene at room temperature for 16 hours and afforded the same compound after purification.

^{1}H-NMR δ(C_6D_6): major diastereomer (minor diastereomer in brackets): 8.0-7.8 (m, 12 H, CH_{arom}); 7.1-6.9 (m, 18 H, CH_{arom}); 3.9-4.0 (4.0-4.1) (m, 3 H, CH); 2.3-2.4 (m, 6 H, CH_2), 1.17 (1.19) (s, 27 H, C-^{t}Bu) [ppm].

^{31}P{^{1}H}-NMR δ(C_6D_6): 42.0 ppm.

Analysis Found: C 68.18 %, H 7.10 %; Calculated: C 68.35 %; H 7.01 %.

5.2.10 Preparation of *rac*-In(L^{tBu})$_3$

To a solution of In{N(SiMe$_3$)$_2$}$_3$ in THF (100 mg, 0.17 mmol, 2 mL) was added a THF solution of HL^{tBu} (132 mg, 0.50 mmol, 2 mL) at 25 °C, and the mixture heated for 7 days at 80 °C. Volatiles were removed under reduced pressure and the residual solid recrystallised from dme to afford colourless ***rac*-In(L^{tBu})$_3$**. The complex isolated was analysed by NMR spectroscopy and found to be a mixture of isomers. Yield 70.9 mg (47 %). Integration of the resonances in the spectra of bulk ***rac*-In(L^{tBu})$_3$** shows the major : minor ratio is 100 : 0.

^{1}H-NMR δ(C_6D_6): 1.15-1.4 (complex mixture, 57 H, P^{t}Bu and C^{t}Bu): 1.7-1.9 (m, 6 H, CH_2), 4.4-4.8 (m, 3 H, CH) [ppm].

$^{31}P\{^{1}H\}$-NMR $\delta(C_6D_6)$: 65.6 (0.5), 68.6 (0.36) and 69.4 (1.0) [relative integrals in brackets].

IR data (nujol in cm^{-1}): 2730, 1357, 1236, 1211, 1186, 1106 (P=O coordinated), 1065 (P=O uncoordinated), 1016, 961, 823, 643.

IR data (toluene solution in cm^{-1}): 2585, 1942, 1802, 1605, 1455, 1249, 1212, 1178, 1107 (P=O coordinated), 1077 (P=O uncoordinated), 1040, 066, 931, 895, 842, 784.

Analysis Found: C 56.07 %, H 10.00 %; Calculated: C 56.12 %, H 10.09 %.

5.2.11 Preparation of *rac*-In(L^{Ph})$_3$

To a solution of In{$N(SiMe_3)_2$}$_3$ in THF (196.7 mg, 0.33 mmol, 5 mL) was added a solution of three equivalents of HL^{Ph} in THF (300 mg, 0.99 mmol, 10 mL) at -78 °C, and allowed to warm slowly to room temperature for 16 hours with stirring. Volatiles were removed under reduced pressure and the residual solid recrystallised from DCM to afford colourless ***rac*-In(L^{Ph})$_3$**. Yield 254.6 mg (76 %). Integration of the resonances in the spectra of bulk ***rac*-In(L^{Ph})$_3$** show that the *rac* isomer is the major isomer present with the minor identified as mixture of *RRS/SSR*-**In(L^{Ph})$_3$**, and the major : minor ratio is 75 : 25.

^{1}H-NMR $\delta(C_6D_6)$: major diastereomer (minor diastereomer in brackets): 8.0-7.6 (m, 12 H, CH_{arom}); 7.1-6.9 (m, 18 H, CH_{arom}); 4.0 (3.7) (m, 3 H, CH); 2.2-2.4 (m, 6 H, CH_2), 1.14 (1.16) (s, 27 H, C-^{t}Bu) [ppm].

$^{31}P\{^{1}H\}$-NMR $\delta(C_6D_6)$: 46.9 (43.6, 41.9 minor) ppm

Analysis Found: C 63.53 %, H 6.45 %; Calculated: C 63.66 %; H 6.53 %.

5.2.12 Preparation of *rac*-Lu(L^{tBu})$_3$

To a solution of Lu{$N(SiMe_3)_2$}$_3$ in THF (250 mg, 0.38 mmol, 5 mL) was added a solution of three equivalents of HL^{tBu} in THF (300 mg, 1.14 mmol, 10 mL) at 78°C, and allowed to warm slowly to RT overnight with stirring. Volatiles were removed

under reduced pressure and the residual solid recrystallised from hexanes to afford colourless ***rac*-Lu(L^{tBu})$_3$**. Yield 348 mg (94 %). Integration of the resonances in the spectra of bulk ***rac*-Lu(L^{tBu})$_3$** show that the *rac* isomer is the major isomer present with the minor identified as mixture of *RRS/SSR*-**Lu(L^{tBu})$_3$**, and the major : minor ratio is 65 : 35.

^{1}H-NMR δ(C_6D_6): major diastereomer (minor diastereomer in brackets): 4.1 (4.6, 4.3) (m, 3 H, CH); 1.7-1.9 (m, 6 H, CH_2); 1.20 (1.19) (d, 27 H, $^2J_{PH}$ = 11.8 Hz, P-^{t}Bu); 1.16 (1.17) (s, 27 H, C-^{t}Bu), 1.11 (1.10) (d, 27 H, $^2J_{PH}$ = 12.9 Hz, P-^{t}Bu) [ppm].

^{31}P{^{1}H}-NMR δ(C_6D_6): 69.9 (70.3, 68.0 and 66.4 minor) ppm.

Analysis Found: C 52.49 %, H 9.48 %; Calculated: C 52.60 %; H 9.46 %.

5.2.13 Preparation of *rac*-Lu(L^{Ph})$_3$

To a solution of Lu{N($SiMe_3$)$_2$}$_3$ in THF (72.3 mg, 0.11 mmol, 5 mL) was added a solution of three equivalents of HL^{Ph} in THF (100 mg, 0.33 mmol, 10 mL) at -78 °C, and allowed to warm slowly to room temperature for 16 hours with stirring. Volatiles were removed under reduced pressure and the residual solid recrystallised from DME to afford colourless ***rac*-Lu(L^{Ph})$_3$**. Yield 89.8 mg (76 %). Integration of the resonances in the spectra of bulk ***rac*-Lu(L^{Ph})$_3$** show that the *rac* isomer is the major isomer present with the minor identified as mixture of *RRS/SSR*-**Lu(L^{Ph})$_3$**, and the major : minor ratio is 65 : 35.

^{1}H-NMR δ(C_6D_6): major diastereomer (minor diastereomer in brackets): 8.1-7.7 (m, 12 H, CH_{arom}); 7.1-6.9 (m, 18 H, CH_{arom}); 4.0 (4.2, 4.1) (m, 3 H, CH); 2.3-2.5 (m, 6 H, CH_2), 1.14 (1.13, 1.05) (s, 27 H, C-^{t}Bu) [ppm].

^{31}P{^{1}H}-NMR δ(C_6D_6): 43.5 (42.9, 42.4 minor) ppm.

Analysis Found: C 60.20 %, H 6.25 %; Calculated: C 60.11 %; H 6.17 %.

5.2.14 Preparation of *rac*-Y(L^{tBu})$_3$

The procedure is the same as published.[10, 11]

^{1}H-NMR δ(C_6D_6): major diastereomer (minor diastereomer in brackets): 4.22 (m, 3 H, CH); 1.78 (m, 6 H, CH_2); 1.24 (1.23) (d, 27 H, $^2J_{PH}$ = 11.4 Hz, P-^{t}Bu); 1.19 (1.20) (s, 27 H, C-^{t}Bu), 1.14 (1.12) (d, 27 H, $^2J_{PH}$ = 11.4 Hz, P-^{t}Bu). ^{1}H-NMR δ(C_7D_8) *tert*-butyl region, major diastereomer; 1.33 (d, 27 H, $^2J_{PH}$ = 8 Hz, P-^{t}Bu). 1.24 (d, 27 H, $^2J_{PH}$ = 8 Hz, P-^{t}Bu); 1.22 (s, 27 H, C-^{t}Bu) [ppm].

^{31}P{^{1}H}-NMR δ(C_6D_6): 68.9 (68.6, 67.6 minor) ppm, δ(C_7D_8): 69.8 (69.4, 68.6 minor) ppm.

Analysis Found: C 57.48 %, H 10.25 %; Calculated: C 57.78; H 10.39.

5.2.15 Preparation of *rac*-Y(L^{Ph})$_3$

To a solution of Y{N($SiMe_3$)$_2$}$_3$ in THF (376.8 mg, 0.66 mmol, 10 mL) was added a solution of three equivalents of HL^{Ph} in THF (600 mg, 2.00 mmol, 10 mL) at -78 °C, and allowed to warm slowly to room temperature for 16 hours with stirring. Volatiles were removed under reduced pressure and the residual solid recrystallised from DME to afford colourless ***rac*-Y(L^{Ph})$_3$**. Yield 595 mg (91 %). Integration of the resonances in the spectra of bulk ***rac*-Y(L^{Ph})$_3$** show that the *rac* isomer is the major isomer present with the minor identified as mixture of *RRS/SSR*-**Y(L^{Ph})$_3$**, and the major : minor ratio is 60 : 40.

A similar reaction was carried out in d_6-benzene at room temperature for 16 hours and afforded the same compound after purification.

^{1}H-NMR δ(C_6D_6): major diastereomer (minor diastereomer in brackets): 8.1-7.7 (m, 12 H, CH_{arom}); 7.1-6.9 (m, 18 H, CH_{arom}); 4.05 (4.25, 4.15) (m, 3 H, CH); 2.3-2.6 (m, 6 H, CH_2), 1.24 (1.13, 1.03) (s, 27 H, C-^{t}Bu) [ppm].

^{31}P{^{1}H}-NMR δ(C_6D_6): 42.9 (42.4, 42.1 minor) ppm.

Analysis Found: C 66.54 %, H 6.86 %; Calculated: C 66.66 %; H 6.92 %.

5.2.16 Preparation of *rac*-Y(L^{Ar})$_3$

To a solution of Y{N(SiMe$_3$)$_2$}$_3$ in C_6D_6 (26.5 mg, 0.047 mmol, 0.2 mL) was added a solution of three equivalents of HL^{Ar} in THF (50 mg, 0.14 mmol, 0.2 mL) at room temperature for 16 hours. Volatiles were removed under reduced pressure and the residual solid recrystallised from DME to afford colourless ***rac*-Y(L^{Ar})$_3$**. Yield 43.5 mg (87 %). Integration of the resonances in the spectra of bulk ***rac*-Y(L^{Ar})$_3$** show that the *rac* isomer is the major isomer present with the minor identified as mixture of *RRS/SSR*-**Y(L^{Ar})$_3$**, and the major : minor ratio is 75 : 25.

A similar reaction was carried out in d_6-benzene at room temperature for 16 hours and afforded the same compound after purification.

^{1}H-NMR δ(C_6D_6): major diastereomer (minor diastereomer in brackets): 7.9-7.6 (m, 12 H, CH_{arom}); 6.75 (d, 6 H, CH_{arom}, $^3J_{HH}$ = 6.5 Hz); 4.25 (4.4) (m, 3 H, CH); 2.5-2.7 (m, 6 H, CH_2), 1.82 (1.87) (s, 36 H, CMe_{arom}), 1.24 (1.13, 1.03) (s, 27 H, C-^{t}Bu) [ppm].

^{31}P{^{1}H}-NMR δ(C_6D_6): 44.5 (43.5, 43.0 minor) ppm.

Analysis Found: C 68.16 %, H 7.68 %; Calculated: C 68.26 %; H 7.81 %.

5.2.17 Preparation of *rac*-Bi(L^{tBu})$_3$

To a solution of Bi{N(SiMe$_3$)$_2$}$_3$ in THF (100 mg, 0.15 mmol, 5 mL) was added a solution of three equivalents of HL^{tBu} in THF (113.9 mg, 0.44 mmol, 5 mL) at -78°C, and allowed to warm slowly to RT overnight with stirring. Volatiles were removed under reduced pressure and the residual solid recrystallised from hexanes to afford colourless ***rac*-Bi(L^{tBu})$_3$**. Yield 25.2 mg (17 %). Integration of the resonances in the spectra of bulk ***rac*-Bi(L^{tBu})$_3$** show that the *rac* isomer is the major isomer present with the minor identified as mixture of *RRS/SSR*-**Bi(L^{tBu})$_3$**, and the major : minor ratio is 30 : 70.

^{1}H-NMR δ(C_6D_6): major diastereomer (minor diastereomer in brackets); 4.8 (5.3, 5.0 and 4.9) (m, 3 H, CH); 1.7-1.9 (m, 6 H, CH_2); 1.2-1.0 (m, 81 H, P-^{t}Bu and C-^{t}Bu) [ppm].

^{31}P{^{1}H}-NMR δ(C_6D_6): 68.9 (68.6, 67.6 minor) ppm.

Analysis Found: C 50.82 %, H 9.15 %; Calculated: C 50.80 %; H 9.13 %.

5.2.18 Preparation of *rac*-Bi(L^{Ph})$_3$

To a solution of Bi{N($SiMe_3$)$_2$}$_3$ in THF (100 mg, 0.15 mmol, 5 mL) was added a solution of three equivalents of HL^{Ph} in THF (131.4 mg, 0.44 mmol, 5 mL) at -78 °C, and allowed to warm slowly to RT overnight with stirring. Volatiles were removed under reduced pressure and the residual solid recrystallised from DCM to afford colourless ***rac*-Bi(L^{Ph})$_3$**. Integration of the resonances in the spectra of bulk ***rac*-Bi(L^{Ph})$_3$** show that the *rac* isomer is the major isomer present with the minor identified as mixture of *RRS/SSR*-**Bi(L^{Ph})$_3$**, and the major : minor ratio is 20 : 80.

^{1}H-NMR δ(C_6D_6): major diastereomer (minor diastereomer in brackets): 7.9-7.7 (m, 12 H, CH_{arom}); 7.1-6.9 (m, 18 H, CH_{arom}); 5.0 (5.25, 4.9) (m, 3 H, CH); 2.8-2.3 (m, 6 H, CH_2), 0.99 (1.00, 0.97) (s, 27 H, C-^{t}Bu).

^{31}P{^{1}H}-NMR δ(C_6D_6): 34.00 (32.42, 33.38, and 33.20 minor) ppm.

Analysis Found: C 58.20 %, H 6.06 %; Calculated: C 58.27 %; H 5.98 %.

5.2.19 Preparation of *rac*-La(L^{tBu})$_3$

To a solution of La{N($SiMe_3$)$_2$}$_3$ in THF (118.2 mg, 0.19 mmol, 5 mL) was added a solution of three equivalents of HL^{tBu} in THF (150.0 mg, 0.57 mmol, 5 mL) at -78°C, and allowed to warm slowly to RT overnight with stirring. Volatiles were removed under reduced pressure and the residual solid recrystallised from DCM to afford colourless ***rac*-La(L^{tBu})$_3$**. Yield 112.5 mg (64 %). Integration of the resonances in the spectra of bulk ***rac*-La(L^{tBu})$_3$** show that the *rac* isomer is the major isomer present with the minor identified as mixture of *RRS/SSR*-**La(L^{tBu})$_3$**, and the major : minor ratio is 40 : 60.

^{1}H-NMR δ(C_6D_6): major diastereomer (minor diastereomer in brackets); 4.25-4.5 (m, 3 H, CH); 1.9-2.2 (m, 6 H, CH_2); 1.24 (1.26) (d, 27 H, $^{2}J_{PH}$ = 12.7 Hz, P-^{t}Bu); 1.20 (1.20) (s, 27 H, C-^{t}Bu), 1.18 (1.19) (d, 27 H, $^{2}J_{PH}$ = 13.2 Hz, P-^{t}Bu) [ppm].

^{31}P{^{1}H}-NMR δ(C_6D_6): 66.6 (66.7, 66.5 minor) ppm

Analysis Found: C 54.62 %; H 9.66 %; Calculated: C 54.65 %; H 9.83 %.

5.2.20 Preparation of $(L^{tBu})_2Y(N(SiMe_3)_2)$

A solution of two equivalents of HL^{tBu} in THF (137.8 mg, 0.53 mmol, 5 mL) was added dropwise to a solution of one equivalent of $Y\{N(SiMe_3)_2\}_3$ in THF (150 mg, 0.26 mmol, 5mL) at -78 °C and stirred for 1 hour at -78 °C. All volatiles were removed under reduced pressure and the residual recrystallised from hexanes to afford colourless crystals. Yield 142.6 mg (71 %). Integration of the resonances in the spectra of bulk $(L^{tBu})_2Y(N(SiMe_3)_2)$ show that the *rac* isomer is the major isomer present with the minor identified as *RS*-$(L^{tBu})_2Y(N(SiMe_3)_2)$, and the major : minor ratio is 65 : 35.

^{1}H-NMR δ(C_6D_6): major diastereomer (minor diastereomer in brackets); 4.21 (m, 2 H, CH); 1.74 (m, 4 H, CH_2); 1.18 (1.17) (d, 18 H, $^{2}J_{PH}$ = 13.7 Hz, P-^{t}Bu); 1.08 (s, 18 H, C-^{t}Bu), 1.08 (1.06) (d, 18 H, $^{2}J_{PH}$ = 13.3 Hz, P-^{t}Bu), 0.58 (s, 18 H, -$NSiCH_3$) [ppm].

^{13}C- NMR δ(C_6D_6): 78.9 (79.2) (CH), 37.7 (37.8) (d, CH, 37.1 Hz), 35.8 (CH_2), 27.5 (27.3) (P-^{t}Bu), 26.5 (26.4) (P-^{t}Bu), 26.2 (C-^{t}Bu), 5.63 (5.73) (-$NSiCH_3$) [ppm].

^{31}P-NMR δ(C_6D_6): 70.5 (70.2) ppm (d, $^{2}J_{YP}$ = 7.6 Hz).

Analysis Found: C 52.83 %, H 10.56 %, N 1.73 %; Calculated: C 52.90 %, H 10.18 %, 1.81 %.

5.2.21 Preparation of $(L^{tBu})_2In(N(SiMe_3)_2)$

To a solution of 1 equivalent of $In\{N(SiMe_3)_2\}_3$ in THF (100.0 mg, 0.17 mmol, 2 mL) was added a solution of 2 equivalents of HL^{tBu} in THF (89.1 mg, 0.34 mmol, 2 mL) at 25 °C, and stirred overnight. Volatiles were removed under reduced pressure and the residual solid recrystallised from hexane to afford colourless **$(L^{tBu})_2In(N(SiMe_3)_2)$**. Yield 96 mg (70 %). Integration of the resonances in the spectra of bulk **$(L^{tBu})_2In(N(SiMe_3)_2)$** show that the *rac* isomer is the major isomer present with the minor identified as *RS*-$(L^{tBu})_2In(N(SiMe_3)_2)$, and the major : minor ratio is 90 : 10.

^{1}H-NMR δ(C_6D_6): 0.62 (s, 18 H, CH_3), 1.12 (d, 18 H, $^2J_{PC}$ = 13.1 Hz, P-^{t}Bu), 1.16 (s, 18 H, C-^{t}Bu), 1.22 (d, 18 H, $^2J_{PC}$ = 13.2 Hz, P-^{t}Bu), 1.7-1.9 (m, 4 H, CH_2), 4.37 (m, 2 H, CH) [ppm].

^{13}C{^{1}H}-NMR δ(C_6D_6): 6.6 (6 C, s, $SiMe_3$), 24.0 (2 C, d, J_{PC} = 57.2 Hz, CH_2), 26.6 (6 C, s, CMe_3), 27.0 (6 C, s, P-CMe_3), 27.1 (6 C, s, P-CMe_3), 79.4 (2 C, d, $^2J_{PC}$ = 6.1 Hz, C-OH) [ppm].

^{31}P{^{1}H}-NMR δ(C_6D_6): 71.8 ppm.

Analysis Found: C 51.14 %, H 9.75 %, N 1.83 %; Calculated: C 51.18 %, H 9.85 %, N 1.76 %.

5.2.22 Preparation of $(L^{Ph})_2In(N(SiMe_3)_2)$

A solution of two equivalents of HL^{Ph} in THF (100 mg, 0.33 mmol, 5 mL) was added dropwise to a solution of one equivalent of $In\{N(SiMe_3)_2\}_3$ in THF (98.5 mg, 0.16 mmol, 5mL) at - 78 °C and stirred for 16 hours All volatiles were removed under reduced pressure and the residual recrystallised from DME to afford colourless solid **$(L^{Ph})_2In(N(SiMe_3)_2)$**. Yield 127.2 mg (91 %). Integration of the resonances in the spectra of bulk **$(L^{Ph})_2In(N(SiMe_3)_2)$** show that the *rac* isomer is the major isomer present with the minor identified as *RS*-$(L^{Ph})_2In(N(SiMe_3)_2)$, and the major : minor ratio is 75 : 25.

^{1}H-NMR δ(C_6D_6): major diastereomer (minor diastereomer in brackets); 8.1-7.7 (m, 8 H, CH_{arom}); 7.0-6.8 (m, 12 H, CH_{arom}) 3.9 (3.6) (m, 2 H, CH); 2.4-2.2 (m, 4 H, CH_2); 1.09 (1.11) (s, 18 H, C-^{t}Bu); 0.83 (s, 18 H, CH_3) [ppm].

^{31}P{^{1}H}-NMR δ(C_6D_6): 48.0 (44.8) ppm.

5.2.23 Preparation of $(L^{tBu})_2Lu(N(SiMe_3)_2)$

A solution of two equivalents of HL^{tBu} in THF (100.0 mg, 0.38 mmol, 5 mL) was added dropwise to a solution of one equivalent of $Lu\{N(SiMe_3)_2\}_3$ in THF (124.9 mg, 0.19 mmol, 5mL) at -78 °C and stirred for 16 hours at RT. All volatiles were removed under reduced pressure and the residual recrystallised from hexanes to afford colourless crystals of **$(L^{tBu})_2Lu(N(SiMe_3)_2)$**. Yield 42.6 mg (26 %). Integration of the resonances in the spectra of bulk **$(L^{tBu})_2Lu(N(SiMe_3)_2)$** show that the *rac* isomer is the major isomer present with the minor identified as *RS*-$(L^{tBu})_2Lu(N(SiMe_3)_2)$, and the major : minor ratio is 70 : 30.

^{1}H-NMR δ(C_6D_6): major diastereomer (minor diastereomer in brackets); 4.3-4.2 (m, 2 H, CH); 1.8-1.6 (m, 4 H, CH_2); 1.18 (d, 18 H, $^{2}J_{PH}$ = 19.7 Hz, P-^{t}Bu); 1.10 (1.07) (d, 18 H, $^{2}J_{PH}$ = 18.3 Hz, P-^{t}Bu) 1.09 (1.11) (s, 18 H, C-^{t}Bu), 0.59 (s, 18 H, -$NSiCH_3$) [ppm].

^{31}P-NMR δ(C_6D_6): 72.6 (72.1) ppm.

5.2.24 Preparation of $(L^{tBu})_2In(NPh_2)$

5.2.24.1 From $(L^{tBu})_2In(N(SiMe_3)_2)$

A teflon tap-equipped NMR tube was charged with $(L^{tBu})_2In[N(SiMe_3)_2]$ (50.0 mg, 0.06 mmol), one equivalent of $HNPh_2$ (10.6 mg, 0.06 mmol), and 0.5 mL C_6D_6. The colourless solution was analysed within 10 minutes by ^{1}H and ^{31}P{^{1}H} NMR spectroscopy. The solution was then heated at 80 °C until no further changes were observed, in this case 3 days. In addition to an equivalent of liberated HN", a product

was observed to have formed quantitatively, characterised as **$(L^{tBu})_2In(NPh_2)$**, Integration of the resonances in the spectra of bulk **$(L^{tBu})_2In(NPh_2)$** show that the *rac* isomer is the major isomer present with the minor identified as *RS*-$(L^{tBu})_2In(NPh_2)$, and the major : minor ratio is 85 : 15.

^{1}H-NMR δ(C_6D_6): major diastereomer (minor diastereomer in brackets);7.66 (d, 4 H, m-Ph), 7.30 (t, 2 H, p-Ph), 7.00 (d, 4 H, o-Ph); 4.3 (m, 2 H, CH); 1.6-1.8 (m, 4 H, CH_2); 1.20 (s, 18 H, C-^{t}Bu); 1.14 (d, 18 H, $^2J_{PC}$ = 6.9 Hz, P-^{t}Bu), 0.79 (d, 18 H, $^2J_{PC}$ = 7.2 Hz, P-^{t}Bu) [ppm].

^{31}P{^{1}H}-NMR δ(C_6D_6): 72.0 (71.9) ppm.

Analysis Found: C 59.58 %, H 8.84 % N 1.64; Calculated: C 59.62 %, H 8.76 %, N 1.74%.

5.2.24.2 From In[(N(SiMe$_3$)$_2$)]$_3$

To a solution of one equivalent of In[(N(SiMe$_3$)$_2$)]$_3$ in C_6D_6 (340.7 mg, 0.57 mmol, 0.5 mL) was added one equivalent $HNPh_2$ (96.7 mg, 0.57 mmol) and two equivalents of HL^{tBu} (300 mg, 1.1 mmol) at 25 °C, and the mixture then heated for 16 h at 80 °C. Volatiles were removed under reduced pressure, the residual solid washed with hexane and dissolved in DME, then the solution evaporated slowly, to afford colourless **$(L^{tBu})_2In(NPh_2)$**. Yield 312.4 mg (68 %).

The product, formed quantitatively, was identified as **$(L^{tBu})_2In(NPh_2)$** by NMR spectroscopy.

5.2.24.3 From In(NPh$_2$)$_3$

A teflon tap-equipped NMR tube was charged with one equivalent of $In(NPh_2)_3$ (50.0 mg, 0.081 mmol), two equivalents of HL^{tBu} (42.3 mg, 0.16 mmol), and 0.5 mL C_6D_6. The colourless solution was analysed within 10 minutes by ^{1}H and ^{31}P NMR spectroscopy. The solution was then heated at 80 °C for 16 hours, the NMR spectrum shows an intractable mixture of compounds

5.2.25 Attempts of Synthesis of various amido $(L^{tBu})_2M(NX_2)$ complexes

5.2.25.1

To a solution of one equivalent of $(L^{tBu})_2InN''$ in d_6-benzene (20.0 mg, 0.025 mmol, 0.5 mL) was added on equivalent of $LiNMe_2$ (1.3 mg, 0.025 mmol), the solution was heated for 16 hours to afford the starting materials.

5.2.25.2

To a solution of one equivalent of $(L^{tBu})_2InN''$ in d_6-benzene (15.0 mg, 0.02 mmol, 0.5 mL) was added on equivalent of $LiNH^tBu$ (1.1 mg, 0.02 mmol), the solution was heated for 16 hours to afford the starting materials.

5.2.25.3

To a solution of one equivalent of $(L^{tBu})_2In(OAr)$ in d_6-benzene (50.0 mg, 0.059 mmol, 0.5 mL) was added on equivalent of $LiNMe_2$ (3.0 mg, 0.059 mmol), the solution was heated for 16 hours to afford the starting materials.

5.2.25.4

To a solution of one equivalent of $(L^{tBu})_2In(OAr)$ in d_6-benzene (50.0 mg, 0.059 mmol, 0.5 mL) was added on equivalent of $HNPh_2$ (10.0 mg, 0.059 mmol), the solution was heated for 16 hours to afford a intractable mixture of compounds.

5.2.25.5

To a solution of one equivalent of $(L^{tBu})_2Y(OAr)$ in d_6-benzene (20.0 mg, 0.024 mmol, 0.5 mL) was added on equivalent of $HNPh_2$ (4.1 mg, 0.024 mmol), the solution was heated for 16 hours to afford a intractable mixture of compounds.

5.2.26 Preparation of $(L^{tBu})_2Y(OAr)$

5.2.26.1 From $(L^{tBu})_2Y(N(SiMe_3)_2)$

A teflon tap-equipped NMR tube was charged with $(L^{tBu})_2Y[N(SiMe_3)_2]$ (90.0 mg, 0.12 mmol), one equivalent of HOAr, HOC_6H_3-^{t}Bu$_2$-2,6 (24 mg, 0.12 mmol), and 0.5 mL C_6D_6. The colourless solution was analysed within 10 minutes by ^{1}H and ^{31}P{^{1}H} NMR spectroscopy. The solution was then heated at 80 °C until no further changes were observed, in this case 16 hours. In addition to an equivalent of liberated HN", a product was observed to have formed quantitatively, characterised as **$(L^{tBu})_2Y(OC_6H_3$-^{t}Bu$_2$-2,6),** [an equal mixture of *RR*-$(L^{tBu})_2Y(OC_6H_3$-^{t}Bu$_2$-2,6) and *SS*-$(L^{tBu})_2Y(OC_6H_3$-^{t}Bu$_2$-2,6), and also meso *RS*-**$(L^{tBu})_2Y(OC_6H_3$-^{t}Bu$_2$-2,6)**] was identified by NMR spectroscopy. Integration of the resonances in the spectra of bulk **$(L^{tBu})_2Y(OC_6H_3$-^{t}Bu$_2$-2,6)** show that the *rac* isomer is the major isomer present with the minor identified as *RS*-**$(L^{tBu})_2Y(OC_6H_3$-^{t}Bu$_2$-2,6)**, and the major : minor ratio is 85 : 15.

^{1}H-NMR δ(C_6D_6): major diastereomer (minor diastereomer in brackets)*;* 7.53 (d, 2 H, ortho-ArH), 6.87 (t, 1 H, para-ArH), 3.63 (t, 2 H, CH); 1.86 (1.85) (s, 18 H, Ar-^{t}Bu), 1.79 (m, 4 H, CH_2); 1.16 (s, 18 H, C-^{t}Bu), 1.02 (d, 36 H, $^2J_{PH}$ = 13.7 Hz, P-^{t}Bu); 0.95 (d, 18 H, $^2J_{PH}$ = 13.3 Hz, P-^{t}Bu) [ppm].

^{13}C{^{1}H}-NMR δ(C_6D_6): 138.4, 125.3, 115.1 (s, 5 C, CH arom), 128.1 (s, C arom), 79.0 (79.7) (CH), 38.4 (37.0) (d, CH_2, 38.5 Hz), 32.3 (32.4) (C-^{t}Bu Arom), 27.5 (27.7) (P-^{t}Bu), 27.0 (27.1) (P-^{t}Bu), 26.9 (C-^{t}Bu) [ppm].

^{31}P{^{1}H}-NMR δ(C_6D_6): 70.7 ppm (d, $^2J_{YP}$ = 8.6 Hz) .

Analysis Found: C 61.66 %, H 10.04 %; Calculated: C 61.75 %, H 9.99 %.

5.2.26.2 From *rac*-$Y(L^{tBu})_3$

A teflon tap-equipped NMR tube was charged with *rac*-$Y(L^{tBu})_3$ (160.0 mg, 0.18 mmol)**,** one equivalent of HOC_6H_3-^{t}Bu$_2$-2,6 (37.8 mg, 0.18 mmol), and 0.5 mL C_6D_6.

The colourless solution was analysed within 10 minutes by ^{1}H and $^{31}P\{^{1}H\}$ NMR spectroscopy. The solution was then heated at 80 °C until no further changes were observed, in this case 16 hours.

The product, formed quantitatively, was identified as **$(L^{tBu})_2Y(OC_6H_3\text{-}^tBu_2\text{-}2,6)$** by NMR spectroscopy.

5.2.26.3 From $Y[N(SiMe_3)_2]_3$

A teflon tap-equipped NMR tube was charged with $HOC_6H_3\text{-}^tBu_2\text{-}2,6$ (8.1 mg, 0.04 mmol) and two equivalents of HL^{tBu} (20.0 mg, 0.08 mmol), and 0.3 mL C_6D_6. To this was added one equivalent of $Y\{N(SiMe_3)_2\}_3$ (22.0 mg, 0.04 mmol) in 0.2 mL C_6D_6. The colourless solution was analysed within 10 minutes by ^{1}H and $^{31}P\{^{1}H\}$ NMR spectroscopy. The solution was then heated at 80 °C until no further changes were observed, in this case 16 hours.

The product, formed quantitatively, was identified as **$(L^{tBu})_2Y(OC_6H_3\text{-}^tBu_2\text{-}2,6)$** by NMR spectroscopy.

5.2.26.4 From $Y(OAr)_3$

A teflon tap-equipped NMR tube was charged with $Y(OAr)_3$ (26.9 mg, 0.04 mmol), two equivalents of HL^{tBu} (20.0 mg, 0.08 mmol), and 0.5 mL C_6D_6. The colourless solution was analysed within 10 minutes by ^{1}H and $^{31}P\{^{1}H\}$ NMR spectroscopy. The solution was then heated at 80 °C until no further changes were observed, in this case 16 hours.

The product, formed quantitatively, was identified as **$(L^{tBu})_2Y(OC_6H_3\text{-}^tBu_2\text{-}2,6)$** by NMR spectroscopy

5.2.26.5 Preparation of *R*-$(L^{tBu})_2Y(OC_6H_3\text{-}^tBu_2\text{-}2,6)$

A teflon tap-equipped NMR tube was charged with $HOC_6H_3\text{-}^tBu_2\text{-}2,6$ (8.1 mg, 0.04 mmol) and two equivalents of *R*-HL^{tBu} (20.0 mg, 0.08 mmol), and 0.3 mL C_6D_6. To

this was added one equivalent of $Y\{N(SiMe_3)_2\}_3$ (22.0 mg, 0.04 mmol) in 0.2 mL C_6D_6. The colourless solution was analysed within 10 minutes by ^1H and $^{31}P\{^1H\}$ NMR spectroscopy. The solution was then heated at 80 °C until no further changes were observed, in this case 16 hours.
The product, formed quantitatively, was identified as ***RR*-$(L^{tBu})_2Y(OC_6H_3$-$^t Bu_2$-2,6)** by NMR spectroscopy.

5.2.27 Preparation of $(L^{tBu})_2In(OC_6H_3$-$^t Bu_2$-2,6)

To a solution of $(L^{tBu})_2InN''$ in C_6D_6 (100.0 mg, 0.125 mmol, 2 mL) was added a solution of HO-C_6H_3-^{t}Bu-2,6 (25.8 mg, 0.125 mmol, 2 mL) at 25 °C, and the mixture then heated for 16 hours at 80 °C. Volatiles were removed under reduced pressure, the residual solid washed with hexane and dissolved in DME, then the solution evaporated slowly, to afford colourless **$(L^{tBu})_2In(OC_6H_3$-$^t Bu_2$-2,6)**. Yield 80.2 mg (76 %). Integration of the resonances in the spectra of bulk **$(L^{tBu})_2In(OC_6H_3$-$^t Bu_2$-2,6)** show that the *rac* isomer is the major isomer present with the minor identified as *RS*-**$(L^{tBu})_2In(OC_6H_3$-$^t Bu_2$-2,6)**, and the major : minor ratio is 90 : 10.

^{1}H-NMR δ(C_6D_6): 0.94 (d, 18 H, $^2J_{PC}$ = 13.7 Hz, P-^{t}Bu), 1.14 (d, 18 H, $^2J_{PC}$ = 13.5 Hz, P-^{t}Bu), 1.15 (s, 18 H, C-^{t}Bu), 1.90. (s, 18 H, Ph-^{t}Bu), 1.7-1.9 (m, 4 H, CH_2), 4.41 (m, 2 H, CH); 6.88 (t, 1 H, p-Ph), 7.44 (d, 2 H, H-meta) [ppm].
$^{13}C\{^1H\}$-NMR δ(C_6D_6): 33.1 (6 C, s, ^{t}Bu), 79.3 (2 C, s, C-OH), 115.62 (1 C, p-Ph), 125.98 (2 C, m-Ph), 141.0 (2 C, o-Ph), 166.9 (1 C, C-O) [ppm].
$^{31}P\{^1H\}$-NMR δ(C_6D_6): 72.94 ppm
Analysis Found: C 59.92 %, H 9.61 %; Calculated: C 59.85 %, H 9.69 %.

5.2.28 Preparation of $(L^{tBu})_2In(O^tBu)$

To a solution of one equivalent of $In\{N(SiMe_3)_2\}_3$ in C_6D_6 (340.7 mg, 0.57 mmol, 0.5 mL) was added one equivalent HO^tBu (42.4 mg, 0.57 mmol) and two equivalents of HL^{tBu} (300 mg, 1.1 mmol) at 25 °C, and the mixture then heated for 16 hours at 80

°C for 2 days. Volatiles were removed under reduced pressure, the residual solid washed with hexane and dissolved in DME, then the solution evaporated slowly, to afford colourless **$(L^{tBu})_2In(O^tBu)$**. Yield 156.8 mg (39 %). Integration of the resonances in the spectra of bulk **$(L^{tBu})_2In(O^tBu)$** show that the *rac* isomer is the major isomer present with the minor identified as *RS*-**$(L^{tBu})_2In(O^tBu)$**, and the major : minor ratio is 85 : 15.

^{1}H-NMR δ(C_6D_6): major diastereomer (minor diastereomer in brackets); 4.2 (4.25) (m, 2 H, CH); 1.75-1.65 (m, 4 H, CH_2); 1.31 (s, 9 H, O-^{t}Bu). 1.12 (d, 18 H, $^2J_{PH}$ = 19.4 Hz, P-^{t}Bu); 1.05 (1.11) (s, 18 H, C-^{t}Bu); 0.98 (0.96) (d, 18 H, $^2J_{PH}$ = 18.9 Hz, P-^{t}Bu) [ppm]

^{31}P-NMR δ(C_6D_6): 71.7 (70.6) ppm.

Analysis Found: C 53.95 %, H 9.70 %; Calculated: C 54.08 %, H 9.79 %.

5.2.29 Preparation of $(L^{tBu})_2In(OCH_2\text{-}C_6H_5)$

To a solution of one equivalent of $(L^{tBu})_2In[(N(SiMe_3)_2)]$ in C_6D_6 (100.0 mg, 0.13 mmol, 0.5 mL) was added one equivalent $HOCH_2\text{-}C_6H_5$ (13.6 mg, 0.13 mmol) at 25 °C and the mixture then heated for 16 hours at 80 °C.

^{1}H and ^{31}P{^{1}H} NMR spectra show the starting materials.

5.2.30 Preparation of $(L^{tBu})_2In(OCH(CH_3)CO_2C(^tBu))$

To a solution of one equivalent of $(L^{tBu})_2In[(N(SiMe_3)_2)]$ in C_6D_6 (100.0 mg, 0.13 mmol, 0.5 mL) was added one equivalent *R*-$OCH(CH_3)CO_2C(^tBu)$ (18.3 mg, 0.13 mmol) at 25 °C, and the mixture then heated for 16 hours at 80 °C.

^{1}H and ^{31}P{^{1}H} NMR spectra show an intractable mixture of compounds.

5.2.31 Preparation of $(L^{tBu})_2In(O^iPr)$

In a NMR tube 3 equivalents of HL^{tBu} (45 mg, 0.17 mmol) and 1 equivalent of $In(O^iPr)_3$ (16.7 mg, 0,06 mmol) were dissolved in C_6D_6 and the reaction were carried out. After 4 hours at RT, the ^1H NMR spectrum shows principally the ligand; the $^{31}P\{^1H\}$ spectrum shows the ligand (63.7 ppm, major resonance) and a new minor resonance (71.4 ppm).

The NMR tube was heated over-night at 80°C; the NMR shows the same resonances. The NMR tube was heated over week-end at 80°C; the NMR shows the same resonances, the reaction was not further investigated.

5.2.32 Preparation of $(L^{tBu})_2In(CH_2SiMe_3)$

Two equivalents of HL^{tBu} (68 mg, 0.26 mmol) and 1 equivalent of $In(CH_2SiMe_3)_3$ (48 mg, 0.13 mmol,) were dissolved in THF and the reaction were carried out over night. The ^1H and $^{31}P\{^1H\}$ NMR spectra show a mixture of the **$(L^{tBu})_2In(CH_2SiMe_3)$** and **$(L^{tBu})In(CH_2SiMe_3)_2$** in ratio 75 : 25 respectively.

5.2.33 Preparation of $(L^{Ph})_2In(CH_2SiMe_3)$

Two equivalents of HL^{Ph} (200 mg, 0.66 mmol) and 1 equivalent of $In(CH_2SiMe_3)_3$ (124.4 mg, 0.33 mmol) were dissolved in pentane and the reaction were carried out over night. $^{31}P\{^1H\}$ and ^1H NMR spectra show just proligand. The reaction was not further investigated.

5.2.34 Other reactions using $(L^{tBu})_2In(NSiMe_3)_2$

5.2.34.1

To a solution of one equivalent of $(L^{tBu})_2InN"$ in *d_6*-benzene (50.0 mg, 0.06 mmol, 0.5 mL) was added one equivalent of $Eu(fod)_3$ (65.0 mg, 0.06 mmol). The NMR

spectrum recorded immediately shows new resonances. Then the solution was heated for 16 hours to afford an intractable mixture of compounds which none of them including ligands resonances.

5.2.34.2

To a solution of one equivalent of $(L^{tBu})_2InN''$ in *d_6*-benzene (50.0 mg, 0.06 mmol, 0.5 mL) was added on equivalent of 9-BBN (15.3 mg, 0.06 mmol), the solution was heated for 16 hours to afford a black glue.

5.2.35 Preparation of $(L^{tBu})In\{(NSiMe_3)_2\}_2$

One equivalents of HL^{tBu} (17.6 mg, 0.067 mmol) and one equivalent of InN''_3 (40 mg, 0.067 mmol) were dissolved in C_6D_6 at RT and was stirred for 16 hours. Volatiles were removed under reduced pressure, the residual solid washed with hexane and dissolved in DME, then the solution evaporated slowly to afford a mixture of products including **$(L^{tBu})In\{(NSiMe_3)_2\}_2$**.

^{1}H-NMR δ(C_6D_6): 4.0 (m, 1 H, CH); 1.65 (m, 2 H, CH_2); 0.91 (s, 9 H, C-^{t}Bu). 0.89 (d, 9 H, $^2J_{PH}$ = 13.2 Hz, P-^{t}Bu); 0.84 (d, 9 H, $^2J_{PH}$ = 12.9 Hz, P-^{t}Bu), 0.40 (s, 18 H, $SiMe_3$); 0.39 (s, 18 H, $SiMe_3$) [ppm].
^{31}P-NMR δ(C_6D_6): 78.8 ppm.

5.2.36 Preparation of $(L^{tBu})In(CH_2SiMe_3)_2$

One equivalent of HL^{tBu} (34.0 mg, 0.13 mmol) and one equivalent of $In(CH_2SiMe_3)_3$ (48 mg, 0.13 mmol) were dissolved in C_6D_6 at RT and was stirred for 16 hours. Volatiles were removed under reduced pressure, the residual solid washed with hexane and dissolved in DME, then the solution evaporated slowly, to afford colourless **$(L^{tBu})In(CH_2SiMe_3)_2$**.

^{1}H-NMR δ(C_6D_6): 4.1 (m, 1 H, CH); 1.8-1.6 (m, 2 H, CH_2); 1.11 (s, 9 H, C-^{t}Bu). 0.96 (d, 9 H, $^{2}J_{PH}$ = 6.5 Hz, P-^{t}Bu); 0.92 (d, 9 H, $^{2}J_{PH}$ = 7.1 Hz, P-^{t}Bu), 0.37 (s, 18 H, $SiMe_3$); 0.30 (s, 18 H, $SiMe_3$); -0.10 (m, 4 H, CH_2) [ppm].

^{31}P-NMR δ(C_6D_6): 73.0 ppm.

5.2.37 Preparation of (L^{tBu})Al(CH_2SiMe_3)$_2$

One equivalent of HL^{tBu} (34.0 mg, 0.13 mmol) and one equivalent of $Al(CH_2SiMe_3)_3$ (39 mg, 0.13 mmol) were dissolved in C_6D_6 at RT and was stirred for 16 hours. Volatiles were removed under reduced pressure, the residual solid washed with hexane and dissolved in DME, then the solution evaporated slowly, to afford colourless **(L^{tBu})Al(CH_2SiMe_3)$_2$**.

^{1}H-NMR δ(C_6D_6): 3.9 (m, 1 H, CH); 1.8-1.7 (m, 2 H, CH_2); 1.02 (s, 9 H, C-^{t}Bu). 0.85 (d, 9 H, $^{2}J_{PH}$ = 12.7 Hz, P-^{t}Bu); 0.81 (d, 9 H, $^{2}J_{PH}$ = 11.9 Hz, P-^{t}Bu), 0.47 (s, 18 H, $SiMe_3$); 0.42 (s, 18 H, $SiMe_3$); -0.65 (m, 4 H, CH_2) [ppm].

^{31}P-NMR δ(C_6D_6): 78.3 ppm.

5.2.38 Preparation of (L^{tBu})Al(Me_3)$_2$

5.2.38.1 (L^{tBu})Al(Me_3)$_2$ from $AlMe_3$

A solution of one equivalent of HL^{tBu} in THF (6.7 mg, 0.025 mmol, 0.2 mL) was added to a solution of one equivalent of $AlMe_3$ in C_6D_6 (0.14 mL, 0.025 mmol, 10 mL) at room temperature and stirred for 16 hours at 70 °C. All volatile compounds were removed under reduced pressure and the residual solid was crystallised in hexanes solution to afford colourless **(L^{tBu})Al(Me_3)$_2$**.

^{1}H-NMR δ(C_6D_6): 1.0-1.2 (54 H, dd, $^{2}J_{PC}$ = 4.5 Hz, P-^{t}Bu); 1.07 (27 H, s, C-^{t}Bu); 1.6 – 1.9 (4 H, m, CH_2); 3.9 – 4.1 (2 H, m, CH) [ppm].

^{31}P-NMR δ(C_6D_6): 78.7 ppm.

5.2.38.2 $(L^{tBu})Al(Me_3)_2$ from DABAL-Me_3

A solution of two equivalents of HL^{tBu} in THF (33.3 mg, 0.106 mmol, 6 mL) was added to a solution of one equivalent of DABAL-Me_3 in toluene (13.7 mg, 0.053 mmol, 10 mL) at room temperature and stirred for 16 hours at 70 °C. All volatile compounds were removed under reduced pressure and the residual solid recrystallised from hexane to afford colourless **$(L^{tBu})Al(Me_3)_2$**.

The product, formed quantitatively, was identified as **$(L^{tBu})Al(Me_3)_2$** by NMR spectroscopy.

5.2.39 Preparation of $(L^{Ph})Al(Me_3)_2$

5.2.39.1 $(L^{Ph})Al(Me_3)_2$ from $AlMe_3$

A solution of one equivalent of HL^{Ph} in THF (6.7 mg, 0.022 mmol, 0.2 mL) was added to a solution of one equivalent of $AlMe_3$ in C_6D_6 (0.10 mL, 0.022 mmol, 10 mL) at room temperature and stirred for 16 hours at 70 °C. All volatile compounds were removed under reduced pressure and the residual solid recrystallised from hexane/DME to afford colourless **$(L^{Ph})Al(Me_3)_2$**.

^{1}H-NMR δ(C_6D_6): 7.6-7.2 (4 H, m, Ph); 6.9-6.7 (6 H, m, Ph); 3.9 – 4.0 (1 H, m, CH); 2.1 – 2.5 (2 H, m, CH_2); 1.0 (9 H, s, C-^{t}Bu); - 0.07 (3 H, s; CH_3); - 0.14 (3 H, s; CH_3) [ppm].

^{31}P{^{1}H}-NMR δ(C_6D_6): 51.1 ppm.

5.2.39.2 $(L^{Ph})Al(Me_3)_2$ from DABAL-Me_3

A solution of two equivalents of HL^{Ph} in THF (100 mg, 0.33 mmol, 5 mL) was added to a solution of one equivalent of DABAL-Me_3 in toluene (42.3 mg, 0.17 mmol, 5 mL) at room temperature and stirred for 16 hours at 70 °C. All volatile

compounds were removed under reduced pressure and the residual solid recrystallised from DME to afford colourless **$(L^{Ph})Al(Me_3)_2$**.

The product, formed quantitatively, was identified as **$(L^{Ph})Al(Me_3)_2$** by NMR spectroscopy.

5.2.40 Preparation of $(L^{tBu})_2In(OSiMe_3)$

To a solution of $(L^{tBu})_2InN"$ in C_6D_6 (50 mg, 0.06 mmol, 2 mL) was going through CO_2 gaz at 25 °C, and the mixture then heated for 16 hours at 80 °C. Volatiles were removed under reduced pressure, the residual solid washed with hexane and dissolved in hexanes, then the solution evaporated slowly, to afford colourless **$(L^{tBu})_2In(OSiMe_3)$**. Integration of the resonances in the spectra of bulk **$(L^{tBu})_2In(OSiMe_3)$** show that the *rac* isomer is the major isomer present with the minor identified as *RS*-**$(L^{tBu})_2In(OSiMe_3)$**, and the major : minor ratio is 90 : 10.

^{1}H-NMR δ(C_6D_6): major diastereomer (minor diastereomer in brackets); 4.3-4.2 (m, 2 H, CH); 1.85-1.7 (m, 4 H, CH_2); 1.18 (1.16) (d, 18 H, $^2J_{PH}$ = 13.1 Hz, P-^{t}Bu); 1.17 (s, 18 H, C-^{t}Bu); 1.05 (1.07) (d, 18 H, $^2J_{PH}$ = 11.8 Hz, P-^{t}Bu); 0.56 (s, 9 H, O-$SiMe_3$) [ppm].

^{31}P-NMR δ(C_6D_6): 71.7 (70.6) ppm.

Analysis Found: C 51.18 %, H 9.48 %; Calculated: C 51.23 %, H 9.57 %.

5.2.41 Preparation of $(L^{tBu})_2In(O_2CNPh_2)$

To a solution of $(L^{tBu})_2In(NPh_2)$ in C_6D_6 (10.0 mg, 0.01 mmol, 2 mL) was going through CO_2 gaz at 25 °C, and the mixture then heated for 16 hours at 80 °C. Volatiles were removed under reduced pressure, the residual solid washed with hexane and dissolved in DME, then the solution evaporated slowly, to afford colourless $(L^{tBu})_2In(O_2CNPh_2)$. Integration of the resonances in the spectra of bulk $(L^{tBu})_2In(O_2CNPh_2)$ how that the *rac* isomer is the major isomer present with the minor identified as *RS*-$(L^{tBu})_2In(O_2CNPh_2)$, and the major : minor ratio is 95 : 5.

^{1}H-NMR δ(C_6D_6): major diastereomer (minor diastereomer in brackets); 7.5 (d, 4 H, m-Ph), 7.1 (t, 2 H, p-Ph), 6.9 (t, 4 H, o-Ph); 4.4 (m, 2 H, CH); 1.95-1.75 (m, 4 H, CH_2); 1.19 (d, 18 H, $^{2}J_{PC}$ = 10.6 Hz, P-^{t}Bu); 1.18 (s, 18 H, C-^{t}Bu); 1.06 (d, 18 H, $^{2}J_{PC}$ = 10.2 Hz, P-^{t}Bu) [ppm].

^{31}P{^{1}H}-NMR δ(C_6D_6): 72.4 (71.9) ppm.

5.3 Synthetic Procedures described in Chapter 3

5.3.1 Polymerisation of lactide in solution

In the glove-box: both chosen quantity of monomer and complex were dissolved in chosen solvent in separate vials, after total dissolution, the solution of complex was added quickly via Pasteur pipette to the solution of monomer and after the desired time the vial was removed from the glove and quenched with hexane. The synthesised colourless polymer was then filtered over Buchner and washed with diethylether, then dried *in vaccuo*. Finally, the polymer was dissolved in the minimum needed quantity of DCM and ran through a flash silica gel column (in a Pasteur pipette) to afford colourless solution (which was dried to afford colourless polymer).

On a shlenk line: according to table entries, the quantity of monomer and complex were loaded in the glove box in different shlenks and were dissolved on a schlenk line with the desired amount of solvent. After complete dissolution of the lactide (sometimes the time needed can be long if the solvent of choosing is toluene or/and the temperature is low), the solution of the complex was added instantly to the solution of the monomer, then after the desired time, an aliquot of the solution was taken and quenched with hexanes solution. The synthesised colourless polymer was then filtered over Buchner and washed with diethylether, then dried *in vaccuo*. Finally, the polymer was dissolved in the minimum needed quantity of DCM and ran through a flash silica gel column (in a Pasteur pipette) to afford colourless solution (which was dried to afford colourless polymer).

Polymerisation tables 3.1, 3.2, 3.3, 3.5, 3.8 and 3.9 are in moles ratio; polymerisarion tables 3.4, 3.6, and 3.7 are in weights ratio

5.3.2 Polymerisation procedure of lactide in melt

The procedure of polymerisation of lactide in melt in similar to the procedure in solution except for the absence of solvent; the desired temperature was 140 °C.

5.3.3 Polymerisation of ε-caprolactone in solution

In an ampoule, 500 mg dried and degassed ε-caprolactone was dissolved in 2 mL toluene at room temperature, 20 mg of **$(L^{tBu})_2Y(OAr)$** dissolved in 1 mL toluene was added via cannula to the vigorously stirred solution and the ampoule was heated at 110 °C for 16 hours. The mixture was quenched by adding 5 drops of MeOH, the solvent was evaporated to afford a opaque polymer.

5.3.4 Copolymerization of ε-caprolactone and *rac*-lactide

In an ampoule, 500 mg dried and degassed ε-caprolactone and 250 mg of *rac*-lactide were dissolved in 2 mL toluene at room temperature, 25 mg of **$(L^{tBu})_2Y(OAr)$** dissolved in 1 mL toluene was added via cannula to the vigorously stirred solution and the ampoule was heated at 110 °C for 16 hours. The mixture was quenched by adding 5 drops of MeOH, the solvent was evaporated to afford a opaque copolymer.

5.3.5 Preparation of the polymer sample for mass spectral analysis of the polymer end groups

In a vial, 10 mg of polylactide was dissolved in 100 mL of acetonitrile, and 1 mL of the previous solution was dissolved in 100 mL of acetonitrile, then 1mL of the previous solution was dissolved in 100 mL of acetonitrile to afford the desired

concentration of polymer in acetonitrile. Finally, the solution was ran through a MALDI-TOF by Ms J. Hanna.

5.3.6 Preparation of polymer sample for NMR spectral analysis of the polymer stereochemistry

In a vial, 10 mg of polylactide was dissolved in 0.5 mL of CDCl3 then introduced an NMR tube, the polymers were characterised by ^{13}C, ^{1}H and $^{1}H\{^{1}H\}$ decoupled on the frequency of the methyl doublet around 1.55 ppm.

5.4 Synthetic Procedures described in Chapter 4

5.4.1 Preparation of $Sn(L^{tBu})_2$

To a solution of $Sn\{N(SiMe_3)_2\}_2$ in THF (126.0 mg, 0.28 mmol, 5 mL) was added a solution of two equivalents of HL^{tBu} in THF (150.0 mg, 0.57 mmol, 5 mL) at room temperature with stirring. Volatiles were removed under reduced pressure and the residual solid recrystallised from DCM to afford colourless **$Sn(L^{tBu})_2$** Yield 127.8 mg (71 %). Integration of the resonances in the spectra of bulk **$Sn(L^{tBu})_2$** show that the *rac* isomer is the major isomer present with the minor identified as *RS*- **$Sn(L^{tBu})_2$**, and the major : minor ratio is 100 : 0.

^{1}H-NMR $\delta(C_6D_6)$: major diastereomer (minor diastereomer in brackets); 1.00 (d, 18 H, $^{2}J_{PC}$ = 10.8 Hz, P-^{t}Bu), 1.18 (s, 18 H, C-^{t}Bu), 1.34 (d, 18 H, $^{2}J_{PC}$ = 14.4 Hz, P-^{t}Bu), 1.71-1.98 (m, 4 H, CH_2), 3.94-4.08 (m, 2 H, CH) [ppm].

$^{31}P\{^{1}H\}$ NMR $\delta(C_6D_6)$: 66.7 ppm (with $^{2}J_{SnP}$ = 255.6 Hz).

Analysis Found: C 52.38 %, H 9.41 %; Calculated: C 52.43 %, H 9.43 %.

5.4.2 Preparation of $Zn(L^{tBu})_2$

To a solution of $Zn\{N(SiMe_3)_2\}_2$ in THF (385.5 mg, 1.0 mmol, 10 mL) was added a solution of two equivalents of HL^{tBu} in THF (522.0 mg, 2.0 mmol, 10 mL) at -78 °C, and allowed to warm slowly to room temperature for 16 hours with stirring. Volatiles were removed under reduced pressure and the residual solid recrystallised from DCM to afford colourless **$Zn(L^{tBu})_2$**. Yield 412.2 mg (70 %). Integration of the resonances in the spectra of bulk **$Zn(L^{tBu})_2$** show that the *rac* isomer is the major isomer present with the minor identified as *RS*- **$Zn(L^{tBu})_2$**, and the major : minor ratio is 75 : 25.

^{1}H-NMR $\delta(C_6D_6)$: major diastereomer (minor diastereomer in brackets): 1.02 (d, 18 H, $^2J_{PC}$ = 11.1 Hz, P-^{t}Bu), 1.05 (d, 18 H, $^2J_{PC}$ = 8.9 Hz, P-^{t}Bu), 1.29 (1.23) (s, 18 H, C-^{t}Bu), 1.79-1.92 (m, 4 H, CH_2), 4.25-4.39 (m, 2 H, CH) [ppm].

$^{31}P\{^1H\}$ NMR $\delta(C_6D_6)$: 72.2 (72.4) ppm.

Analysis Found: C 57.33 %, H 10.29 %; Calculated: C 57.18 %, H 10.28 %.

5.4.3 Preparation of $Ca(L^{tBu})_2$

A solution of two equivalents of HL^{tBu} in C_6D_6 (10.4 mg, 0.04 mmol, 0.25 mL) was added to a solution of one equivalent of $Ca\{N(SiMe_3)_2\}_2$ $(THF)_2$ in C_6D_6 (10.0 mg, 0.02 mmol, 0.25 mL) at room temperature and stirred for 16 hours at 70 °C. All volatile compounds were removed under reduced pressure to afford colourless **$Ca(L^{tBu})_2$.** Integration of the resonances in the spectra of bulk **$Ca(L^{tBu})_2$** show that the *rac* isomer is the major isomer present with the minor identified as *RS*- **$Ca(L^{tBu})_2$**, and the major : minor ratio is 90 : 10.

^{1}H-NMR $\delta(C_6D_6)$: major diastereomer (minor diastereomer in brackets): 0.95 (d, 18 H, $^2J_{PC}$ = 13.7 Hz, P-^{t}Bu), 1.11 (d, 18 H, $^2J_{PC}$ = 13.5 Hz, P-^{t}Bu), 1.11 (s, 18 H, C-^{t}Bu), 1.7-1.9 (m, 4 H, CH_2), 3.15-3.35 (m, 2 H, CH) [ppm].

^{13}C-NMR δ(C_6D_6): 25.3 (2 C, d, J_{PC} = 56.8 Hz, CH_2); 26.3 (6 C, ^{t}Bu); 27.2 (6 C, ^{t}Bu); 26.3 (6 C, ^{t}Bu); 68.1 (2 C, d, $^2J_{PC}$ = 5.7 Hz, CH) [ppm].

^{31}P{^{1}H}-NMR δ(C_6D_6): 68.87 (69.14) ppm.

Analysis Found: C 59.71 %, H 10.63 %; Calculated: C 59.75 %, H 10.75 %.

5.4.4 Preparation of Mg(L^{tBu})$_2$

5.4.4.1 From Mg[N(SiMe$_3$)$_2$]$_2$(THF)$_2$

A solution of two equivalents of HL^{tBu} in C_6D_6 (50.0 mg, 0.19 mmol, 0.25 mL) was added to a solution of one equivalent of Mg{N(SiMe$_3$)$_2$}$_2$(THF)$_2$ in C_6D_6 (46.6 mg, 0.095 mmol, 0.25 mL) at room temperature and the solution was heated at 80 °C for 16 hours to afford a intractable mixture of compounds.

5.4.4.2 From (L^{tBu})Mg(OAr)

A solution of one equivalent of HL^{tBu} in C_6D_6 (25.0 mg, 0.095 mmol, 0.25 mL) was added to a solution of one equivalent of (L^{tBu})Mg(OAr) in C_6D_6 (23.5 mg, 0.05 mmol, 0.25 mL) at room temperature and the solution was heated at 80°C for 16 hours to afford a intractable mixture of compounds.

5.4.5 Preparation of [Mg(L^{Ph})$_2$]$_2$

To a solution of Mg{N(SiMe$_3$)$_2$}$_2$ (THF)$_2$ in THF (82.7 mg, 0.17 mmol, 5 mL) was added a solution of two equivalents of HL^{Ph} in THF (100.0 mg, 0.33 mmol, 5 mL) at room temperature and the solution was heated for 16 hours at 80 °C. Volatiles were removed under reduced pressure and the residual solid recrystallised from THF/DME solution to afford colourless **[Mg(L^{Ph})$_2$]$_2$**. Yield 45.1 mg (42 %).

^{1}H-NMR δ(C_6D_6): major diastereomer (minor diastereomer in brackets); 1.13 (1.15) (s, 18 H, C-^{t}Bu); 2.16-2.50 (m, 4 H, CH_2); 3.79-4.11 (4.11-4.37) (m, 2 H, CH); 6.84-7.15 (m, 12 H, CH_{arom}); 7.34-8.21 (m, 8 H, CH_{arom}) [ppm].

^{31}P{^{1}H}-NMR δ(C_6D_6): 40.15 (40.35) ppm.

Analysis Found: C 68.85 %, H 7.13 %; Calculated: C 68.96 %, H 7.07 %.

5.4.6 Preparation of $[Sn(L^{Ph})_2]_2$

To a solution of $Sn\{N(SiMe_3)_2\}_2$ in THF (218.6 mg, 0.5 mmol, 5 mL) was added a solution of two equivalents of HL^{Ph} in THF (300.0 mg, 0.99 mmol, 5 mL) at room temperature and the solution was heated for 16 hours at 80 °C. Volatiles were removed under reduced pressure and the residual solid recrystallised from DME to afford colourless **$[Sn(L^{Ph})_2]_2$**. Yield 223.5 mg (62 %).

^{1}H-NMR δ(C_6D_6): 0.91 (s, 18 H, C-^{t}Bu); 0.94 (s, 18 H, C-^{t}Bu); 2.05-2.19 (m, 2 H, CH_2); 2.23-2.37 (m, 2 H, CH_2), 2.39-2.56 (m, 2 H, CH_2); 2.57-2.72 (m, 2 H, CH_2); 3.65-3.81 (m, 1 H, CH); 4.15-4.4.23 (m, 1 H, CH); 4.35-4.55 (m, 1 H, CH); 6.79-7.04 (m, 12 H, CH_{arom}); 7.43-7.85 (m, 8 H, CH_{arom}) [ppm].

^{31}P{^{1}H}-NMR δ(C_6D_6): 37.55 ppm (with $^{2}J_{SnP}$ = 198.0 Hz) and 38.56 ppm (with $^{2}J_{SnP}$ = 241.2 Hz).

Analysis Found: C 59.90 %, H 6.22 %; Calculated: C 59.94 %, H 6.15 %.

5.4.7 Preparation of $[Zn(L^{Ph})_2]_2$

To a solution of $Zn\{N(SiMe_3)_2\}_2$ in THF (190.7 mg, 0.5 mmol, 5 mL) was added a solution of two equivalents of HL^{Ph} in THF (300 mg, 0.99 mmol, 5 mL) at room temperature and the solution was heated for 16 hours at 80 °C. Volatiles were removed under reduced pressure and the residual solid recrystallised from DME to afford an intractable mixture of compounds.

5.4.8 Preparation of $[Co(L^{Ph})_2]_2$

To a solution of $Co\{N(SiMe_3)_2\}_2$ in THF (86.1 mg, 0.17 mmol, 5 mL) was added a solution of two equivalents of HL^{Ph} in THF (100.0 mg, 0.33 mmol, 5 mL) at room temperature and the solution was heated for 16 hours at 80 °C. Volatiles were removed under reduced pressure and the residual solid recrystallised from hexane to afford purple **$[Co(L^{Ph})_2]_2$**. Yield 96.8 mg (88 %).

^{1}H-NMR $\delta(C_6D_6)$: - 40 to 60 ppm.

$^{31}P\{^1H\}$-NMR $\delta(C_6D_6)$: 34 ppm (very broad).

Analysis Found: C 65.35 %, H 6.74 %; Calculated: C 65.35 %, H 6.70 %.

5.4.9 Preparation of $[Mg(L^{Ar})_2]_2$

To a solution of $Mg\{N(SiMe_3)_2\}_2(THF)_2$ in THF (34.2 mg, 0.07 mmol, 10 mL) was added a solution of two equivalents of HL^{Ar} in THF (50.0 mg, 0.14 mmol, 10 mL) at room temperature and the solution was heated for 16 hours at 80 °C. Volatiles were removed under reduced pressure and the crystallised in a Hexanes/DME solution to afford colourless **$[Mg(L^{Ar})_2]_2$**.

5.4.10 Preparation of $(L^{tBu})Mg(OAr)$

A teflon tap-equipped NMR tube was charged with HOC_6H_3-Bu^t_2-2,6 (157.4 mg, 0.76 mmol) and one equivalent of HL^{tBu} (200.0 mg, 0.76 mmol), and 0.3 mL C_6D_6. To this was added one equivalent of $Mg\{N(SiMe_3)_2\}_2(THF)_2$ (373.0 mg, 0.76 mmol) in 0.2 mL C_6D_6. The solution was heated at 80 °C for 16 hours. Volatiles were removed under reduced pressure and the residual solid recrystallised from hexane, The colourless crystal was identified as **$(L^{tBu})Mg(OAr)$** by NMR spectroscopy. Yield 303.5 mg (81 %).

^{1}H-NMR δ(C_6D_6): 0.95 (d, 9 H, $^{2}J_{PC}$ = 13.4 Hz, P-^{t}Bu), 1.04 (d, 9 H, $^{2}J_{PC}$ = 12.7 Hz, P-^{t}Bu), 1.14 (s, 9 H, C-^{t}Bu), 1.91. (s, 18 H, Ph-^{t}Bu), 1.66-1.83 (m, 2 H, CH_2), 3.92-4.02 (m, 1 H, CH); 6.62-6.87 (m, 1 H, p-Ph), 7.34-7.52 (d, 1 H, o-Ph), 7.23-7.32 (m, 1 H, m-Ph) [ppm].

^{31}P{^{1}H}-NMR δ(C_6D_6): 74.54 ppm.

Analysis Found: C 68.38 %, H 10.38 %; Calculated: C 68.50 %, H 10.47 %.

5.4.11 Preparation of [{Co(L^{Ph})$_2$}{L^{Ph}Co(O_2CL^{Ph})}]

A solution of **[Co(L^{Ph})$_2$]$_2$** in THF was left in a Schlenk tube with a small leak over a period of 11 months then volatiles were removed under reduced pressure, the residual solid recrystallised from hexane/THF to afford purple [{Co(L^{Ph})$_2$} {L^{Ph}Co(O_2CL^{Ph})}].

^{1}H-NMR δ(C_6D_6): -40 to 60 ppm. List major resonances, include fwhm if very broad.

^{31}P{^{1}H}-NMR δ(C_6D_6): 27 ppm (fwhm =).

5.4.12 Preparation of {L^{Ph}Co(O_2CL^{Ph})}$_2$

To a solution of **[Co(L^{Ph})$_2$]$_2$** in C_6D_6 (32.0 mg, 0.05 mmol, 0.5 mL) was going through CO_2 gaz at 25 °C, and the mixture then heated for 16 hours at 80 °C. Volatiles were removed under reduced pressure, the residual solid washed with hexane and dissolved in DME, then the solution evaporated slowly, to afford dark blue {L^{Ph}Co(O_2CL^{Ph})}$_2$

5.4.13 Preparation of [(HL^{tBu})$_2$MgCl].Cl

A solution of two equivalents of HL^{tBu} in toluene (500.0 mg, 1.91 mmol, 10 mL) was added to a solution of one equivalent of $MgCl_2$ in toluene (90.1 mg, 0.95 mmol, 10 mL) at room temperature and stirred for 16 hours at 70 °C. All volatile

compounds were removed under reduced pressure and the residual solid recrystallised from hexane to afford colourless **[(HL^{tBu})$_2$MgCl].Cl** 416.9 mg (71 %).

^{1}H-NMR δ(C_6D_6): 1-1.1 (54 H, m, C-CH_3); 1.8 – 1.9 (4 H, m, CH_2); 5.22 (2 H, bs, OH); 5.3 – 5.4 (2 H, m, CH) [ppm].

^{13}C-NMR δ(C_6D_6): 22.5 (2 C, d, J_{PC} = 14.1 Hz, CH_2); 25.7 (6 C, ^{t}Bu); 25.9 (6 C, ^{t}Bu); 26.1 (6 C, ^{t}Bu); 34.6 (2 C, C-^{t}Bu); 35.4 (2 C, d, J_{PC} = 13.8 Hz, P-^{t}Bu); 36.3 (2 C, ^{t}Bu); 66.6 (2 C, d, $^2J_{PC}$ = 8.2 Hz, CH) [ppm].

^{31}P{^{1}H}-NMR δ(C_6D_6): 70.0 and 70.6 ppm.

m/z (11.5 %) = 582.6 [**[(HL^{tBu})$_2$MgCl].Cl** - HCl] and m/z (7.1 %) = 546.6 [**[(HL^{tBu})$_2$MgCl].Cl** – 2 HCl].

Analysis Found: C 54.26 %, H 10.14 %; Calculated: C 54.25 %, H 10.08 %.

A solution of two equivalents of ***R*-HL^{tBu}** in C_6D_6 (40.0 mg, 0.153 mmol, 0.25 mL) was added to a solution of one equivalent of $MgCl_2$ in C_6D_6 (7.3 mg, 0.08 mmol, 0.25 mL) at room temperature and stirred for 16 hours at 70 °C. All volatile compounds were removed under reduced pressure and the residual solid recrystallised from hexane to afford colourless ***R*-[(HL^{tBu})$_2$MgCl].Cl**.

5.4.14 Preparation of (HL^{tBu})$_2$SnCl$_2$

A solution of two equivalents of HL^{tBu} in toluene (100.0 mg, 0.38 mmol, 10 mL) was added to a solution of one equivalent of $SnCl_2$ in toluene (36.2 mg, 0.19 mmol, 10 mL) at room temperature and stirred for 16 hours at 70 °C. All volatile compounds were removed under reduced pressure and the residual solid recrystallised from hexane to afford colourless **(HL^{tBu})$_2$SnCl$_2$** 108.6 mg (80 %).

^{1}H-NMR δ(C_6D_6): 0.98 (18 H, s, C-^{t}Bu); 1.3-1.4 (36 H, dd, $^2J_{PC}$ = 12.4 Hz, P-^{t}Bu); 1.9 – 2.0 (4 H, m, CH_2); 3.9 – 4.0 (2 H, m, CH) [ppm].

^{31}P{^{1}H}-NMR δ(C_6D_6): 76.1 ppm.

Analysis Found: C 47.08 %, H 8.75 %; Calculated: C 47.13 %, H 8.86 %.

5.4.15 Preparation of [(HL^{tBu})$_2$ZnCl].Cl

A solution of two equivalents of HL^{tBu} in toluene (200.0 mg, 0.66 mmol, 10 mL) was added to a solution of one equivalent of $ZnCl_2$ in toluene (45.1 mg, 0.33 mmol, 10 mL) at room temperature and stirred for 16 hours at 70 °C. All volatile compounds were removed under reduced pressure and the residual solid recrystallised from hexane to afford colourless [**(HL^{tBu})$_2$ZnCl].Cl**. Yield 179.1 mg (82 %).

^{1}H-NMR δ(C_6D_6): 1.02 (18 H, s, C-^{t}Bu); 1.1-1.4 (36 H, dd, $^2J_{PC}$ = 4.5 Hz, P-^{t}Bu); 1.7 – 1.9 (4 H, m, CH_2); 4.1 – 4.2 (2 H, m, CH); 4.63 (2 H, s, OH) [ppm].

^{13}C{^{1}H}-NMR δ(C_6D_6): 23.4 (2 C, d, J_{PC} = 56.8 Hz, CH_2); 25.8 (6 C, ^{t}Bu); 26.2 (6 C, ^{t}Bu); 26.3 (6 C, ^{t}Bu); 35.0 (2 C, d, J_{PC} = 56.8 Hz, P-^{t}Bu); 35.9 (2 C, d, J_{PC} = 58.1 Hz, P-^{t}Bu); 36.0 (2 C, ^{t}Bu); 73.4 (2 C, d, $^2J_{PC}$ = 5.7 Hz, CH) [ppm].

^{31}P{^{1}H}-NMR δ(C_6D_6): 72.6 ppm.

m/z (10.5 %) = 623.0 [[**(HL^{tBu})$_2$ZnCl].Cl** - HCl] and m/z (7.1 %) = 587.0 [[**(HL^{tBu})$_2$ZnCl].Cl** – 2 HCl].

Analysis Found: C 50.88 %, H 9.23 %; Calculated: C 50.87 %, H 9.45 %.

5.4.16 Preparation of [(HL^{Ph})$_2$MgCl].Cl

A solution of two equivalents of HL^{Ph} in toluene (1.0 g, 3.31 mmol, 10 mL) was added to a solution of one equivalent of $MgCl_2$ in toluene (157.6 mg, 1.66 mmol, 10 mL) at room temperature and stirred for 16 hours at 70 °C. All volatile compounds were removed under reduced pressure and the residual solid recrystallised from DME to afford colourless [**(HL^{Ph})$_2$MgCl].Cl. Yield** 867.4 mg (76 %).

^{1}H-NMR δ(C_6D_6): 0.83 (18 H, s, C-^{t}Bu); 2.1 – 2.3 (4 H, m, CH_2); 3.65 (2 H, s, O-H); 3.9 – 4.1 (2 H, m, CH); 6.9-7.1 (12 H, m, P-Ar); 7.7-7.9 (8 H, m, P-Ar) [ppm].

^{31}P{^{1}H}-NMR δ(C_6D_6): 41.2 ppm.

m/z (8.49 %) = 663.1 [(HL^{Ph})$_2$$MgCl_2$ - HCl]

5.4.17 Preparation of $(HL^{Ph})_2SnCl_2$

A solution of two equivalents of HL^{Ph} in toluene (500.0 mg, 1.66 mmol, 10 mL) was added to a solution of one equivalent of $SnCl_2$ in toluene (157.0 mg, 0.83 mmol, 10 mL) at room temperature and stirred for 16 hours at 70 °C. All volatile compounds were removed under reduced pressure and the residual solid recrystallised from DME to afford colourless **$(HL^{Ph})_2SnCl_2$ Yield** 583.2 mg (89 %).

^{1}H-NMR δ(C_6D_6): 0.9 (18 H, s, C-^{t}Bu); 2.3 – 2.6 (4 H, m, CH_2); 3.9 – 4.0 (2 H, m, CH); 4.61 (2 H, s, O-H); 7.0-7.1 (12 H, m, P-Ar); 7.8-7.9 (8 H, m, P-Ar) [ppm].

^{13}C{^{1}H}-NMR δ(C_6D_6): 25.2 (2 C, d, J_{PC} = 16.8 Hz, CH_2); 25.7 (6 C, ^{t}Bu); 25.9 (6 C, ^{t}Bu); 26.0 (6 C, ^{t}Bu); 35.2 (2 C, C-^{t}Bu); 35.5 (2 C, d, J_{PC} = 8.8 Hz, P-^{t}Bu); 36.3 (2 C, CMe_3); 74.7 (2 C, CH) [ppm].

^{31}P{^{1}H}-NMR δ(C_6D_6): 39.7 ppm.

Analysis Found: C 54.65 %, H 5.52 %; Calculated: C 54.44 %, H 5.84 %.

5.4.18 Preparation of $[(HL^{Ph})_2ZnCl].Cl$

A solution of two equivalents of *rac*-HL^{Ph} in toluene (500.0 mg, 1.66 mmol, 10 mL) was added to a solution of one equivalent of $ZnCl_2$ in toluene (112.8 mg, 0.83 mmol, 10 mL) at room temperature and stirred for 16 hours at 70 °C. All volatile compounds were removed under reduced pressure and the residual solid recrystallised from DME/THF to afford colourless **$[(HL^{Ph})_2ZnCl].Cl$. Yield** 522.4 mg (85 %).

^{1}H-NMR δ(C_6D_6): 0.9 (18 H, s, C-^{t}Bu); 2.3 – 2.6 (4 H, m, CH_2); 4.0 – 4.1 (2 H, m, CH); 4.95 (2 H, s, O-H); 7.0-7.1 (12 H, m, P-Ar); 7.8-7.9 (8 H, m, P-Ar) [ppm].

^{31}P{^{1}H}-NMR δ(C_6D_6): 41.6 ppm.

Analysis Found: C 58.44 %, H 6.14 %; Calculated: C 58.35 %, H 6.26 %.

5.4.19 Reactions of deprotonation of $(HL^{R})_2MCl_2$

5.4.19.1 Reaction of DABCO and $(HL^{tBu})_2SnCl_2$

A solution of three equivalents of DABCO in toluene (23.6 mg, 0.21 mmol, 5 mL) was added dropwise on a solution of one equivalent of **$(HL^{tBu})_2SnCl_2$** in toluene (50.0 mg, 0.07 mmol, 5 mL) cooled at -78 °C, then the reaction was stirred for 16 hours and allowed to warm to room temperature over x h. The reaction afforded a white solid and colourless solution, after filtration the solution was dried under vacuum to afford colourless glue. Analysis of the glue by NMR spectroscopy confirmed it to be proligand.

5.4.19.2 Reaction of LiN" and $(HL^{tBu})_2SnCl_2$

A solution of two equivalents of LiN" in C_6D_6 (23.3 mg, 0.14 mmol) was added on a solution of one equivalent of **$(HL^{tBu})_2SnCl_2$** in C_6D_6 (50 0mg, 0.07 mmol) at room temperature, the reaction was heated for 16 hours at 80 °C, the NMR shows an intractable mixture of compounds.

5.4.19.3 Reaction of DABCO and $[(HL^{tBu})_2MgCl].Cl$

A solution of three equivalents of DABCO in toluene (24.1 mg, 0.22 mmol, 3 mL) was added dropwise on a solution of one equivalent of **$[(HL^{tBu})_2MgCl].Cl$** in toluene (50.0 mg, 0.072 mmol, 3 mL) cooled at -78 °C, then the reaction was stirred for 16 hours and leaved warm-up. The volatiles were removed under vacuum to afford colourless solid. The NMR spectroscopy shows an intractable mixture of compounds.

5.5 X-Ray Crystallography Tables

	$Y(L^{Ph})_3$	$Y(L^{Ar})_3$	$Bi(L^{tBu})_3$
Chemical formula	$C_{54}H_{66}O_6P_3Y$	$C_{76}H_{111}O_8P_3Y$	$C_{42}H_{90}BiO_6P_3$
M_r	992.89	1334.47	993.03
Cell setting, space group	Monoclinic, $P12_1/n1$	Monoclinic, $P12_1/c1$	Monoclinic, $P12_1/c1$
Temperature (K)	150 (2)	150 (2)	150 (2)
a, b, c (Å)	11.5546 (3), 28.9231 (5), 15.5901 (3)	17.3521 (10), 14.9501 (8), 29.6647 (18)	21.3948 (8), 17.4131 (7), 13.4824 (5)
b (°)	96.3760 (10)	101.097 (4)	90.00, 93.353 (2), 90.00
V (Å^3)	5177.90 (19)	7551.6 (8)	5014.3 (3)
Z	4	4	4
D_x (Mg m^{-3})	1.274	1.174	1.315
Radiation type	Mo Ka	Mo $K\alpha$	Mo Ka
μ (mm^{-1})	1.27	0.89	3.65
Crystal form, colour	Prism, colourless	Block, colourless	Block, colourless
Crystal size (mm)	0.22 × 0.22 × 0.16	0.54 × 0.36 × 0.29	0.53 × 0.35 × 0.29
Diffractometer	Bruker SMART APEX CCD area detector	Bruker SMART APEX CCD area detector	Bruker SMART APEX CCD area detector
Data collection method	ω scans	ω scans	ω scans
Absorption correction	Multi-scan	Multi-scan	Multi-scan
T_{min}	0.610	0.602	0.3648
T_{max}	0.746	0.745	0.7454
No. of measured, independent and observed reflections	27949, 10382, 8428	74446, 15365, 10170	45751, 10274, 8207
Criterion for observed reflections	$I > 2\sigma(I)$	$I > 2\sigma(I)$	$I > 2\sigma(I)$
R_{int}	0.061	0.074	0.086
θ_{max} (°)	26.4	26.4	26.5
Refinement on	F^2	F^2	F^2
$R[F^2 > 2s(F^2)]$, $wR(F^2)$,S	0.074, 0.143, 1.24	0.051, 0.134, 1.02	0.075, 0.190, 1.15
No. of relections	10382 reflections	15365 reflections	10274 reflections
No. of parameters	586	818	469
H-atom treatment	Riding	Riding	Riding

	Lu(L^{Ph})$_3$	***fac*-In(L^{tBu})$_3$**	***mer*-In(L^{tBu})$_3$**
Chemical formula	$C_{54}H_{66}LuO_6P_3$	$C_{46}H_{100}InO_8P_3$	$C_{42}H_{90}InO_6P_3$
M_r	1078.95	988.99	898.87
Cell setting, space group	Monoclinic, $P2_1/n$	Tetragonal, $P4_3$	Monoclinic, $P12_1/c1$
Temperature (K)	150 (2)	150 (2)	150 (2)
a, b, c (Å)	11.5228 (6), 28.9135 (14), 15.5726 (8)	12.5537 (18), 35.309 (7)	19.2795 (5), 12.5166 (3), 21.7618 (5)
β (°)	96.499 (3)		105.1100 (10)
V (Å^3)	5154.9 (5)	5564.6 (16)	5069.9 (2)
Z	4	4	4
D_x (Mg m^{-3})	1.390	1.181	1.178
Radiation type	Mo $K\alpha$	Mo $K\alpha$	Mo $K\alpha$
μ (mm^{-1})	2.06	0.55	0.60
Crystal form, colour	Block, colourless	Prism, colorless	Prism, colourless
Crystal size (mm)	0.35 × 0.25 × 0.18	0.20 × 0.10 × 0.03	0.65 × 0.40 × 0.25
Diffractometer	Bruker Smart Apex CCD area detector	Bruker SMART APEX CCD area detector	Bruker SMART APEX CCD area detector
Data collection method	Phi and ω scans	ω scans	ω scans
Absorption correction	Multi-scan	Multi-scan	Multi-scan
T_{min}	0.581	0.766	0.609
T_{max}	0.745	1.000	0.746
No. of measured, independent and observed reflections	70511, 10556, 9260	27886, 9546, 6239	76637, 14888, 13246
Criterion for observed reflections	$I > 2\sigma(I)$	$I > 2\sigma(I)$	$I > 2\sigma(I)$
R_{int}	0.055	0.155	0.044
θ_{max} (°)	26.4	25.3	30.5
Refinement on	F^2	F^2	F^2
$R[F^2 > 2\sigma(F^2)]$, $wR(F^2)$, S	0.027, 0.062, 1.02	0.096, 0.302, 1.01	0.047, 0.106, 1.16
No. of relections	10556 reflections	9546 reflections	14888 reflections
No. of parameters	577	495	517
H-atom treatment	Riding	Riding	Riding
$(\Delta/\sigma)_{max}$	0.001	<0.0001	0.012
$\Delta\rho_{max}$, $\Delta\rho_{min}$ (e Å^{-3})	1.13, –0.32	1.19, –1.60	2.12, –0.67

	$(L^{tBu})_2YN''$	$(L^{tBu})_2InN''$	$(L^{tBu})_2In(NPh_2)$
Chemical formula	$C_{34}H_{78}NO_4P_2Si_2Y$	$C_{34}H_{78}InNO_4P_2Si_2$	$C_{40}H_{70}InNO_4P_2$
M_r	772.00	797.91	805.73
Cell setting, space group	Orthorhombic, *Pbcn*	Monoclinic, *P*12/*n*1	Monoclinic, *C*2/*c*
Temperature (K)	150 (2)	150 (2)	150 (2)
a, *b*, *c* (Å)	14.4604 (3), 19.6725 (5), 15.8916 (4)	13.5420 (7), 10.9614 (6), 14.4927 (8)	44.6208 (11), 16.1104 (4), 20.4816 (5)
β (°)		92.340 (2)	115.8270 (10)
V (Å^3)	4520.72 (19)		13252.7 (6)
Z	4	2	12
D_x (Mg m^{-3})	1.134	1.233	1.211
Radiation type	Mo *K*α	Mo *K*α	Mo *K*α
μ (mm^{-1})	1.45	0.71	0.64
Crystal form, colour	Prism, colourless	Prism, colourless	Block, colourless
Crystal size (mm)	0.53 × 0.33 × 0.18	0.53 × 0.33 × 0.18	0.43 × 0.30 × 0.23
Diffractometer	Bruker SMART APEX CCD area detector	Bruker SMART APEX CCD area detector	Bruker SMART APEX CCD area detector
Data collection method	ω scans	ω scans	ω scans
Absorption correction	Multi-scan	Multi-scan	Multi-scan
T_{min}	0.631	0.631	0.630
T_{max}	0.746	0.746	0.745
No. of measured, independent and observed reflections	23957, 6244, 4094	25829, 6157, 5864	72036, 13660, 11223
Criterion for observed reflections	$I > 2\sigma(I)$	$I > 2\sigma(I)$	$I > 2\sigma(I)$
R_{int}	0.068	0.031	0.072
θ_{max} (°)	30.5	30.5	26.5
Refinement on	F^2	F^2	F^2
$R[F^2 > 2\sigma(F^2)]$, $wR(F^2)$, *S*	0.081, 0.154, 1.16	0.036, 0.084, 1.18	0.067, 0.140, 1.21
No. of relections	6244 reflections	6157 reflections	13660 reflections
No. of parameters	212	234	677
H-atom treatment	Riding	Riding	Riding
$(\Delta/\sigma)_{max}$	0.001	0.001	0.002
$\Delta\rho_{max}$, $\Delta\rho_{min}$ (e Å^{-3})	0.85, –0.43	1.15, –0.73	0.96, –1.53

	$(L^{tBu})_2In(OAr)$	$(L^{tBu})_2Y(OAr)$	$(L^{tBu})_2(OSiMe_3)$
Chemical formula	$C_{42}H_{81}InO_5P_2$	$C_{44.56}H_{81}O_5P_2Y$	$C_{31}H_{69}InO_5P_2Si$
M_r	842.83	847.61	726.71
Cell setting, space group	Orthorhombic, $P2_12_12_1$	Trigonal, $R3$	Orthorhombic, $P2_12_12_1$
Temperature (K)	150 (2)	150 (2)	293 (2)
a, b, c (Å)	10.5951 (2), 18.1438 (4), 24.2262 (5)	36.1964 (8), 36.1964 (8), 10.8303 (3)	10.0066 (3), 18.2326 (6), 22.2333 (7)
β (°)		92.340 (2)	115.8270 (10)
V (Å^3)	4657.13 (17)	12288.6 (5)	4056.4 (2)
Z	4	9	4
D_x (Mg m^{-3})	1.202	1.031	1.190
Radiation type	Mo $K\alpha$	Mo $K\alpha$	Mo $K\alpha$
μ (mm^{-1})	0.61	1.16	0.72
Crystal form, colour	Prism, colourless	Block, colourless	Block, colourless
Crystal size (mm)	0.35 × 0.32 × 0.21	0.55 × 0.21 × 0.20	0.30 × 0.29 × 0.21
Diffractometer	Bruker SMART APEX CCD area detector	Bruker SMART APEX CCD area detector	Bruker SMART APEX CCD area detector
Data collection method	ω scans	ω scans	ω scans
Absorption correction	Multi-scan	Multi-scan	Multi-sca
T_{min}	0.628	0.614	0.582
T_{max}	0.746	0.745	0.745
No. of measured, independent and observed reflections	47190, 13576, 12674	44332, 11071, 9043	43617, 8490, 8066
Criterion for observed reflections	$I > 2\sigma(I)$	$I > 2\sigma(I)$	$I > 2\sigma(I)$
R_{int}	0.041	0.054	0.061
θ_{max} (°)	30.5	26.4	26.6
Refinement on	F^2	F^2	F^2
$R[F^2 > 2\sigma(F^2)]$, $wR(F^2)$, S	0.050, 0.113, 1.17	0.048, 0.130, 1.04	0.045, 0.112, 1.07
No. of relections	13576 reflections	11071 reflections	8490 reflections
No. of parameters	475	471	382
H-atom treatment	Riding	Riding	Riding
$(\Delta/\sigma)_{max}$	<0.0001	0.001	0.002

	$(L^{tBu})_2(CO_2)(NPh_2)$
Chemical formula	$C_{41}H_{70}InNO_6P_2$
M_r	849.74
Cell setting, space group	Monoclinic, $P12_1/c1$
Temperature (K)	273 (2)
a, b, c (Å)	23.0920 (5), 10.3958 (2), 19.1988 (4)
β (°)	101.9970 (10)
V (Å^3)	4508.20 (16)
Z	4
D_x (Mg m^{-3})	1.252
Radiation type	Mo $K\alpha$
μ (mm^{-1})	0.64
Crystal form, colour	Plate, colourless
Crystal size (mm)	0.35 × 0.25 × 0.1
Diffractometer	Bruker SMART APEX CCD area detector
Data collection method	ω scans
Absorption correction	Multi-scan (based on symmetry-related measurements)
T_{min}	0.613
T_{max}	0.745
No. of measured, independent and observed reflections	9175, 9176, 8386
Criterion for observed reflections	$I > 2\sigma(I)$
R_{int}	0.000
θ_{max} (°)	26.4
Refinement on	F^2
$R[F^2 > 2\sigma(F^2)]$, $wR(F^2)$, S	0.050, 0.108, 1.15
No. of relections	9176 reflections
No. of parameters	461
H-atom treatment	Riding

	$Zn(L^{tBu})_2$	$Sn(L^{tBu})_2$	$(HL^{tBu})ZnCl_2$
Chemical formula	$C_{28}H_{60}O_4P_2Zn$	$C_{28}H_{60}O_4P_2Sn$	$C_{14}H_{31}Cl_2O_2PZn$
M_r	588.07	641.39	398.63
Crystal system, space group	Orthorhombic, $P2_12_12_1$	Monoclinic, $P2_1/c$	Monoclinic, $P2_1/c$
Temperature (K)	150	150	120
a, b, c (Å)	12.3735 (14), 15.5890 (18), 17.696 (2)	16.1829 (19), 11.6147 (12), 19.157 (2)	13.9351 (4), 17.9494 (5), 15.8272 (3)
β (°)		108.278 (2)	92.680 (2)
V (Å^3)	3413.5 (7)	3419.1 (7)	3954.48 (18)
Z	4	4	8
D_x (Mg.m^{-3})		1.339	1.246
Radiation type	Mo $K\alpha$	Mo $K\alpha$	Mo $K\alpha$
μ (mm^{-1})	0.84	0.87	1.59
Crystal shape	Colourless	Block	Block
Colour	Needle	Colourless	Colourless
Crystal size (mm)	0.1 × 0.1 × 0.03	0.64 × 0.34 × 0.21	0.58 × 0.49 × 0.34
Diffractometer	Bruker *SMART APEX* CCD area detector	Bruker *SMART APEX* CCD area detector	Soton kappa CCD dataset
Scan method	dtprofit.ref scans	ω scans	ω scans
μ (mm^{-1})	0.84	1.59	0.87
Absorption correction	Multi-scan	Multi-scan	Multi-scan
T_{min}, T_{max}	0.855, 1.000	0.610, 0.756	0.631, 0.735
No. of measured, independent and observed reflections	22113, 6229, 5730	21659, 6229, 4513	40698, 9038, 6719
θ values (º)	θ_{max} = 25.4, θ_{min} = 1.7		θ_{max} = 25.4, θ_{min} = 2.1
R_{int}	0.046	0.089	0.072
$R[F^2 > 2\sigma(F^2)]$, $wR(F^2)$, S	0.033, 0.081, 0.82	0.071, 0.143, 1.08	0.090, 0.258, 1.16
No. of reflections	6229	6229	9038
No. of parameters	335	316	387
No. of restraints	0	0	0
H-atom treatment	Riding	Riding	Riding
$\Delta\rangle_{max}$, $\Delta\rangle_{min}$ (e Å^{-3})	0.27, -0.44	1.13, -0.61	5.57, -1.95
Flack parameter	0.574 (9)		

	$(HL^{tBu})_2SnCl_2$	$(HL^{tBu})_2MgCl_2$	$(HL^{tBu})_2MgCl_2.(H_2O)$
Chemical formula	$C_{28}H_{58}Cl_2O_6P_2Sn$	$C_{30}H_{66}Cl_2MgO_{4.50}P_2$	$C_{32}H_{68}Cl_{14}MgO_5P_2$
M_r	742.27	655.98	1115.41
Crystal system, space group	Monoclinic, $P2_1/n$	Tetragonal, $I4_1/a$	Monoclinic, $P2_1/c$
Temperature (K)	150	150	150
a, b, c (Å)	14.2569 (5), 13.7155 (5), 19.8179 (7)	20.2211 (4), 38.8148 (17)	20.169 (14), 13.459 (9), 22.181 (15)
β (º)	103.318 (2)	15871.1 (8)	113.854 (10)
V (Å^3)	3771.0 (2)		5507 (6)
Z	4	16	4
F(000)	1552	5728	2320
D_x (Mg m^{-3})	1.307	1.098	1.345
Radiation type	Mo $K\alpha$	Mo $K\alpha$	Mo $K\alpha$
No. of reflections for cell measurement	10915	10028	9672
μ (mm^{-1})	0.94	0.29	0.80
Crystal shape	Irregular	Block	Block
Colour	Colourless	Colourless	Colourless
Crystal size (mm)	0.49 × 0.37 × 0.34	0.56 × 0.32 × 0.21	0.33 × 0.27 × 0.09
Diffractometer	Bruker *SMART APEX* CCD area detector	Bruker *SMART APEX* CCD area detector	Bruker *SMART APEX* CCD area detector
Scan method	ω scans	ω scans	ω scans
Absorption correction	Multi-scan *SADABS*	Multi-scan *SADABS*	Multi-scan *SADABS*
T_{min}, T_{max}	0.604, 0.746	0.628, 0.746	0.778, 0.931
No. of measured, independent and observed reflections	42413, 10915, 10205	94250, 10028, 6116	9672, 9672, 7589
R_{int}	0.048	0.119	0.0000
θ values (º)	θ_{max} = 30.6, θ_{min} = 1.8	θ_{max} = 28.9, θ_{min} = 1.1	θ_{max} = 25.0, θ_{min} = 2.0
$R[F^2 > 2\sigma(F^2)]$, $wR(F^2)$, S	0.101, 0.236, 1.25	0.099, 0.310, 1.07	0.051, 0.138, 1.03
No. of parameters	370	383	551
No. of restraints	0	0	64
H-atom treatment	Riding	Riding	Riding
$(\Delta/\sigma)_{max}$	0.001	0.740	0.001

	$[Mg(L^{Ar})_2]_2$	$[Co(L^{Ph})_2]_2$	$[Co(L^{Ph)}{}_2]_2(CO_2)$
Chemical formula	$C_{102}H_{148}Mg_2O_{10}P_4$	$C_{79}H_{96}Co_2O_{10}P_4$	$C_{77}H_{95}Co_2O_{10}P_4$
M_r	1706.70	1447.30	1422.27
Crystal system, space group	Monoclinic, *C*2/*c*	Triclinic, P^-1	Monoclinic, $P2_1/n$
Temperature (K)	150	150	150
a, *b*, *c* (Å)	15.583 (3), 22.961 (5), 28.341 (7)	17.3893 (5), 17.9940 (5), 19.7239 (5)	13.1674 (5), 20.0144 (9), 31.0267 (12)
α, β, γ (º)	90.00(0), 103.104 (16), 90.00(0)	104.2510 (10), 101.7940 (10), 116.9530 (10)	90.00(0), 92.448 (2), 90.00(0)
V (Å^3)	9876 (4)	4962.6 (2)	8169.2 (6)
Z	4	2	4
D_x (Mg m^{-3})	1.148	0.969	1.156
Radiation type	Mo *K*α	Mo *K*α	Mo *K*α
No. of reflections for cell measurement	12315	20327	16638
μ (mm^{-1})	0.14	0.44	0.54
Crystal shape	Block	Block	Block
Colour	Colourless	Purple	Purple
Crystal size (mm)	0.43 × 0.38 × 0.31	0.48 × 0.41 × 0.32	0.61 × 0.49 × 0.41
Diffractometer	Bruker *SMART APEX* CCD area detector	Bruker *SMART APEX* CCD area detector	Bruker *SMART APEX* CCD area detector
Scan method	ω scans	ω scans	ω scans
Absorption correction	Multi-scan *SADABS*	Multi-scan *SADABS*	Multi-scan *SADABS*
T_{min}, T_{max}	0.577, 0.746	0.635, 0.745	0.608, 0.745
No. of measured, independent and observed [$I > 2\sigma(I)$] reflections	48669, 12315, 10096	55050, 20327, 16211	62308, 16638, 13121
R_{int}	0.055	0.037	0.055
$R[F^2 > 2\sigma(F^2)]$, $wR(F^2)$, *S*	0.112, 0.254, 1.26	0.096, 0.309, 1.10	0.118, 0.305, 1.19
No. of reflections	12315	20327	16638
No. of parameters	546	832	850
No. of restraints	0	0	0
H-atom treatment	Riding	Riding	Riding
$(\Delta/\sigma)_{max}$	0.046	0.185	5.764

[1] D. C. Bradley, M. B. Hursthouse, A. A. Ibrahim, K. M. Abdul Malik, M. Motevalli, R. Moseler, H. Powell, J. D. Runnacles, A. C. Sullivan, *Polyhedron* **1990**, *9*, 2959.
[2] K. J. Fisher, D. C. Bradley, *J. Am. Chem. Soc.* **1971**, *93*, 2058.
[3] P. J. Davidson, D. H. Harris, M. F. Lappert, *J. Chem. Soc., Dalton Trans.* **1976**, 2268.
[4] H. Buerger, W. Sawodry, U. Wannagat, *J. Organomet. Chem.* **1965**, *3*, 113.
[5] H. Buerger, J. Cichon, U. Goetze, U. Wannagat, H. J. Wismar, *J. Organometal. Chem.* **1971**, *33*, 1.
[6] D. C. Bradley, J. S. Ghotra, F. A. Hart, *J. Chem. Soc., Dalton Trans.* **1973**, 1021.
[7] L. Farrugia, *J. Appl. Crystallogr.* **1999**, *32*, 837.
[8] L. Farrugia, *J. Appl. Crystallogr.* **1997**, *30*, 565.
[9] G. Sheldrick, *Acta Cryst.* **2008**, *A64*, 112.
[10] P. L. Arnold, J.-C. Buffet, R. P. Blaudeck, S. Sujecki, A. J. Blake, C. Wilson, *Angew. Chem., Int. Ed.* **2008**, *47*, 6033.
[11] R. P. Blaudeck, PhD thesis University of Nottingham, UK (Nottingham), **2007**.
[12] M. I. Ali, PhD thesis University of Edinburgh, UK (Edinburgh), **2009**.
[13] S. E. Gorringe, University of Edinburgh, UK (Edinburgh), **2009**.
[14] J. Baran, A. Duda, A. Kowalski, R. Symanski, S. Penczek, *Macromol. Rapid Commun.* **1997**, *18*, 325.